FRMD8 is a novel regulator of iRhom-dependent ADAM17 activity



Ulrike Künzel

Lincoln College
University of Oxford

A thesis submitted to the University of Oxford
for the degree of Doctor of Philosophy

Trinity Term 2017

Table of contents

Acknowledgements **7**

Abstract **9**

Abbreviations **11**

1 Introduction **14**

1.1 The role of ectodomain shedding in intercellular signalling **14**

1.1.1 Epidermal growth factor receptor (EGFR) signalling 14

1.1.2 Regulation of EGFR signalling by ectodomain shedding 15

1.2 The shedding enzyme ADAM17 ..... **17**

1.2.1 ADAM17 substrates 17

1.2.2 Physiological function of ADAM17 18

1.2.3 Regulation of ADAM17 activity 19

1.3 iRhoms regulate ADAM17 activity **22**

1.3.1 The rhomboid-like superfamily 22

1.3.2 iRhom structure and expression 24

1.3.3 iRhoms and their functions 25

1.3.3.1 Protein degradation 25

1.3.3.2 Regulation of ADAM17 activity 27

1.3.3.3 Innate immune response to viral infection 29

1.3.4 Physiological function of mammalian iRhoms 29

1.3.5 Regulation of iRhoms 31

1.3.5.1 Transcriptional regulation of iRhoms 32

1.3.5.2 Posttranscriptional regulation of iRhoms 32

1.4 FERM domain-containing protein 8 (FRMD8) **34**

1.5 Aim of this project **36**

2 Materials and methods 38

2.1 Molecular biology methods 38

2.1.1 Molecular cloning 38

2.1.1.1 Polymerase chain reaction (PCR) 38

2.1.1.2 Agarose gel electrophoresis and gel purification 42

2.1.1.3 Restriction Digest 42

2.1.1.4 DNA assembly 42

2.1.1.5 Transformation 43

2.1.1.6 Plasmid preparation 43

2.1.1.7 Sequencing 44

2.1.2 mRNA isolation and quantitative PCR 45

2.1.3 Isolation of genomic DNA 46

2.1.4 CRISPR/Cas9 constructs 46

2.2 Cell biology methods 48

2.2.1 Mammalian cell lines 48

2.2.1.1 Cell lines and culture 48

2.2.1.2 DNA transfection 48

2.2.1.3 siRNA transfection 49

2.2.1.4 Lentiviral transduction 50

2.2.1.5 CRISPR/Cas9 genome editing in HEK293T cells 50

2.2.2 Human stem cell culture 51

2.2.2.1 Culture of human induced pluripotent stem cells (iPSCs) 51

2.2.2.2 CRISPR/Cas9 genome editing in iPSCs 51

2.2.2.3 Differentiation of iPSCs into macrophages 52

2.2.2.4 TNFα ELISA 53

2.3 Biochemical methods 54

2.3.1 Interactome studies using mass spectrometry 54

2.3.1.1 Cross-linking 54

2.3.1.2 Cell lysis and co-immunoprecipitation 54
2.3.1.3 Sample preparation 55
2.3.1.4 Mass spectrometry data analysis 55
2.3.2 Cell lysis 56
2.3.3 Bicinchoninic acid (BCA) assay 56
2.3.4 Co-immunoprecipitation 57
2.3.5 Concanavalin A enrichment 57
2.3.6 Deglycosylation assay 57
2.3.7 SDS-PAGE and western blotting 57
2.3.8 Shedding assay 59
2.3.9 Immunofluorescence staining and confocal microscopy 59
2.3.10 Flow cytometry 60
2.4 Mouse work 62
2.4.1 Generation of KO mice 62
2.4.2 Genotyping 62
2.4.3 Lysis of mouse tissues 63
2.4.4 Culture of bone marrow-derived macrophages (BMDM) 63
2.5 Work with Drosophila melanogaster 65
2.5.1 Fly lines 65
2.5.2 Generation of KO line with CRISPR/Cas9 65
2.5.3 Negative geotaxis assay 67
2.5.4 Longevity assay 68
3 Identification of FRMD8 as a novel iRhom interaction partner 70
3.1 Introduction 70
3.2 Results 73
3.2.1 Design and optimisation of a mass spectrometry-based screen for novel iRhom interaction partners 73

3.2.2 Generation of different truncated iRhom constructs 76
3.2.3 Mass spectrometry-based screen reveals potential new iRhom interaction partners 80
3.2.4 Validation of the FRMD8-iRhom interaction 84
3.3 Discussion 88
3.3.1 Identification of novel cytosolic interaction partners of iRhoms 88
3.3.2 A role for the iRhom N-terminus in the nucleus? 89
4 Investigating FRMD8 function within the iRhom/ADAM17 pathway 91
4.1 Introduction 91
4.2 Results 93
4.2.1 FRMD8 knockdown reduces mature ADAM17 levels 93
4.2.2 FRMD8 KO cells generated by CRISPR/Cas9 show reduced ADAM17 shedding activity 95
4.2.3 FRMD8 binds to iRhom2 N-terminus throughout the secretory pathway 102
4.2.4 FRMD8 loss does not affect ER-to-Golgi trafficking of iRhom2 106
4.2.5 FRMD8 stabilises iRhom2 beyond the Golgi 109
4.2.6 FRMD8 stabilises endogenous iRhom2 levels 113
4.3 Discussion 116
4.3.1 Proposed model for FRMD8 function 116
4.3.2 A potential role of the FRMD8 C-terminus 117
4.3.3 The relationship between FRMD8 and iRhom1 117
5 Physiological roles of FRMD8 120
5.1 Introduction 120
5.2 Results 122
5.2.1 FRMD8 KO macrophages show impaired TNFα release 122
5.2.2 Generation of FRMD8 KO mice 125
5.2.3 Bili KO Drosophila show reduced locomotion and activity 128

5.3 Discussion 133

5.3.1 Analysis of the first FRMD8 KO animals 133

5.3.2 A role for FRMD8/Bili in regulating iRhom in flies? 134

5.3.3 FRMD8 regulates TNFα signalling in human macrophages 135

6 Discussion and future directions 137

6.1 The role of FRMD8 in the iRhom/ADAM17 pathway 137

6.2 The function of FRMD8 in other pathways 140

6.3 The role of the iRhom2 N-terminus in regulating ADAM17 activity 141

6.3.1 Regions required for ADAM17-dependent shedding 143

6.3.2 The region required for mature ADAM17 stability 143

6.3.3 The iRhom2 cub mutation 144

6.4 Importance of analysing endogenous iRhom levels 146

6.5 FRMD8, iRhoms and ADAM17 as potential drug targets 147

6.5.1 ADAM17 inhibitors 148

6.5.2 iRhom2 as a drug target? 149

6.5.3 FRMD8 as a drug target? 150

Appendix 152

References 161

Acknowledgements

First, I would like to thank my supervisor, Matthew Freeman, for the opportunity to work in his lab on this exciting project. I am grateful for his support and guidance throughout my PhD time, for the freedom and trust to peruse my own ideas, and finally for advice and feedback on this thesis.

I am very grateful to all current and past members of the Freeman lab - Iqbal Dulloo, Stefan Düsterhöft, Adam Grieve, Kyojiro Ikeda, Nina Jajčanin-Jozić, Clémence Levet, Viorica Liebe, Ángela Moncada Pazos, Sonia Muliyil, Xin Shen, Boris Sieber and Hongmei Xu - for their support during the last 4 years. I especially thank Adam, Boris, Iqbal, Nina, and Stefan for their encouragement and scientific and non-scientific discussions that helped me to complete this project. Many thanks to Adam for feedback and proofreading of various scientific reports in the past and for organising several reagents or constructs for my project. I also thank Yao Meng, who was a Master's student in the lab, for her hard work in establishing an endogenously tagged iRhom2 cell line. And, of course, thanks to Clémence for keeping the lab running.

Furthermore, I would like to thank the Oxford scientists and research facilities who contributed to this project: first of all, I am very grateful to Monika Stegmann for her time and help with the statistical analysis of mass spectrometry results. I would also like to thank the rest of the Oxford Proteomics facility, particularly Svenja Hester for advice on developing a mass spectrometry screen and the help with processing the samples. Thanks to Andrew Bassett and Joey Riepsaame from Genome Engineering Oxford for their help with the CRISPR/Cas9 technique used during this project. I am also thankful to Sally Cowley and the entire stem cell lab for their advice and support with the iPSC work. I am grateful to Sonia Muliyil, Clémence Levet and Osamu Suyari for their help and advice with fly work. The generation of FRMD8 KO mice would not have been possible without help from Elizabeth Robertson, Jonathan Godwin, and Adam Grieve - I am deeply thankful for that. Thanks also to the team in the mouse facility and to Clémence Levet and Ángela Moncada Pazos for their help with mouse work.

I am very grateful for the support from the Boehringer Ingelheim Fonds and the Medical Research Council during this project and beyond.

Furthermore, I would like to thank Lincoln College for the support and the opportunity to meet so many wonderful people.

Many thanks to my friends for their support and welcome distractions from PhD life.

I am very grateful to my family, particularly my parents, who have supported and encouraged me throughout my entire life, and without whom all my years of study would not have been possible.

Above all, I would like to thank Johannes for his love and support - thanks for being an endless source of motivation and encouragement during the challenges of (PhD) life!

Abstract

A disintegrin and metalloprotease (ADAM) 17 cleaves and releases membrane-tethered pro-forms of several signalling molecules from the plasma membrane, including the inflammatory cytokine tumour necrosis factor alpha (TNFα) and ligands of the epidermal growth factor receptor (EGFR). Due to the important functions of its substrates, ADAM17 activity has to be tightly controlled, and its misregulation has implications for inflammation and cancer. The multi-pass membrane proteins iRhom1 and iRhom2 are members of the conserved rhomboid-like superfamily and control ADAM17 activity by several mechanisms throughout the secretory pathway. First, iRhoms facilitate trafficking of the catalytically inactive proenzyme form of ADAM17 from the endoplasmic reticulum (ER) to the Golgi apparatus, where the inhibitory pro-domain of ADAM17 is removed. Subsequently, iRhoms exert a different form of control of ADAM17 at the plasma membrane, this time on stimulus-induced ADAM17 activity, its substrate specificity, and its stability. iRhoms ultimately regulate the release of ADAM17 substrates, and are consequently key players in TNFα and EGFR signalling. However, it remains unclear how iRhom function itself is regulated posttranslationally, and whether iRhoms require co-factors to exert their roles as ADAM17 regulators. The goal of my project was to shed light into these questions by identifying new iRhom interaction partners.

I developed a mass spectrometry-based screen to identify new binding partners of human iRhoms using co-immunoprecipitation. The top hit of the screen was the poorly characterised FERM domain-containing protein 8 (FRMD8), which binds to both iRhom1 and iRhom2. FRMD8 was found to play a crucial role in the iRhom/ADAM17 pathway because FRMD8 knockdown and knockout in HEK293T cells significantly reduced the levels of mature ADAM17 and the release of ADAM17 substrates. The closely related metalloprotease ADAM10 was not affected by the loss of FRMD8, implying that FRMD8 is not a general regulator of ADAM metalloproteases. Interaction studies revealed that FRMD8 binds to the cytosolic N-terminus of iRhom2 throughout the entire secretory pathway. FRMD8 loss does not affect the ER-to-Golgi trafficking of iRhom2 but plays a

role in stabilising iRhom2 at the plasma membrane by preventing the lysosomal degradation of both iRhom2 and mature ADAM17.

Using human induced pluripotent stem cell (hiPSC)-derived macrophages, I showed that FRMD8 regulates mature ADAM17 levels and the ADAM17-dependent release of TNFα in human macrophages. Studies in FRMD8 knockout (KO) mice confirmed the reduced mature ADAM17 levels in all mouse tissues tested, further supporting the conclusion that FRMD8 is a novel regulator of the iRhom/ADAM17 pathway with physiological relevance in mammals.

Finally, I showed that the interaction of FRMD8 and iRhom, which are both conserved from *Drosophila* to human, is also conserved. Furthermore, loss of the FRMD8 orthologue in flies, Bili, leads to motility defects and shows similarity to the loss of iRhom in flies. These results suggest that FRMD8 is a novel regulator of iRhom function in mammals and *Drosophila*.

Abbreviations

aa	amino acid
ADAM	a disintegrin and metalloprotease
AREG	amphiregulin
BCA	bicinchoninic acid
bp	base pair
BSA	bovine serum albumin
BMDM	bone marrow-derived macrophage
BTC	betacellulin
cDNA	complementary DNA
CHAPS	3-[(3-Cholamidopropyl)dimethylammonio]-1-propanesulfonate
co-IP	co-immunoprecipitation
CRISPR/Cas	clustered regularly interspaced short palindromic repeats/CRISPR-associated
DDM	n-dodecyl β-D-maltoside
DKO	double knockout
DMSO	dimethyl sulfoxide
DNA	deoxyribonucleic acid
DSP	dithiobis(succinimidyl propionate)
DSS	dextran sulfate sodium
DTT	dithiothreitol
EDTA	ethylenediaminetetraacetic acid
EGF	epidermal growth factor
EGFR	epidermal growth factor receptor
Endo H	endoglycosidase H
ER	endoplasmic reticulum
ERAD	ER-associated degradation
EREG	epiregulin
FACS	fluorescence-activated cell sorting
FASP	filter-assisted sample preparation
FCS	fetal calf serum
FERM	four-point-one, ezrin, radix, moesin
FRMD8	FERM domain-containing protein 8
gDNA	genomic DNA
GFP	green fluorescent protein
GPCR	G-protein-coupled receptor
HB-EGF	heparin-binding epidermal growth factor
HEK cells	human embryonic kidney (cells)
HSV-1	herpes simplex virus type 1

Ig	immunoglobulin
IL	interleukin
IP	immunoprecipitation
iPSC	induced pluripotent stem cell
IRHD	iRhom homology domain
KO	knockout
LDS	lithium dodecyl sulfate
LPS	lipopolysaccharide
LRP6	low-density lipoprotein receptor-related protein 6
MAPK	mitogen-activated protein kinase
M-CSF	macrophage colony-stimulating factor
MEF	mouse embryonic fibroblast
mRNA	messenger RNA
NLS	nuclear localisation sequence
NMD	nonsense-mediated decay
PAC	proteasome assembling chaperone
PAGE	polyacrylamide gel electrophoresis
PAM	protospacer adjacent motif
PBS	phosphate-buffered saline
PCR	polymerase chain reaction
PMA	phorbol 12-myristate 13-acetate
PNGase F	peptide: N-glycosidase F
PPI	protein-protein interaction
PVDF	polyvinylidene fluoride
RNA	ribonucleic acid
RNAi	RNA interference
RSK	ribosomal protein S6 kinase
SDS	sodium dodecyl sulfate
sgRNA	single-guide RNA
siRNA	small interfering RNA
TBS	Tris-buffered saline
TfR	transferrin receptor
TGFα	transforming growth factor alpha
TMD	transmembrane domain
TMEM115	transmembrane protein 115
TNFα	tumour necrosis factor alpha
TNFR	TNFα receptor
TOC	tylosis with oesophageal cancer
WT	wild-type

CHAPTER 1

Introduction

1 Introduction

1.1 The role of ectodomain shedding in intercellular signalling

1.1.1 Epidermal growth factor receptor (EGFR) signalling

The communication between cells, referred to as intercellular signalling, is essential for multicellular organisms to orchestrate cell functions; but even unicellular organisms can communicate to coordinate their actions (Alberts et al., 2002). Epidermal growth factor receptor (EGFR) signalling is a well-studied example of an intercellular signalling pathway that regulates cell differentiation, proliferation, survival, and tissue repair in metazoans. The EGFR belongs to the family of receptor tyrosine kinases which are single-pass membrane proteins with a ligand-binding domain in their extracellular region and an intracellular kinase domain (Adrain and Freeman, 2014). Mammals express four different EGFR proteins (ErbB1-4), for which eleven ligands are known: the epidermal growth factor (EGF), the transforming growth factor alpha (TGFα), amphiregulin (AREG), heparin-binding EGF (HB-EGF), epiregulin (EREG), betacellulin (BTC), epigen, as well as neuregulin 1-4 (NRG1-4) (Citri and Yarden, 2006).

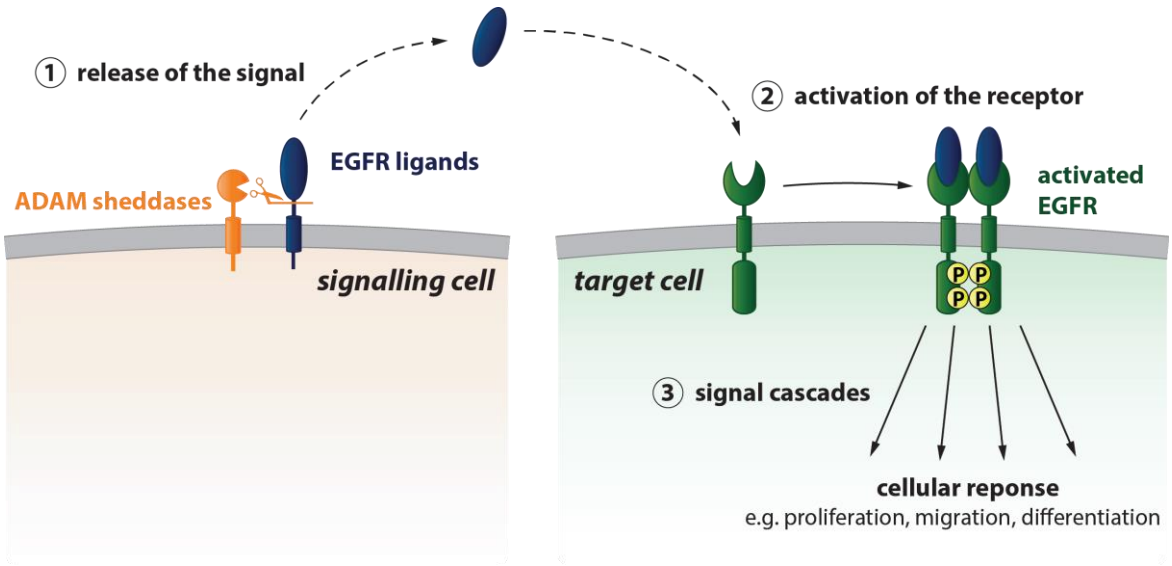


Figure 1.1 | The role of ectodomain shedding in intercellular signalling illustrated on the example of EGFR signalling. The sheddases ADAM10 and ADAM17 have a key role in regulating EGFR signalling by controlling the release of EGFR ligands from the signalling cell.

EGFR signalling requires three main steps (Fig. 1.1): first, signalling molecules are released from the signalling cell, which then in the second step bind to a receptor on the target cell, thereby activating the receptor. Ligand binding leads to homo- or heterodimerisation of ErbB1-4, which results in autophosphorylation of the receptor by its kinase domain. In the third step, signalling proteins are recruited to the activated receptor and trigger downstream signalling cascades, ultimately leading to a cellular response, such as proliferation, differentiation or cell migration (Holbro and Hynes, 2004).

1.1.2 Regulation of EGFR signalling by ectodomain shedding

EGFR signalling has to be tightly regulated because hyperactivation has been linked to various types of cancer (Yarden and Sliwkowski, 2001). Although, current cancer therapeutics focus on blocking EGFR signalling in the target cell (Yarden and Pines, 2012), one important mechanism to control the access of the ligand to the receptor is regulating the release of the signalling molecules from the signalling cell. All EGFR ligands are synthesised as membrane-tethered precursors that are cleaved by proteases to be released from cells (Harris et al., 2003) (Fig.1.1). The proteolytic processing of membrane proteins that results in the release of the extracellular part is referred to as ectodomain shedding and is executed by proteases called sheddases. With 2% to 4% of cell surface proteins undergoing ectodomain shedding, this is an important mechanistic principle that regulates the release of signalling molecules and the activity of signalling receptors and adhesion molecules (Blobel, 2005, Hayashida et al., 2010).

In mammals, a disintegrin and metalloprotease (ADAM) proteins, a family of membrane-bound zinc metalloproteases, mediate ectodomain shedding of several EGFR ligands (Blobel et al., 2009). Although there is some overlap between several ADAM proteases in cleaving EGFR ligands, ADAM17 and ADAM10 are the key enzymes in releasing EGFR ligands: ADAM17 is the main sheddase of TGFα, HB-EGF, AREG, EREG, and epigen, whereas ADAM10 is the principal protease in EGF and BTC

processing (Sahin et al., 2004, Sahin and Blobel, 2007). In addition, both ADAM10 and ADAM17 are involved in the cleavage of NRG1 (Fleck et al., 2013).

Stimulation of G-protein-coupled receptors (GPCRs), another group of cell surface receptors, can activate ADAM protease-dependent EGFR signalling (reviewed in (Ohtsu et al., 2006)). This crosstalk between two signalling pathways is referred to as EGFR transactivation and has been implicated in several types of cancer (Kose, 2017). Stimulated GPCRs lead to the activation of ADAM protease-mediated shedding of EGFR ligands, which subsequently trigger EGFR signalling. As EGFR transactivation requires metalloprotease activity, a triple membrane-passing signal pathway was suggested, opposed to an intracellular activation pathway (Fig.1.2) (Prenzel et al., 1999, Fischer et al., 2003).

In summary, ectodomain shedding by ADAM proteases plays a crucial role in the activation of EGFR signalling, and consequently in development, tissue repair, and cancer (Blobel, 2005). Importantly, the principle of ectodomain shedding is not restricted to EGFR ligands and also required for the regulation of other signalling pathways, for example in tumour necrosis factor alpha (TNFα) signalling as described in 1.2.1.

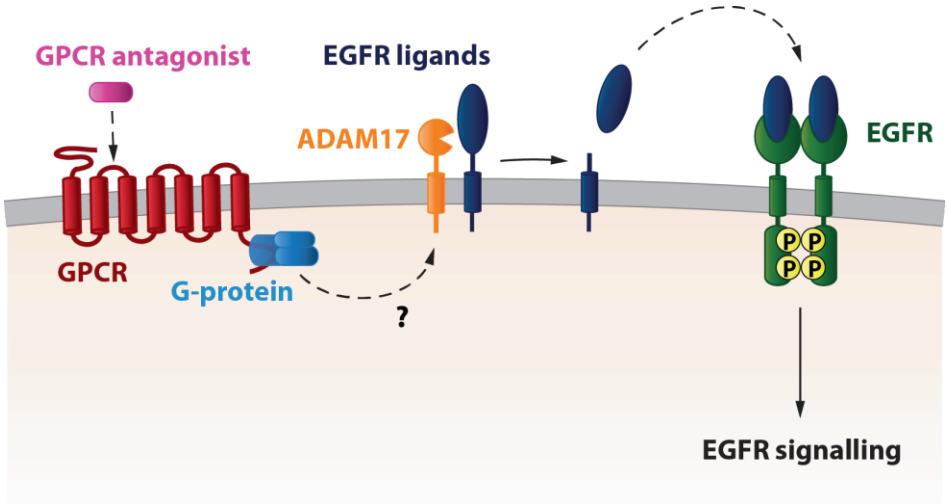


Figure 1.2 | Role of ADAM17 in EGFR transactivation by G-protein-coupled receptors (GPCRs). ADAM17 has a central role in EGFR transactivation by GPCRs through a triple membrane-spanning pathway, in which the signal crosses the membrane three times: activation of GPCRs lead to the downstream activation of ADAM17, which results in the release of EGFR ligands that finally trigger EGFR signalling.

1.2 The shedding enzyme ADAM17

The metalloprotease ADAM17 is, together with its close relative ADAM10, the principal sheddase in mammalian cells. ADAM17 is conserved from *Drosophila* to human and consists of an inhibitory pro-domain, followed by the catalytic metalloproteinase domain, a disintegrin domain, the membrane proximal domain, a transmembrane domain (TMD), and a cytoplasmic region (Zunke and Rose-John, 2017) (Fig.1.3). Although only the catalytic domain, which contains the catalytic zinc ion, is required for proteolytic activity of ADAM17 (Milla et al., 1999), the other domains are involved in regulating ADAM17 activity (Grotzinger et al., 2017).

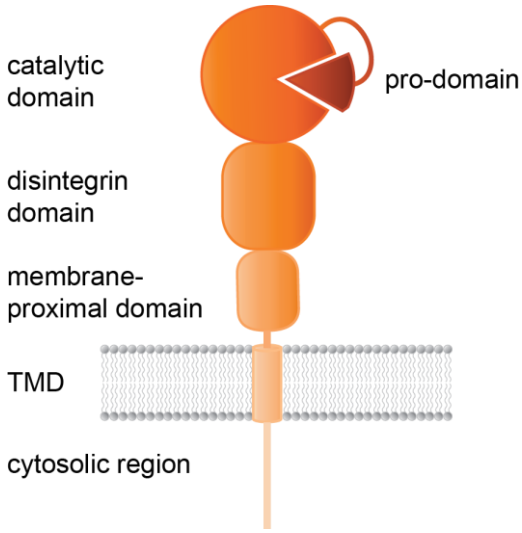


Figure 1.3 | Domain organisation of ADAM17. Schematic representation of the ADAM17 domain structure, adapted from (Rose-John, 2013).

1.2.1 ADAM17 substrates

ADAM17 was initially discovered as the enzyme responsible for the shedding and release of the membrane-bound pro-inflammatory cytokine TNFα, and is therefore also known as TNFα-converting enzyme (TACE) (Black et al., 1997, Moss et al., 1997). TNFα can activate two receptors, TNFα receptor 1 (TNFR1) and TNFR2 (Lewis et al., 1991), which leads to the transcriptional activation of pro-inflammatory cytokines. TNFα consequently orchestrates the innate immune response in bacterial infection and is a key

player in inflammatory diseases like rheumatoid arthritis and inflammatory bowel disease (reviewed in (Kalliolias and Ivashkiv, 2016)). TNFα-deficient mice are susceptible to pathogen infection but resistant to lethal doses of lipopolysaccharide (LPS) (Marino et al., 1997), a bacteria-derived molecule which induces septic shock, an uncontrolled, often fatal immune response that can occur after infection (Huet and Chin-Dusting, 2014).

In addition to TNFα, there have been more than 80 substrates reported for ADAM17, among those are several cytokine receptors (e.g. TNFR1 and TNFR2), cell adhesion molecules, and, as mentioned above, the EGFR ligands AREG, TGFα, HB-EGF, EREG, and epigen (Zunke and Rose-John, 2017). All five EGFR ligands have roles in tissue proliferation and homeostasis in the skin, as well as in the development of other organs (Table 1.1). Despite the large number of substrates that can be shed by ADAM17, not all of them seem to be physiologically relevant, as for instance seen by the phenotypes of ADAM17-deficient mice (1.2.2).

Table 1.1 | Overview of the function of EGFR ligands cleaved by ADAM17

	Biological function	**Reference(s)**
TGFα	eye development, hair follicle development, skin architecture	(Mann et al., 1993, Luetteke et al., 1993)
	epidermal thickening and development	(Vassar and Fuchs, 1991)
AREG	development of the mammary gland	(Luetteke et al., 1999)
	epidermal proliferation and wound healing	(Cook et al., 1997, Cook et al., 2004, Stoll et al., 2010)
HB-EGF	heart development	(Jackson et al., 2003, Iwamoto et al., 2003)
	cutaneous wound healing	(Tokumaru et al., 2000, Shirakata et al., 2005)
EREG	skin homeostasis	(Shirasawa et al., 2004)
epigen	role in sebaceous glands in the skin	(Dahlhoff et al., 2010)

1.2.2 Physiological function of ADAM17

Due to its substrate repertoire, which includes EGFR ligands, cytokines, and cytokine receptors, ADAM17 is an important regulator of inflammation and tissue repair *in vivo* with

implications for cancer and other diseases (Scheller et al., 2011). *Adam17*-deficient mice die perinatally with open eyes at birth, skin and hair follicle defects, and enlarged heart valves, at least partially phenocopying the loss of several EGFR ligands and ErbB1 in mice (Peschon et al., 1998, Jackson et al., 2003). As ADAM17 loss is lethal in mice, ADAM17 function was studied in several conditional knockout models. Myeloid-specific ADAM17 knockout (KO) mice show a strong reduction in TNFα levels in sera upon LPS treatment, which leads to resistance to LPS-induced septic shock (Horiuchi et al., 2007a). A hypomorphic ADAM17 mouse model, called *Adam17*$^{ex/ex}$, in which about 95% of the ADAM17 mRNA contains an early stop codon, shows a drastic reduction of ADAM17 protein levels in all tissues. *Adam17*$^{ex/ex}$ mice are viable but deficient in TNFα shedding and susceptible to dextran sulfate sodium (DSS)-induced intestinal inflammation (Chalaris et al., 2010). Keratinocyte-specific loss of ADAM17 leads to a defect in epidermal barrier function and chronic skin inflammation (Franzke et al., 2012).

In humans, homozygous *ADAM17* loss-of-function mutations have been reported in three families (Blaydon et al., 2011, Bandsma et al., 2015, Tsukerman et al., 2015). All patients showed reduced secretion of TNFα from peripheral blood mononuclear cell (PBMCs) after stimulation and suffered from reoccurring bacterial infections, diarrhoea, hair defects, skin lesions, and skin inflammations. Two patients died from their symptoms before the age 2 years (Bandsma et al., 2015, Tsukerman et al., 2015), whereas two other patients reached teenage age (Blaydon et al., 2011).

In summary, ADAM17-deficient mouse models and human patients show similar phenotypes, which clearly demonstrate the physiological relevance of ADAM17-mediated shedding of TNFα and EGFR ligands *in vivo*.

1.2.3 Regulation of ADAM17 activity

Proteolysis, such as ADAM17-dependent shedding, is a posttranslational modification that irreversibly changes the properties of a protein. For this reason, ADAM17 activity is tightly regulated at multiple levels from protein synthesis to degradation.

ADAM17 is synthesised as a zymogen, a catalytically inactive pro-form of an enzyme, and contains an inhibitory pro-domain. The pro-domain coordinates the zinc ion in the active centre of the sheddase and keeps proADAM17 inactive until it is proteolytically removed in the *trans*-Golgi network by furin-like pro-protein convertases (Endres et al., 2003), resulting in mature ADAM17. Mature ADAM17 is enzymatically active but not necessarily able to shed its substrates because enzymatic activity and shedding activity of mature ADAM17 are two distinct functions (Sommer et al., 2016): the enzymatic activity is demonstrated by the ability of the catalytic centre to cleave peptides, whereas the shedding activity refers to the actual release of ADAM17 substrates. Much work has been done on the regulation of ADAM17, although some of it is contradictory and details still need to be resolved. Nevertheless, to illustrate the complexity, I will outline here some of the main proposed mechanisms. For example, an important regulatory theme is the conformation of ADAM17 and its accessibility to substrates (reviewed in (Grotzinger et al., 2017). In resting cells, the majority of mature ADAM17 is stored intracellularly and only a small amount is present at the cell surface (Soond et al., 2005, Lorenzen et al., 2016). The trafficking of mature ADAM17 to the cell surface can be activated by mitogen-activated protein kinases (MAPKs) (Soond et al., 2005, Xu and Derynck, 2010). At the plasma membrane, ADAM17 shedding activity can be inhibited by the interaction of ADAM17 with $\alpha_5\beta_1$integrin (Gooz et al., 2012, Bax et al., 2004, Trad et al., 2013), by the tissue inhibitor of metalloproteinases 3 (TIMP3) (Amour et al., 1998) or by dimerisation of ADAM17, which favours TIMP3 binding (Xu et al., 2012). Furthermore, the accessibility of mature ADAM17 to the cell surface is regulated by endocytosis, followed by endocytic recycling or lysosomal degradation. The cytosolic protein phosphofurin acidic cluster sorting protein 2 (PACS-2) binds to ADAM17 and promotes its endocytic recycling (Dombernowsky et al., 2015).

Beyond conformational regulation and compartmentalisation, shedding activity of ADAM17 can also be rapidly activated by various stimuli, including phorbol esters and GPCR agonists. Although, there is some controversy, this appears not to require the cytoplasmic tail of ADAM17, but instead relies on its TMD (Reddy et al., 2000, Horiuchi et

al., 2007b, Le Gall et al., 2010, Maretzky et al., 2011). Different mechanisms have been suggested for the rapid stimulated ADAM17 shedding activity (Le Gall et al., 2010, Xu et al., 2012, Sommer et al., 2016, Grieve et al., 2017), many of which imply conformational changes of ADAM17. One study showed for instance that stimulation leads to the exposure of phosphatidylserine (PS) in the outer leaflet of the plasma membrane, where the membrane-proximal domain of ADAM17 interacts with PS leading to a conformational change in the membrane-proximal domain and the activation of ADAM17 shedding activity (Sommer et al., 2016).

Of primary relevance to my work, it has been shown that almost all steps of ADAM17 regulation are controlled by membrane proteins, called iRhoms, which will be discussed in detail below (1.3.3.2).

1.3 iRhoms regulate ADAM17 activity

1.3.1 The rhomboid-like superfamily

iRhoms belong to the rhomboid-like superfamily, a conserved family of multi-pass membrane proteins found in all three kingdoms of life (Freeman, 2014). The superfamily is named after its founding member, *Drosophila* Rhomboid-1, which was first described to cause a pointed head skeleton in the *Drosophila* embryo when mutated (Jurgens et al., 1984). In 2001, Rhomboid-1 was the first intramembrane serine protease to be discovered, when it was shown to cleave its substrates within their TMDs (Urban et al., 2001). Rhomboid-1 cleaves the TGFα-like EGFR ligand Spitz in *Drosophila*, leading to the release of soluble Spitz and subsequently to the activation of the EGFR (Lee et al., 2001, Urban et al., 2001). Homologues of rhomboid proteases are present in many pro- and eukaryotic species and perform various cellular functions including quorum sensing in bacteria, host cell invasion in *Plasmodium* and *Toxoplasma* parasites, regulating mitochondrial function, wound healing, and ER-associated degradation (ERAD) in metazoans (reviewed in (Dusterhoft et al., 2017)). In addition to the rhomboid proteases, bioinformatic analysis identified rhomboid homologues in eukaryotes that lack catalytic residues (Koonin et al., 2003, Lemberg and Freeman, 2007), leading to the proposal of a superfamily of rhomboid-like proteins, comprising both rhomboid proteases and pseudoproteases (Freeman, 2009). In mammals, the rhomboid-like superfamily consists of 14 members, nine of which are pseudoproteases (Fig. 1.4A). Inactive rhomboid-like proteins, like iRhoms, presumably evolved by gene duplications of ancient active rhomboids followed by the loss of catalytic function, diversification, and gain of new functions (Adrain and Freeman, 2012). Accordingly, rhomboid proteases and their inactive homologues have distinct cellular functions, but share structural similarities. For instance, all members of the rhomboid-like superfamily share a core of six conserved TMDs, the rhomboid fold, which can be extended by a seventh TMD at the C- or N-terminus (Fig. 1.4A). The active centre of rhomboid proteases consists of a conserved serine-histidine

dyad (Lemberg et al., 2005), located in the fourth and sixth TMD of the rhomboid fold (Fig. 1.4A).

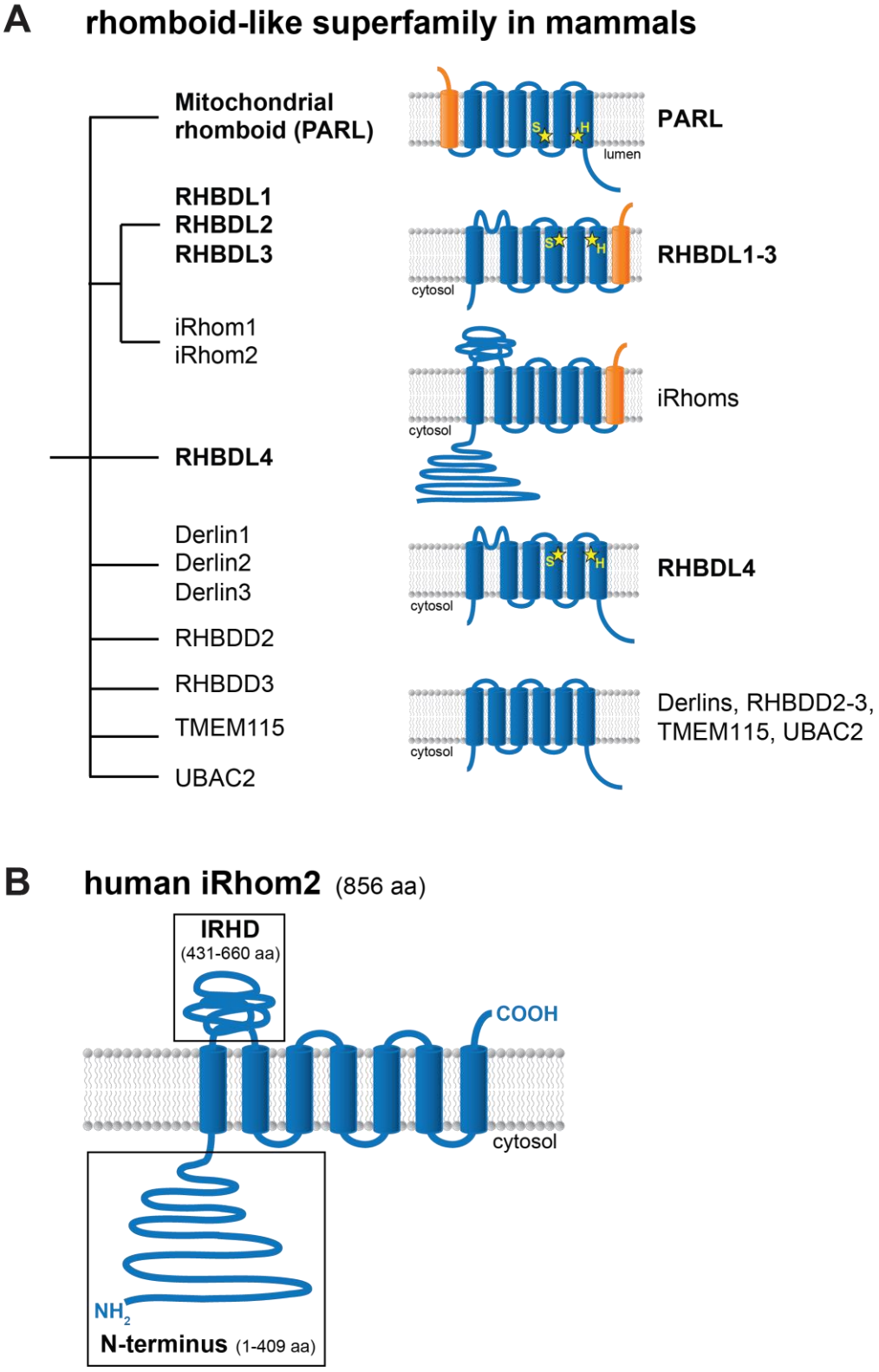


Figure 1.4 | iRhoms are members of the rhomboid-like superfamily. A) Overview of the rhomboid-like superfamily in mammals. Paralogues are represented in the diagram. Active rhomboid proteases are written in bold. The domain structure of representatives of the rhomboid-

like family is shown on the right. The six TMD rhomboid fold is shown in blue and the additional seventh TMD is highlighted in orange. The position of catalytic serine (S) and histidine (H) is indicated by a yellow star. **B)** Schematic representation of human iRhom2 with its characteristic cytosolic N-terminus and the iRhom homology domain (IRHD) located between TMD1 and TMD2. iRhom1 shows the same domain organisation.

1.3.2 iRhom structure and expression

iRhoms are inactive rhomboid-like proteins that are phylogenetically and structurally closely related to the rhomboid proteases RHBDL1-3 (Bergbold and Lemberg, 2013). iRhoms contain seven TMDs and lack either one or two residues of the serine-histidine dyad that makes up the catalytic centre of rhomboid proteases. The exceptions are iRhom1 and iRhom2 in *Caenorhabditis elegans*, which still contain an intact serine-histidine dyad (Lemberg and Freeman, 2007). However, all iRhoms contain a conserved proline N-terminal of the expected location of catalytic serine, which presumably eliminates proteolytic activity of iRhoms (Lemberg and Freeman, 2007). Supporting this, the insertion of a proline residue in the active site of rhomboid proteases impaired their catalytic activity (Zettl et al., 2011). iRhoms have been tested for the cleavage of a variety of known rhomboid substrates but, as predicted, were not able to cleave any (Zettl et al., 2011).

In contrast to rhomboid proteases, iRhoms contain a long N-terminus that constitutes approximately half of the entire protein (Fig. 1.4B). Furthermore, iRhoms comprise a highly conserved cysteine-rich loop between TMD1 and TMD2, termed the iRhom homology domain (IRHD). The IRHD contains 16 conserved cysteines which might form disulfide bonds (Lemberg and Freeman, 2007). The function of the IRHD has not been well characterised yet but was suggested to play an essential role in the binding and maturation of ADAM17 (Grieve et al., 2017).

iRhoms are conserved in all metazoans but not in unicellular eukaryotes or prokaryotes. Whereas *Drosophila* only contains one iRhom gene, most vertebrates contain two paralogues, called *RHBDF1* (encoding iRhom1) and *RHBDF2* (encoding

iRhom2) (Ensembl genome browser (Yates et al., 2016)). iRhom1 and iRhom2 show 56% identity in their amino acid sequence in humans but differ in their tissue expression: iRhom2 is highly expressed in immune cells and skin (Christova et al., 2013), whereas iRhom1 is more ubiquitously expressed (Christova et al., 2013, Li et al., 2015). iRhoms localise to the ER, the Golgi apparatus (Nakagawa et al., 2005, Zou et al., 2009, McIlwain et al., 2012, Hosur et al., 2014, Maney et al., 2015, Luo et al., 2016), and the plasma membrane (Maney et al., 2015, Grieve et al., 2017). iRhom2 was also detected in lysosomes (Luo et al., 2016).

1.3.3 iRhoms and their functions

A variety of cellular functions throughout the secretory pathway have been described for iRhoms mainly regulating protein degradation, protein transport, and growth factor and cytokine signalling.

1.3.3.1 Protein degradation

The first mechanistic insight into iRhom function came from *Drosophila*, where iRhom was found as a negative regulator of EGFR signalling. iRhom KO flies showed increased periods of inactivity, which phenocopied hyperactivation of EGFR signalling (Zettl et al., 2011). On a cellular level, overexpression of *Drosophila* iRhom or mammalian iRhoms resulted in the proteasomal degradation of EGFR ligands and consequently in their reduced secretion (Fig. 1.5). In *Drosophila*, the degradation of EGFR ligands required components of the ERAD machinery *in vivo*. Although mammalian iRhom1 and iRhom2 were shown to interact with EGF and drive its degradation by ERAD (Zettl et al., 2011) a physiological role of this function has not yet been proven.

Furthermore, a genome-wide screen identified human iRhom1 as a stimulator of proteasomal activity, suggesting a more general role for iRhom1 in protein degradation (Lee et al., 2015). iRhom1 overexpression increased the proteasomal activity in human cells and flies, particularly under ER stress. Mechanistically, it was suggested that iRhom1

binds to the proteasome assembling chaperone (PAC) 1 and PAC2, thereby regulating their stability and heterodimerisation (Lee et al., 2015), which is essential for the assembly of the 20S proteasome (Hirano et al., 2005). Whether the role of iRhom in regulating the assembly of the 20S proteasome is related to iRhom-mediated ERAD of EGFR ligands is unclear. Notably, iRhom1 also affected the stability and degradation of cytoplasmic proteins, such as a Huntington mutant and a GFP degron (Lee et al., 2015), suggesting that this function is not directly related to ERAD. Whether iRhom2 also has a redundant role in regulating proteasomal activity has not been assessed, although there are hints that several rhomboid-like proteins have a functional relationship with the proteasome, as the rhomboid proteases RHBDL1 and RHBDL2 also increased proteasomal activity, and this was independent of their proteolytic activity (Lee et al., 2015).

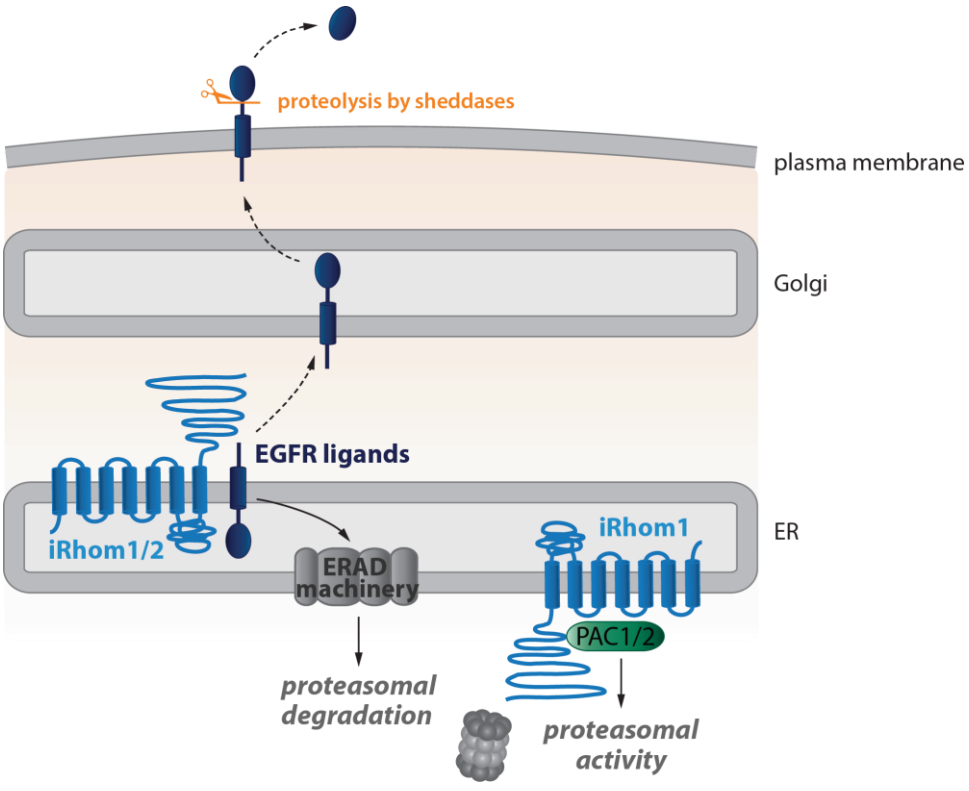


Figure 1.5 | The role of iRhoms in protein degradation. Drosophila iRhom and mammalian iRhom1/2 mediate the proteasomal degradation of EGFR ligands by ERAD (Zettl et al., 2011). Drosophila iRhom and human iRhom1 were also shown to positively regulate the proteasomal activity through the proteasome assembling chaperone-1 (PAC1) and PAC2 (Lee et al., 2015).

1.3.3.2 Regulation of ADAM17 activity

The best-characterised role of mammalian iRhoms is the regulation of ADAM17 activity. iRhom1 and iRhom2 bind to pro- and mature ADAM17 (Adrain et al., 2012, McIlwain et al., 2012, Christova et al., 2013) but not to the closely related metalloprotease ADAM10 (Adrain et al., 2012), and regulate ADAM17 activity at multiple stages throughout the secretory pathway. Firstly, iRhoms act as cargo-specific transporters of ADAM17 and control the trafficking of ADAM17 from the ER to the Golgi apparatus (Adrain et al., 2012, McIlwain et al., 2012), where the inhibitory pro-domain of ADAM17 is removed by furin-like pro-protein convertases resulting in mature ADAM17 (Fig. 1.6). iRhoms are ultimately required for the release of ADAM17 substrates, and the loss of both iRhoms results in a complete loss of mature ADAM17 and ADAM17-dependent shedding (Christova et al., 2013, Li et al., 2015). However, if only one of the iRhoms is deleted, the other iRhom can partly rescue the loss in most tissues (Christova et al., 2013, Li et al., 2015), except for tissues in which only one iRhom is expressed, such as macrophages, where iRhom2 controls all ADAM17 maturation and activity (Issuree et al., 2013).

Secondly, iRhoms are required for the rapid, stimuli-induced activation of ADAM17-dependent shedding (Maretzky et al., 2013, Grieve et al., 2017). It has long been shown that the cytoplasmic tail of ADAM17 is not required for the rapid activation of ADAM17-dependent shedding upon stimulation of cells (Le Gall et al., 2010) but that the cytoplasmic N-terminus of iRhom2 is required (Maretzky et al., 2013). This is consistent with reports that iRhom1 and iRhom2 participate in the GPCR-mediated transactivation of EGFR signalling (Zou et al., 2009, Christova et al., 2013, Maretzky et al., 2013). Mechanistically, the stimulation of cells with phorbol ester or GPCR agonists leads to the MAPK1/3-dependent phosphorylation of three distinct sites within the iRhom2 N-terminus, to which 14-3-3 proteins are subsequently recruited (Grieve et al., 2017). The binding of 14-3-3 proteins to the iRhom2 N-terminus alters the interaction between iRhom2 and mature ADAM17 at the plasma membrane, leading to the upregulation of ADAM17-dependent shedding (Grieve et al., 2017). Furthermore, iRhom2 was suggested to control

the substrate selectivity of ADAM17 upon stimulation (Maretzky et al., 2013). The cytoplasmic region, the TMD and the membrane-proximal region of the substrate seem to play an important role in the substrate selectivity, but further mechanistic details are not understood (Maretzky et al., 2013).

Thirdly, iRhom2 stabilises mature ADAM17 at the plasma membrane and prevents its degradation through the lysosomal pathway (Grieve et al., 2017). This stabilisation was dependent on the cytosolic N-terminus of iRhom2, implying that it contains signals or interaction partners that mediate the stability of ADAM17 at the cell surface. Further details are, however, not understood.

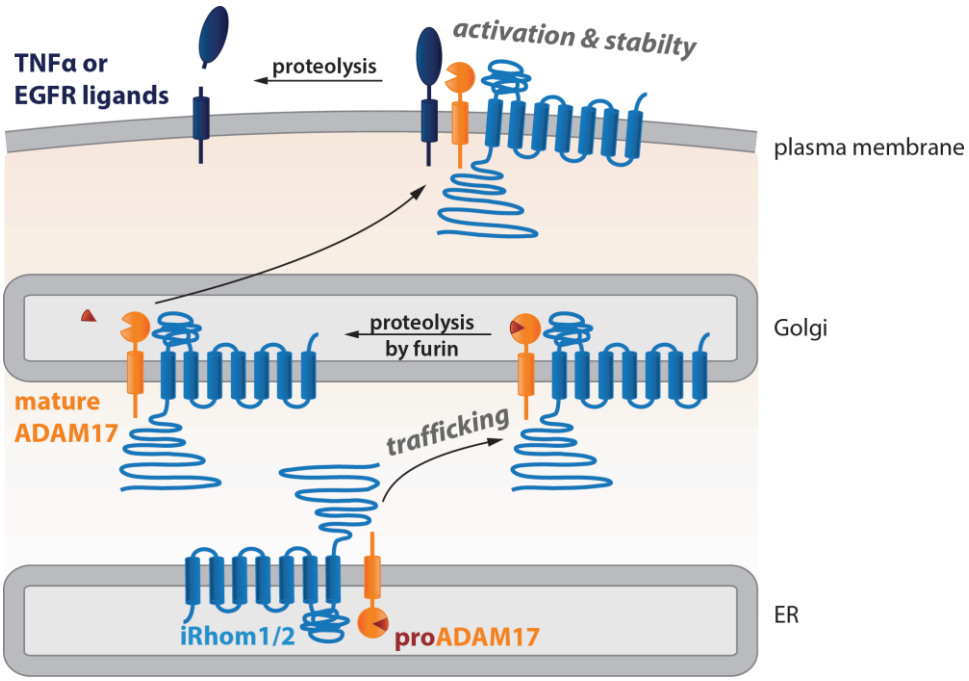


Figure 1.6 | iRhoms regulate ADAM17 activity and consequently the ADAM17-dependent release of EGFR ligands and TNFα. Mammalian iRhoms enable the trafficking of proADAM17 from the ER to the Golgi apparatus (Adrain et al., 2012, McIlwain et al., 2012). At the plasma membrane, iRhom2 controls the stability and stimuli-dependent shedding activity of mature ADAM17 (Grieve et al., 2017).

In summary, iRhom2 was described to exert three distinct functions in the regulation of ADAM17 activity: iRhoms mediate ADAM17 maturation through controlling the ER-to-Golgi trafficking of ADAM17, they maintain ADAM17 stability at the cell surface, and finally

they enable rapid, stimuli-induced ADAM17-dependent shedding (Grieve et al., 2017). Consequently, it was proposed that iRhom2 can be considered as a regulatory subunit of ADAM17 (Grieve et al., 2017). The stoichiometric composition of such an iRhom2-ADAM17 complex has not been investigated, but iRhom1 was reported to form homodimers (Nakagawa et al., 2005) suggesting that iRhom2 might also dimerise.

1.3.3.3 Innate immune response to viral infection

Recently, iRhom2 was linked to another role in innate immunity, as it was shown to regulate the trafficking and the stability of the stimulator of interferon genes (STING) (Luo et al., 2016). STING is a polytopic membrane protein, which is involved in the activation of antiviral type I interferon (IFN) genes upon infection of the cells with DNA viruses (Ishikawa et al., 2009). iRhom2 constitutively binds STING, as well as the STING interactor translocon-associated protein (TRAP) complex subunit beta (TRAPβ) (Luo et al., 2016) (Luo et al., 2016). Upon viral infection iRhom2 enhances the interaction of STING with TRAPβ, thereby facilitating the trafficking of STING to perinuclear vesicles, which is required for the downstream activation of type I IFN genes. Second, and independently of STING trafficking, iRhom2 promotes the interaction of the deubiquitinase EIF3S5 with STING, which enhances the deubiquitination and consequently the stability of STING (Luo et al., 2016).

The modulation of the innate immune response to DNA viruses by iRhom2 was also demonstrated *in vivo*. iRhom2 KO mice died upon infection with herpes simplex virus type 1 (HSV-1), having significantly lower serum levels of type I IFN (Luo et al., 2016).

1.3.4 Physiological function of mammalian iRhoms

Physiological roles of mammalian iRhoms have been demonstrated in mouse models and patients. iRhom2 KO mice are viable and show no obvious defects (Adrain et al., 2012, McIlwain et al., 2012, Siggs et al., 2012, Luo et al., 2016) but exhibit, under closer examination, defects in their innate immune response to viruses and bacteria (McIlwain et

al., 2012, Luo et al., 2016) as well as skin defects (Maruthappu et al., 2017). iRhom2-deficient macrophages are impaired in secreting TNFα after stimulation with LPS (Adrain and Freeman, 2012, McIlwain et al., 2012, Siggs et al., 2012), and iRhom2 KO mice were consequently protected from septic shock but were susceptible to infection with *Listeria monocytogenes* (McIlwain et al., 2012). In addition, iRhom2 KO mice were protected from rheumatoid arthritis in a mouse model (Issuree et al., 2013), leading to the idea that iRhom2 might be an immune cell-specific drug target for TNFα-related inflammatory diseases (Issuree et al., 2013, Lichtenthaler, 2013).

Furthermore, iRhom2 gain-of-function mutations lead to skin and hair follicle defects in mice and humans. Single point mutations in the human iRhom2 N-terminus are linked to tylosis with oesophageal cancer (TOC) (Blaydon et al., 2012, Saarinen et al., 2012), an autosomal dominant disease characterised by thickening of the skin on palms and soles (palmoplantar keratoderma) with a high risk of developing squamous cell carcinoma in the oesophagus. iRhom2 TOC mutations were shown to lead to elevated constitutive ADAM17-dependent shedding (Brooke et al., 2014, Maney et al., 2015). A mouse model of human TOC mutations (*Rhbdf2*$^{P159L/P159L}$) shows a loss of hair coat and enhanced wound healing presumably caused by elevated amphiregulin signalling (Hosur et al., 2017). In addition to the TOC mouse model, two genomic deletions in the *Rhbdf2* locus also causes skin and hair follicle defects: the curly-bare (cub) mutation results in an N-terminally truncated iRhom2 lacking amino acids 1 to 268 (Hosur et al., 2014, Siggs et al., 2014) and the uncovered (uncv) mutation is an in-frame deletion ranging amino acids 118 to 191 (Leilei et al., 2014, Yang et al., 2016), therefore, both deletions have lost the TOC locus. *Rhbdf2*$^{uncv/uncv}$ and *Rhbdf2*$^{cub/cub}$ mice are hairless, whereas *Rhbdf2*$^{-/-}$ mice have a normal hair coat (Hosur et al., 2014, Leilei et al., 2014, Siggs et al., 2014). *Rhbdf2*$^{cub/cub}$ show enhanced wound healing, similar to *Rhbdf2*$^{P159L/P159L}$ mice, as well as accelerated tumourigenesis, both of which might be caused by elevated EGFR signalling (Hosur et al., 2014). In addition to regulating ADAM17-dependent shedding of EGFR ligands in the skin, iRhom2 was also proposed to directly regulate keratin 16 levels, leading to a thinner epidermis on the paws of iRhom2 KO mice (Maruthappu et al., 2017). Taken together,

several independent studies have demonstrated a crucial function of iRhom2 in hair and skin homeostasis in mice and humans.

The physiological role of iRhom1 is controversial because two different *Rhdbf1* KO mouse models showed distinct phenotypes ranging from no obvious defects (Li et al., 2015) to prenatal lethality (Christova et al., 2013). It was speculated that iRhom1 plays a role in the brain (Lichtenthaler et al., 2015) as iRhom1 loss completely eliminated ADAM17 maturation in the brain with the exception of brain-resident macrophages (microglia), in which ADAM17 maturation was entirely dependent on iRhom2 (Li et al., 2015). Supporting the hypothesis for a function for iRhom1 in the brain, one iRhom1 KO mouse model suffered from brain haemorrhages (Christova et al., 2013). However, no other data have been reported yet to further support this hypothesis.

iRhom1 might be involved in different types of cancer as iRhom1 levels were elevated in breast cancer patients and correlated with a poorer survival rate and enhanced disease progression (Zhou et al., 2014). In line with this, knockdown of iRhom1 in head and neck squamous cell cancer and breast cancer cell lines affected EGFR signalling and reduced cell migration and proliferation (Yan et al., 2008, Zou et al., 2009). In addition to its role in ADAM17-dependent EGFR signalling, which might explain the link of iRhom1 to cancer, iRhom1 was suggested to play a role in the cellular response to oxygen deficiency in cancer cells by enhancing the stability of the transcription factor hypoxia-inducible factor 1-alpha (HIF1α) (Zhou et al., 2014).

In summary, mouse models and patient data suggest that iRhom2 is a key regulator in skin biology and innate immunity *in vivo*, whereas iRhom1 has been linked to cancer and might also have a role in the brain.

1.3.5 Regulation of iRhoms

Increasing evidence shows that the expression, stability and function of iRhoms can be regulated, but mechanistic details are still poorly understood.

1.3.5.1 Transcriptional regulation of iRhoms

The importance of tightly regulating iRhom expression is supported by the fact that increased levels of both iRhoms are associated with disease: iRhom1 expression was elevated in breast cancer patients (Yan et al., 2008), and iRhom2 expression was increased in brains of Alzheimer's disease patients (De Jager et al., 2014). Several studies have reported that iRhom expression can be induced by different stimuli: iRhom2 expression was upregulated by LPS (Adrain et al., 2012, McIlwain et al., 2012) and DNA viruses but not by cytokines like TNFα, IL-1β, IFN-β and IFN-γ (Luo et al., 2016). iRhom1 levels were increased by ER stress induced by thapsigargin and tunicamycin (Lee et al., 2015). Together these data suggest that iRhoms are upregulated under different cellular stress conditions, but a complete picture of the transcriptional regulation of iRhoms is missing.

1.3.5.2 Posttranscriptional regulation of iRhoms

iRhom levels and functions are also regulated posttranslationally which occurs at cytosolic N-terminus of iRhoms. The N-terminus of iRhom2, and presumably of iRhom1, is phosphorylated upon stimulation, which results in the rapid, stimulation-dependent activation of ADAM17 activity (Grieve et al., 2017). An iRhom2 mutant lacking essential phosphorylation sites within the iRhom2 N-terminus still supported constitutive ADAM17-dependent shedding but not stimulated shedding, demonstrating that phosphorylation of iRhoms is required for the rapid activation of ADAM17 shedding activity. As described before (1.3.3.2), the mechanistic link between phosphorylation of the iRhom2 N-terminus and its ability to induce ADAM17 shedding activity is mediated through its interaction with 14-3-3 proteins.

Furthermore, the iRhom N-terminus seems to harbour regulatory sites that downregulate iRhom function as demonstrated by different N-terminal iRhom gain-of-function mutations that enhanced ADAM17-dependent shedding (Brooke et al., 2014, Hosur et al., 2014, Maney et al., 2015). Mouse iRhom1$^{\Delta 166}$ and iRhom2$^{\Delta 212}$, as well as the

human iRhom2 TOC mutation I186T resulted in an increase in constitutive ADAM17-dependent shedding (Brooke et al., 2014, Maney et al., 2015). This might mechanistically work by regulating iRhom2 localisation because iRhom2$^{\Delta 212}$ resulted in higher iRhom2 levels at the plasma membrane compared to wild-type iRhom2 (Maney et al., 2015), and the localisation of iRhom2 was altered in tylotic skin (Blaydon et al., 2012). Furthermore, the cub mutation (iRhom2$^{\Delta 268}$) was suggested to be a gain-of-function mutation that increases the constitutive release of amphiregulin (Hosur et al., 2014). However, analysing the release of TNFα upon LPS injection, *Rhbdf2*$^{cub/cub}$ mice resembled *Rhbdf2*$^{-/-}$ mice, suggesting that ADAM17 activity is strongly impaired (Hosur et al., 2014). How secretion of EGFR ligands is increased while TNFα release is impaired in *Rhbdf2*$^{cub/cub}$ mice remains to be shown.

Finally, it was suggested that mutations in the iRhom2 N-terminus affect the stability of iRhom2: exogenous expression of human iRhom2 containing TOC or cub mutations was reported to show increased protein stability compared to overexpressed wild-type iRhom2 presumably by circumventing proteasomal degradation (Hosur et al., 2014). Although mechanistic details and physiological relevance of the proteasomal degradation of iRhoms are unclear, these findings suggest that iRhom2 levels are subject to regulations at a posttranscriptional level.

In summary, the iRhom N-terminus is posttranslationally modified and linked to diseases when mutated. Several studies emphasise the importance of the iRhom2 N-terminus in controlling iRhom function and consequently ADAM17 activity, but mechanistic details are currently poorly understood. In this study, I have identified the iRhom N-terminus as the site of interaction with a novel protein, the FERM domain-containing protein 8 (FRMD8).

1.4 FERM domain-containing protein 8 (FRMD8)

FRMD8 is a poorly studied protein that is conserved from *Drosophila* to human. The only report about the function of FRMD8 describes it as a negative regulator of Wnt signalling in flies, zebrafish and human cells (Kategaya et al., 2009). This study identified FRMD8 in an RNAi screen in *Drosophila* cells aiming to find regulators of the low-density lipoprotein receptor-related protein 6 (LRP6)-mediated Wnt/β-catenin signalling pathway. Loss of FRMD8 led to the hyperactivation of the canonical Wnt signalling pathway as seen in the activation of a β-catenin reporter in *Drosophila* and human cells. In addition, FRMD8 loss phenocopied Wnt overexpression phenotypes in *Drosophila* and zebrafish embryos. Mechanistically, FRMD8 was shown to bind to the Wnt signalling receptor and single-pass membrane protein LRP6 and to weaken its downstream interaction with axin, which is required to activate β-catenin-dependent transcription of downstream genes (Nusse and Clevers, 2017). No further work on FRMD8 and its role in Wnt signalling has been reported.

FRMD8 is expressed in all tissues (The Human Protein Atlas (Uhlen et al., 2015), BioGPS (Wu et al., 2016)) and its expression in the lung correlated with a higher survival rate of lung adenocarcinoma patients (Galvan et al., 2013). FRMD8 belongs to the family of FERM (four-point-one, ezrin, radixin, moesin) domain-containing proteins, which comprises around 50 proteins, such as talin, merlin, ezrin/radixin/moesin, several myosins, kinases, phosphatases, and guanine nucleotide exchange factors (Frame et al., 2010). All family members contain a structurally conserved FERM domain of around 300 amino acids, which mediates protein-protein and protein-lipid interactions (Bosanquet et al., 2014). The FERM domain exhibits a clover leaf-shaped structure consisting of the three subdomains F1, F2 and F3. The F1 domain adopts a ubiquitin-like fold, the F2 subdomain resembles an acyl-CoA binding protein, and the F3 lobe is related to a pleckstrin homology (PH)/phosphotyrosine-binding (PTB) domain (Pearson et al., 2000). FERM-domain containing proteins have diverse cellular functions, many of which involve

linking the plasma membrane proteins to the cytoskeleton and regulating signal transduction (Moleirinho et al., 2013, Bosanquet et al., 2014).

1.5 Aim of this project

iRhoms play an essential role in ADAM17-dependent shedding, but it is still unclear how iRhoms regulate ADAM17 function or how iRhoms are regulated themselves at a molecular level. The aim of this project was to identify novel interaction partners of human iRhoms in a mass spectrometry-based approach and to further characterise these candidates to gain new insight into iRhom function. In the subsequent chapters, I will report the identification of FRMD8 as a novel iRhom1 and iRhom2 interaction partner in a mass spectrometry screen and the impact of FRMD8 on the iRhom-dependent regulation of ADAM17. I will further show the characterisation of FRMD8-deficient cells and FRMD8 KO model organisms to dissect the molecular mechanism of FRMD8 in the iRhom/ADAM17 pathway. I will then finish in chapter 6 with an overview of my conclusions, their implications for future work, and an attempt to integrate my findings with what is known about iRhom regulation of ADAM17.

CHAPTER 2

Materials and methods

2 Materials and methods

2.1 Molecular biology methods

2.1.1 Molecular cloning

2.1.1.1 Polymerase chain reaction (PCR)

DNA fragments were amplified by polymerase chain reaction (PCR) using the Q5 High-Fidelity DNA polymerase (New England Biolabs) in a 96-well thermal cycler (Applied Biosystems) according to the protocol in Table 2.1. Expression constructs consisting of several fragments were annealed by overlap extension PCR (Nelson and Fitch, 2011) following the protocol in Table 2.2. Primers for the PCR reaction were ordered from Invitrogen or Sigma-Aldrich and are listed in Table 2.3.

Table 2.1 | Q5 PCR protocol

PCR mix (25 µl)		**PCR programme**		
5x Q5 reaction buffer (New England Biolabs)	5.00 µl	98°C	1 min	1x
dNTP mix (10 mM) (Bioline)	0.50 µl	98°C	30 s	
Forward primer (25 µM)	0.50 µl	70°C	30 s	35x
Reverse primer (25 µM)	0.50 µl	72°C	1 min / 1kb	
Template DNA (< 1,000 ng/µl)	0.50 µl	72°C	4 min	1x
Q5 High-Fidelity DNA polymerase	0.25 µl	4°C		Hold
water	17.75 µl			

Table 2.2 | Overlap extension PCR protocol

PCR mix (25 µl)		**PCR programme**		
5x Q5 reaction buffer (New England Biolabs)	5.00 µl	98°C	1 min	1x
dNTP mix (10 mM) (Bioline)	0.50 µl	98°C	30 s	
Template DNA 1	0.1 pmol	60°C	1 min	13x
Template DNA 2	0.1 pmol	68°C	1 min / 1kb	
Q5 High-Fidelity DNA polymerase	0.25 µl	72°C	8 min	1x
water	add up to 25 µl	4°C		Hold

Table 2.3 | PCR primers

primer name	sequence (5'- 3')
P1/hiRhom2_NotI fw	AGCACAGTGGCGGCCGCATGGCCTCTGCTGACAAGAATGG
P7/hUnc93b1_NotI fw	AGCACAGTGGCGGCCGCATGGAGGCGGAGCCG
P24/3xHA-hiRhom2 fw	CGCTTCTGCGAGAAGTATGAGCTGGACCAGGTGCTGCACGC ATACCCGTACGACGTCCCT
P25/3xHA-hiRhom2 rev	TGGATAGCCCGCATAGTCAGGGACGTCGTACGGGTATGCGT GCAGCACCTGGTCCAGCT
P26/3xHA_NotI rev	TAGACTCGAGCGGCCGCTTAGCCGGCGTAATCCGGCAC
P32/3xHA-hUNC93B1 fw	TACGAACAGGCGCAGGGGGGAGACGGGCCGGAGGAGCAG GCATACCCGTACGACGTCCCT
P33/3xHA-hUNC93B1 rev	TGGATAGCCCGCATAGTCAGGGACGTCGTACGGGTATGCCT GCTCCTCCGGCCCGTCTCC
P38/hiRhom2_IRHD rev	CATGTAGGAAGAGAGACAGCCAGAGCCTGGTGACGTGCTGG GCAAAGC
P39/hiRhom2_IRHD fw	CGTGGGCTTTGCCCAGCACGTCACCAGGCTCTGGCTGTCTC TCTTCC
P41/hiRhom1_NotI fw	AGCACAGTGGCGGCCGCATGAGTGAGGCCCGCAGGGACA
P42/hiRhom2_N-term 3xHA rev	AGGGACGTCGTACGGGTATGCGGTGACGTGCTGGGCAAAG C
P43/hiRhom2_N-term 3xHA fw	GCTTTGCCCAGCACGTCACCGCATACCCGTACGACGTCCCT
P46/hiRhom2_w/oN-term_NotI fw	AGCACAGTGGCGGCCGCATGCGCCGCAGCATCAGCAGCAC
P47/hiRhom1_w/oN-term_NotI fw	AGCACAGTGGCGGCCGCATGGTGGGACGGCTCACCAAC
P51/hiRhom1_N-term 3xHA rev	AGGGACGTCGTACGGGTATGCCGTCTCATGCTGCGAGAAG
P52/hiRhom1_N-term 3xHA fw	TGGGCTTCTCGCAGCATGAGACGGCATACCCGTACGACGTC CCT
P54/hFRDM8 fw	TACCGAGCTCGGATCCATGGACGGGACAGAAGGCA
P55/hFRDM8_V5 rev	GCCCTCTAGACTCGAGCTACGTAGAATCGAGACCGAGGAGA GGGTTAGGGATAGGCTTACCGCCCTGCTCCAGGCTGTCG
P70/hiRhom1_N-term 3xHA fw	AGCACAGTGGCGGCCGCATGGCATACCCGTACGACGTCC
P71/hiRhom1_N-term 3xHA rev	AGGCTGCTCGTGCTGTCCCTGCGGGCCTCACTGCCGGCGTA ATCCGGCACATC
P72/hiRhom1_N-term fw	TACCCCTATGATGTGCCGGATTACGCCGGCAGTGAGGCCCG CAGGGACA
P73/ hiRhom1_N-term rev	TAGACTCGAGCGGCCGCTTACGTCTCATGCTGCGAGAAGC
P113/hiRhom2Δ100 fw	AGCACAGTGGCGGCCGCATGAGTTCAGAGAAGCGCCCTG
P114/hiRhom2Δ200 fw	AGCACAGTGGCGGCCGCATGGAGATGGACAGGCCCCAC

primer name	sequence (5'- 3')
P115/hiRhom2Δ300 fw	AGCACAGTGGCGGCCGCATGTCCATGCCTGATGATGTCT
P116/hiRhom2Δ270 fw	AGCACAGTGGCGGCCGCATGAGCTTTGCCTTCCCGAGCT
P117/hiRhom2Δ330 fw	AGCACAGTGGCGGCCGCATGGGGGTGCAAATCCCTCTGA
P122/hiRhom2Δ242 fw	AGCACAGTGGCGGCCGCATGAGCTTGCAAGCTGCC
P142/hFRDM8ΔC_V5 rev	GCCCTCTAGACTCGAGCTACGTAGAATCGAGACCGAGGAGA GGGTTAGGGATAGGCTTACCGGGGCCTGCGGGCTCCGCC
P157/pcDNA3.1 Bili fw	TACCGAGCTCGGATCC ATGGAGCCAAATCATTATTAC
P177/pcDNA3.1 Bili-HA rev	GCCCTCTAGACTCGAGCTAAGCGTAATCTGGAACATCGTATG GGTA ATAGCTTATAGATAATGATC
P233/5'HA fw	GGGAGACCCAAGCTGGCTAGCGTTTAAACTTATGAGAGGGA ACAGTGATGCTCTTG
P234/5' HA rev	AGTGACACCAGGATGAGTGCCCGCTTGCGGTACTTGTCGCT GGTGCCGAAGGTGATGTAGG
P235/3'HA fw	CTGGGGCGTGAGGCCTGTGAGATCCTGACCCAAGCTCAGG CACACCCAAGGCACCTGC
P236/3'HA rev	AGTCGAGGCTGATCAGCGGGTTTAAACGGGCCCTCTAGACC CAGTTTCATGCTACCTGAGGTC

All expression constructs generated during this project are listed in Table 2.4. Other plasmids used in this project are listed in Table 2.5.

Table 2.4 | Generated expression constructs. Primer sequences are listed in Table 2.3. #construct cloned by Yao Meng.

generated construct	PCR template(s)	primer pair(s)	target vector
human iRhom2^{WT}-3xHA	iRhom2 isoform 1 cDNA (NM_024599; OriGene clone SC122961); human iRhom1^{WT}-3xHA	P1 + P25; P24 + P26	pLEX.puro (NotI)
human UNC93B1-3xHA	UNC93B1 cDNA (BC025669.1; GI:19343917); human iRhom1^{WT}-3xHA	P7 + P33; P32 + P26	pLEX.puro (NotI)
human iRhom2$^{\Delta 100}$-3xHA	human iRhom2^{WT}-3xHA	P113 + P26	pLEX.puro (NotI)
human iRhom2$^{\Delta 200}$-3xHA	human iRhom2^{WT}-3xHA	P114 + P26	pLEX.puro (NotI)
human iRhom2$^{\Delta 242}$-3xHA	human iRhom2^{WT}-3xHA	P122 + P26	pLEX.puro (NotI)
human iRhom2$^{\Delta 270}$-3xHA	human iRhom2^{WT}-3xHA	P116 + P26	pLEX.puro (NotI)

generated construct	PCR template(s)	primer pair(s)	target vector
human iRhom2$^{\Delta 300}$-3xHA	human iRhom2^{WT}-3xHA	P115 + P26	pLEX.puro (NotI)
human iRhom2$^{\Delta 330}$-3xHA	human iRhom2^{WT}-3xHA	P117 + P26	pLEX.puro (NotI)
human iRhom2$^{\Delta 382}$-3xHA	human iRhom2^{WT}-3xHA	P46 + P26	pLEX.puro (NotI)
human iRhom2$^{\Delta IRHD}$-3xHA	human iRhom2^{WT}-3xHA	P1 + P38; P39 + P26	pLEX.puro (NotI)
human iRhom2$^{1-440}$-3xHA	human iRhom2^{WT}-3xHA	P1 + P42; P43 + P26	pLEX.puro (NotI)
human iRhom1$^{\Delta 374}$-3xHA	human iRhom1^{WT}-3xHA	P47 + P26	pLEX.puro (NotI)
human iRhom1$^{1-437}$-3xHA	human iRhom1^{WT}-3xHA	P41 + P51; P52 + P26	pLEX.puro (NotI)
human 3xHA-iRhom1$^{1-437}$	human iRhom1^{WT}-3xHA	P70 + P71; P72 + P73	pLEX.puro (NotI)
human FRMD8-V5	human FRMD8 cDNA (NM_031904; OriGene clone SC107202)	P54 + P55	pcDNA3.1(+) (BamHI, XhoI)
human FRMD8$^{\Delta C}$-V5	human FRMD8-V5	P54 + P142	pcDNA3.1(+) (BamHI, XhoI)
Drosophila Bili-HA	*Drosophila* Bili cDNA (GH28553 from DGRC)	P157 + P177	pcDNA3.1(+) (BamHI, XhoI)
human iRhom2 homology construct$^{\#}$	gDNA isolated from HEK293T cells; 3xHA tag gBlock (Integrated DNA Technologies)	P233 + P234; P235 + P236	pcDNA3.1(+) (HindIII, XhoI)

Table 2.5 | Other plasmids used

construct	vector	source
human iRhom1^{WT}-3xHA	pLEX.puro	Colin Adrain
mouse iRhom2^{WT}-3xHA	pM6P.blast	Adam Grieve (Siggs et al., 2014)
human iRhom2^{cub}-3xHA	pM6P.blast	Adam Grieve (Siggs et al., 2014)
Drosophila iRhom-3xFlag	pEGFP-N1 w/o eGFP	Markus Zettl (Zettl et al., 2011)
lentiviral packaging plasmid	pCMV-delta8.91	Colin Adrain (Adrain et al., 2011)
lentiviral envelope plasmid	pMD-VSV-G	Colin Adrain (Adrain et al., 2011)

2.1.1.2 Agarose gel electrophoresis and gel purification

PCR products and digested plasmids were analysed on a 1% agarose gel supplemented with SYBR safe (1:10,000 dilution; Invitrogen) in 1x Tris-Borate-EDTA (TBE) buffer (Sigma-Aldrich). DNA bands were excised with a scalpel and purified using a gel purification kit (Macherey-Nagel) according to the manufacturer's instructions.

2.1.1.3 Restriction Digest

Plasmid DNA was incubated with restriction endonucleases to at 37°C for 2 h to 16 h (Table 2.6). For a digest with two restriction enzymes the reaction buffer was selected according to the manufacturer's instructions. After the restriction digest, DNA fragments were separated on a 1% agarose gel and the vector was excised and purified as described above (2.1.1.2).

Table 2.6 | Restriction digest protocol

restriction digest (20 µl)	
10x Reaction Buffer (New England Biolabs)	2 µl
Restriction enzyme(s) (New England Biolabs)	1 µl each
Vector DNA	2-3 µg
Water	add up to 20 µl

2.1.1.4 DNA assembly

Purified PCR products were either ligated with the vector DNA using Gibson Assembly (Gibson et al., 2009). This DNA assembly methods requires a homology of at least 15 bp between the DNA fragments to be assembled, which was introduced by using overhanging primers during PCR (see Table 2.4). Gel-purified PCR products and vector fragments were incubated with Gibson Assembly Master Mix (New England Biolabs) according to the protocol in Table 2.7 for 15-60 min.

Table 2.7 | Gibson assembly

Gibson assembly (up to 20 µl)	
2x Gibson Assembly Master Mix (New England Biolabs)	up to 10 µl
PCR product	50 - 200 ng
Vector DNA	50 ng

2.1.1.5 Transformation

Assembled plasmid DNA was transformed into competent *E. coli* (strain DH5α, New England Biolabs). 2 µl of the ligated vector was added to 30 µl competent bacteria, which were then incubated for 15 min on ice. Bacteria were heat shocked at 42°C for 1 min and afterwards placed back on ice. 0.25 ml LB medium was added and the bacteria suspension was incubated for at least 20 min at 37°C. Bacteria were plated on LB agar plates supplemented with 100 µg/ml ampicillin or 30 µg/ml kanamycin and incubated overnight at 37°C.

2.1.1.6 Plasmid preparation

For small-scale plasmid preparation 6 ml LB supplemented with the corresponding antibiotics were inoculated with bacteria transformed with the plasmid of interest. Bacteria were grown in a shaker overnight at 37°C and 180 rpm. The overnight cultures were pelleted by centrifugation (2500 g, 10 min, 4°C), and DNA was isolated from bacteria using the QIAprep Spin Miniprep kit (Qiagen) according the manufacturer's manual.

For large-scale plasmid preparation bacteria from 200 ml overnight cultures were centrifuged for 10 min at 2,500 g at 4°C. DNA was isolated from bacteria pellets using a Plasmid Midi kit (Qiagen) following the manufacturer's instructions.

2.1.1.7 Sequencing

Generated DNA constructs were sequenced using the Sanger Sequencing Service from Source BioScience, Nottingham. Sequencing primers provided by the sequencing company, as well as self-designed primers were used (Table 2.8).

Table 2.8 | Sequencing primers

primer name	sequence (5'- 3')	target
designed primers		
P3/hiRhom2_int fw	GGTGTGTACGAGAGCGTG	human iRhom2 cDNA
P4/hiRhom2_int rev	CCAAAGTCTCCGAGCAGTC	human iRhom2 cDNA
P5/pLEX-MCS fw	CACCAAAATCAACGGGACTT	pLEX.puro
P5/pLEX-MCS rev	ATATAGACAAACGCACACCGGCCT	pLEX.puro
P48/hiRhom2_int2 fw	ACGCCGCAAGAGAATGTCT	human iRhom2 cDNA
P49/hiRhom1_int fw	AGGTGCACAGCTTCATTC	human iRhom1 cDNA
P50/hiRhom1_int rev	AGCCAAACTGTCTCTTGTG	human iRhom1 cDNA
P53/hiRhom1_int2 fw	TGGCCAAGATGAGCTTC	human iRhom1 cDNA
P84/Bili fw	GCAGCAAGAATACTGCCAACG	Drosophila Bili cDNA
P85/Bili rev	ATGTTGGTGCTGATGCGGCT	Drosophila Bili cDNA
P112/Bili_int fw	TCACAAGTGCAACAATGGG	Drosophila Bili cDNA
P180/FRMD8_exon 6 fw	TGCAGATCCATGACGAGGA	human FRMD8 gDNA/cDNA
P181/FRMD8_exon 6 rev	AACAACTGCCTAGGGCCA	human FRMD8 gDNA
P182/FRMD8_exon 7 fw	GCCAGAGTCTCTTTGCTG	human FRMD8 gDNA/cDNA
P183/FRMD8_exon 7 rev	GTGCTCGTGACAAGACAC	human FRMD8 gDNA
P239/hiRhom2 endog. 3xHA rev	CGTAATCCGGCACATCATAG	3xHA tag
P240/hiRhom2 endog. fw	CTGCTGCTCCTATTCCAC	human iRhom2 gDNA
P241/hiRhom2 endog. rev	CTGGCCCAACTAATTCCC	human iRhom2 gDNA
primers provided by Source BioScience		
CMVF_pCDNA3	CAACGGGACTTTCCAAAATG	pcDNA3.1(+)
BGH Reverse	TAGAAGGCACAGTCGAGG	pcDNA3.1(+)
primers received from Andrew Bassett, Genome Engineering Oxford		
dBiliHRMF	CACTGCAGTATAATCGAAAA	Drosophila Bili gDNA
dBiliHRMR	TAGTAATCATCGCGACACTTC	Drosophila Bili gDNA

2.1.2 mRNA isolation and quantitative PCR

RNA was isolated from mammalian cells using the RNeasy kit (Qiagen) according to the manufacturer's instructions. RNA concentration was determined using a Nanodrop spectrophotometer (Thermo Fisher Scientific) and equal amounts of RNA were reverse transcribed using the SuperScript VILO cDNA synthesis kit (Invitrogen) according to Table 2.9. cDNA was diluted 1:10 in ultrapure water and used for quantitative PCR (qPCR) using the TaqMan Gene Expression Master Mix (Applied Biosystems) following the protocol in Table 2.10. qPCR was performed in Fast Optical 96-Well Reaction plates (Applied Biosystems) on a StepOnePlus system (Applied Biosystems) using the standard settings (Table 2.10). TaqMan probes used for qPCR are listed in Table 2.11. Gene expression was normalized to β-actin (*ACTB*) expression and analysed with the StepOne software (Applied Biosystems).

Table 2.9 | Reverse transcription

reverse transcription (10 µl)	
SuperScript VILO master mix	2 µl
RNA	up to 2.5 µg
RNase-free water	add to 10 µl

Table 2.10 | qPCR protocol

TaqMan PCR mix (10 µl)		**PCR programme (standard settings)**		
TaqMan Gene Expression Master Mix	5.00 µl	95°C	20 s	1x
TaqMan probe	0.50 µl	95°C	20 s	1x
cDNA	1.50 µl	95°C	1 s	40x
water	3.00 µl	60°C	20 s	

Table 2.11 | TaqMan probes for qPCR

target gene	product number	company
Human *ACTB*	Hs99999903_m1	Thermo Fisher Scientific
Human *ADAM17*	Hs01041915_m1	Thermo Fisher Scientific
Human *FRMD8*	Hs00607699_mH	Thermo Fisher Scientific
Human *RHBDF1*	Hs01102745_m1	Thermo Fisher Scientific
Human *RHBDF2*	Hs00226277_m1	Thermo Fisher Scientific
Human *TNF*	Hs00174128_m1	Thermo Fisher Scientific
Drosophila *act42A*	Dm02362162_s1	Thermo Fisher Scientific
Drosophila *bili*	Dm02144595_g1	Thermo Fisher Scientific

2.1.3 Isolation of genomic DNA

Cells were pelleted at 2,500 g for 5 min, resuspended in DNA extraction buffer (10 mM Tris-HCl (pH 8.0), 1 mM EDTA, 25 mM NaCl, 200 µg/ml proteinase K (Thermo Scientific; added freshly)), and incubated at 65°C for 30 min. Proteinase K was inactivated by incubating the sample at 95°C for 2 min. The isolated genomic DNA (gDNA) was then used as a template for PCR.

2.1.4 CRISPR/Cas9 constructs

The CRISPR/Cas9 technology is a simple, two-component systems that enables targeted genome editing in many organisms (Jinek et al., 2012, Doudna and Charpentier, 2014). In brief, the wild-type Cas9 endonuclease from *Streptococcus pyogenes* is directed to a specific genomic locus by a specific single-guide RNA (sgRNA), where it then introduces a double strand break, which is repaired by the error-prone non-homologous end joining (NHEJ), often creating insertions and deletions, or by homologous recombination. The recognition of the genomic target sequence by the sgRNA/Cas9 complex requires the base pairing of an approximately 20-nt long sgRNA with the genomic DNA, as well as the presence of 3-nt long protospacer adjacent motif (PAM) 5’ of the target sequence in the DNA. Target sequences in the genome can be identified using bioinformatic tools (e.g. www.sanger.ac.uk/htgt/wge).

For the generation of KO and knock-in cell lines in this project, wild-type *S. pyogenes* Cas9 endonuclease and the sgRNA were expressed from one vector. The sgRNA design and cloning was conducted by the Genome Engineering Facility at the University of Oxford. The sequence and target regions of sgRNAs used are listed in Table 2.12.

To endogenously 3xHA-tag human iRhom2, a 3xHA tag was knocked into the *RHBDF2* locus by repairing the Cas9-introduced double-strand break by homologous recombination. For this purpose, a homology construct consisting of a 3xHA tag flanked by two homology arms of approximately 800 bp was cloned as described before (2.1.1). Homology arms 3' and 5' of the 3xHA tag were amplified from gDNA isolated from HEK293T cells by PCR and all fragments were assembled into pcDNA3.1(+) (Table 2.4).

Table 2.12 | CRISPR/Cas9 plasmids

target gene	**sgRNA target site with PAM (5'-3')**	**plasmid backbone**	**selection**
Human *FRMD8* – exon 6	TTGGGCCCTACCAGCCCGGCCGG	pSpCas9(BB)-2A-Puro (pX459)	Puromycin
Human *FRMD8* – exon 7	CCACGAGCTGCCGTTTTATGGGT	pSpCas9(BB)-2A-Puro (pX459)	Puromycin
Human *RHBDF2* – exon 19	CCCAGCGGTCAGTGCAGCACCT	epX459(1.1)[#]	Puromycin
Human *RHBDF2* – exon 19	CAGCGGTCAGTGCAGCACCTGG	epX459(1.1) [#]	Puromycin
Drosophila *bili* – exon 4	GCATTTATATTACAACACTACGG	pCFD3 (Addgene plasmid 49410)	---

[#] generated by Joey Riepsaame based on pX459 V2.0 and eSpCas9(1.1)

2.2 Cell biology methods

2.2.1 Mammalian cell lines

2.2.1.1 Cell lines and culture

Human embryonic kidney (HEK) 293T cells were cultured in DMEM (Sigma-Aldrich) supplemented with 10% fetal calf serum (FCS), 100 U/ml penicillin and 100 µg/ml streptomycin (all Gibco) at 37°C in a humidified incubator with 5% CO_2. Cells were split twice a week using trypsinisation (TrypLE Select, Gibco).

Table 2.13 | Cell lines used and generated. Plasmids used for the generation of the cell lines are listed in Tables 2.4 and 2.12.

cell line	strategy and details	source
HEK293T + human iRhom1^{WT}	lentiviral transduction	Freeman lab
HEK293T + human iRhom2^{WT}	lentiviral transduction	generated in this project
HEK293T + human iRhom2$^{\Delta IRHD}$	lentiviral transduction	generated in this project
HEK293T + human iRhom2$^{\Delta 382}$	lentiviral transduction	generated in this project
HEK293T FRMD8 KO, clone 1-2	CRISPR/Cas9; *FRMD8* targeted in exon 7	generated in this project
HEK293T FRMD8 KO, clone 3-1	CRISPR/Cas9; *FRMD8* targeted in exon 6	generated in this project
HEK293T FRMD8 KO, clone 1-2 + human iRhom2^{WT}	CRISPR/Cas9; *FRMD8* targeted in exon 7	generated in this project
HEK293T endogenous iRhom2-3xHA, clone A8	CRISPR/Cas9; *RHBDF2* endogenously 3xHA-tagged before stop codon in exon 19	generated by Yao Meng

2.2.1.2 DNA transfection

For transient transfections cells were seeded 4 h to 24 h before transfection in cell culture plates or dishes. HEK293T cells were transfected with the nonliposomal transfection reagent FuGENE HD (Promega). FuGENE HD was added to OptiMEM (Gibco) and incubated for 5 min at room temperature before it was added to a second tube containing DNA in OptiMEM. The volumes of the transfection mix used for different

plate sizes are indicated in Table 2.14. The transfection mix was incubated for 15-20 min at room temperature and added to the cells.

Table 2.14 | Transfection mix

plate size	FuGENE HD	DNA	total volume of the transfection mix
10 cm	10 -15 µl	1-3 µg	1,000 µl
6-well	4 µl	0.7 - 1.2 µg	500 µl
12-well	2 µl	0.5 - 0.8 µg	200 µl
24-well	0.75 µl	0.03 µg	50 µl

2.2.1.3 siRNA transfection

For knockdown experiments, cells were seeded a day before transfection to reach about 50% confluency on the day of transfection. Cells were transfected with siRNA using Lipofectamine RNAiMax (Thermo Fisher Scientific) according to the manufacturer's protocol: per 6-well 5 µl Lipofectamine RNAiMax were mixed with 250 µl OptiMEM and added to 5 µl smart pool siRNA (10 µM) or 5 µl of each single siRNA (10 µM) (Table 2.15) diluted in 250 µl OptiMEM. The reaction mix was incubated for 15-20 min at room temperature before adding to cells. Protein expression was analysed 72 h after transfection using western blot or qPCR.

Table 2.15 | siRNA for knockdown

target	siRNA sequence and manufacturer
human *FRMD8*	siGENOME SMARTpool for human FRMD8 (Dharmacon; M-018955-01-0010): GCCACGAGCUGCCGUUUUA; UGGUAUACCUAGCGGAUGA; GCACGUCAUCGAUAGCAGA; GGUGGGCGCAAGCCAGUUU
human *RHBDF2*	Stealth siRNAs (Thermo Fisher Scientific): AACCCAGAAGUUCUCCUGCUGGAUG (HSS128594); UACUCCUUCAGAGGGAUUUGCACCC (HSS128595)
non-targeting control	non-targeting siGENOME control pool (Dharmacon; D-001206-13-50): UAGCGACUAAACACAUCAA; UAAGGCUAUGAAGAGAUAC; AUGUAUUGGCCUGUAUUAG; AUGAACGUGAAUUGCUCAA

2.2.1.4 Lentiviral transduction

HEK293T stable cell lines were generated by lentiviral transduction with the pLEX.puro vector. HEK293T cells were transfected with 1 µg pLEX.puro plasmid, 0.7 µg packaging plasmid (pCMV-delta8.91) and 0.3 µg envelope plasmid (pMD-VSV-G; Table 2.5) using FuGENE HD (see 2.2.1.2). The transfection medium was exchanged 5 h to 16 h after transfection for fresh medium. The medium was collected 48 h later and filtered through a 45-µm filter (Sartorius). 70% confluent HEK293T cells growing in a 6-well plate were transduced with the filtered medium supplemented with 10 µg/ml polybrene (Millipore). Fresh medium was added to the virus-producing HEK293T cells and 24 h later the supernatant was collected for a second round of transduction. 48 h after the second transduction, cells were selected in DMEM medium supplemented with 2.5 µg/ml puromycin (Gibco) for at least 48 h.

2.2.1.5 CRISPR/Cas9 genome editing in HEK293T cells

To generate FRMD8 KO cell lines, HEK293T cells were transfected with 1 µg of one Cas9/sgRNA plasmid (Table 2.12) per 6-well. HEK293T cells were selected with 2 µg/ml puromycin 48 h after transfection to eliminate non-transfected cells. After 48 h of selection, cells were seeded at low density in a 15-cm culture dish to select single colonies for the generation of clonal cell lines. The cell lines were analysed for FRMD8 expression by western blot and qPCR.

For knock-in cell lines, HEK293T cells were treated with 200 ng/ml nocodazole (Sigma-Aldrich) for 17 h and then transfected with 0.5 µg of one Cas9/sgRNA plasmid (Table 2.12) and 0.5 µg homology plasmid (Table 2.4) per 6-well. 2 days after transfection HEK293T cells were selected with 2 µg/ml puromycin for 48 h and then seeded into 15-cm culture dish for the selection of single clones. Selected clones were grown in 96-well plates and screened for the presence of the inserted 3xHA tag by PCR using primers P239-241 (Table 2.8) according to the protocol in Table 2.1. Positive clones were further analysed by western blot.

2.2.2 Human stem cell culture

2.2.2.1 Culture of human induced pluripotent stem cells (iPSCs)

The human induced pluripotent stem cell (iPSC) lines AH017-13 were derived from skin biopsies of healthy donors in the James Martin Stem Cell Facility at the University of Oxford according to standardised protocols as published previously (Fernandes et al., 2016). Donors had given signed informed consent for the derivation of human iPSC lines from skin biopsies (Ethics Committee: National Health Service, Health Research Authority, NRES Committee South Central, Berkshire, UK (REC 10/H0505/71)).

AH017-13 iPSCs were cultured in feeder layer-free conditions in mTeSR1 (STEMCELL Technologies) in Geltrex (Thermo Fisher Scientific)-coated wells. Culture medium was changed every day to prevent the differentiation of iPSCs. Cells were passaged with TrypLE Express (Gibco) and plated in media containing 10 µmol/l Rho kinase inhibitor Y-27632 (Abcam).

2.2.2.2 CRISPR/Cas9 genome editing in iPSCs

FRMD8 KO iPSC lines were generated by targeting exon 7 of the *FRMD8* gene as described before (2.1.4). AH017-13 iPSCs were transfected with the Cas9/sgRNA plasmid by electroporation using the Neon Transfection System (Invitrogen). $3 \cdot 10^6$ AH017-13 iPSCs were electroporated (1,400 mV, 20 ms, 1 pulse) in a 100 µl tip (Invitrogen) with 15 µg pX459-FRMD8-exon7 plasmid (Table 2.12) of endotoxin-free DNA quality. After electroporation, iPSCs were plated at a density of $4 \cdot 10^5$ cells/cm^2 into Geltrex-coated 24-well plates and selected 48 h after transfection with 0.25 µg/ml puromycin. After 2 days of selection, surviving cells were plated on a feeder-layer of $4 \cdot 10^6$ irradiated mouse embryonic fibroblasts (MEFs) in 0.1% gelatin-coated 10-cm culture dishes and cultured in hES medium (KnockOut DMEM, 20% KnockOut serum replacement, 2 mM L-Glutamine, 100 µM nonessential amino acids, 50 µM 2-mercaptoethanol (all Gibco) and 10 ng/mL human basic fibroblastic growth factor (R&D)). Colonies of iPSCs were manually selected and grown on Geltrex in mTeSR1. Clones were analysed by western blot using the anti-

FRMD8 antibody. Potential FRMD8 KO clones were further analysed by PCR followed by Sanger sequencing. gDNA was isolated from iPSCs as described above (2.1.3) and PCR was performed to Table 2.1 using primers P180 and P183 (Table 2.8). The PCR product was purified (2.1.1.2) and sequenced using the primer P182 (Table 2.8).

2.2.2.3 Differentiation of iPSCs into macrophages

AH017-13 wild-type and FRMD8 KO clones were analysed for single nucleotide polymorphism (SNP) at the Wellcome Trust Centre for Human Genetics at the University of Oxford to confirm normal karyotypes before differentiation into macrophages.

iPSCs were differentiated into embryoid bodies (EBs) by mechanically dissociation and differentiated into macrophages as described previously (van Wilgenburg et al., 2013). Briefly, iPSCs were grown on a feeder layer of MEFs in hES medium. A dense 6-well of iPSCs was scored into 10x10 sections using a plastic pipette tip. The resulting 100 patches were lifted with a cell scraper and cell clumps were transferred into a 6-well ultra-low adherence plate (Corning) containing EB formation medium (hES medium supplemented with 50ng/ml human bone morphogenetic protein 4 (Invitrogen), 50ng/ml human vascular endothelial growth factor (PeproTech) and 20 ng/ml human stem cell factor (Miltenyi Biotec)) to form EBs. A 50% medium change was performed every second day. EBs were harvested on day 5. Approximately 60 to 80 EBs were transferred into a T75 flask containing factory medium (X-VIVO 15 (Lonza) supplemented with 2 mM L-glutamine, 50 µM 2-mercaptoethanol, 100 ng/ml human macrophage colony-stimulating factor (M-CSF) and 25 ng/ml interleukin 3 (IL-3), 100 U/ml penicillin and 100 µg/ml streptomycin (all Gibco)). The EBs were fed weekly with fresh factory medium. After approximately 2 weeks EBs started to produce non-adherent, premature macrophages, which were harvested from the supernatant of EB cultures through a 40-µm cell strainer (BD Bioscience). About $1 \cdot 10^5$ cells were seeded per cm^2 growth area and differentiated into mature, adherent macrophages for 7 days in macrophage medium (X-VIVO 15

supplemented with 2 mM L-glutamine, 100 ng/ml M-CSF, 100 U/ml penicillin and 100 µg/ml streptomycin) with a 50% medium change on day 4.

2.2.2.4 TNFα ELISA

iPSC-derived macrophages harvested from EB cultures were counted (Moxi Z, Orflo Technologies) and seeded at a density of 25,000 cells per well into 96-well tissue culture plates. After 7 days of differentiation into mature macrophages in macrophage differentiation medium (2.2.2.3), macrophages were analysed for TNFα secretion. The medium was changed for fresh macrophage differentiation medium supplement with 50 ng/ml LPS (Sigma-Aldrich) and with 2 µM GW280264X (GW) or 2 µM GI254023X (GI) (synthesized by Iris Biotech, Marktredwitz, Germany)) where indicated. Cell culture supernatants were collected after 4 h of stimulation and analysed by TNFα ELISA (eBioscience, 88-7346-86) according to the manufacturer's instructions.

Macrophages were lysed in Triton X-100 lysis buffer and protein concentration was determined using a bicinchoninic acid (BCA) assay (Thermo Scientific) as described in 2.3.3. The release of TNFα was normalised to the cell lysate concentration to adjust for potential differences in cell numbers. Each experiment was performed in biological triplicates. Three independent experiments were analysed using an unpaired, non-parametric test (Mann-Whitney test).

2.3 Biochemical methods

2.3.1 Interactome studies using mass spectrometry

2.3.1.1 Cross-linking

Five confluent 150 mm dishes of HEK293T cells were put on ice and washed with ice-cold phosphate-buffered saline (PBS) and proteins were cross-linked *in vivo* using 1 mg/ml dithiobis(succinimidyl propionate) (DSP) (Thermo Scientific). DSP was freshly dissolved in dimethyl sulfoxide (DMSO) at a concentration of 10 mg/ml and then diluted to 1 mg/ml in PBS, which was added to the cells on ice for 45 min. 100 mM Tris-HCl (pH 8.0) was added to the cells to inactivate the crosslinker. Before lysis cells were washes with 50 mM Tris-HCl (pH 8.0) on ice for 5-10 min.

2.3.1.2 Cell lysis and co-immunoprecipitation

Cells were lysed in DDM RIPA lysis buffer (1% n-dodecyl β-D-maltoside (DDM), 150 mM NaCl, 50 mM Tris-HCl (pH 7.5), 0.1% SDS, 0.5% sodium deoxycholate) supplemented with EDTA-free protease inhibitor mix (Roche) and 10 mM 1,10-Phenanthroline (Sigma-Aldrich) for 20 min on ice. Other lysis buffers tested contained the same buffer composition but 1% CHAPS, 1% Triton X-100, or 1% Tergitol-type NP-40 instead of DDM. Cell lysates were centrifuged (20,000 g, 10 min, 4°C) and the post-nuclear supernatant was pre-cleared by incubation with mouse IgG (Sigma-Aldrich) for 1 h at 4°C. The supernatant was added to magnetic anti-HA beads (Thermo Scientific) and incubated for 1 h at 4°C. Beads were washed four times with DDM RIPA wash buffer (1% DDM, 300 mM NaCl, 50 mM Tris-HCl (pH 7.5), 0.1% SDS, 0.5% sodium deoxycholate) and once with PBS. Bound proteins were eluted by incubation with 1 mg/ml HA peptide (Roche; dissolved in 20 mM Tris (pH 7.5), 100 mM NaCl) for 15 min at 37°C. This step was repeated twice, the eluates were pooled and concentrated with a vivaspin concentrator 500 (10,000 kDa MWCO; Sartorius). The spin filter was washed five times with PBS while centrifuging at 12,000 g at room temperature.

2.3.1.3 Sample preparation

Proteins samples were prepared for analysis by mass spectrometry using filter-aided sample preparation as described in (Wisniewski et al., 2009). Briefly, proteins were denatured on the vivaspin filter with 8 M urea at room temperature for 1 h (or at 4°C overnight), then reduced in 8 M urea supplemented with 10 mM DTT for 1 h at room temperature. The filter was cleared from urea by centrifugation (12,000 g at room temperature) and proteins were then acetylated by incubation with 2 mg/ml iodoacetamide at room temperature for 1 h (in the dark). The filter was cleared and then washed twice with 25 mM ammonium bicarbonate (NH_4HCO_3). After this step, the collection tube was changed for a fresh tube and proteins were digested in 1 µg trypsin (Promega; diluted in 25 mM NH_4HCO_3) overnight at 37 ˚C with gentile agitation. Peptides were eluted from the filter with 0.1% formic acid, 0.1% formic acid in 50% acetonitrile (ACN) and finally with 0.1% formic acid in 80% ACN. The eluate was concentrated and peptides were loaded on C18 spin columns (Thermo Scientific) to remove salt. Peptides were eluted with 0.1% formic acid in 50% ACN and with 0.1% formic acid in 80% ACN and concentrated.

2.3.1.4 Mass spectrometry data analysis

Peptides were resolved in 0.1% trifluoroacetic acid in 5% ACN and separated by nano-flow reversed-phase liquid chromatography coupled to Q Exactive Hybrid Quadrupole-Orbitrap mass spectrometer (Thermo Scientific). Data was analysed using the SINQ analysis of the central proteomics facility Oxford (Trudgian et al., 2011).

For statistical analysis, the raw data files generated were processed using the MaxQuant (version 1.5.0.35) software, integrated with the Andromeda search engine as described previously (Cox et al., 2011, Cox and Mann, 2008). The MS/MS spectra were searched against the human proteome (UniProt, 2013/04/03), precursor mass tolerance was set to 20 ppm, variable modifications defined as acetylation (protein N-terminus), C_3H_4OS (on L and N-terminus), phosphorylation (on S, T and Y), and oxidation (on M). Carbamidomethylation (on C) was defined as a fixed modification. Enzyme specificity was

set to trypsin with a maximum of 2 missed cleavages and protein and peptide spectral matches (PSM) false discovery rate (FDR) was set at 0.01.

Differential protein abundance analysis was performed on three biological replicates using the Perseus (version 1.5.5.3) by Dr Monika Stegmann from the central proteomics facility Oxford. Log_2-transformed protein intensity distributions were analysed using a two-tailed t-test to assess the statistical significance of protein abundance fold-changes. P-values were adjusted for multiple hypothesis testing with the Benjamini-Hochberg correction (Hochberg and Benjamini, 1990). Log_{10}-transformed p-values and log_2-transformed differences between the means of protein intensities were plotted. Proteins with less than 3 unique peptides were manually filtered out.

2.3.2 Cell lysis

Cells were harvested on ice and washed once with ice-cold PBS before they were lysed in Triton X-100 lysis buffer (1% Triton X-100, 150 mM NaCl, 50 mM Tris-HCl (pH 7.5)) supplemented with EDTA-free protease inhibitor mix and 10 mM 1,10-Phenanthroline for 15 min. Cell debris were pelleted by centrifugation at 20,000 g at 4°C for 10 min.

2.3.3 Bicinchoninic acid (BCA) assay

A BCA assay kit (Thermo Scientific) was used to determine protein concentrations of cell lysates. 10 µl diluted protein lysates were mixed with 200 µl working reagent (BCA reagent A and B mixed 1:50) in a 96-well plate according to the manufacturer's instructions. Serial dilutions of BSA (2 mg/ml; Thermo Scientific) were measured as standards in parallel. After an incubation of 30 min at 37°C, the absorbance of cell lysates and BSA standards was measured at 562 nm with a plate reader (SpectraMax M3, Molecular Devices).

2.3.4 Co-immunoprecipitation

Lysates were added to anti-HA magnetic beads (Thermo Scientific), anti-V5 magnetic beads (MBL International) or magnetic Flag M2 beads (Sigma-Aldrich), that had been washed once in Triton X-100 lysis buffer. Beads were incubated with the lysate at 4°C for 1 h with over-head rotation and then washed three times with Triton X-100 wash buffer (1% Triton X-100, 300 mM NaCl, 50 mM Tris-HCl (pH 7.5)). Proteins were eluted in 2x LDS buffer (Invitrogen) supplemented with 50 mM DTT for 10 min at 65°C.

2.3.5 Concanavalin A enrichment

To enrich for N-glycosylated proteins, cells lysates were incubated with concanavalin A sepharose (Sigma-Aldrich) at 4°C for 3 h with over-head rotation. Beads were pelleted (2,500 g, 5 min, 4°C) and washed with Triton X-100 wash buffer. Proteins were eluted in 2x LDS buffer supplemented with 50 mM DTT for 10 min at 65°C.

2.3.6 Deglycosylation assay

Cells lysates were denatured with Glycoprotein Denaturing Buffer (New England Biolabs) at 65°C for 15 min and then incubated with 1 µl endoglycosidase H (Endo H), 1 µl peptide: N-glycosidase F (PNGase F) (both New England Biolabs) or without enzyme for 2 h according to the manufacturer's instructions. Samples incubated in 4x LDS buffer at 65°C for 10 min and then analysed by western blot.

2.3.7 SDS-PAGE and western blotting

Proteins were separated by sodium dodecyl sulfate polyacrylamide gel electrophoresis (SDS-PAGE) using 4-20% Bis-Tris NuPAGE gradient gels (Invitrogen) and MOPS running buffer (50 mM MOPS, 50 mM Tris, 0.1 % SDS, 1 mM EDTA). After SDS-PAGE, proteins were either stained using the ProteoSilver Silver Stain Kit (Sigma-Aldrich) or proteins were transferred to a polyvinylidene difluoride (PVDF) membrane (Millipore). The PVDF membrane was activated with methanol before proteins were transferred from the gel to

the membrane in transfer buffer (25 mM Bicine, 25 mM Bis-Tris, 15% methanol, 1 mM EDTA) at 100 V for 75 min. Membranes were blocked in 5% milk-TBS-T (150 mM NaCl, 10 mM Tris-HCl (pH 7.5), 0.05% Tween 20, 5% dry milk powder) at room temperature and then incubated with the primary antibody diluted in 5% milk-TBS-T (Table 2.14) at 4°C overnight. Three washing steps with TBS-T (150 mM NaCl, 10 mM Tris-HCl (pH 7.5), 0.05% Tween 20) were performed at room temperature. Membranes were then incubated with the secondary antibody diluted in 5% milk-TBS-T (Table 2.16) at room temperature for 1 h and then washed three times with TBS-T again. Antibody binding was detected using enhanced chemiluminescence (ECL) reagent (GE Healthcare). Membranes were incubated in ECL reagent and then exposed in a dark room to X-ray films (Thermo Scientific) or high sensitivity films (Amersham Hyperfilm ECL, GE Healthcare), which were developed using a SRX-101A medical film processor (Konica). All western blots shown constitute one representative experiment of at least three independent replicates with a similar outcome (unless otherwise stated in the figure legend). For quantification the band intensity was normalised to the background and the loading control using ImageJ from least three independent experiments.

Table 2.16 | Antibodies for western blot

antibody	dilution	manufacturer
primary antibody		
anti-β-actin-HRP, mouse monoclonal (clone AC-15)	1:5,000	Sigma-Aldrich (A3854)
anti-ADAM17, rabbit polyclonal	1:2,000	Abcam (ab39162)
anti-Flag, mouse monoclonal	1:2,000	Sigma-Aldrich (F1804)
anti-FRMD8, rabbit polyclonal	1:500	Abcam (ab169933)
anti-HA-HRP, rat monoclonal (clone 3F10)	1:2,000	Roche (11867423001)
anti-iRhom2, rabbit polyclonal	1:500	(Adrain et al., 2012)
anti-transferrin receptor 1, mouse monoclonal (clone H68.4)	1:2,000	Invitrogen (13-6800)
anti-V5, goat polyclonal	1:2,000	Santa Cruz (sc-83849)
secondary antibody		
anti-goat-HRP, mouse monoclonal	1:5,000	Santa Cruz (sc-2354)
anti-mouse-HRP, goat polyclonal	1:5,000	Santa Cruz (sc-2055)
anti-rabbit-HRP, goat polyclonal	1:20,000	Sigma-Aldrich (A9169)

2.3.8 Shedding assay

To determine the ability of ADAM17 to cleave its substrates, alkaline phosphatase (AP)-conjugated ADAM17 substrates were transfected into cells and the AP activity in cell lysates and supernatants was determined in a colorimetric assay. $8 \cdot 10^4$ HEK293T cell lines were seeded in triplicates into poly-(L)-lysine (PLL)-coated 24-well plates. The following day cells was transfected with 30 ng plasmid DNA encoding AP-AREG or AP-TGFα (received from Prof Carl Blobel) using FuGENE HD as described in 2.2.1.2. 48 h after transfection, cells were washed with OptiMEM and then incubated at 37°C for 30 min with 200 µl colourless OptiMEM (Gibco, 11058-021) containing DMSO, 200 nM phorbol 12-myristate 13-acetate (PMA) or 200 nM PMA and 1 µM GW. Then cell supernatants were collected, the cells were washed in PBS and lysed in 200 µl Triton X-100 lysis buffer. 100 µl cell lysate or cell supernatant was incubate with 100 µl AP substrate p-nitrophenyl phosphate (PNPP) (Thermo Scientific) at room temperature until wells turned yellow. The absorption was measured at 405 nm with a plate reader. The percentage of AP-conjugated material released from each well was calculated by dividing the signal from the supernatant by the sum of the signal from the lysate and the supernatant. The data was expressed as mean of at least three independent experiments, each of which was performed with three biological replicates per condition. For statistical analysis, an unpaired, non-parametric test (Mann-Whitney test) was performed using the Prism 7 software (GraphPad).

For shedding assays after siRNA-mediated knockdown, cells were seeded at a lower density of $1 \cdot 10^4$ cells per 24-well and transfected the next day with siRNA as described in 2.2.1.3. 24 h after the siRNA transfection, the plasmids expressing the AP-conjugates were transfected the protocolled continued as described above.

2.3.9 Immunofluorescence staining and confocal microscopy

$1.5 \cdot 10^4$ HEK293T cells were seeded in a poly-L-lysine (PLL)-coated 8-well culture slide (Corning) and transfected as described before (2.2.1.2). 48 h after transfection, cells

were washed with PBS and then fixed with 4% paraformaldehyde (PFA; in PBS) (Electron Microscopy Sciences) for 20 min. After three washes in PBS, cells were permeabilised with 0.2% Triton X-100 (in PBS) for 10 min and washed again in PBS three times. Cells were blocked with 1% Bovine Serum Albumin (BSA; in PBS) for 1 h at room temperature and incubated with the primary antibody (diluted in 1% BSA) (Table 2.17). After three PBS washes, cells were incubated with Alex Fluor-conjugated secondary antibodies (diluted in 1% BSA) for 40 min at room temperature. Cells were washed three times with PBS and then mounted in Fluoromount-G with DAPI (eBioscience). Slides were analysed using an inverted Olympus FV1000 confocal system using a 100x/1.40 Oil UPlanSApo objective (Olympus).

Table 2.17 | Antibodies for immunocytochemistry

antibody	dilution	manufacturer
primary antibody		
anti-calnexin	1:500	Roche (11 867 423 001)
anti-HA, rat monoclonal (clone 3F10)	1:500	Roche (11 867 423 001)
anti-V5, goat polyclonal	1:500	Santa Cruz (sc-83849)
secondary antibody		
anti-mouse Alexa Fluor 488, donkey polyclonal	1:500	Invitrogen (A-21202)
anti-rabbit Alexa Fluor 647, donkey polyclonal	1:500	Invitrogen (A-31573)

2.3.10 Flow cytometry

For the cell surface staining of HEK293T cells for ADAM10 and ADAM17, cells were stimulated with 200 nM PMA for 5 min. Cells stained for iRhom2-HA were not stimulated. Cells were harvested in PBS and washed with ice-cold FACS buffer (0.25% BSA, 0.1% sodium azide in PBS). $0.5 \cdot 10^6$ HEK293T cells were pelleted by centrifugation (400 g, 5 min, 4°C) and resuspended in primary antibody (Table 2.18) diluted in 50 µl FACS buffer. Cells were incubated in primary antibody on ice for 45 min. After two washes with FACS buffer, the cells were incubated with Alexa Fluor 488-coupled secondary antibody (diluted in 50 µl FACS buffer) on ice for 30 min. Cells were washed twice with ice-cold

FACS buffer, fixed in 2% PFA and then analysed with a BD FACSCalibur (BD Biosciences) and FlowJo software (version 10.0.7). Cells stained only with the secondary antibody or HA-negative cells served as control. Flow cytometry blots shown represent one from at least three experiments with similar outcome. The geometric mean fluorescence intensity of stained cells was compared to the control using FlowJo. The mean with error bars representing the standard deviation was plotted using Prism 7. An unpaired t-test was used for statistical analysis.

Macrophages used for cell surface staining were harvested in 2 mM EDTA (in PBS) and washed with ice-cold macrophage FACS buffer (1% FCS, 10 µg/ml human IgG, 0.01% sodium azide in PBS). The staining was performed as described for HEK293T cells above using an anti-TNFα as the primary antibody and a secondary antibody conjugated to Alexa Fluor 647 (Table 2.18), both in macrophage FACS buffer.

Table 2.18 | Antibodies for flow cytometry

antibody	**dilution**	**manufacturer**
primary antibody		
anti-ADAM10, mouse monoclonal (clone SHM14)	4 µg in 50 µl	BioLegend (352702)
anti-ADAM17, mouse monoclonal (clone A300E)	8 µg in 50 µl	(Yamamoto et al., 2012); received from S. Düsterhöft
anti-HA, rabbit polyclonal	0.5 µg in 50 µl	Santa Cruz (sc-805)
anti-TNFα, rabbit polyclonal	2.5 µg in 50 µl	Abcam (ab9739)
secondary antibody		
anti-mouse Alexa Fluor 488, donkey polyclonal	1:1,000	Invitrogen (A-21202)
anti-rabbit Alexa Fluor 488, donkey polyclonal	1:1,000	Invitrogen (A-21206)
anti-rabbit Alexa Fluor 647, donkey polyclonal	1:1,000	Invitrogen (A-31573)

2.4 Mouse work

2.4.1 Generation of KO mice

Commercially available *Frmd8*$^{-/-}$ mouse ES cells from KOMP Repository at UC Davis were used to generate *Frmd8*$^{-/-}$ mice in-house. The mouse ES cells (C57BL/6NTac strain) were grown up by Prof Elizabeth Robertson and injected into blastocysts of Balb/c mice by Jonathan Godwin. Chimeras were bred to C57BL/6 under project licenses 80/2584 and 30/2306 with the help of Dr Adam Grieve. Pups with a black coat, potentially *Frmd8*$^{+/-}$, were genotyped as described below (2.4.2). 2 heterozygous FRMD8 KO mice (*Frmd8*$^{+/-}$) were crossed to generate *Frmd8*$^{-/-}$ mice.

2.4.2 Genotyping

Mouse genomic DNA was isolated from ear notching or tail samples using the Hot Sodium Hydroxide and Tris (HotSHOT) method (Truett et al., 2000). Skin samples were boiled in 75 µl HotSHOT buffer (25 mM NaOH, 0.2 mM EDTA) at 95°C for 1 h. Then 75 µl neutralisation buffer (40 mM Tris-HCl (pH 5.5)) were added, the sample was vortexed and centrifuged at 1,500 g for 3 min. Isolated DNA was used as a template for the genotyping PCR (Table 2.19). The PCR products were separated in a 2% agarose gel and the size of the bands compared to the expected sizes shown in the genotyping scheme in Fig. 2.1.

Table 2.19 | genotyping PCR protocol

PCR mix (10µl)		**PCR programme**		
10x PCR reaction buffer (Invitrogen)	1.00 µl	94°C	3 min	1x
$MgSO_4$ (50 mM) (Invitrogen)	0.30 µl	94°C	30 s	
dNTP mix (10 mM) (Bioline)	0.20 µl	62°C	30 s	35x
Primers (10 µM)	0.25 µl	72°C	90 s / 1kb	
Template DNA	2.00 µl	72°C	4 min	1x
Platinum Taq polymerase (Invitrogen)	0.04 µl	4°C		Hold
water	5.71 µl			

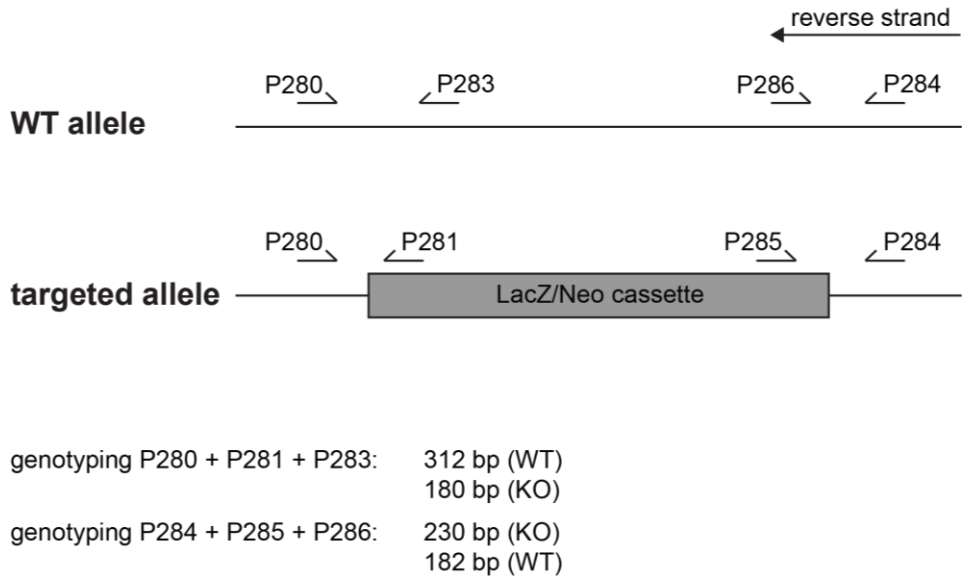


Figure 2.1 | Genotyping strategy for FRMD8 KO mice. Schematic representation of the location of the genotyping primers and the expected PCR products.

2.4.3 Lysis of mouse tissues

Mouse tissues were collected from sacrificed animals and stored on dry ice or at -80°C. Tissues were lysed in Triton X-100 RIPA buffer (1% Triton X-100, 150 mM NaCl, 50 mM Tris-HCl (pH 7.5), 0.1% SDS, 0.5% sodium deoxycholate) supplemented with EDTA-free protease inhibitor mix (Roche) and 10 mM 1,10-Phenanthroline (Sigma-Aldrich) using a tissue homogeniser (Omni International). Lysates were cleared from cell debris by centrifugation (20,000 g, 4°C, 10 min) and stored at -80°C until analysis by western blot. Protein concentrations of tissue lysates were determined using the BCA assay (2.3.3)

2.4.4 Culture of bone marrow-derived macrophages (BMDM)

Hind legs were isolated from sacrificed mice and bone marrow was flushed into PBS using a 26G needle (Terumo). The cell suspension was passed through a 70-µm cell strainer and cells were pelleted by centrifugation (250 g, 5 min, room temperature). Bone marrow-derived cells were resuspended in macrophage growth medium (DMEM supplemented with 10% FCS, 2 mM L-glutamine, 100 U/ml penicillin and 100 µg/ml streptomycin, and 15% L929 cell-conditioned medium). Cells were differentiated into

macrophages for 7 days with addition of 50% fresh macrophage growth medium on day 4 of culture. Macrophages were harvested after 7 days of culture in macrophage growth medium by incubation in ice-cold 2 mM EDTA (in PBS), and then pelleted by centrifugation (400 g, 5 min, 4°C).

2.5 Work with *Drosophila melanogaster*

2.5.1 Fly lines

Flies were kept in polyethylene vials containing fly food in incubators at 25°C. The fly lines used (Table 2.20) were obtained from Bloomington Drosophila stock collection, a kind gift from Andrew Bassett or generated during this project.

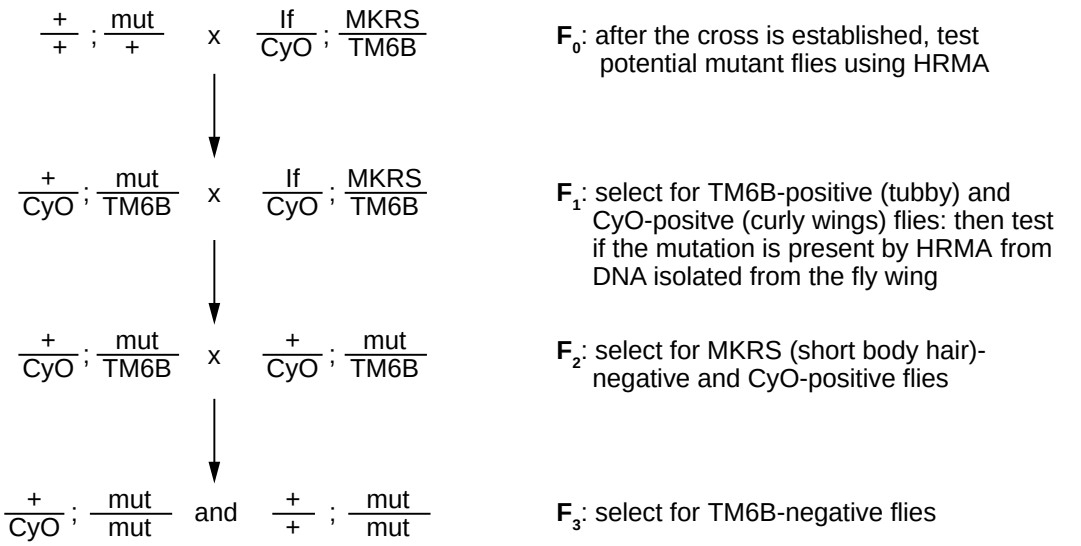
Table 2.20 | Fly lines used and generated

Fly line	source	description
w^{1118}; If/CyO; MKRS/TM6B	Andrew Bassett	balancer line for the 2nd and 3rd chromosome
y^1 P(act5c-cas9, w^+) M(3xP3-RFP.attP)ZH-2A w*	Bloomington stock 54590	ubiquitous Cas9 expression under the Act5C promotor
w^{1118}; Bili KO/Bili KO	generated	Bili KO line (8-nt deletion in *bili* gene)
w^{1118}	generated	wild-type control line for Bili KO

2.5.2 Generation of KO line with CRISPR/Cas9

200 act5-cas9 fly embryos were injected with 0.1 µg/ml plasmid DNA (dissolved in ultrapure water) encoding the sgRNA at the fly facility at the University of Cambridge. Flies eclosing from the injected embryos were crosses to a balancer fly line (Fig. 2.2) as described in (Bassett and Liu, 2014). Once the cross was established, potential mosaic flies were analysed for disruptions in the *bili* gene by high resolution melt analysis (HRMA). DNA was extracted from the whole fly using DNA extraction buffer as described in 2.1.3, and used as a template for melt analysis. For HRMA a PCR in the presence of the fluorescent DNA dye LCGreen Plus (BioFire Diagnostics) was performed using a Rotor-Gene Q PCR cycler (Qiagen) according to the protocol in Table 2.21 using primers dBiliHRMF and dBiliHRMR (Table 2.8). As mutations lead to a change in the melting curve of the PCR product, changes of the fluorescent signal with increasing temperature were analysed using the Rotor-Gene Q software (Qiagen). Only crosses from mosaic flies that showed a change in the melt curve were maintained.

A Bili KO flies



B WT control flies

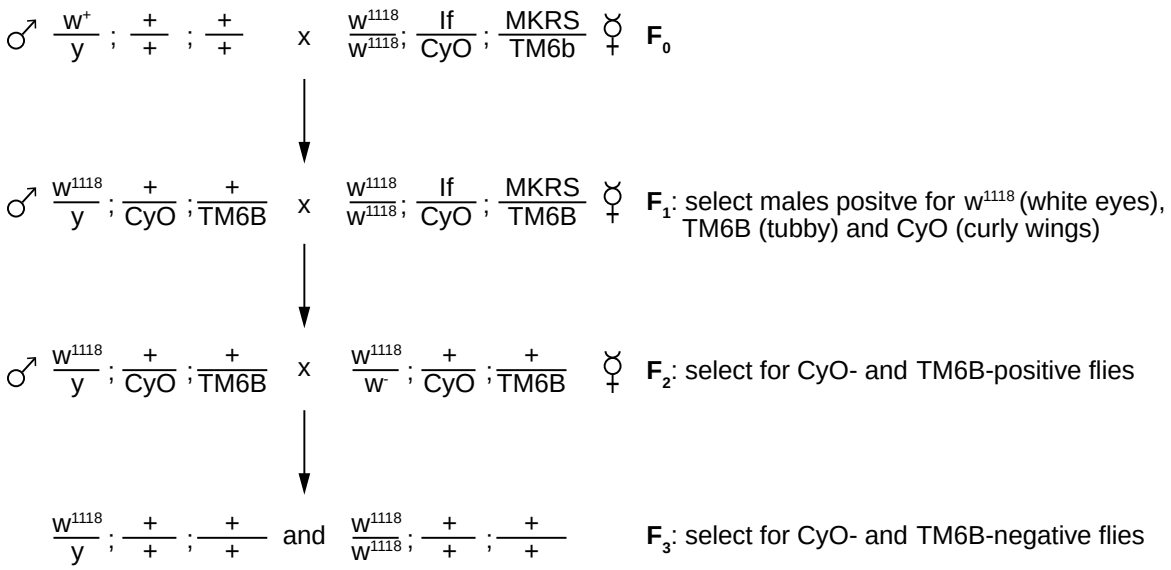


Figure 2.2 | Crossing scheme for the generation of Bili KO and WT control flies. A) Flies eclosing from injected embryos were crossed a balancer fly line. Offspring (F_1) was selected for the presence of the CyO and TM6B balancers (curly wings; shorter pupae and additional hair on the shoulder) and tested for the presence of a mutation in the *bili* gene. Flies carrying a *bili* mutation were further crossed to the balancer line, and their progeny was used to generate homozygous *bili* knockout flies in the third generation (F_3). **B)** Males of the same fly line (BL54590) as the injected embryos in A) were crossed a balancer fly line. Offspring (F_1) was selected for the presence of the CyO and TM6B balancers and crossed to the balancer line again until wild-type flies were generated in the third generation (F_3).

The progeny (F_1 generation) of these flies was selected for the presence of the balancer chromosome and were subsequently analysed for the presence of a *bili* mutation. For this reason, DNA was extracted from a single fly wing (see 2.1.3.) and analysed by HRMA (Table 2.21). When a change in the melt curve was detected, HRMA PCR products were treated with ExoSAP-IT clean-up reagent (Applied Biosystems), and then sequenced using primer dBiliHRMF (Table 2.8) to determine the nature of the *bili* mutation. Flies carrying a frameshift mutation in the *bili* gene were further crossed to marker/balancer fly line (Fig. 2.2).

Table 2.21 | High resolution melt analysis (HRMA) protocol

HRMA mix (10µl)		**PCR programme**		
2x HotShot Diamond PCR master mix (Clent Lifescience)	5.0 µl	95°C	5 min	1x
LCGreen Plus+ (BioFire Diagnostics)	1.0 µl	95°C	30 s	45x
Primers (10 µM)	0.2 µl	55°C	30 s	
Template DNA	1.0 µl	72°C	30 s	
water	2.6 µl	70-98°C	hold 2 s per cycle	

2.5.3 Negative geotaxis assay

On the day of eclosion, female flies were collected in groups of around 20-30 flies under CO_2 anaesthesia. The flies were kept in an incubator at 25°C and allowed to recover from anaesthesia for at least 18 h before the assay. The climbing apparatus was prepared for a group of Bili KO and wild-type flies by connecting two empty polystyrene vials vertically using tape. At the lower vial, a circle marked the vertical distance of 8 cm above the bottom surface. Flies were rapidly transferred into the climbing apparatus without applying anaesthesia, and were allowed to acclimatise to the new environment for 20-30 min before starting the assay. Flies were gently tapped 3x down to the bottom of the vial and 10 s after the tap a photo was taken to count the number of flies above the 8-cm mark in several vials in parallel. The assay was repeated ten times, allowing 1 min of

rest between the trials. For each trial, the number of flies above the 8-cm mark was expressed as a percentage of total flies. The data was statistically analysed using an unpaired t-test in GraphPad Prism 7.

2.5.4 Longevity assay

Male adult flies of the Bili KO line and the corresponding wild-type were collected on the day of eclosion. Groups of 8-18 flies were placed into a vial with fresh fly food and kept in an incubator at 25°C. The flies were flipped into a fresh food vial every two to three days and the number of dead flies was counted until all flies were dead. Data was depicted in a Kaplan-Meier survival plot using GraphPad Prism 7.

CHAPTER 3

Identification of FRMD8 as a novel iRhom interaction partner

3 Identification of FRMD8 as a novel iRhom interaction partner

3.1 Introduction

As described in chapter 1, mammalian iRhoms exert different cellular roles, ranging from the regulation of ADAM17 in intercellular signalling and the cellular response to viral infection, to protein degradation. Their functions in different cellular pathways require iRhoms to interact with other proteins, and consequently, several interaction partners of mammalian iRhom1 and iRhom2 have been reported, although only ADAM17 could be confirmed by several different studies (Table 3.1).

Table 3.1 | Published interaction partners of mammalian iRhoms. All interactions were confirmed by co-immunoprecipitation in the indicated studies.

	interaction partner(s)	reference(s)
iRhom1	EGF	(Zettl et al., 2011)
	ADAM17	(Christova et al., 2013)
	TGFα	(Nakagawa et al., 2005)
	HB-EGF	(Nakagawa et al., 2005)
	PAC1 and PAC2	(Lee et al., 2015)
	hypoxia-inducible factor 1-alpha (HIF1α)	(Zhou et al., 2014)
	receptor of activated protein C kinase 1 (RACK1)	(Zhou et al., 2014)
iRhom2	EGF	(Zettl et al., 2011)
	ADAM17	(Adrain et al., 2012, McIlwain et al., 2012, Christova et al., 2013)
	AREG	(Hosur et al., 2014)
	STING	(Luo et al., 2016)
	TRAPβ	(Luo et al., 2016)
	Sec5	(Luo et al., 2016)
	14-3-3 gamma, epsilon, eta, tau, zeta	(Grieve et al., 2017)
	Keratin 16	(Maruthappu et al., 2017)

The initial identification of several membrane proteins as interactors of iRhoms led to the hypothesis that, while diverging from rhomboid proteases and losing their proteolytic activity, iRhoms have kept the ability to recognise and bind TMDs during evolution (Adrain

and Freeman, 2012). In case of the membrane protein STING, it was indeed shown that the interaction with iRhom2 occurs through the TMDs of both proteins (Luo et al., 2016).

Another site of protein-protein interactions is the cytosolic N-terminus of iRhoms, which is involved in regulating iRhom localisation, as well as ADAM17-dependent shedding (Brooke et al., 2014, Hosur et al., 2014, Maney et al., 2015). It is likely that interacting proteins play a role in that, but only few protein interactions have yet been identified for the iRhom N-terminus (Grieve et al., 2017, Maruthappu et al., 2017). The large luminal loop between the first two TMDs, the IRHD, might constitute a third site for protein-protein interaction. The function of the IRHD is still largely uncharacterised, but it was found to be essential for iRhom2 binding to ADAM17 (Grieve et al., 2017).

Despite the different cellular roles described for iRhoms, how iRhoms function at a molecular level is not well understood. Open questions include whether iRhoms require co-factors to exert their functions as regulators of ADAM17, how iRhoms themselves are regulated and whether iRhoms transport and regulate other client proteins than ADAM17 or STING. The identification of new iRhom interaction partners will help to understand the molecular mechanism underlying known cellular roles of iRhoms. Mass spectrometry-based screens or the yeast two-hybrid system are high-throughput methods commonly used to identify protein-protein interactions (Gingras et al., 2007). Mass spectrometry approaches have the advantage that protein complexes can be studied under the physiological conditions in the relevant species and cell types, whereas yeast two-hybrid screens are typically performed in *Saccharomyces cerevisiae.* Although a recent study applied the yeast two-hybrid technology to screen for interaction partners of the human iRhom2 N-terminus (Maruthappu et al., 2017), the interactome of full-length human iRhoms has never been studied systematically. The aim of my PhD project was therefore to identify new interaction partners of human iRhoms using a mass spectrometry-based approach. First, this required establishing a robust co-immunoprecipitation (co-IP) protocol to purify iRhoms and their interaction partners from cells. Second, the isolated proteins were analysed by mass spectrometry. ADAM17, as a known interaction partner of iRhoms, supported the establishment and validation of the screen. Finally, identified

candidates were validated using truncated versions of iRhoms, as the screen might also have identified false positives that nonspecifically bound iRhoms. The top hit of the screen was further validated in western blot and co-localisation studies.

3.2 Results

3.2.1 Design and optimisation of a mass spectrometry-based screen for novel iRhom interaction partners

To identify new interaction partners of human iRhoms by mass spectrometry, a robust co-IP protocol for human iRhoms had to be established first. I used a HEK293T cell line stably expressing C-terminally 3xHA-tagged human iRhom1 (iRhom1-3xHA) to optimise the co-IP conditions with ADAM17 serving as a positive control. First, I tested different lysis buffers containing either Triton X-100, Tergitol-type NP-40, n-dodecyl β-D-maltoside (DDM), or CHAPS because the choice of the detergent is crucial for the isolation of integral membrane proteins (Arachea et al., 2012, Vuckovic et al., 2013). ADAM17 was successfully co-immunoprecipitated with iRhom1 in all lysis buffers tested, whereas the isolation of iRhom1 was most efficient in the buffers containing 1% Triton X-100, 1% DDM, and 1% Tergitol-type NP-40 (Fig. 3.1A). A RIPA lysis buffer containing 1% DDM was finally chosen for mass spectrometry analysis.

In the next step, I optimised the elution of proteins from HA beads. To avoid the elution of beads-coupled antibodies, which would lead to a contamination in the mass spectrometry analysis, I used HA peptides to specifically elute HA-tagged proteins. The elution with HA peptides was less efficient than the standard elution with lithium dodecyl sulfate (LDS) sample buffer (Fig. 3.2A-B) but, in contrast to LDS sample buffer (Fig. 3.2B), HA peptides did not elute immunoglobulin (Ig). For this reason, the elution with HA peptides was included in the co-IP protocol used for mass spectrometry analysis.

Finally, an *in vivo* crosslinking step was added to the established co-IP protocol to keep transiently bound proteins associated to iRhoms during the co-IP. Dithiobis(succinimidyl propionate) (DSP) was used as crosslinking reagent because it is cleavable in DTT, membrane-permeable, and contains a spacer of only 12.0 Å (8 atoms) reducing nonspecific crosslinking. For mass spectrometry analysis, the established co-IP protocol was scaled up and eluted proteins were trypsin digested using filter-assisted sample

preparation (FASP) (Wisniewski et al., 2009) (Fig. 3.3), before the peptides were submitted for mass spectrometry analysis to the local proteomics facility.

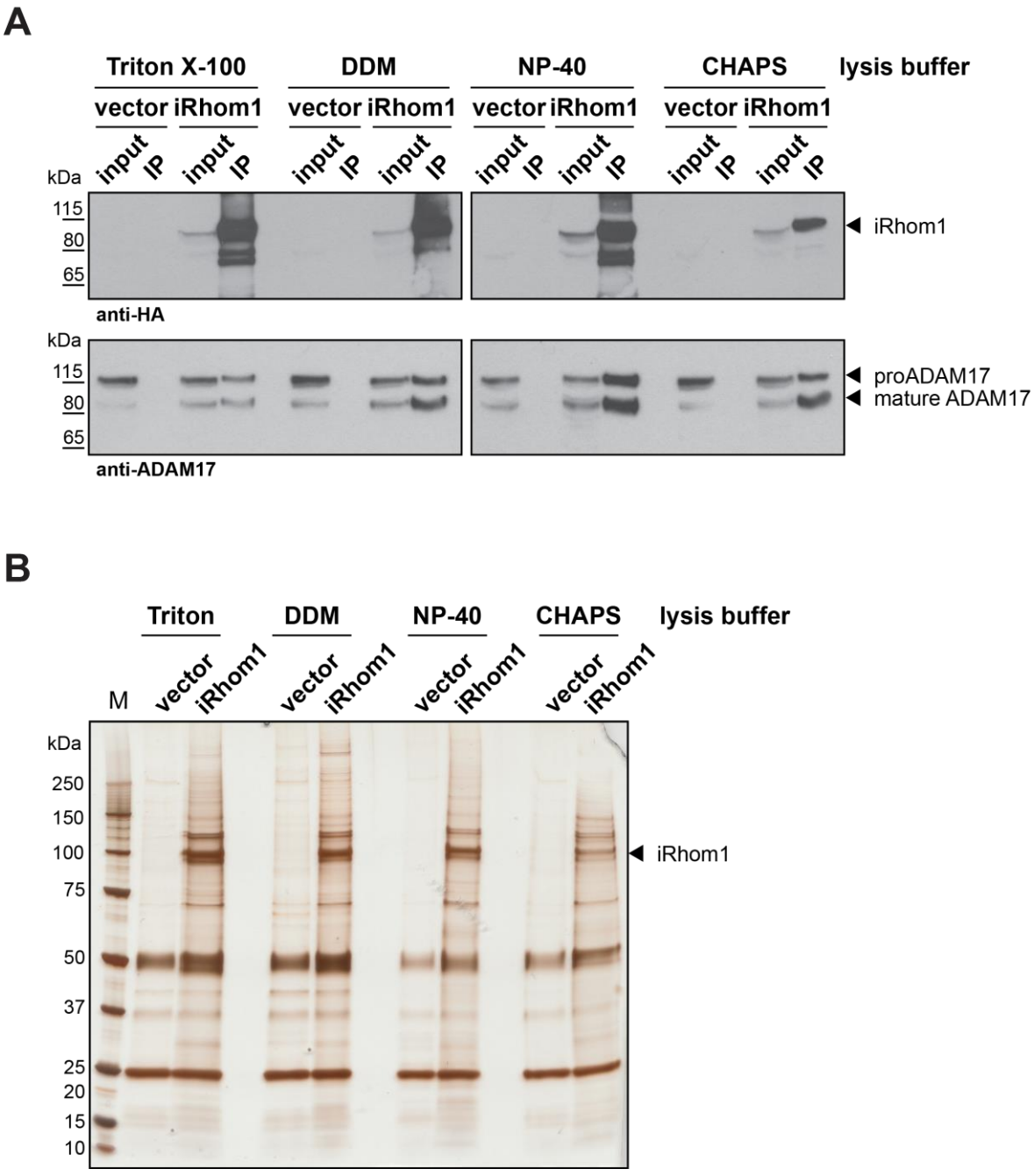


Figure 3.1 | ADAM17 is co-immunoprecipitated with iRhom1 in different lysis buffers. Lysis buffers containing either 1% Triton X-100, 1% DDM, 1% Tergitol-type NP-40, or 1% CHAPS in 150 mM NaCl, 50 mM Tris-HCl (pH 7.5), 0.5% sodium deoxycholate and 0.1% SDS were used. **A)** Western blot of anti-HA immunoprecipitated iRhom1 (IP) and cell lysates (input), after anti-HA or anti-ADAM17 staining. One representative western blot out of three independent experiments is shown. **B)** SDS-PAGE of anti-HA immunoprecipitated iRhom1 eluted from HA beads using LDS sample buffer, after silver staining.

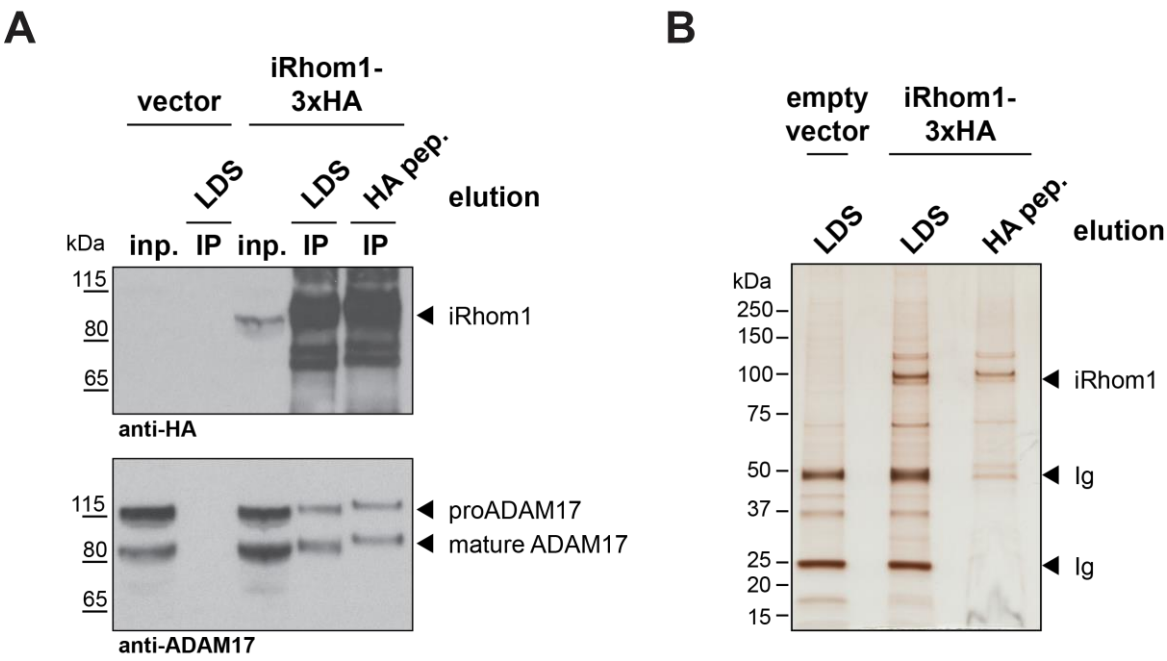


Figure 3.2 | Elution of ADAM17 and iRhom1 from anti-HA beads using HA peptide. A) Western blot of anti-HA immunoprecipitated iRhom1 (IP) and cell lysate input (inp.), after anti-HA or anti-ADAM17 staining. Proteins were eluted either with 4x LDS sample buffer (LDS) or 1 mg/ml HA peptide (HA pep.). One representative western blot out of three independent experiments is shown. **B)** SDS-PAGE of anti-HA immunoprecipitated iRhom1, after silver staining.

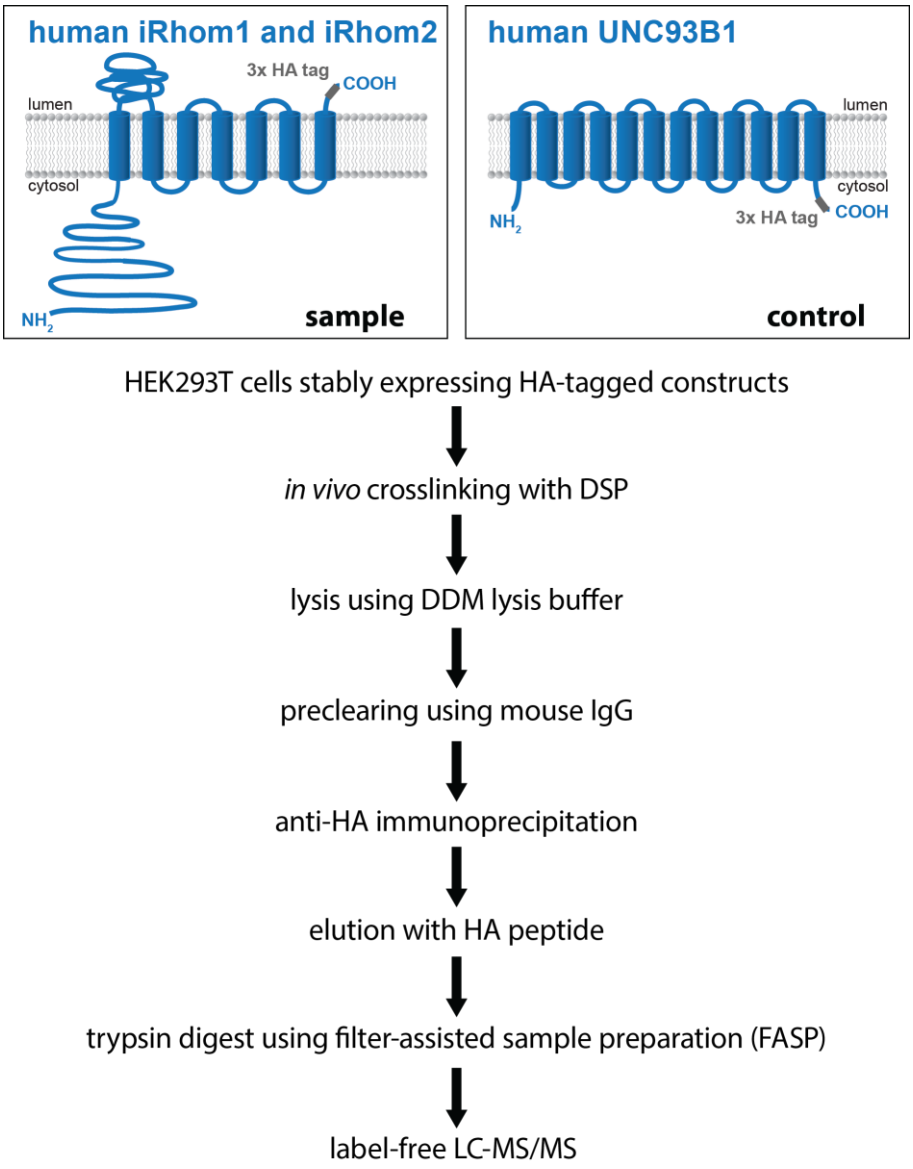
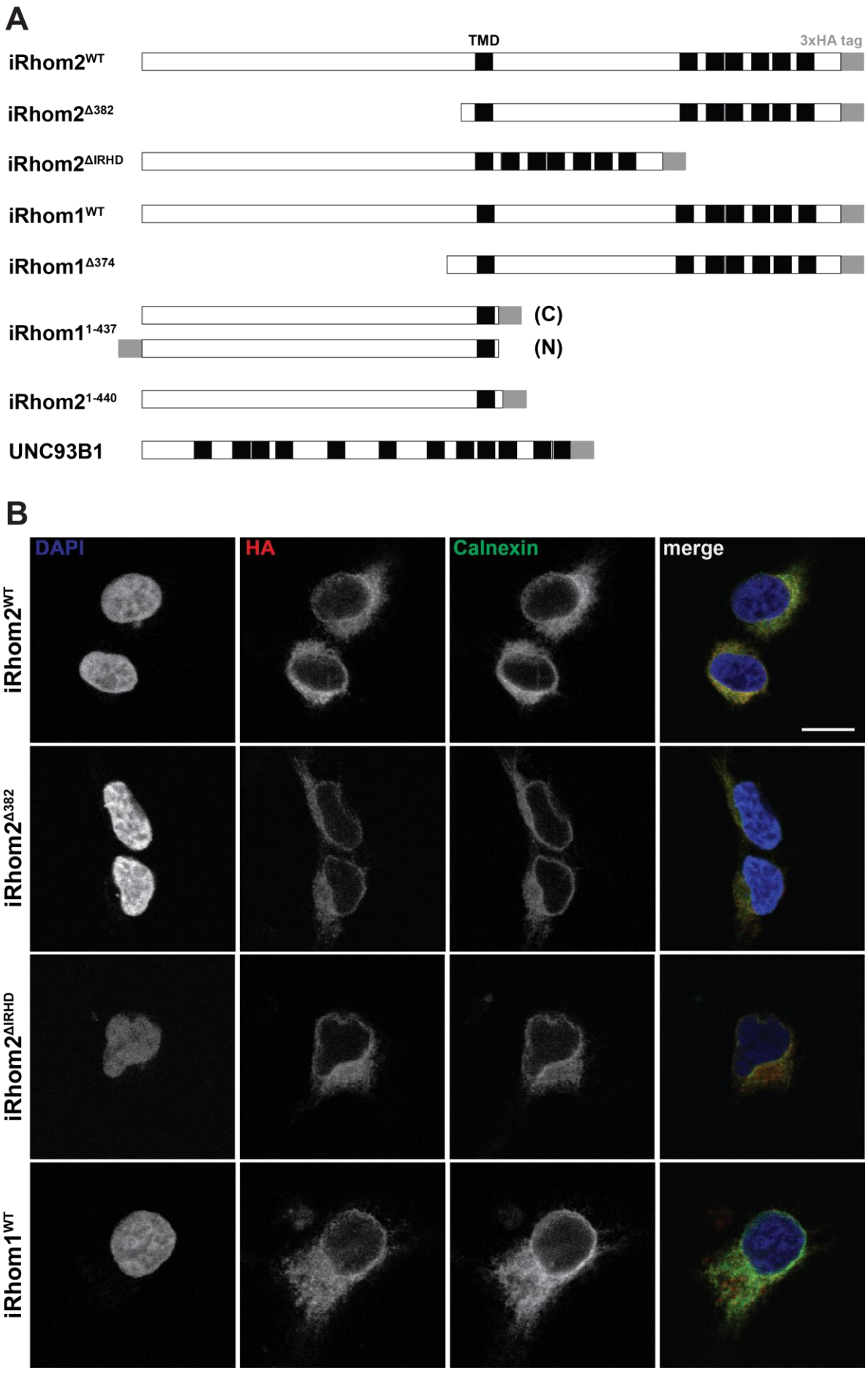


Figure 3.3 | Established protocol for co-immunoprecipitation and mass spectrometry analysis. HEK293T cells stably expressing human iRhom1^{WT}, iRhom2 ^{WT}, iRhom2$^{\Delta 382}$, iRhom2$^{\Delta IRHD}$ or UNC93B1 were cross-linked *in vivo* using 1 mg/ml DSP. Cells were lysed in DDM RIPA lysis buffer and the post-nuclear supernatant was pre-cleared with mouse IgG. Proteins were immunoprecipitated using magnetic anti-HA beads. Bound proteins were eluted by incubation with 1 mg/ml HA peptide. Eluates were concentrated with a vivaspin concentrator and proteins prepared for mass spectrometry analysis by trypsin digestion using FASP (Wisniewski et al., 2009). Peptides were injected into a nano-flow reversed-phase liquid chromatography (LC) coupled to a Q Exactive Hybrid Quadrupole-Orbitrap mass spectrometer (MS/MS) (Thermo Scientific).

3.2.2 Generation of different truncated iRhom constructs

Establishing a mass spectrometry-based screen for interaction partners of iRhom1 and iRhom2 also required the generation of suitable controls. Human UNC93B1 is, like

iRhoms, a multi-pass membrane protein mainly localised in the ER (Koehn et al., 2007), therefore, it was used as a negative control for nonspecific interactions in the co-IPs. I also cloned different truncated versions of human iRhoms (Fig. 3.4A), which served as additional controls and can be used to identify which regions of iRhoms interact with potential new partners. I tested the correct cellular localisation of all generated constructs by immunofluorescence (Fig. 3.4B) finding that UNC93B1, iRhom1^{WT}, iRhom2^{WT}, and iRhom2$^{\Delta 382}$ co-localised with calnexin in the ER. Surprisingly, the C-terminally truncated iRhom1$^{1-437}$ and iRhom2$^{1-440}$ constructs, which only contain the first TMD, localised to the ER and the nucleus (Fig. 3.4B). The same nuclear localisation was observed for iRhom1$^{1-437}$ with the 3xHA tag on the N-terminus (iRhom1$^{1-437}$ (N); Fig. 3.4B), suggesting that the localisation of the tag was not the problem. It is possible that the C-terminally truncated versions of iRhom1 and iRhom2 were not properly integrated in the ER but translocated to the nucleus due to a nuclear localisation (NLS) present in the both iRhom1 and iRhom2 N-terminus (Fig. A1, Appendix). For this reason, the C-terminally truncated iRhom constructs were not used for the mass spectrometry screen. Finally, I generated stable HEK293T cell lines for UNC93B1, iRhom2^{WT}, iRhom2$^{\Delta IRHD}$, and iRhom2$^{\Delta 382}$ by lentiviral transduction, which I used for the mass spectrometry-based screen in addition to the already existing stable iRhom1^{WT}-expressing HEK293T cell line.


A
TMD
3xHA tag
iRhom2WT
iRhom2Δ382
iRhom2ΔIRHD
iRhom1WT
iRhom1Δ374
iRhom11-437
(C)
(N)
iRhom21-440
UNC93B1
B
DAPI
HA
Calnexin
merge
iRhom2WT
iRhom2Δ382
iRhom2ΔIRHD
iRhom1WT

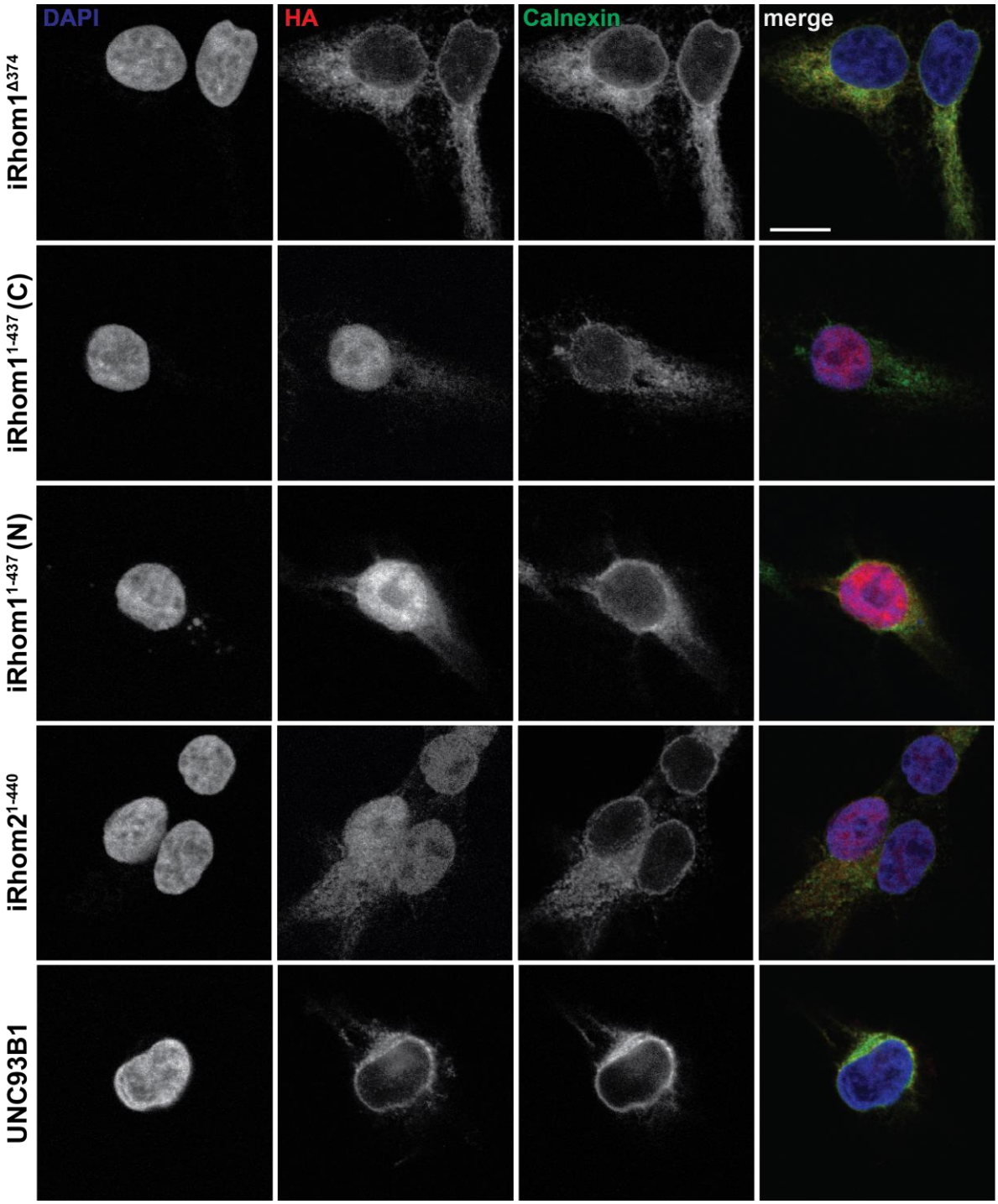


Figure 3.4 | iRhom constructs and their localisation. A) Schematic representation of iRhom and control constructs generated for the mass spectrometry screen. **B)** Immunofluorescence staining of HEK293T cells transfected with different constructs of human iRhom1, iRhom2 or UNC93B1, using 4',6-diamidino-2-phenylindole (DAPI; blue), anti-HA (red), and anti-calnexin (green) antibodies. Non-transfected cells served as a control for the antibody staining with epitope tag antibodies (data not shown).

3.2.3 Mass spectrometry-based screen reveals potential new iRhom interaction partners

Having established all required tools for the mass spectrometry screen, I performed the screen in HEK293T cell lines, following the optimised co-IP and mass spectrometry protocol (Fig. 3.3). Three independent experiments using iRhom2^{WT} and UNC93B1 were statistically analysed with the help of Dr Monika Stegmann from the Oxford proteomics facility. Figure 3.5 shows the volcano plot of identified iRhom2^{WT} interaction partners compared to UNC93B1 as a control. Both bait proteins, iRhom2^{WT} and UNC93B1, were significantly enriched in the corresponding co-IP (Fig. 3.5) demonstrating that both co-IPs had worked as anticipated. 80 statistically significant hits were identified in the iRhom2^{WT} co-IP, among them the known iRhom2 interactor ADAM17, which provides further evidence of the functionality of the screen. The top hit of the iRhom2^{WT} mass spectrometry analysis was the poorly characterised FERM domain-containing protein 8 (FRMD8) (Fig. 3.5), which was also reproducibly detected in the iRhom1^{WT} co-IP (Table A1, Appendix).

To further analyse the 80 statistically significant hits of the iRhom2^{WT} co-IP, I grouped them according to the biological processes they are involved in, as defined by genome ontology (GO) terms in the UniProt database. The significant iRhom2^{WT} hits were mainly linked to three cellular processes: signal transduction, protein folding and degradation, and protein transport (Fig. 3.6A). This is consistent with the known functions of iRhoms in ADAM17 transport (McIlwain et al., 2012, Adrain et al., 2012), EGFR ligand degradation (Zettl et al., 2011), regulation of proteasomal activity (Lee et al., 2015), and STING localisation and stability (Luo et al., 2016), and might suggest that these pathways are the most important cellular functions of iRhoms, at least in the HEK293T cells used for this study. STING and EGF itself, however, were not among the identified interaction partners, presumably due to their low expression in HEK293T cells (Sun et al., 2013, Uhlen et al., 2015).

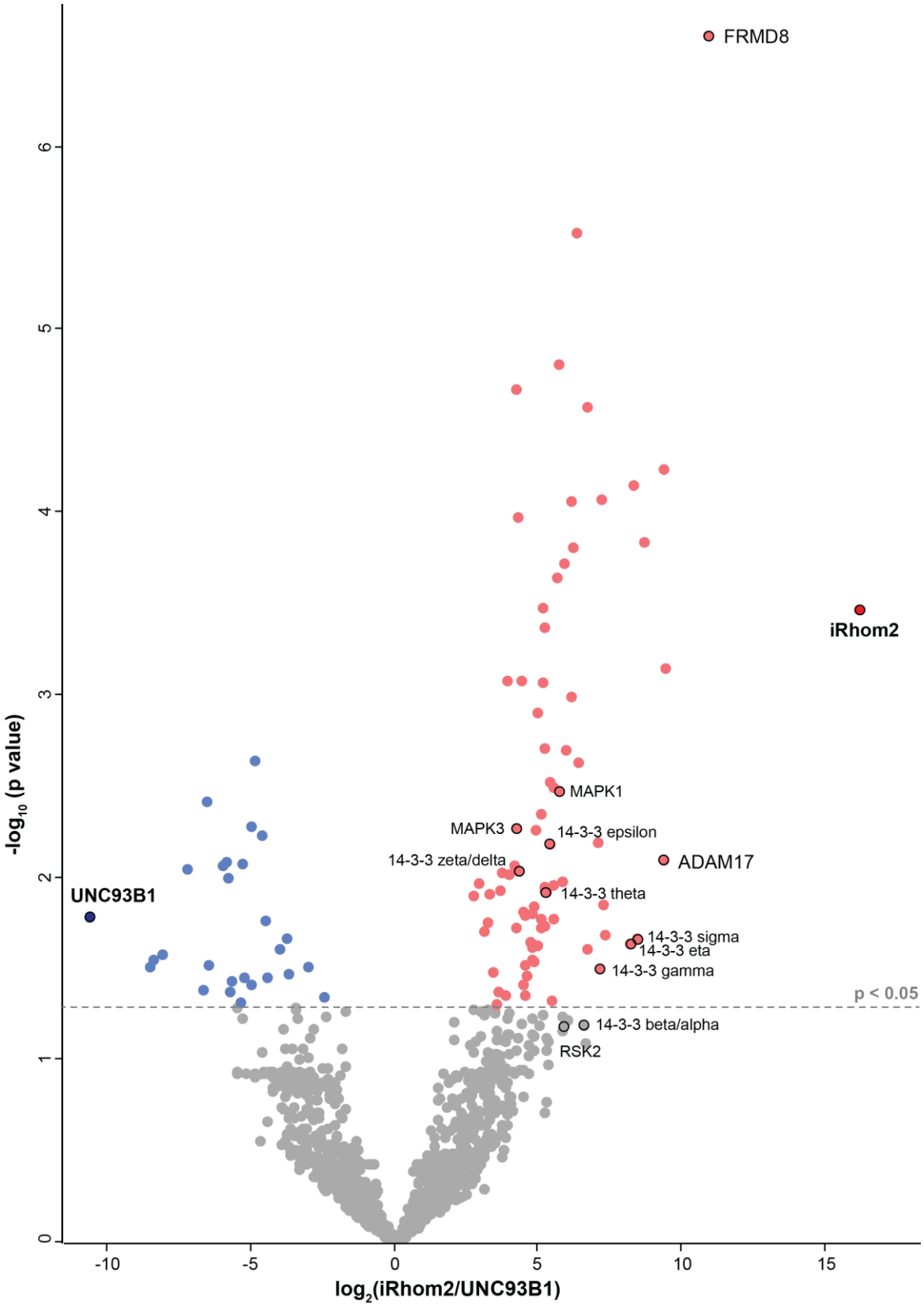


Figure 3.5 | Identification of potential iRhom2 interaction partners by mass spectrometry. The Volcano blot shows the enrichment in the iRhom2^{WT} co-IP compared to the control IP (UNC93B1) on the x-axis, whereas the statistical significance of each hit is plotted on the y-axis. Statistical analysis was performed with Perseus by Dr Monika Stegmann as described in 2.3.1.4.

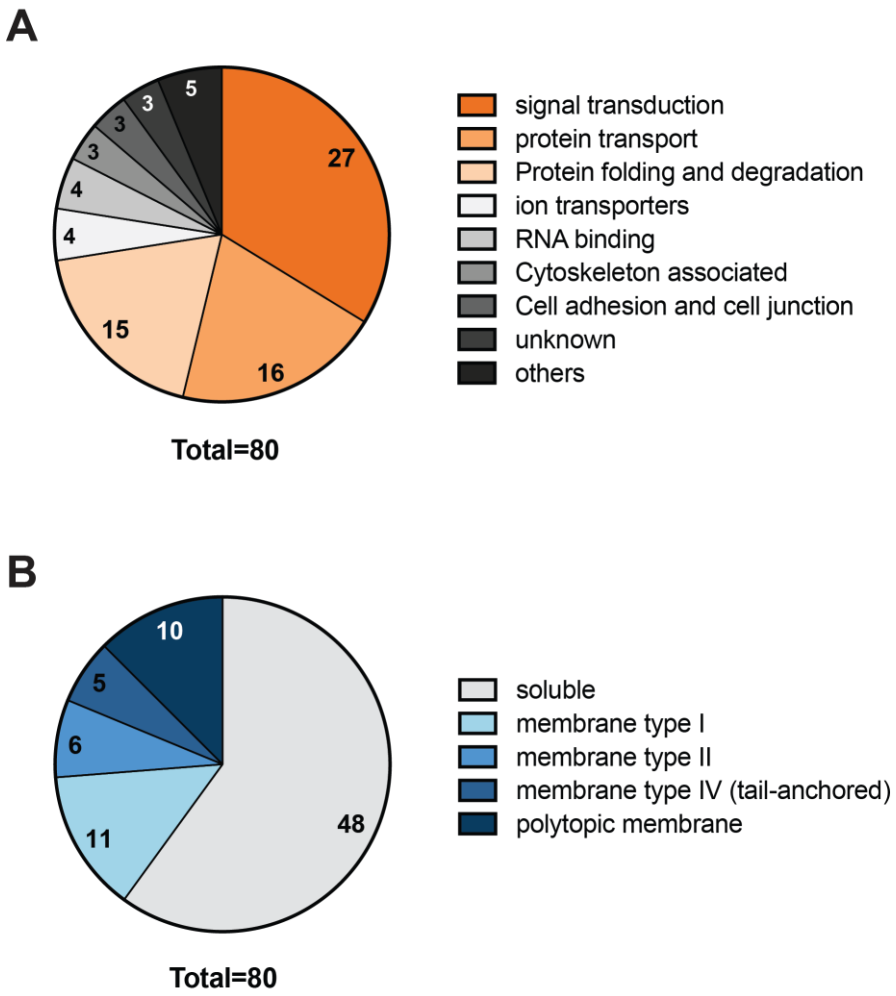


Figure 3.6 | Mass spectrometry hits for iRhom2^{WT} are linked to signal transduction, protein transport or protein folding and degradation. A) Grouping of identified mass spectrometry hits for iRhom2^{WT} according to their predicted topology based on the UniProt database (www.uniprot.org). **B) I**dentified mass spectrometry hits for iRhom2 were grouped according to the biological processes GO term indicated in the UniProt database. Each protein was only grouped into one category.

Further analysing the mass spectrometry hits, I found that the majority (60%) of the 80 significant iRhom2^{WT} hits were soluble proteins (Fig. 3.6B). Most of the soluble mass spectrometry hits are proteins localised in the cytoplasm (39 out of 48 proteins), which either suggests either that the majority of interactions happens through the cytosolic N-terminus of iRhoms or that soluble proteins were easier to detect in this screen. To further investigate the potential cytosolic interaction partners, I performed mass spectrometry analysis using truncated iRhom2 versions. iRhom2$^{\Delta IRHD}$ and the N-terminally truncated

iRhom2$^{\Delta382}$ (Fig. 3.4A) served as additional controls for the iRhom2^{WT} co-IP by testing whether identified interaction partners bound specifically to the N-terminus or to the IRHD of iRhom2. I found that several cytosolic proteins, such as FRMD8, 14-3-3 proteins, ribosomal protein S6 kinase alpha-3 (RSK2), MAPK1, and MAPK3, were specifically reduced or lost in the iRhom2$^{\Delta382}$ co-IP compared to iRhom2^{WT} (Table 3.2). However, these cytosolic proteins were still able to bind to iRhom2$^{\Delta IRHD}$ (Table 3.2), demonstrating specificity of these proteins for the iRhom2 N-terminus.

Table 3.2 | Validation of the cytosolic hits of the iRhom2^{WT} mass spectrometry screen using truncated iRhom2 constructs. The binding of candidate interactors to iRhom2$^{\Delta382}$ and iRhom2$^{\Delta IRHD}$ was investigated in one experiment using HEK293T cells stably expressing human iRhom2^{WT}, iRhom2$^{\Delta382}$, iRhom2$^{\Delta IRHD}$ or UNC93B1. Mass spectrometry analysis was performed using SINQ analysis (Trudgian et al., 2011) and the ratio of the spectral index in the iRhom2 mutant to iRhom2^{WT} is indicated in brackets. A ratio below 0.33 was considered no binding (No), a ratio above 0.33 was considered as an interaction (Yes).

Prot. ID	Protein name	Gene	iRhom2$^{\Delta382}$ binding (ratio $^{\Delta382}/_{WT}$)	iRhom2$^{\Delta IRHD}$ binding (ratio $^{\Delta IRHD}/_{WT}$)
P78536	ADAM17	ADAM17	Yes (0.43)	No (0.07)
Q9BZ67	FRMD8	FRMD8	No (0.00)	Yes (0.89)
P31947	14-3-3 protein sigma	SFN	No (0.00)	Yes (0.58)
P62258	14-3-3 protein epsilon	YWHAE	No (0.04)	Yes (1.28)
P61981	14-3-3 protein gamma	YWHAG	No (0.03)	Yes (0.71)
Q04917	14-3-3 protein eta	YWHAH	No (0.10)	Yes (0.58)
P27348	14-3-3 protein theta	YWHAQ	No (0.05)	Yes (1.45)
P63104	14-3-3 protein zeta/delta	YWHAZ	---	Yes (0.81)
P31946	14-3-3 protein alpha/beta	YWHAB	No (0.03)	Yes (0.60)
P28482	MAPK1	MAPK1	No (0.00)	Yes (1.72)
P27361	MAPK3*	MAPK3	No (0.00)	Yes (1.74)
P51812	RSK2	RPS6KA3	No (0.00)	Yes (1.42)
O00629	Importin subunit alpha-3	KPNA4	No (0.00)	Yes (2.59)
Q96P70	Importin-9	IPO9	Yes (0.87)	Yes (2.39)

*only identified with iRhom2

Interestingly, when analysing the binding of ADAM17 to iRhom2$^{\Delta 382}$ and iRhom2$^{\Delta IRHD}$ by mass spectrometry, I found that ADAM17 was still detected in the iRhom2$^{\Delta 382}$ co-IP (although it was slightly reduced in this sample), but it was drastically reduced in iRhom2$^{\Delta IRHD}$ samples (Table 3.2), suggesting that the IRHD is required for the interaction between iRhom2 and ADAM17. Consistent with my findings, it was recently shown that binding of mouse iRhom2$^{\Delta IRHD}$ to mature and proADAM17 was impaired, while N-terminally truncated mouse iRhom2 was still able to bind proADAM17 but not mature ADAM17 (Grieve et al., 2017).

In summary, I identified potential new iRhom2 interaction partners using a mass spectrometry-based screen. It is necessary to validate these hits to exclude false positives. The use of the truncated iRhom2 constructs for mass spectrometry provided preliminary data about the specificity of potential cytosolic interactors and showed that the top candidate from the screen, FRMD8, specifically interacts with the iRhom2 N-terminus. Therefore, FRMD8 seems a promising candidate to pursue.

3.2.4 Validation of the FRMD8-iRhom interaction

FRMD8, the top hit of my mass spectrometry screen (Fig. 3.5), was further investigated using western blot and co-localisation studies. I cloned a C-terminally V5-tagged construct of human FRMD8 (FRMD8-V5) and co-expressed it with human iRhom1-3xHA and iRhom2-3xHA. FRMD8 was co-immunoprecipitated specifically with iRhom1 and iRhom2, and vice versa (Fig. 3.7A), proving that FRMD8 was not an artefact of the mass spectrometry screen, and that it interacts both with iRhom1 and iRhom2. In addition, I also detected an interaction of iRhom2-3xHA with endogenous FRMD8 using an FRMD8-specific antibody (Fig. 3.7B). The specificity of the FRMD8 antibody was confirmed in FRMD8 KO cells (Fig. A2, Appendix).

To better understand the nature of the FRMD8-iRhom interaction, I tested which part of FRMD8 is required to bind to iRhom2. Unlike most FERM domain-containing proteins, which contain several domains in addition to the FERM domain (Pearson et al., 2000,

Moleirinho et al., 2013), there are no additional domains predicted for FRMD8. The only significant part of FRMD8 outside of its FERM domain is an 88-amino acid long C-terminus. I deleted the C-terminus of FRMD8 (Fig. 3.8A) to test whether this region affects the binding to iRhom2. The C-terminally truncated FRMD8 (FRMD8$^{\Delta C}$) was still able to bind to iRhom2 (Fig. 3.8B) demonstrating that the C-terminus of FRMD8 is not required for the interaction with iRhom2. This implies that the interaction depends on the N-terminus of FRMD8, which contains the FERM domain.

Using immunofluorescence, I further investigated where in the cell the interaction between iRhoms and FRMD8 occurs. FRMD8 showed a cytosolic localisation and was also present at the plasma membrane (Fig. 3.9) consistent with a previous report (Kategaya et al., 2009). FRMD8 and iRhom2 partially co-localised at sites which are likely to be the early secretory pathway (Fig. 3.9) because, as seen in Figure 3.4B, iRhom2 mainly localises to the ER.

Taken these findings together, FRMD8 is a novel iRhom interaction partner identified in my mass spectrometry screen. FRMD8 binds both to iRhom1 and iRhom2 and partially co-localises with iRhom2 in the cell.

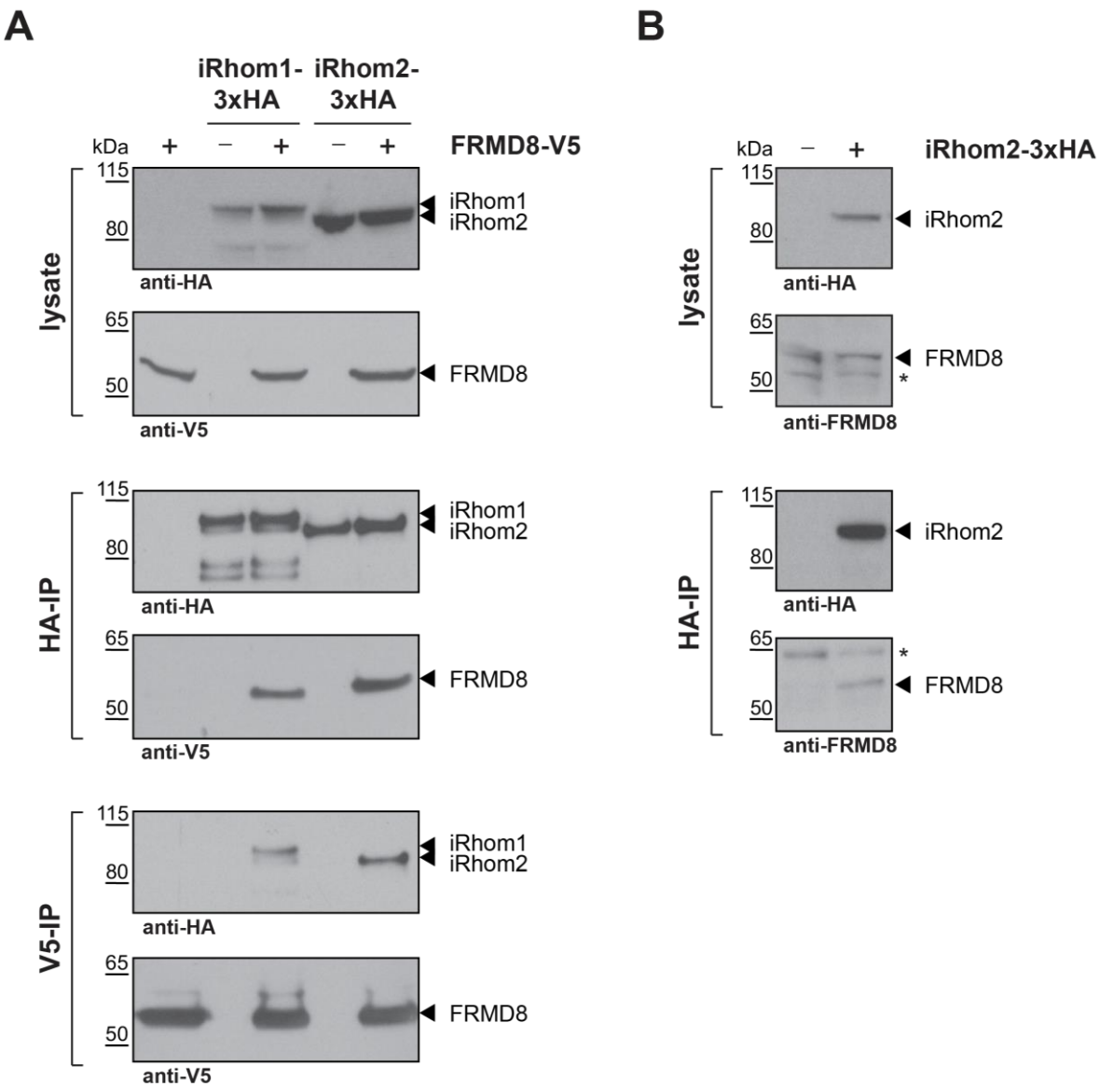


Figure 3.7 | FRMD8 co-immunoprecipitates with iRhom1 and iRhom2. A) Western blot of HEK293T cells stably expressing human iRhom1-3xHA or iRhom2-3xHA transfected with human FRMD8-V5 (where indicated) and subjected to anti-HA and anti-V5 immunoprecipitation (HA-IP, V5-IP), after anti-HA and anti-V5 staining. One representative western blot out of four independent experiments is shown. **B)** Western blot of lysates and anti-HA IP from wild-type HEK293T and HEK293T cells stably expressing iRhom2-HA, after anti-HA and anti-FRMD8 staining. An asterisk (*) indicates nonspecific bands detected by the FRMD8 antibody. One representative western blot out of three independent experiments is shown.

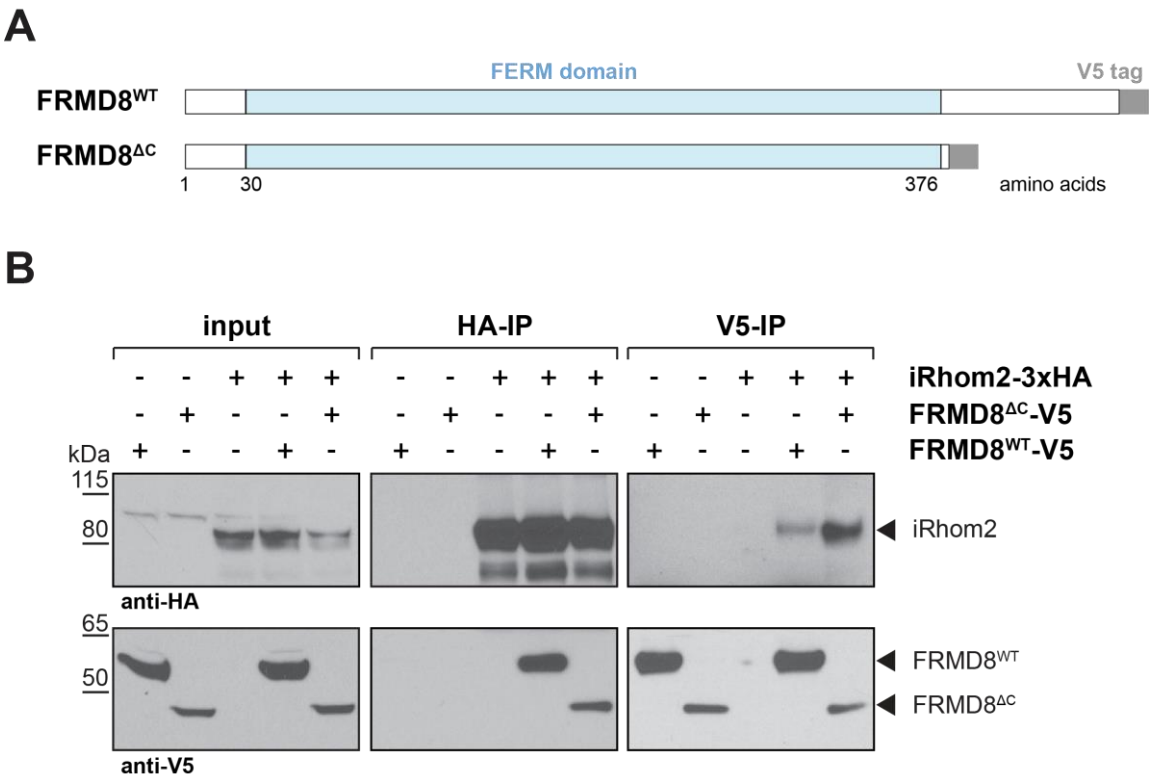


Figure 3.8 | FRMD8 binds to iRhom2 through its FERM domain. A) Schematic representation of the V5-tagged full-length and C-terminally truncated human FRMD8 constructs (FRMD8^{WT}-V5, FRMD8$^{\Delta C}$-V5). **B)** Western blot of lysates, anti-HA and anti-V5 immunoprecipitation (input, HA-IP, V5-IP) of HEK293T cells co-expressing human iRhom2-3xHA with human FRMD8^{WT}-V5 or FRMD8$^{\Delta C}$-V5, after anti-HA or anti-V5 staining. One representative western blot out of three independent experiments is shown.

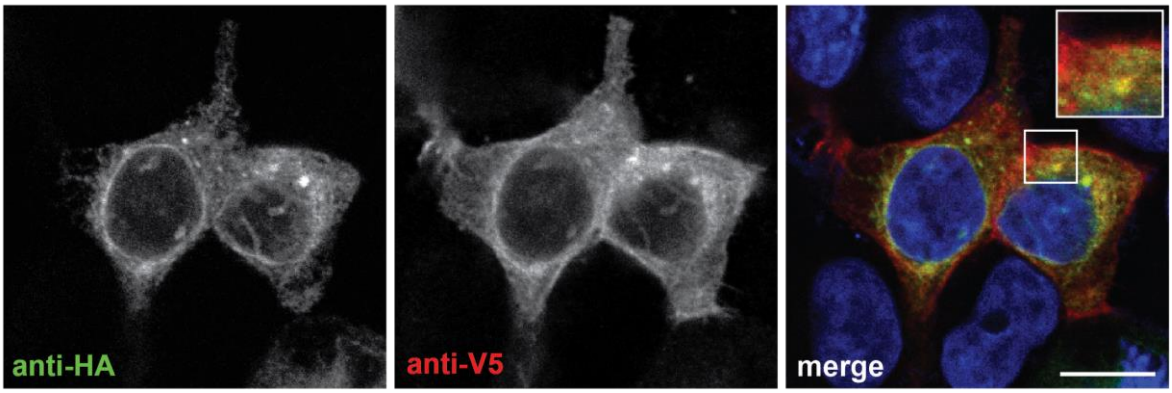


Figure 3.9 | FRMD8 localises to the cytosol and plasma membrane. Immunofluorescence microscopy of MCF-7 cells transfected with iRhom2-3xHA and FRMD8-V5 and stained with anti-HA antibody (green), anti-V5 antibody (red) and DAPI for DNA (blue). Regions of iRhom2 and FRMD8 colocalisation have been magnified. The white scale bar represents 10 µm.

3.3 Discussion

3.3.1 Identification of novel cytosolic interaction partners of iRhoms

Here, I showed the identification of FRMD8 as a new interaction partner of human iRhom1 and iRhom2. This poorly studied protein, about which nothing has been reported other than having been suggested to inhibit Wnt signalling in *Drosophila*, zebrafish, and humans (Kategaya et al., 2009), was the top hit of a mass spectrometry-based approach to identify potential novel interaction partners of human iRhoms. FRMD8 is localised in the cytosol and presumably binds to the N-terminus of iRhoms. In subsequent chapters I will describe further experiments to elucidate the role of this largely uncharacterised protein, and to investigate the cellular function of its interaction with iRhoms.

14-3-3 proteins, which have also been identified as hits in my mass spectrometry screen, were confirmed as iRhom2 interaction partners in mouse embryonic fibroblasts by my colleague Dr Hongmei Xu. She found that several 14-3-3 proteins (gamma, epsilon, eta, tau, zeta) are recruited to three different sites in the iRhom2 N-terminus upon PMA-stimulated iRhom2 phosphorylation. The recruitment of 14-3-3 alters the interaction of iRhom2 and mature ADAM17 at the plasma membrane and allows ADAM17 to cleave its substrates (Grieve et al., 2017). My screen was performed under basal conditions but, even without stimulation, I found that both iRhom1 and iRhom2 can be phosphorylated (Table A2, Appendix), explaining why I was able to detect 14-3-3 binding.

The kinases MAPK1 and MAPK3 were shown to be required for phosphorylation of iRhom2 and 14-3-3 recruitment (Grieve et al., 2017). The fact that MAPK1/3 were identified in my screen as interactors of iRhom2 suggests that MAPK1/3 might phosphorylate iRhom1 and iRhom2 directly. Further supporting this idea, both MAPK1 and MAPK3 were predicted by the software Scansite3 (Obenauer et al., 2003) to have binding sites within the N-terminus of human iRhom2, and MAPK1 sites within the human iRhom1 N-terminus. Another kinase identified in my screen, RSK2, might be a negative regulator of ADAM17-dependent shedding because RSK inhibition resulted in an increase in shedding of the ADAM17 substrate AREG (Grieve et al., 2017). Its role in

phosphorylating iRhoms has not been further investigated, but it is possible that it binds the iRhom N-terminus and phosphorylates either iRhoms or iRhom interaction partners.

In conclusion, the mass spectrometry-based screen identified 80 statistically significant hits for iRhom2^{WT}, which are mainly linked to signal transduction, protein transport, or protein folding and degradation. While several hits linked to signal transduction have been confirmed and followed up, future experiments will have to validate untested candidates involved in protein transport, folding, and degradation.

3.3.2 A role for the iRhom N-terminus in the nucleus?

The mass spectrometry screen identified a few significant candidates that are linked to nuclear import (Fig. 3.6A), which were mainly different importin proteins (Table A1, Appendix). This finding could be linked to the observed nuclear localisation of the C-terminally truncated iRhom2 constructs (Fig. 3.4B). Considering that both iRhoms have several potential NLS (Fig. A1, Appendix), it is likely that the generated truncated versions, which were supposed to be single-pass TMD constructs, were not properly integrated into the ER membrane and therefore became localised to the nucleus. Whether that phenomenon is biologically relevant is unclear. Interestingly, tagged iRhom1 and iRhom2 have been observed in many studies to appear in two versions - a full-length and an approximately 50 kDa version (Nakagawa et al., 2005, Adrain et al., 2012, Maney et al., 2015). The latter was suggested to result from proteolytic cleavage of the full-length version (Nakagawa et al., 2005), and corresponds in size approximately to the C-terminally truncated iRhom versions used in this study. For this reason, it can be speculated that C-terminally truncated iRhoms also exist in cells and might also translocate into the nucleus. Further work has to be done to prove the existence of truncated iRhoms, preferably on endogenous levels, as well as their cellular localisation and their physiological relevance.

CHAPTER 4

Investigating FRMD8 function within the iRhom/ADAM17 pathway

4 Investigating FRMD8 function within the iRhom/ADAM17 pathway

4.1 Introduction

Among the different cellular functions described of iRhoms, their role in the regulation of the metalloprotease ADAM17 is the best characterised and has been assessed in various cell types in mouse and human. iRhoms regulate ADAM17 activity at multiple levels: first, iRhoms are required for the ER-to-Golgi trafficking of proADAM17, consequently allowing the generation of mature ADAM17 in the Golgi (Adrain et al., 2012, McIlwain et al., 2012). Second, iRhoms also regulate the shedding activity of ADAM17 at the plasma membrane, which requires the phosphorylation of the iRhom2 N-terminus (Grieve et al., 2017). Finally, the N-terminus of iRhom2 is required to stabilise mature ADAM17 at the cell surface and protect it from lysosomal degradation (Grieve et al., 2017), although mechanistic details are not understood.

Several studies have stressed the important role of the cytosolic N-terminus of iRhoms in regulating ADAM17-dependent shedding (Brooke et al., 2014, Maney et al., 2015, Grieve et al., 2017), but the N-terminus might also play a role in iRhom stability and localisation: truncations in the iRhom2 N-terminus showed elevated levels of iRhom2 at the cell surface (Maney et al., 2015) and were suggested to increase iRhom2 stability (Hosur et al., 2014). Despite these observations, mechanistic understanding of how the iRhom N-terminus affects stability, localisation, and ADAM17 shedding activity are lacking. It is possible that cytosolic interaction partners of iRhoms play an important role in all the described effects of the N-terminus.

FRMD8 is a novel interaction partner of iRhoms identified in this study. FRMD8 was initially discovered in a *Drosophila* screen aiming to identify inhibitors of canonical Wnt signalling (Kategaya et al., 2009). Kategaya and colleagues (2009) suggested that FRMD8 binds to the Wnt cell surface receptor LRP6 to attenuate the interaction of LRP6 with the downstream protein axin. This led to impaired activation of β-catenin and ultimately reduced canonical Wnt signalling. The inhibitory role of FRMD8 in Wnt

signalling was described in *Drosophila*, zebrafish and human cells (Kategaya et al., 2009), however, there is currently no mechanistic insight into FRMD8 function. There have not been any other reports describing FRMD8 protein function, therefore, the cellular role of FRMD8 is largely unknown.

Having identified FRMD8 as a new cytosolic interaction partner of iRhom1 and iRhom2, my main aim was to assess whether FRMD8 has a role in iRhom function. To address this question, I focused on the well-characterised role of iRhoms in regulating ADAM17 activity. I studied effects on the iRhom/ADAM17 pathway in FRMD8-deficient cells generated either using RNAi or CRISPR/Cas9. The CRISPR/Cas9 technique enables targeted changes in the genome (Jinek et al., 2012) and was also used in this project to generate a cell line with endogenously tagged iRhom2, which allowed me to investigate the effect of FRMD8 on endogenous iRhom2. Furthermore, I aimed to further validate and characterise the binding of FRMD8 to the iRhom2 N-terminus that was indicated by the mass spectrometry data (Table 3.2). Considering that the iRhom2 N-terminus is an important site of phosphorylation, I also addressed the role of phosphorylation for the FRMD8-iRhom interaction.

4.2 Results

4.2.1 FRMD8 knockdown reduces mature ADAM17 levels

Loss of mammalian iRhom function can be analysed by assessing mature ADAM17 levels, which are reduced or lost in iRhom-deficient cells (Adrain et al., 2012, McIlwain et al., 2012, Christova et al., 2013). To analyse whether FRMD8 affects the iRhom/ADAM17 pathway, I knocked down FRMD8 in HEK293T cells and analysed ADAM17 levels by western blot. FRMD8 loss resulted in significantly reduced levels of mature ADAM17, whereas the levels of proADAM17 were unchanged (Fig. 4.1A). FRMD8 siRNA reduced the levels of FRMD8 mRNA by 80% (Fig. 4.1B) proving the successful knockdown of FRMD8. The levels of ADAM17 mRNA were unaffected by the knockdown of FRMD8 (Fig. 4.1B), implying that the reduction of mature ADAM17 protein levels in FRMD8 knockdown cells was not caused by a change in ADAM17 transcription.

As an additional approach to assaying ADAM17 function, I analysed the release of ADAM17 substrates from FRMD8 knockdown cells by transfecting cells with the alkaline phosphatase (AP)-tagged ADAM17 substrates AREG, TGFα, and HB-EGF. Phorbol 12-myristate 13-acetate (PMA) treatment activates ADAM17 shedding activity and stimulates the release of ADAM17 substrates (Sahin et al., 2004, Horiuchi et al., 2007b). However, HEK293T cells transfected with FRMD8 siRNA secreted significantly less AP-AREG, AP-TGFα and AP-HB-EGF under unstimulated and PMA-stimulated conditions, compared to cells transfected with non-targeting control siRNA (Fig. 4.2A-C). EGF, which is shed by ADAM10 but not by ADAM17 (Sahin et al., 2004), served as a control for the specificity of FRMD8. There was no difference in the release of AP-EGF from control and FRMD8 knockdown cells (Fig. 4.2D), implying that FRMD8 does not affect ADAM10 function. ADAM10 activity is not inducible by PMA (Sahin et al., 2004), therefore, the release of AP-EGF was, unlike ADAM17-dependent substrates (Fig. 2A-C), not increased after PMA stimulation.

In conclusion, these results show that FRMD8 loss led to reduced mature ADAM17 levels and consequently reduced release of ADAM17 substrates under stimulated and

unstimulated conditions. However, ADAM10-dependent shedding was not affected by FRMD8 knockdown, suggesting that FRMD8 regulates the iRhom/ADAM17 pathway specifically.

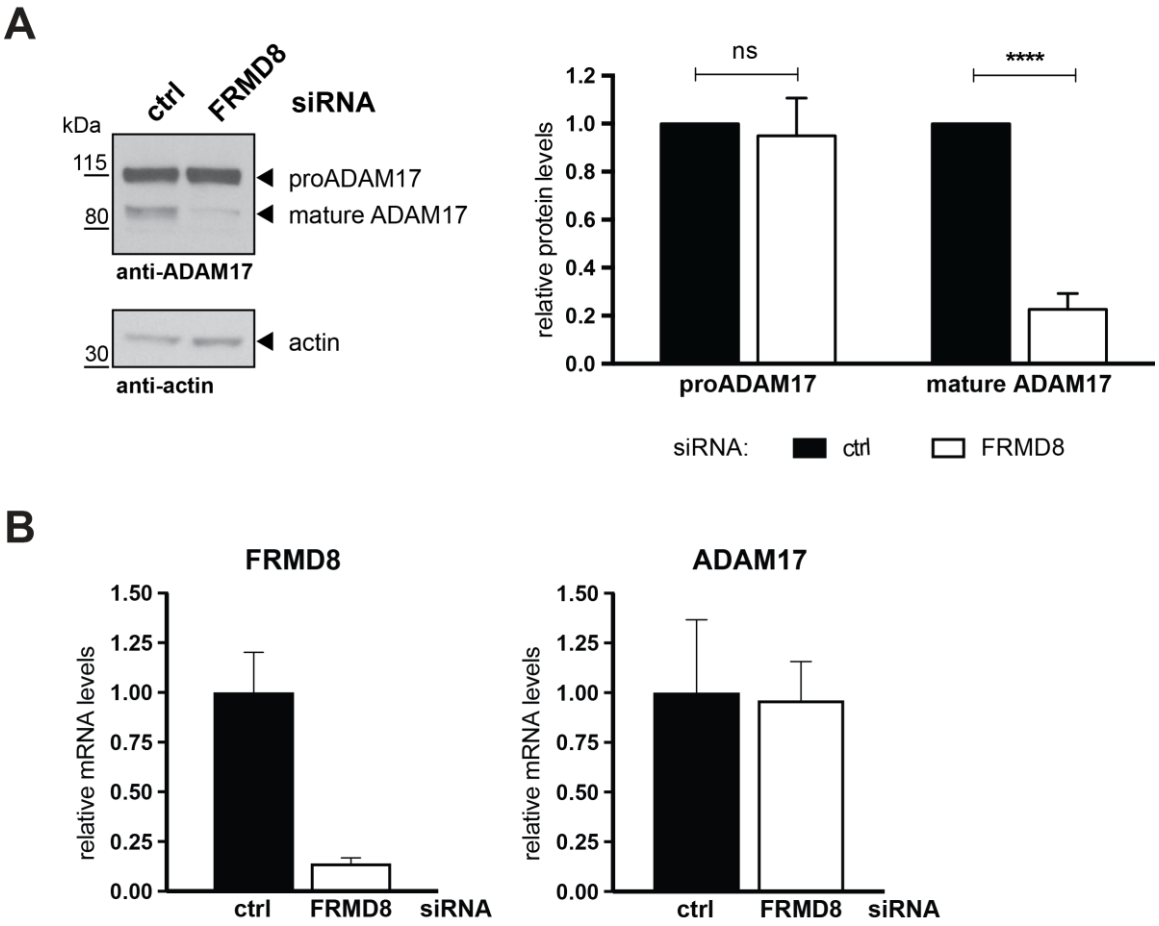


Figure 4.1 | FRMD8 knockdown reduces mature ADAM17 levels. A) Western blot of HEK293T cell lysates transfected with non-targeting siRNA control pool (ctrl) or FRMD8 pre-designed SMARTpool siRNA, after anti-ADAM17 and anti-actin staining. One representative western blot out of four independent experiments is shown. ADAM17 protein levels were quantified from western blots of four independent experiments and normalised to actin controls using ImageJ. Statistical analysis was performed using an unpaired t-test (n=4); ns = p value > 0.05; **** = p value < 0.0001. **B)** mRNA levels of FRMD8 and ADAM17 relative to actin levels determined by TaqMan PCR.

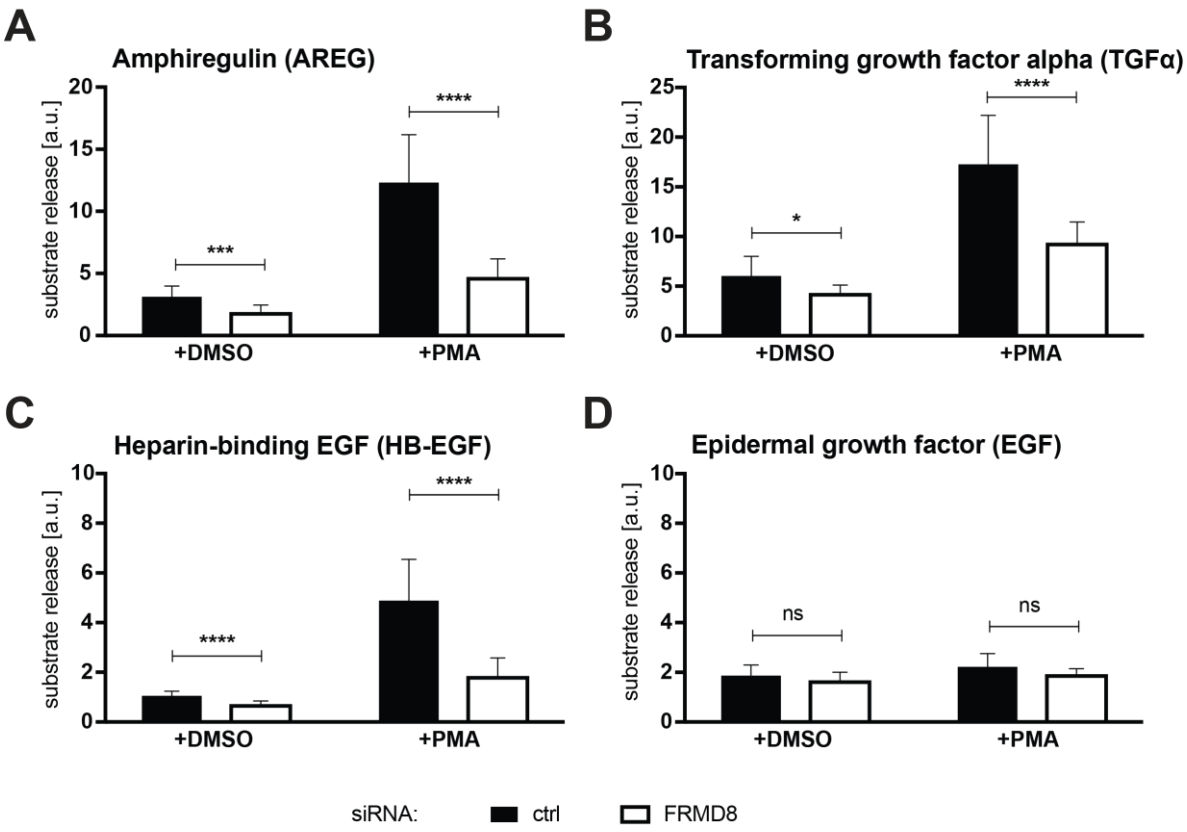


Figure 4.2 | FRMD8 knockdown reduces release of ADAM17 substrates. A) - D) HEK293T cells were transfected with non-targeting siRNA control pool (ctrl) or FRMD8 pre-designed SMARTpool siRNA as well as with AP-AREG, AP-TGFα, AP-HB-EGF, and AP-EGF. Cells were stimulated with 200 nM PMA for 30 min and supernatants were collected and AP activity measured. The substrate release was calculated by dividing the AP activity in the supernatant by the sum of AP activity in the lysate and the supernatant. Experiments were performed in biological triplicates. The results of four independent experiments are shown. Statistical analysis was performed on n=12 (combining three replicates from four independent experiments) using an unpaired, non-parametric test (Mann-Whitney test); ns = p value > 0.05; * = p value < 0.05; *** = p value < 0.001; **** = p value < 0.0001.

4.2.2 FRMD8 KO cells generated by CRISPR/Cas9 show reduced ADAM17 shedding activity

To examine further the role of FRMD8 in the iRhom/ADAM17 pathway, I generated FRMD8 KO HEK293T cell lines by CRISPR/Cas9 genome editing. As potential splice variants of *FRMD8* exist (Yates et al., 2016), which lack either exon 3 or exon 4 (Fig. A3A, Appendix), only exons 5 to 8 were considered as target sites for sgRNAs to knockout all three *FRMD8* isoforms. Two sgRNAs targeting exon 6 and exon 7 (Fig. 4.3A) were

designed and cloned by Andrew Bassett from the local facility, Genome Engineering Oxford. The two clonal FRMD8 KO cell lines, which I generated using either of the sgRNAs, showed a loss of FRMD8 protein expression and a strong reduction of mature ADAM17 levels (Fig. 4.3B). I also analysed the FRMD8 mRNA levels in both cell lines to examine if the FRMD8 mRNA was degraded by nonsense-mediated decay (NMD) (Popp and Maquat, 2016), as would be expected. FRMD8 mRNA levels were only reduced in the cell line in which exon 7 had been targeted (Fig. 4.3C). As the FRMD8 mRNA in the other FRMD8 KO cell line (targeting exon 6) was not reduced, it is probably not degraded by NMD. Therefore, it is possible that a truncated FRMD8 protein is generated in this cell line, which is either unstable or hard to detect by western blot with the FRMD8 antibody. For this reason, I continued to work only with the FRMD8 KO cell line in which exon 7 had been targeted (hereafter simply named “FRMD8 KO”) and which showed both loss of mRNA and protein. When I sequenced the genomic DNA from the FRMD8 KO cell line, I detected a 2-nt deletion in exon 7 of the FRMD8 gene (Fig. A3B, Appendix), which resulted a premature stop codon at amino acid 273 (Fig. A3C, Appendix).

FRMD8 KO cells showed 75% reduction of mature ADAM17 levels, which was similar to the observations in FRMD8 knockdown cells (Fig. 4.1A). As with the knockdown, the levels of mature ADAM10 were not affected by FRMD8 loss (Fig. 4.4A), demonstrating FRMD8 specificity for ADAM17. The reduced levels of mature ADAM17 in FRMD8 KO cells were rescued by expressing FRMD8-V5 in FRMD8 KO cells (Fig. 4.4B), proving that the reduction of mature ADAM17 levels is specifically caused by the loss of FRMD8. However, the expression of the C-terminally truncated FRMD8$^{\Delta C}$ (Fig. 3.8A) did not fully rescue the levels of mature ADAM17 (Fig. 4.4B), although I had shown that it was still able to bind to iRhom2 (Fig. 3.8B). This implies that binding alone of FRMD8 to iRhom2 is not sufficient for its function, and that the FRMD8 C-terminus is required for the role of FRMD8 in the iRhom/ADAM17 pathway.

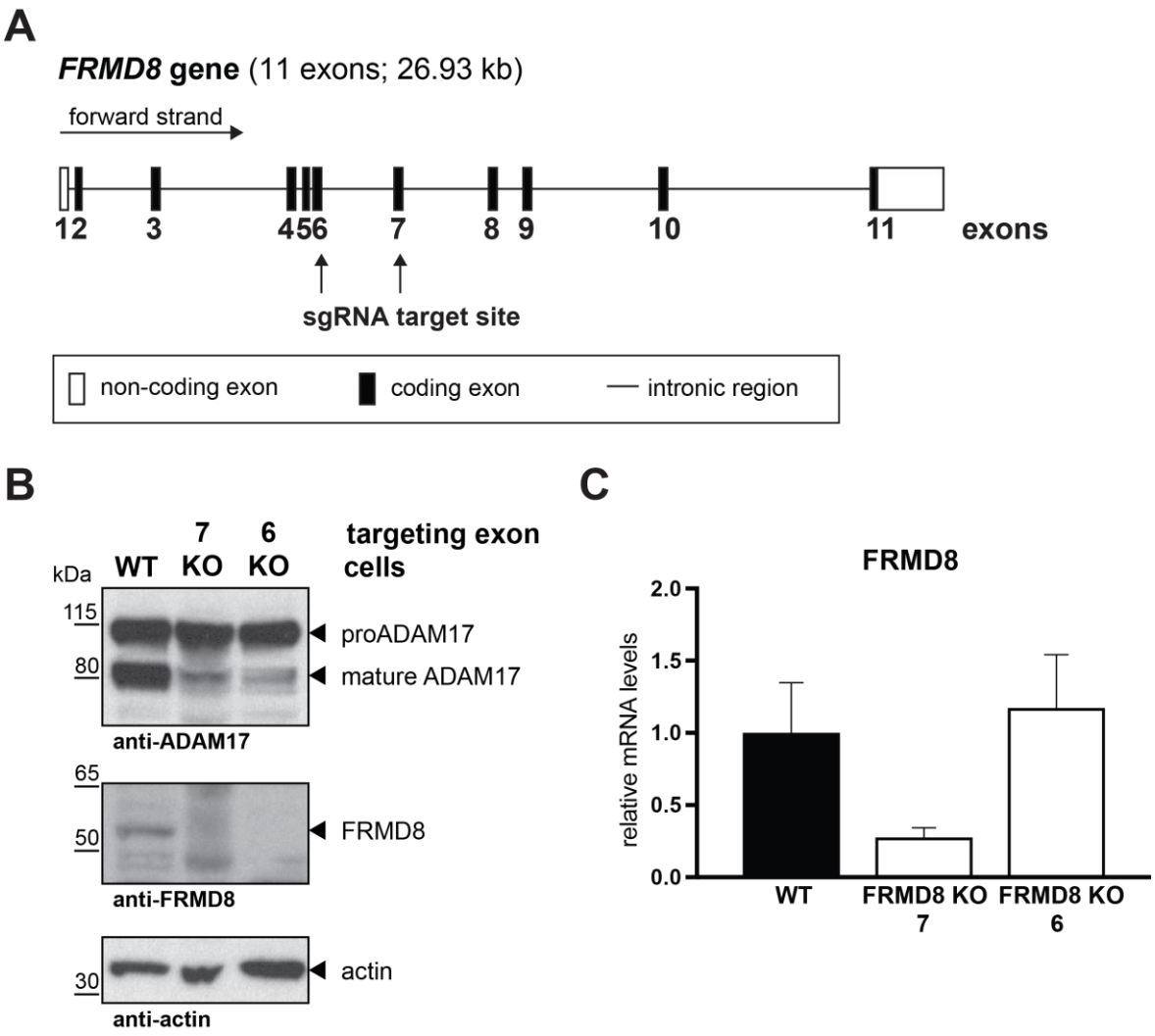


Figure 4.3 | Generation of FRMD8 KO cells using CRISPR/Cas9 genome editing. A) Map of FRMD8 gene based on the Ensembl genome browser (Yates et al., 2016). **B)** Western blot of wild-type (WT) HEK293T and FRMD8 KO cell lysates after anti-ADAM17, anti-FRMD8 and anti-actin staining. **C)** FRMD8 mRNA relative to actin mRNA levels analysed by TaqMan PCR in WT and FRMD8 KO cell lines.

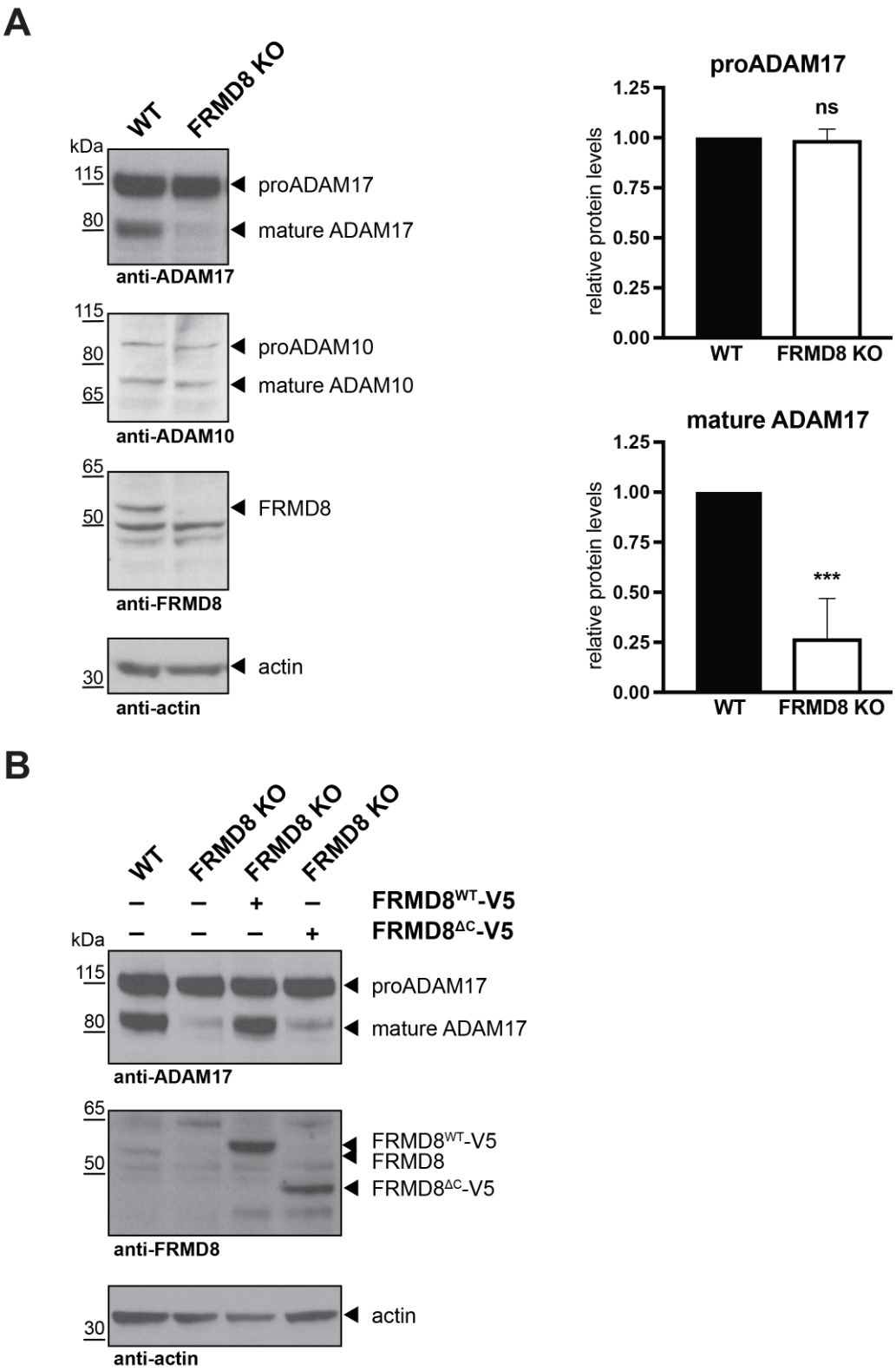


Figure 4.4 | FRMD8 KO specifically reduces mature ADAM17 levels. A) Western blot of wild-type (WT) HEK293T and FRMD8 KO cell lysates probed for endogenous ADAM17, ADAM10, FRMD8 and actin. Protein levels were quantified from western blots were normalised to actin (n=3). Statistical analysis was performed using an unpaired t-test; ns = p value > 0.05; *** = p value < 0.001. **B)** Western blot of wild-type (WT) HEK293T and FRMD8 KO cells transiently transfected with $FRMD8^{WT}$-V5 and $FRMD8^{\Delta C}$-V5 (where indicated), after anti-ADAM17, anti-FRMD8 or anti-actin staining. One representative western blot out of three independent experiments is shown.

To confirm the requirement of FRMD8 for the production of mature ADAM17 with a second, independent approach, I examined the cell surface levels of endogenous ADAM17 using flow cytometry. ADAM17 cell surface levels were significantly reduced in FRMD8 KO cells, whereas the cell surface levels of ADAM10 were not affected (Fig. 4.5). This confirms that the FRMD8 specifically regulates ADAM17 but not ADAM10, further demonstrating that FRMD8 is not a general trafficking factor for metalloproteases.

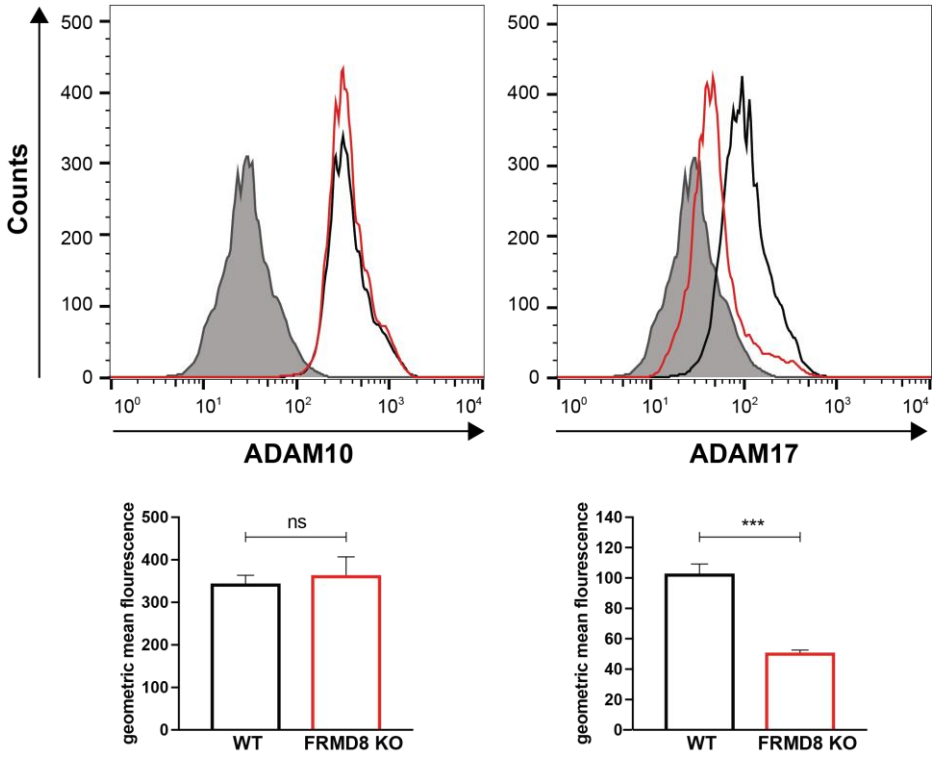


Figure 4.5 | FRMD8 KO reduces cell surface levels of ADAM17. Flow cytometry analysis of wild-type (WT) HEK293T and FRMD8 KO cells after stimulation with 200 nM PMA for 5 min. Unpermeabilised cells were stained on ice for endogenous ADAM10 and ADAM17, or with secondary antibody only as a control (grey). The shown flow cytometry graph is one representative experiment out of four independent experiments. Statistical analysis was performed using an unpaired t-test (n=4); ns = p value > 0.05; *** = p value < 0.001.

To study the release of ADAM17 substrates in FRMD8 KO cells, I analysed the shedding of AP-tagged EGFR ligands in FRMD8 KO cells. As in FRMD8 knockdown cells (Fig. 4.2A, C), the release of AP-AREG and AP-HB-EGF from FRMD8 KO was reduced after stimulation of cells with PMA (Fig. 4.6A). Stimulation with PMA and simultaneous

inhibition of ADAM10 and ADAM17 with GW280264X (GW) (Hundhausen et al., 2003), eliminated shedding in wild-type and FRMD8 KO cells, implying that the release of AP-tagged EGFR ligands was caused by ADAM17-dependent proteolysis. To exclude the possibility that FRMD8 KO cells are unable to correspond to PMA-induced stimulation of ADAM17, I also analysed unstimulated, constitutive shedding. FRMD8 KO cells released significantly less AP-TGFα compared to wild-type cells after 20 h of constitutive shedding (Fig. 4.6B), showing that FRMD8 loss also leads to a defect in ADAM17-dependent shedding under unstimulated conditions. Furthermore, the treatment with the ADAM10/17 inhibitor GW for 20 h blocked shedding of AP-TGFα in wild-type and FRMD8 KO cells, which verifies that the observed release of AP-TGFα was caused by ADAM17-dependent shedding and not leakage of AP-TGFα from apoptotic cells. PMA-stimulated shedding of AP-TGFα after PMA treatment was significantly reduced in FRMD8 KO cells as seen before for AP-AREG and AP-HB-EGF (Fig. 4.6A).

In summary, FRMD8 KO cells showed a significant reduction in the release of ADAM17 substrates from cells due to reduced levels of mature ADAM17 in the cell and at the cell surface. The maturation and levels of the related metalloprotease ADAM10 were not changed in FRMD8 KO cells, indicating that FRMD8 is a specific regulator of the iRhom/ADAM17 pathway rather than a general trafficking factor, although that does not exclude other cellular roles of FRMD8.

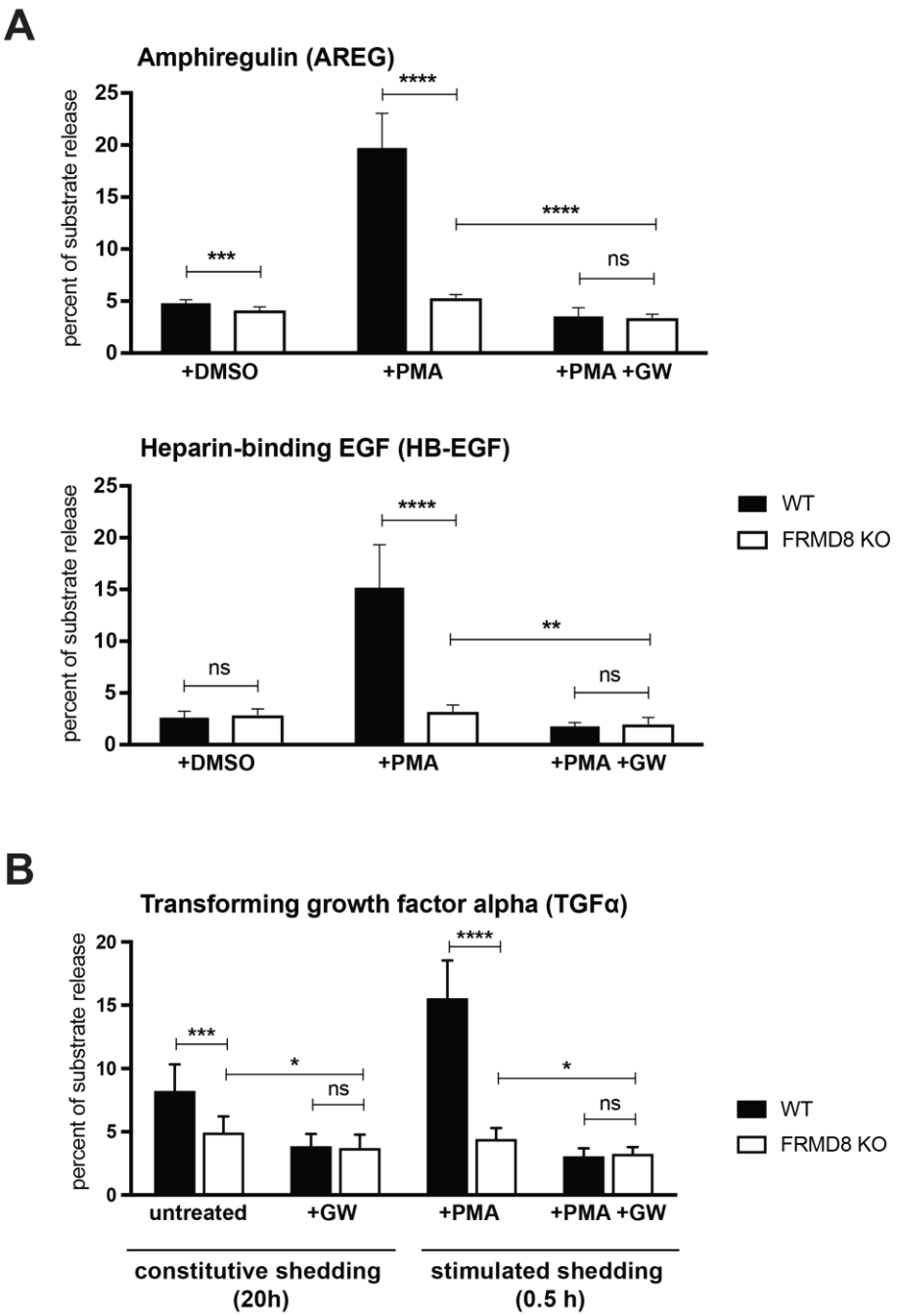


Figure 4.6 | FRMD8 KO reduces constitutive and stimulated shedding of ADAM17 substrates. A) - B) HEK293T cells transfected with AP-tagged AREG, HB-EGF or TGFα were either incubated with 200 nM PMA, with 200 nM PMA and 1 µM GW (ADAM10/ADAM17 inhibitor), or with DMSO for 30 min. In addition, cells transfected with AP-TGFα were either left unstimulated for 20 h or incubated with 1 µM GW for 20 h. Each experiment was performed in biological triplicates. The results of three independent shedding experiments are shown. Statistical analysis was performed on n=9 (combining three replicates from three independent experiments) using an unpaired, non-parametric test (Mann-Whitney test); ns = p value > 0.05; * = p value < 0.05; ** = p value < 0.01; *** = p value < 0.001; **** = p value < 0.0001.

4.2.3 FRMD8 binds to iRhom2 N-terminus throughout the secretory pathway

Although I have clearly shown the interaction of FRMD8 with iRhom1 and iRhom2 (Fig. 3.7), I wanted to further investigate the binding of FRMD8 to iRhoms to better understand the mechanism by which FRMD8 affects iRhom function. First, I tested which region of iRhoms is bound by FRMD8. The long cytosolic iRhom2 N-terminus was the obvious candidate: it is the only significant cytoplasmic region in iRhom2, and preliminary mass spectrometry data indicated the requirement of the iRhom2 N-terminus for FRMD8 binding (Table 2.3). Co-expression of different N-terminal truncations of human iRhom2-3xHA (Fig. 4.7D) with FRMD8-V5, followed by anti-HA IP revealed that FRMD8 co-immunoprecipitates with truncations up to 200 amino acids, however, deleting 300 amino acids and more within the human iRhom2 N-terminus eliminated its ability to bind to FRMD8 (Fig. 4.7A). To refine the site of interaction, further deletions of the iRhom2 N-terminus were generated. Whereas iRhom2$^{\Delta 242}$ was still able to bind FRMD8, iRhom2$^{\Delta 270}$ was strongly impaired in FRMD8 binding (Fig. 4.7B). These data indicate that the N-terminal region in iRhom2 starting from amino acid 243is necessary for FRMD8 binding.

The mouse iRhom2^{cub} mutant is a deletion of the amino acid 1-268 in the iRhom2 N-terminus (Siggs et al., 2014) and, by aligning mouse and human sequences, corresponds to a deletion of 298 amino acids in the human iRhom2 N-terminus (Fig. 4.7D and 4.8A). Mouse iRhom2^{WT} was able to bind human FRMD8, presumably due to the high sequence homology between mouse and human iRhom2, but mouse iRhom2$^{\Delta 268}$ (iRhom2^{cub}) did not co-immunoprecipitate human FRMD8 (Fig. 4.7C). This is in line with the lack of interaction of FRMD8 and human iRhom2$^{\Delta 300}$ (Fig. 4.7A, B) and suggests that loss of FRMD8 binding might contribute to the mouse iRhom2^{cub} phenotype, although further work would be required to confirm this prediction.

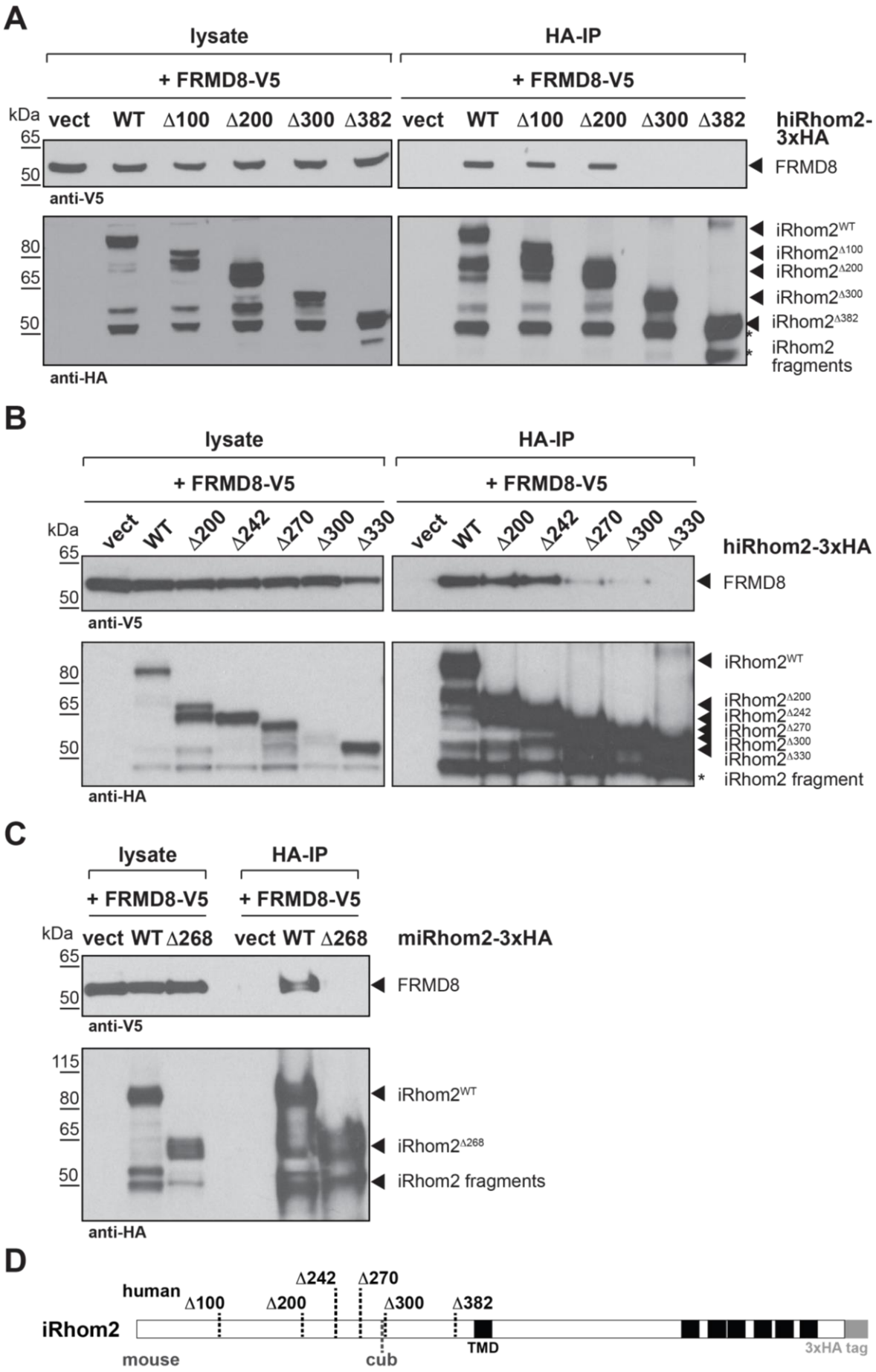

A
lysate
HA-IP
+ FRMD8-V5
+ FRMD8-V5
kDa
vect WT Δ100 Δ200 Δ300 Δ382
vect WT Δ100 Δ200 Δ300 Δ382
hiRhom2-3xHA
65
50
anti-V5
FRMD8
80
65
50
anti-HA
iRhom2WT
iRhom2Δ100
iRhom2Δ200
iRhom2Δ300
iRhom2Δ382
*
*
iRhom2 fragments
B
lysate
HA-IP
+ FRMD8-V5
+ FRMD8-V5
kDa
vect WT Δ200 Δ242 Δ270 Δ300 Δ330
vect WT Δ200 Δ242 Δ270 Δ300 Δ330
hiRhom2-3xHA
65
50
anti-V5
FRMD8
80
65
50
anti-HA
iRhom2WT
iRhom2Δ200
iRhom2Δ242
iRhom2Δ270
iRhom2Δ300
iRhom2Δ330
* iRhom2 fragment
C
lysate
HA-IP
+ FRMD8-V5
+ FRMD8-V5
kDa
vect WT Δ268
vect WT Δ268
miRhom2-3xHA
65
50
anti-V5
FRMD8
115
80
65
50
anti-HA
iRhom2WT
iRhom2Δ268
iRhom2 fragments
D
human
Δ100
Δ200
Δ242
Δ270
Δ300
Δ382
iRhom2
mouse
cub
TMD
3xHA tag

Figure 4.7 | FRMD8 binds to the iRhom2 N-terminus. A) - C) Western blot of lysates and anti-HA immunoprecipitation (HA-IP) of HEK293T cells transiently transfected with FRMD8-V5 and either empty vector (vect), **A) - B)** truncated human iRhom2-3xHA constructs or **C)** truncated mouse iRhom2-3xHA constructs after anti-HA or anti-V5 staining. One representative western blot out of at least three independent experiments is shown. **D)** Schematic representation of the truncated iRhom2 constructs used in A)-C).

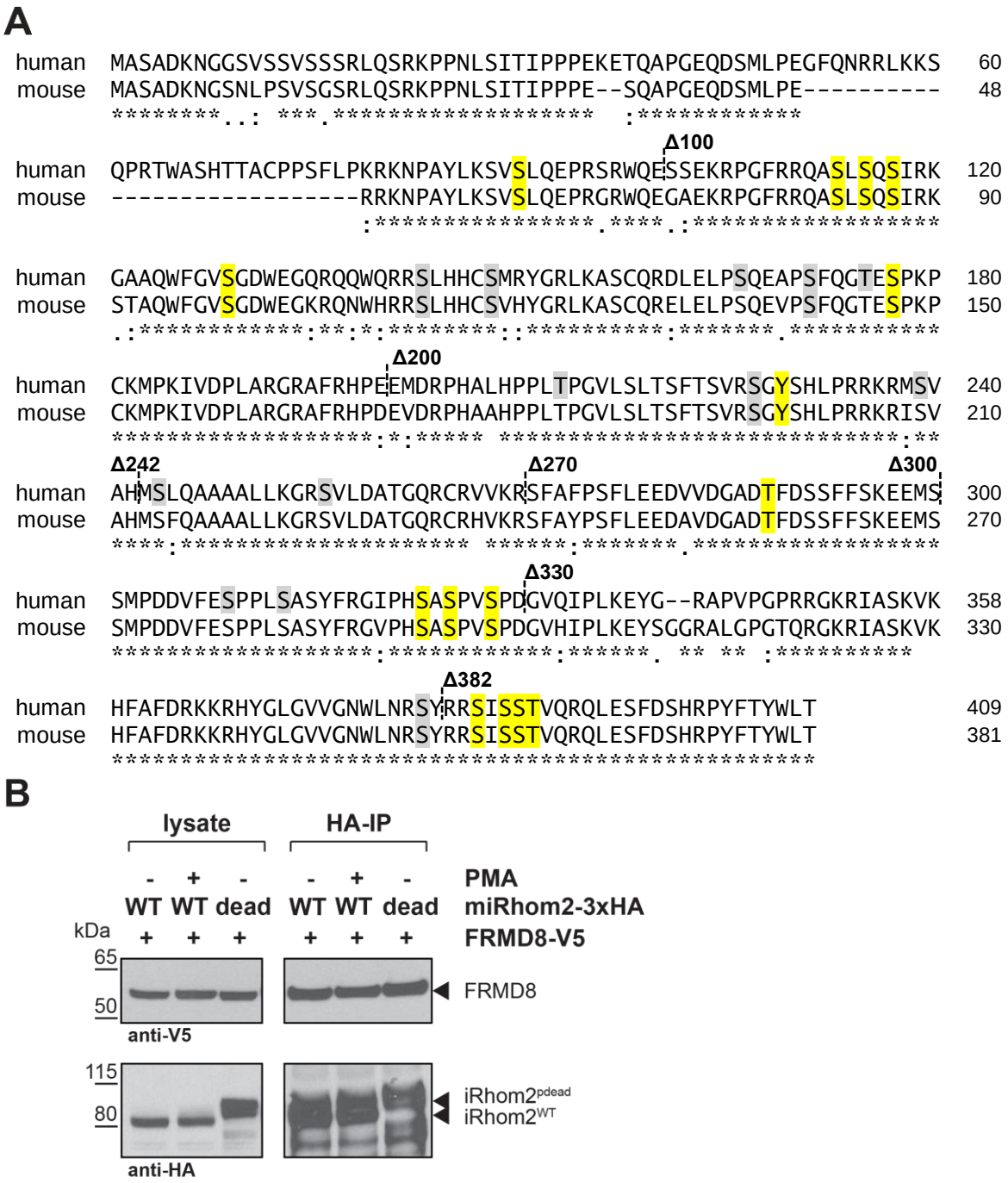


Figure 4.8 | FRMD8 binds to a conserved stretch in the iRhom2 N-terminus. A) Alignment of the cytosolic N-terminus of human and mouse iRhom2 using Clustal Omega (www.ebi.ac.uk/Tools/msa/clustalo). The potential interaction site is highlighted in red. Potential phosphorylation sites that have been mutated to alanine in the iRhom2^{pDEAD} mutant (used in Fig.

4.8B) are highlighted in yellow. Additional phosphorylation sites reported on PhosphoSitePlus (www.phosphosite.org) are highlighted in grey. An asterisk (*) indicates positions which have a fully conserved residue, a colon (:) indicates strongly similar properties of the amino acids, and a period (.) indicates weakly similar properties according to the Clustal Omega tool. **B)** Western blot of cell lysates and anti-HA immunoprecipitation (HA-IP) of HEK293T cells transiently transfected with mouse iRhom2^{WT} or iRhom2^{pDEAD} (dead), after anti-V5 and anti-HA staining. Where indicated cells have been stimulated with 200 nM PMA for 30 min. One representative western blot out of three independent experiments is shown.

The iRhom2 N-terminus can be phosphorylated, which is an important step in regulating ADAM17 activity (Grieve et al., 2017). Therefore, I tested whether stimulation of cells with PMA, which leads to iRhom2 phosphorylation (Grieve et al., 2017), affects FRMD8 binding. Neither stimulation of cells with PMA, nor using an iRhom2 mutant (iRhom2^{pDEAD}), in which 15 conserved phosphorylation sites have been mutated to alanine (Grieve et al., 2017), impaired the binding of FRMD8 to mouse iRhom2 (Fig. 4.8B). This indicates that phosphorylation of iRhom2 is not required for FRMD8 binding.

Next, I addressed the question of where in the secretory pathway FRMD8 binds to iRhom2. My immunofluorescence data showed that FRMD8 was localised in the cytosol and at the plasma membrane (Fig. 3.9). As iRhoms stay associated with ADAM17 from the ER to the plasma membrane, and regulate ADAM17 activity throughout its entire life cycle (Grieve et al., 2017), FRMD8 could bind and affect iRhom function at different points throughout the secretory pathway. For this reason, I investigated the interaction between FRMD8 and iRhom2 by assessing which form of ADAM17 was bound to iRhom2. Both mature and proADAM17 were co-immunoprecipitated with FRMD8 when co-overexpressing exogenous iRhom2 (Fig. 4.9), indicating that FRMD8 is a constitutive interaction partner of iRhom2 that binds to iRhom2 throughout its entire life cycle. These data further show that binding of FRMD8 to iRhom2 does not eliminate the interaction between iRhom2 and mature ADAM17, suggesting that FRMD8, iRhom2 and ADAM17 form a tripartite complex. The binding between FRMD8 and ADAM17 is probably not

direct, though, as I could not detect FRMD8 binding to ADAM17 in absence of iRhoms (Fig. A4, Appendix).

In summary, my data demonstrate that FRMD8 binds the iRhom2 N-terminus in the region of amino acids 243-298, and that this is independent of PMA-stimulation and phosphorylation. Furthermore, FRMD8, iRhom2 and ADAM17 form a tripartite complex throughout the entire secretory pathway with iRhom2 binding to both FRMD8 and mature and proADAM17 simultaneously.

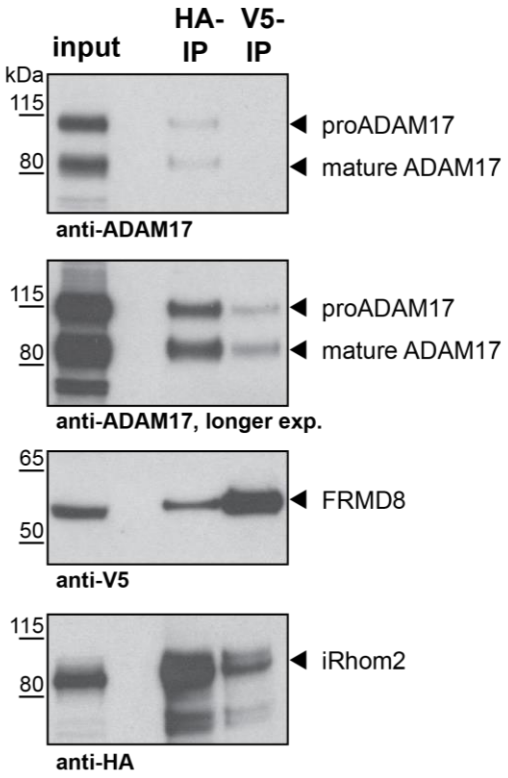


Figure 4.9 | FRMD8 binds to iRhom2 throughout the secretory pathway. Western blot of lysates, anti-HA and anti-V5 immunoprecipitation (HA-IP, V5-IP) of HEK293T cells co-expressing human iRhom2-3xHA with human FRMD8-V5 after anti-ADAM17, anti-HA and anti-V5 staining. One representative western blot out of three independent experiments is shown.

4.2.4 FRMD8 loss does not affect ER-to-Golgi trafficking of iRhom2

As FRMD8 loss reduces mature ADAM17 levels, this raises the question of what is the molecular mechanism by which FRMD8 affects the iRhom/ADAM17 pathway? To further investigate at which stage in the iRhom/ADAM17 life cycle FRMD8 plays a role, I

investigated whether FRMD8 impairs ADAM17 maturation by affecting the ER-to-Golgi trafficking of iRhoms and proADAM17. First, I examined whether the interaction between iRhoms and proADAM17 in the ER is impaired in the absence of FRMD8, consequently preventing the transport of proADAM17 to the Golgi. I did not observe differences in the ability of iRhom2-3xHA to bind to proADAM17 in wild-type and FRMD8 KO cells (Fig. 4.10A), suggesting that FRMD8 plays no role in the binding of iRhom2 to proADAM17 in the ER.

I then analysed whether FRMD8 affects iRhom2 trafficking to the Golgi apparatus. I investigated whether iRhom2 reaches the Golgi apparatus in absence of FRMD8 by examining the N-glycosylation of mouse iRhom2. As N-glycosylation of proteins changes throughout the secretory pathway (Stanley et al., 2009), ER and *medial*-/*trans*-Golgi localisation of proteins can be distinguished by their N-glycosylation. By treating cell lysates with the endoglycosidase H (Endo H), which removes high mannose and hybrid N-glycosylation restricted to ER and *cis*-Golgi proteins, or with peptide: N-glycosidase F (PNGase F), which cleaves all N-glycans (Stanley et al., 2009), the localisation of N-glycosylated proteins can be distinguished (Fig. 4.10B). Both in wild-type and FRMD8 KO cells, about one fourth of the total iRhom2 levels was Endo H-resistant (Fig. 4.10C), which corresponds to *medial*/*trans*-Golgi-glycosylated iRhom2. This indicates that iRhom2 is still able to reach the Golgi in absence of FRMD8, suggesting that there is no major defect in ER-to-Golgi trafficking of iRhom2 in FRMD8 KO cells. Attempts to analyse iRhom2 localisation using immunofluorescence were ambiguous, as in HEK293T cells iRhom2 could only be detected in the Golgi apparatus when significantly overexpressed (Fig. A5, Appendix). This is in line with published immunofluorescence data of tagged iRhoms, which are predominantly localised to the ER with little co-localisation with Golgi markers (Nakagawa et al., 2005, Zou et al., 2009, McIlwain et al., 2012, Hosur et al., 2014, Maney et al., 2015).

In summary, my data imply that there are no major defects in the ER-to-Golgi trafficking of iRhom2. This suggests that the maturation of ADAM17 is not impaired in

FRMD8 KO cells and hints on FRMD8 affecting the regulation of mature ADAM beyond the Golgi.

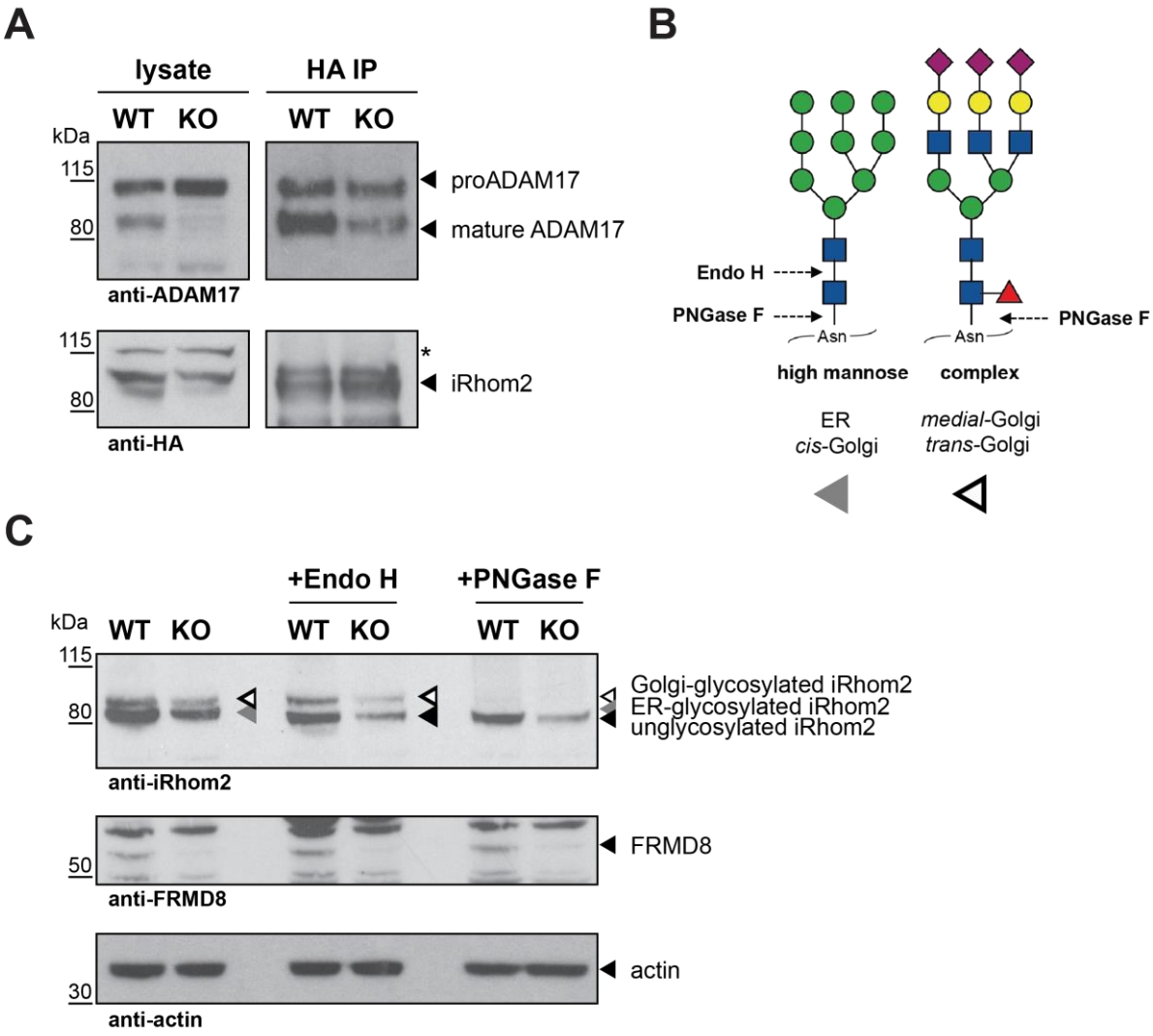


Figure 4.10 | iRhom2 binds ADAM17 and reaches the Golgi in absence of FRMD8. A) Western blot of wild-type (WT) HEK293T and FRMD8 KO cell lysates and anti-HA IP after anti-ADAM17and anti-HA staining. An asterisk (*) marks nonspecific bands of the HA antibody. One representative western blot out of four independent experiments is shown. **B)** Schematic representation of different N-glycosylation based on (Stanley et al., 2009). **C)** Western blot of wild-type (WT) HEK293T and FRMD8 KO cells transiently transfected with mouse iRhom2 after anti-iRhom2, anti-FRMD8, or anti-actin staining. Cell lysates were denatured and treated with Endo H or PNGase F where indicated. One representative western blot out of three independent experiments is shown.

4.2.5 FRMD8 stabilises iRhom2 beyond the Golgi

As I did not detect a defect in the ER-to-Golgi trafficking of iRhom2, I investigated whether iRhom function was affected at the plasma membrane. When staining for cell surface iRhom2-3xHA with an anti-HA antibody, I discovered that FRMD8 KO cells showed reduced levels of iRhom2 at the plasma membrane (Fig. 4.11A). This was not caused by different transduction levels of iRhom2-3xHA in wild-type and FRMD8 KO cell lines, as proven by whole cell anti-HA staining (Fig. 4.11B) and western blot (Fig. 4.10A), further suggesting that it is specifically the relatively small pool of iRhom2 at the cell surface that is affected by FRMD8 loss. This could result either from a defect in Golgi-to-plasma membrane trafficking or from a decrease in iRhom2 stability at the cell surface in the absence of FRMD8.

Further investigating whether FRMD8 affects iRhom stability, I found that FRMD8 overexpression substantially increased the amount of exogenously expressed iRhom2 (Fig. 4.12A), suggesting that FRMD8 stabilises iRhom2. Interestingly, iRhom2 overexpression also increased the levels of endogenous FRMD8 (Fig. 4.12B). This stabilisation of FRMD8 by iRhoms was not caused by changes in FRMD8 mRNA levels upon iRhom2 overexpression (Fig. 4.12C), indicating that FRMD8 is stabilised at the protein level. Although, I have not pursued this observation, it indicates a mutual stabilisation of iRhom2 and FRMD8.

The observed stabilisation of iRhom2 by FRMD8 implies that iRhom2 might normally be subject to degradation. Treatment of HEK293T cells stably expressing iRhom2-3xHA with the lysosomal inhibitor bafilomycin A1 increased the protein levels of iRhom2 (Fig. 4.12D), consistent with the idea that there is a basal level of iRhom2 degradation by the lysosomal pathway. This finding is in line with observations in MEFs showing that exogenous iRhom2 levels increased upon bafilomycin treatment (Grieve et al., 2017) and a study that reported that iRhom2 can localise to lysosomes (Luo et al., 2016).

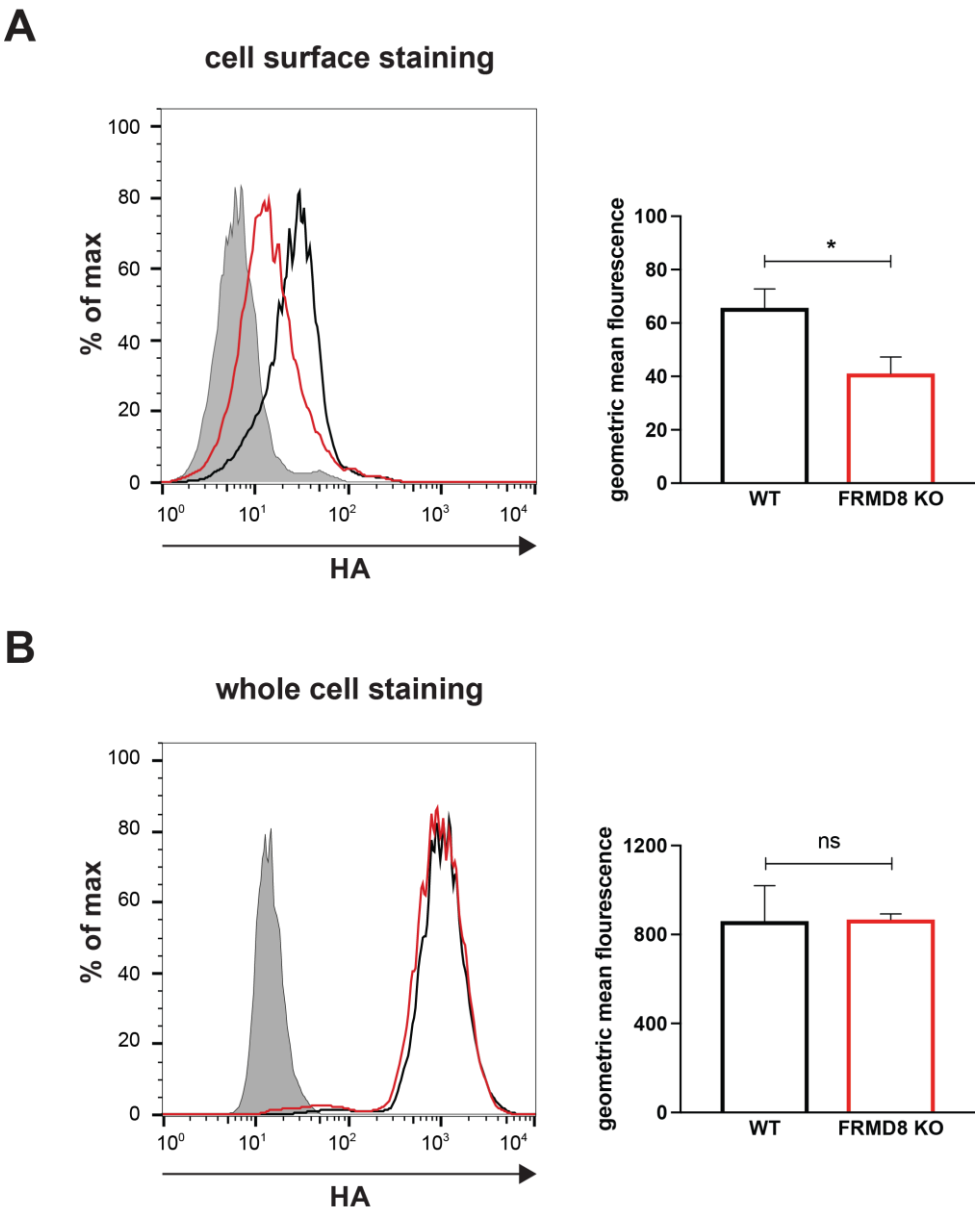


Figure 4.11 | Cells surface levels of overexpressed iRhom2 levels are decreased in FRMD8 KO cells. Flow cytometry analysis of wild-type (WT) HEK293T and FRMD8 KO cells stably expressing human iRhom2-3xHA. **A)** Unpermeabilised cells were stained on ice using an anti-HA antibody and an Alexa Fluor 488-coupled secondary antibody. Wild-type HEK293T cells served as a control (grey). The shown flow cytometry graph is one representative experiment out of three experiments. **B)** Cells were permeabilised and stained at room temperature with an anti-HA antibody. Staining with the Alexa Fluor 488-coupled secondary antibody served as a control (grey). The shown flow cytometry graph is one representative experiment out of two experiments. Statistical analysis was performed using an unpaired t-test (n=3 (A) and n=2 (B)); ns = p value > 0.05; * = p value < 0.05.

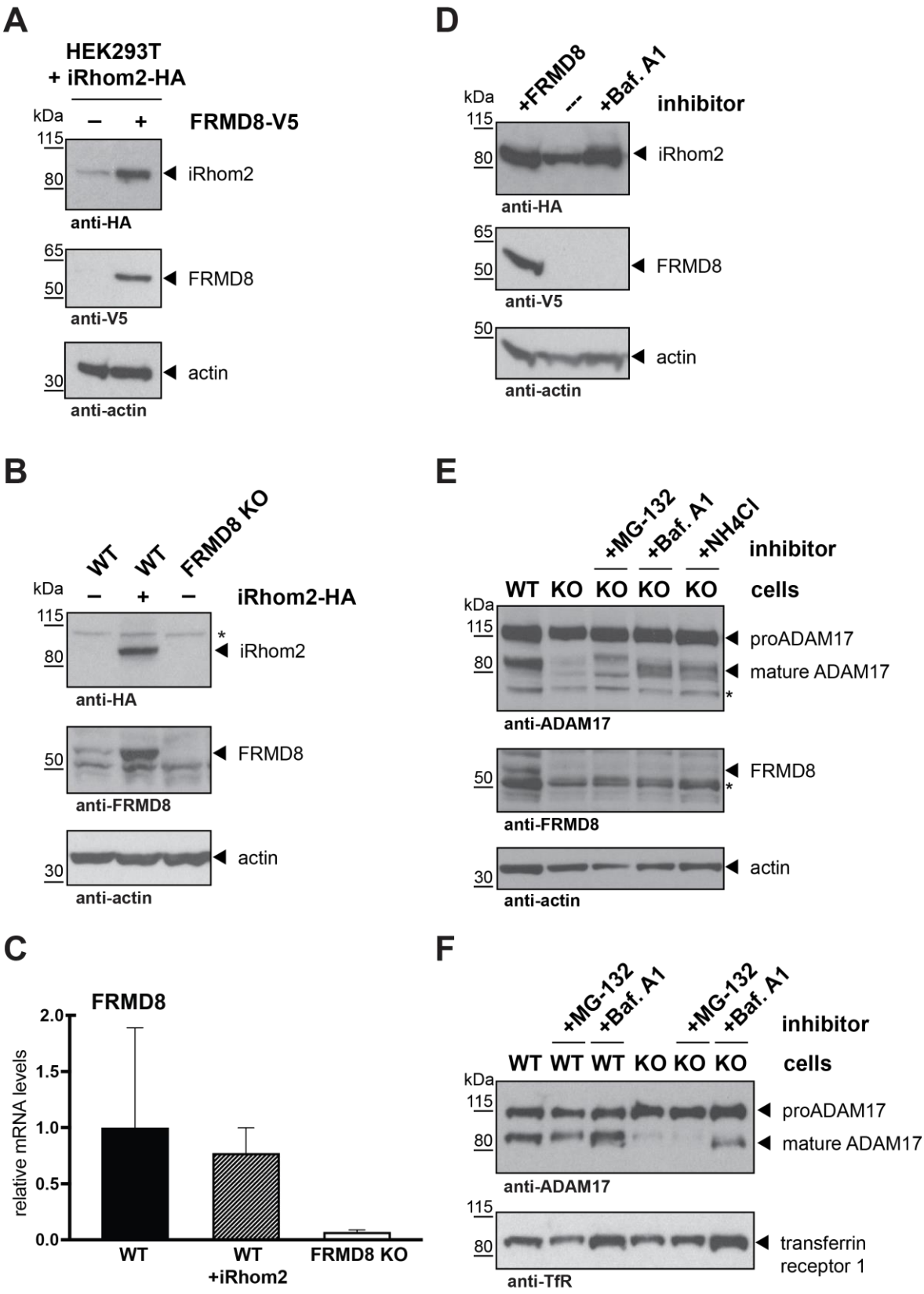


Figure 4.12 | FRMD8 stabilises iRhom2 and prevents lysosomal degradation of iRhom2 and mature ADAM17. A) Western blot of HEK293T cells stably expressing human iRhom2-3xHA and transfected with FRMD8-V5 (where indicated) after anti-HA, anti-V5 and anti-actin staining. **B)** Western blot of HEK293T cells transfected with human iRhom2-3xHA (where indicated) after anti-HA, anti-FRMD8 and anti-actin staining. An asterisk (*) marks a nonspecific band. **C)** FRMD8

mRNA levels relative to actin mRNA levels determined by TaqMan PCR in wild-type HEK293T (WT), HEK293T cells transfected with human iRhom2-3xHA (WT+iRhom2), and in FRMD8 KO cells. **D)** Western blot of HEK293T cells stably expressing human iRhom2-3xHA after anti-HA, anti-V5 and anti-actin staining. Where indicated cells have been transfected with FRMD8-V5 or treated with 200 nM bafilomycin A1 (Baf. A1) for 16 h. **E)** Western blot of cell lysates of wild-type (WT) HEK293T and FRMD8 KO treated with 10 µM MG-132, 200 nM bafilomycin A1 (Baf. A1) or 50 mM ammonium chloride (NH_4Cl) for 16 h. An asterisk (*) marks a nonspecific band. **F)** Cell lysates of wild-type (WT) HEK293T and FRMD8 KO cells treated with 10 µM MG-132 or 200 nM bafilomycin A1 (Baf. A1) for 16 h have been enriched for glycosylated proteins using concanavalin A beads to improve the anti-ADAM17 staining. Transferrin receptor 1 (TfR) was used as a loading control although it is also susceptible to bafilomycin treatment. **A) - B)** and **D) - F)** One representative western blot out of three independent experiments is shown.

In order to test whether the low levels of mature ADAM17 in FRMD8-deficient cells are linked to the degradation of iRhom2 by the lysosomal pathway, FRMD8 KO cells were treated with the lysosomal inhibitors bafilomycin A1 and ammonium chloride (NH_4Cl). Both treatments rescued the reduced mature ADAM17 levels in FRMD8 KO cells (Fig.4.12E), whereas the proteasomal inhibitor MG-132 did not increase mature ADAM17 levels (Fig. 4.12E-F). This indicates that mature ADAM17 is degraded through the lysosomal pathway in the absence of FRMD8, which could be linked to the degradation of iRhoms through the same pathway.

In conclusion, FRMD8 and iRhom2 stabilise each other. Although we do not understand the mechanism of this mutual stabilisation, their binding might, for example, obscure degradation signals on each protein. My observation that FRMD8 KO cells have less iRhom2 at the cell surface suggests that the role of FRMD8 might be limited to the cell surface pool of iRhom2. Mature ADAM17 is rapidly degraded through the lysosomal pathway in FRMD8 KO cells, demonstrating that FRMD8 plays a role in stabilising mature ADAM17. Although mechanistic details of how mature ADAM17 stability is linked to iRhom2 stability, both controlled by FRMD8, are still unclear, my findings provide a potential explanation for the role of FRMD8 in regulating ADAM17 activity.

4.2.6 FRMD8 stabilises endogenous iRhom2 levels

Due to the lack of available antibodies detecting endogenous human iRhom1 or iRhom2, all experiments investigating the effect of FRMD8 on iRhom function described so far used exogenously expressed iRhoms. In order to study the effect of FRMD8 on endogenous iRhoms, iRhom2 was tagged at the *RHBDF2* locus with a 3xHA tag by CRISPR/Cas9. The tag was added at the C-terminus of iRhom2 by targeting the last exon of the *RHBDF2* gene. The strategy shown in Fig. 4.13A involved arresting the cells in G2/M phase with nocodazole, targeting the endogenous *RHBDF2* locus with a sgRNA, while supplying a homology construct containing the 3xHA tag flanked by two homology arms of about 800 bp length. If the double strand break was successfully repaired by homologous recombination, the 3xHA tag would be inserted just before the stop codon of the *RHBDF2* gene. The cloning of the homology construct and the selection of HA-tagged colonies was performed in collaboration with Yao Meng, a Master's student in the Freeman lab. Although the expression of iRhom2 in HEK293T cells is low (The Human Protein Atlas (Uhlen et al., 2015)), we used this cell line for endogenous tagging of iRhom2 because all other experiments in this project were performed in HEK293T cells, and they are easy to modify by CRISPR/Cas9.

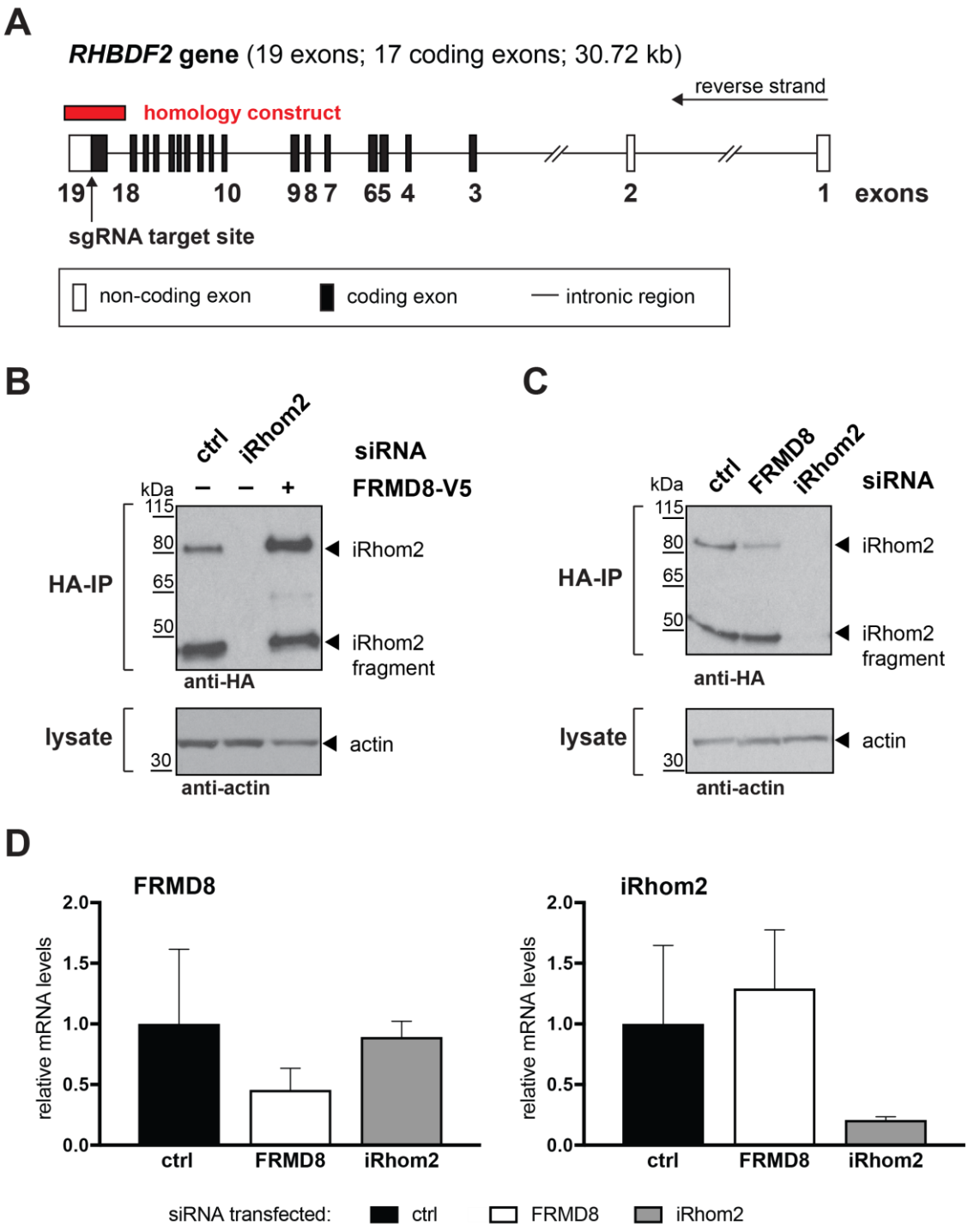


Figure 4.13 | Endogenous iRhom2 levels are stabilised by FRMD8. A) Schematic representation of the CRISPR/Cas9-mediated knock-in of the 3xHA tag (cloned into a homology construct) into the endogenous *RHDBF2* locus. Map of RHBDF2 gene (encoding iRhom2) based on the Ensembl database (Yates et al., 2016). **B) - C)** Western blot of endogenously tagged HEK293T iRhom2-3xHA cells transfected with FRMD8-V5 plasmid, siRNAs targeting iRhom2, non-targeting siRNA control pool (ctrl) or FRMD8 pre-designed SMARTpool siRNA. Protein lysates were anti-HA immunoprecipitated to detect endogenous iRhom2-3xHA levels. One representative western blot out of three independent experiments is shown. **D)** FRMD8 and iRhom2 mRNA levels relative to actin mRNA levels determined by TaqMan PCR in cells used for the experiment shown in C).

Due to the low expression of iRhom2 in HEK293T cells, lysates had to be anti-HA immunoprecipitated to detect the 3xHA tag. The knockdown of iRhom2 led to the loss of the HA-specific band (Fig. 4.13B), verifying that the *RHBDF2* locus had been tagged as expected. In these cells, FRMD8 overexpression resulted in a strong increase of endogenous iRhom2 in the HEK293T cells (Fig. 4.13B). This result verifies the earlier data that relied on the expression of tagged iRhom2 and demonstrates that FRMD8 indeed has a role in stabilising endogenous iRhom2. The knockdown of FRMD8 led only to a small reduction of the iRhom2 band (Fig. 4.13C). This is probably explained by the fact that the knockdown efficiency of FRMD8 was only 50% in the experiment shown (Fig. 4.13D). Furthermore, the mRNA levels of iRhom2 were not reduced upon FRMD8 knockdown (Fig. 4.13D), further implying that FRMD8 affects iRhom2 stability at the protein level.

In summary, these findings confirm the stabilising function of FRMD8 on iRhom2 and show that this role of FRMD8 also applies to endogenous iRhom2.

4.3 Discussion

4.3.1 Proposed model for FRMD8 function

In this chapter, I have shown that FRMD8 is an important novel regulator of ADAM17 and iRhom function. Although there are details that remain to be understood, my data lead to the following model of FRMD8 function: FRMD8 binds the iRhom2 N-terminus throughout the entire secretory pathway. FRMD8 and iRhom2 reciprocally stabilise each other, which is particularly important at the cell surface where FRMD8 prevents lysosomal degradation of iRhom2. FRMD8 might, for instance, control the balance between endocytic recycling and degradation of iRhom2 and ADAM17. ADAM17, but not iRhoms, has been shown to undergo endocytic recycling to limit cell surface accessibility (Dombernowsky et al., 2015).

The destabilisation of iRhom2 in the absence of FRMD8 leads to enhanced lysosomal degradation of mature ADAM17 levels, ultimately resulting in the reduced release of ADAM17 substrates. ProADAM17 levels are not affected by FRMD8 loss. Given that proADAM17 does not get beyond early Golgi compartments, this is consistent with the model that lysosomal degradation of iRhom2 and mature ADAM17 occurs as a consequence of endocytic internalisation from the plasma membrane.

My model and my data do not explain how the destabilisation of the plasma membrane iRhom2 pool leads to a reduction in mature ADAM17 levels. It is currently not known whether mature ADAM17 and iRhom2 are degraded together through the lysosomal pathway, or whether they dissociate and are degraded independently. Interestingly, it has been observed that iRhom2 protein levels were downregulated by ADAM17 knockdown (Brooke et al., 2014). Although it is unclear if this is a transcriptional or posttranslational effect, it might suggest that ADAM17 and iRhoms mutually stabilise each other. This would argue for a mechanism by which iRhom2 and ADAM17 have to dissociate in order to be destabilised. Consistent with this hypothesis, I showed that the decline of the iRhom2 cell surface pool was only around 50% in FRMD8 KO cells (Fig. 4.11A), whereas mature ADAM17 levels were decreased by about 75% upon FRMD8 loss (Fig.4.1A, 4.4A,

4.5) suggesting that ADAM17 and iRhom2 were not degraded in the same stoichiometry. Further experiments will need to address whether iRhoms and mature ADAM17 are degraded together or independently, and which role FRMD8 plays in the degradation of both proteins.

4.3.2 A potential role of the FRMD8 C-terminus

Although the C-terminal region of FRMD8 is not required for the binding to iRhom2 (Fig.3.8B), it appears to have a role in stabilising mature ADAM17 levels (Fig. 4.4B). Hypothetically, the FRMD8 C-terminus could be required to block lysosomal degradation, and ultimately stabilise, iRhom2. This might happen through protein interactions of the FRMD8 C-terminus with unknown interaction partners. However, my data cannot exclude the possibility that the FRMD8$^{\Delta C}$ construct is fully functional and able to rescue mature ADAM17 levels but that this takes longer than wild-type FRMD8. I have observed that the rescue of mature ADAM17 levels in FRMD8 KO cells with wild-type FRMD8 requires more than 48 h after transfection of the construct, probably due to the very slow maturation of proADAM17 (Lorenzen et al., 2016). Hence, it is possible that FRMD8$^{\Delta C}$ is more difficult to express or more unstable than wild-type FRMD8 and therefore takes longer to rescue the mature ADAM17 levels. In conclusion, the role of the FRMD8 C-terminus remains minimally explored and has to be addressed in future experiments.

4.3.3 The relationship between FRMD8 and iRhom1

Even though I have not determined the exact region of interaction between FRMD8 and iRhom1, it is likely that the binding between FRMD8 and iRhom1 also depends on the iRhom1 N-terminus. As shown in Figure A1 (Appendix) the sequence similarity between the iRhom1 and iRhom2 N-termini is high, and mammalian iRhom1 and iRhom2 have shown overlapping function in regulating ADAM17 (Christova et al., 2013, Maney et al., 2015), further supporting the hypothesis that FRMD8 regulates both iRhoms in a similar

fashion. Future experiments will have to address the role of FRMD8 for iRhom1 function in more detail.

In summary, FRMD8 is a novel component of the iRhom/ADAM17 pathway affecting the stability of iRhom2 and mature ADAM17 in mammalian cell lines. The biological role of FRMD8 in different tissues or a whole organism is unclear and needs further studies to obtain a more complete picture of FRMD8 function in the iRhom/ADAM17 pathway. I will report the investigation of FRMD8 in flies and mice in the next chapter.

CHAPTER 5

Physiological roles of FRMD8

5 Physiological roles of FRMD8

5.1 Introduction

The physiological function of FRMD8 is largely unclear. Like iRhoms, FRMD8 is conserved from fruit flies to human. In *Drosophila melanogaster*, zebrafish and human cells FRMD8 was described as a negative regulator of Wnt/β-catenin signalling (Kategaya et al., 2009). The role of FRMD8 was analysed by RNAi in zebrafish and *Drosophila* embryos (Kategaya et al., 2009), however, no FRMD8 KO organism has been generated yet. The biological role of iRhoms, on the other hand, has been studied in KO flies and mice. iRhom KO flies are viable and fertile but show reduced daytime activity, and increased periods of sleep (Zettl et al., 2011). This sleep-like phenotype is caused by hyperactivation of EGFR signalling in the absence of iRhom, which normally promotes the degradation of EGFR ligands by ERAD in flies (Zettl et al., 2011). In mice, iRhom2 loss does not have any obvious defects (Adrain et al., 2012, McIlwain et al., 2012, Luo et al., 2016, Siggs et al., 2012) unless the mice are challenged with bacterial or viral infections. Upon infection with *Listeria* (McIlwain et al., 2012) or HSV-1 (Luo et al., 2016), iRhom2 KO mice die due to defects in the generation of cytokines, such as TNFα and type I IFN. The phenotype of iRhom1 KO mice is controversial, as two different deletions of the *Rhbdf1* gene led to different phenotypes. The first iRhom1 KO mouse line, generated by deletion of exons 2-18, was postnatally lethal due to a wasting phenotype (Christova et al., 2013). Dependent on the genetic background of the mouse strain, these iRhom1 KO mice died between 9 days (C57BL/6J) and 6 weeks (129S6/SvEvTac) of age (Christova et al., 2013). iRhom1/2 double KO (DKO) mice resulting from this iRhom1 KO line were embryonically lethal. A different iRhom1 KO mouse line, in which exons 4-11 were deleted, resulted in viable iRhom1 KO mice with no obvious defects (Li et al., 2015). The resulting iRhom1/2 DKO mice died perinatally with open eyes and misshaped heart valves (Li et al., 2015), similarly to *Adam17*$^{-/-}$ mice. Overall, the lethality of both iRhom DKO mouse lines emphasises the importance of iRhoms *in vivo*.

Having shown that FRMD8 plays a major role in regulating iRhom-dependent ADAM17 activity in a cell culture system, I wanted to investigate the role of FRMD8 *in vivo*. Therefore, my aim was to generate FRMD8 KO mice and flies to analyse the role of FRMD8 in these model organisms, and to determine the physiological importance of FRMD8. First, I generated *Drosophila* FRMD8 (Bili) KO flies using CRISPR/Cas9 and studied the phenotype of adult flies, in relation to the known phenotype of iRhom KO flies. Second, I started to generate FRMD8 KO mice from commercial ES cells, as no mouse consortium has generated a FRMD8-deficient mouse line yet. The long-term aim is to analyse the phenotype of the first mammalian FRMD8 KO model organism. Whilst waiting for the generation of FRMD8 KO mice, I generated and studied human FRMD8 KO macrophages to investigate the biological relevance of FRMD8 in macrophages, a cell type in which iRhom2 and ADAM17 play an essential role in the release of TNFα (Adrain et al., 2012, McIlwain et al., 2012). To generate genetically modified macrophages, I used iPSC lines, which can be differentiated into a variety of cell types, including macrophages (van Wilgenburg et al., 2013). Since the first reprogramming of murine fibroblasts into iPSCs by Takahashi and Yamanaka in 2006 (Takahashi and Yamanaka, 2006), iPSCs have developed into an important tool in disease modelling and drug discovery (Shi et al., 2017). In combination with the CRISPR/Cas9 technology, human iPSCs can be used to study gene deletions in cell types that are otherwise challenging to genetically manipulate. By using iPSC-derived macrophages, I avoided common problems when manipulating macrophages, such as low transfection and knockdown efficiency.

Studying FRMD8 loss in flies, mice, and human macrophages will help to reveal the physiological relevance of FRMD8 in mammals and *Drosophila*.

5.2 Results

5.2.1 FRMD8 KO macrophages show impaired TNFα release

As iRhom2 plays an essential role in TNFα release in macrophages (Adrain et al., 2012, McIlwain et al., 2012), and FRMD8 regulates iRhom2 function, investigating FRMD8 KO macrophages should provide valuable information about the biological function of FRMD8. I generated human FRMD8 KO iPSC lines in the James Martin Stem Cell Facility, Oxford and analysed two different FRMD8 KO clones derived from the same iPSC parental line, AH017-13, which had previously been generated in the facility from a skin biopsy of a female donor (Fernandes et al., 2016). Both FRMD8 KO iPSC lines had indels in exon 7 of the FRMD8 gene (Fig. A6A-B, Appendix), which are predicted to lead to premature stop codons (Fig. A6C, Appendix).

The two iPSC lines were differentiated into macrophages following standard protocols (Fig. 5.1A) (van Wilgenburg et al., 2013). FRMD8 protein levels were undetectable in both FRMD8 KO macrophages lines (Fig. 5.1B), and FRMD8 mRNA levels were drastically reduced (Fig. 5.1C), confirming that both lines were indeed FRMD8-deficient. Similar to my results in FRMD8 KO HEK293T cells, both FRMD8 KO macrophage lines showed a reduction in mature ADAM17 protein levels by about 75% compared to the wild-type control (Fig. 5.1B).

To further examine whether the reduced mature ADAM17 levels in FRMD8 KO cells also affect the release of TNFα, an ELISA was used to measure TNFα levels in cell supernatants. When stimulated with LPS, FRMD8 KO macrophages released significantly less TNFα compared to wild-type iPSC-derived macrophages (Fig. 5.2A). The treatment the ADAM10 inhibitor GI had no effect on TNFα release in wild-type and FRMD8 KO macrophages, proving that the release of TNFα is ADAM10-independent. However, the ADAM10/ADAM17 inhibitor GW blocked the release of TNFα in LPS-stimulated wild-type and FRMD8 KO macrophages (Fig. 5.2B), demonstrating that TNFα release is mediated by ADAM17-dependent shedding, and implying that a defect in ADAM17 leads to the reduced TNFα release in FRMD8 KO macrophages.

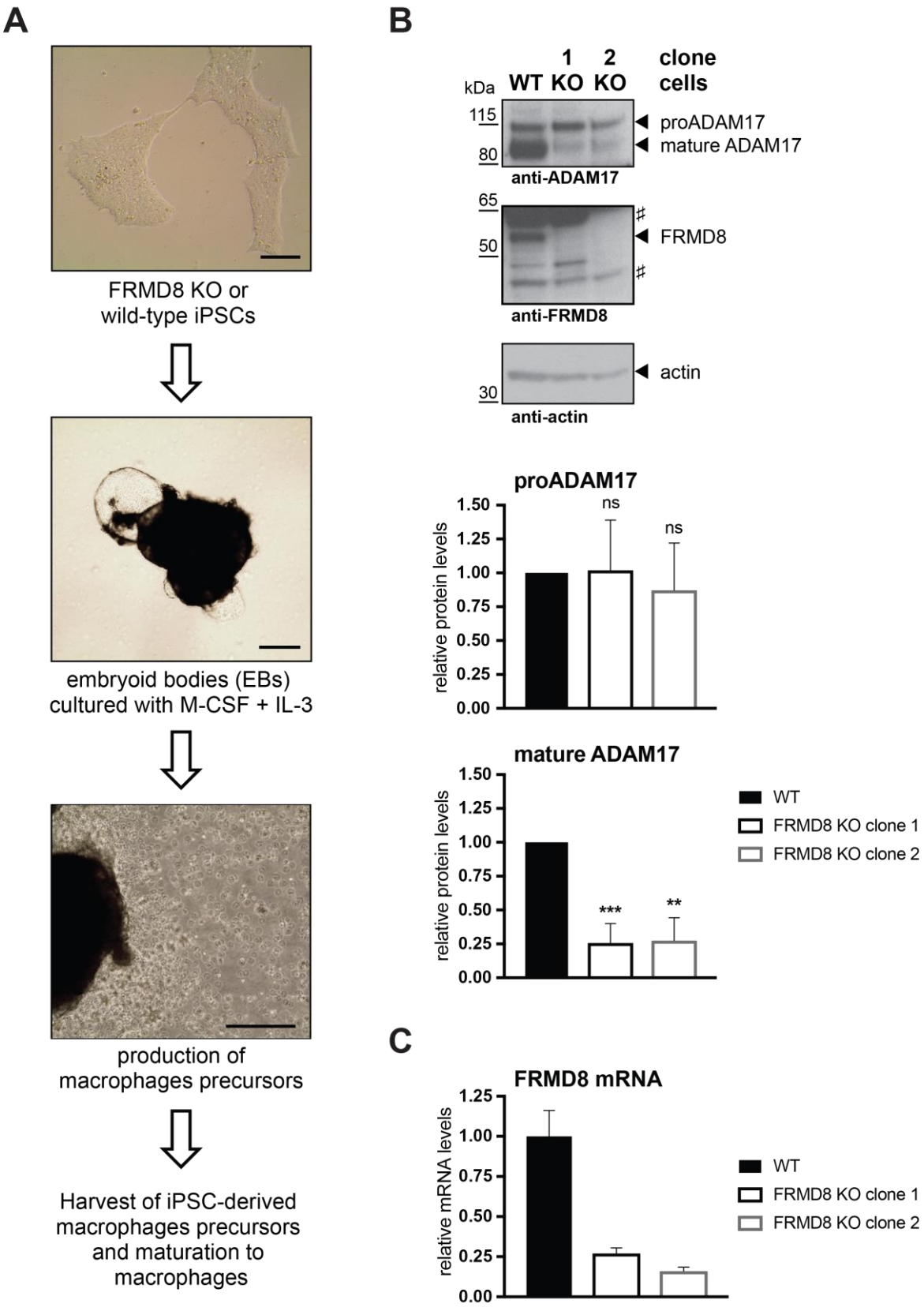


Figure 5.1 | FRMD8 KO macrophages have reduced mature ADAM17 levels. A) Differentiation protocol of iPSCs into macrophages based on (van Wilgenburg et al., 2013). Scale bars represent 10 µm. **B)** Western blot of iPSC-derived macrophage lysates after anti-ADAM17, anti-FRMD8 or anti-actin staining. ♯ indicates nonspecific bands. One representative western blot out of three independent experiments is shown. ADAM17 protein levels were quantified from western blots and

normalised to actin controls using data from three independent experiments. Statistical analysis was performed using an unpaired, non-parametric test (Mann-Whitney test); ns = p value > 0.05; ** = p value < 0.01; *** = p value < 0.001. **C)** FRMD8 mRNA levels relative to actin mRNA levels analysed by TaqMan PCR in wild-type (WT) and FRMD8 KO iPSC-derived macrophages.

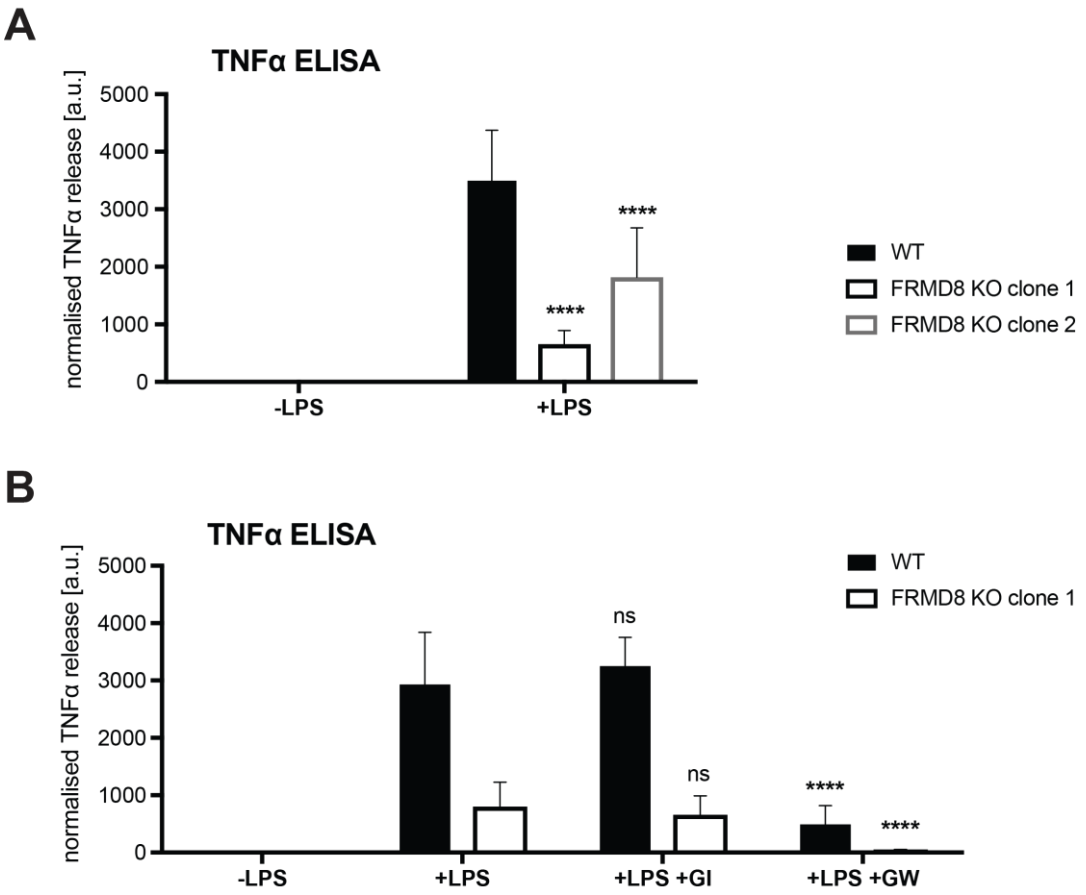


Figure 5.2 | FRMD8 KO macrophages show reduced release of TNFα. A) - B) iPSC-derived macrophages were either left unstimulated, stimulated with 50 ng/ml LPS, or with 50 ng/ml LPS and simultaneously with 2 µM GI or 2 µM GW for 4 h. TNFα amounts in the supernatants were measured by ELISA and then normalised to the concentration of macrophage cell lysates. Statistical analysis was performed on n=9 (combining three replicated from 3 independent replicates) using an unpaired, non-parametric test (Mann-Whitney test); ns = p value > 0.05; **** = p value < 0.0001.

To show that the impaired TNFα release from FRMD8 KO macrophages is not caused by a deficiency in TNFα expression and induction, I analysed TNFα levels in the iPSC-derived macrophages. Cell surface staining of TNFα confirmed that wild-type and FRMD8 KO macrophages have similar cell surface levels of TNFα (Fig. A7A, Appendix). The

TNFα surface levels in FRMD8 KO macrophage line 1 were slightly lower potentially explaining the lower release of TNFα compared to FRMD8 KO macrophage line 2 (Fig. 5.2A). Analysis of TNFα mRNA levels demonstrated that FRMD8 KO macrophages have no defect in the LPS-induced TNFα transcription (Fig. A7B, Appendix), further indicating that the reduced release of TNFα from FRMD8 KO macrophages is caused by the impaired levels of mature ADAM17.

In summary, my data prove that FRMD8 affects mature ADAM17 levels and activity in human macrophages and demonstrate that the role of FRMD8 in regulating iRhom function and ultimately ADAM17 activity has physiological relevance.

5.2.2 Generation of FRMD8 KO mice

Given the important role of FRMD8 in human macrophages, the phenotypic analysis of FRMD8 KO mice will help to get a broader picture of the physiological relevance of FRMD8 in mammals. To generate *Frmd8*$^{-/-}$ mice in-house, commercially available FRMD8 KO mouse ES cells, which have a neomycin cassette inserted in the *Frmd8* gene locus spanning all coding exons (2-11) (Fig. 5.3A), from KOMP Repository at UC Davis were used. This work is ongoing at the time of writing, but the first two litters of a cross of two *Frmd8*$^{+/-}$ mice resulted in two *Frmd8*$^{-/-}$ pups (Fig. 5.3B), one of which died at the age of 3 days. Although the number of pups analysed from *Frmd8*$^{+/-}$ mouse crosses were low, preliminary data showed that *Frmd8*$^{-/-}$ mice were born below the expected Mendelian ratio of 25% (Fig. 5.3C), suggesting that there might be increased embryonic or perinatal lethality in these mice. Furthermore, three pups died before the age of 3 days before the genotype could be determined. More crosses will have to be generated to further analyse the possible lethality of *Frmd8*$^{-/-}$ mice.

One *Frmd8*$^{-/-}$ mouse survived and was healthy when it was culled for experiments at the age of 15 days. Western blot analysis of tissues from the 15-day old *Frmd8*$^{-/-}$ pup showed that mature ADAM17 levels were reduced in all analysed tissue compared to tissues from a wild-type littermate (Fig. 5.4A). This clearly demonstrates that FRMD8 also

plays a role in controlling ADAM17 levels *in vivo*. Furthermore, the reduction of mature ADAM17 levels in the brain, a tissue in which iRhom2 is almost completely absent (Christova et al., 2013, Li et al., 2015), suggests that FRMD8 regulates mature ADAM17 levels through iRhom1, in addition to iRhom2, *in vivo*. Furthermore, I detected FRMD8 expression in all tissues tested, which include brain, liver, kidney and skin (Fig. 5.4B), which is consistent with the predicted ubiquitous expression of FRMD8 (The Human Protein Atlas (Uhlen et al., 2015), BioGPS (Wu et al., 2016)). FRMD8 expression was lost in the *Frmd8*$^{-/-}$ pup confirming the successful generation of *Frmd8*$^{-/-}$mice at the protein level.

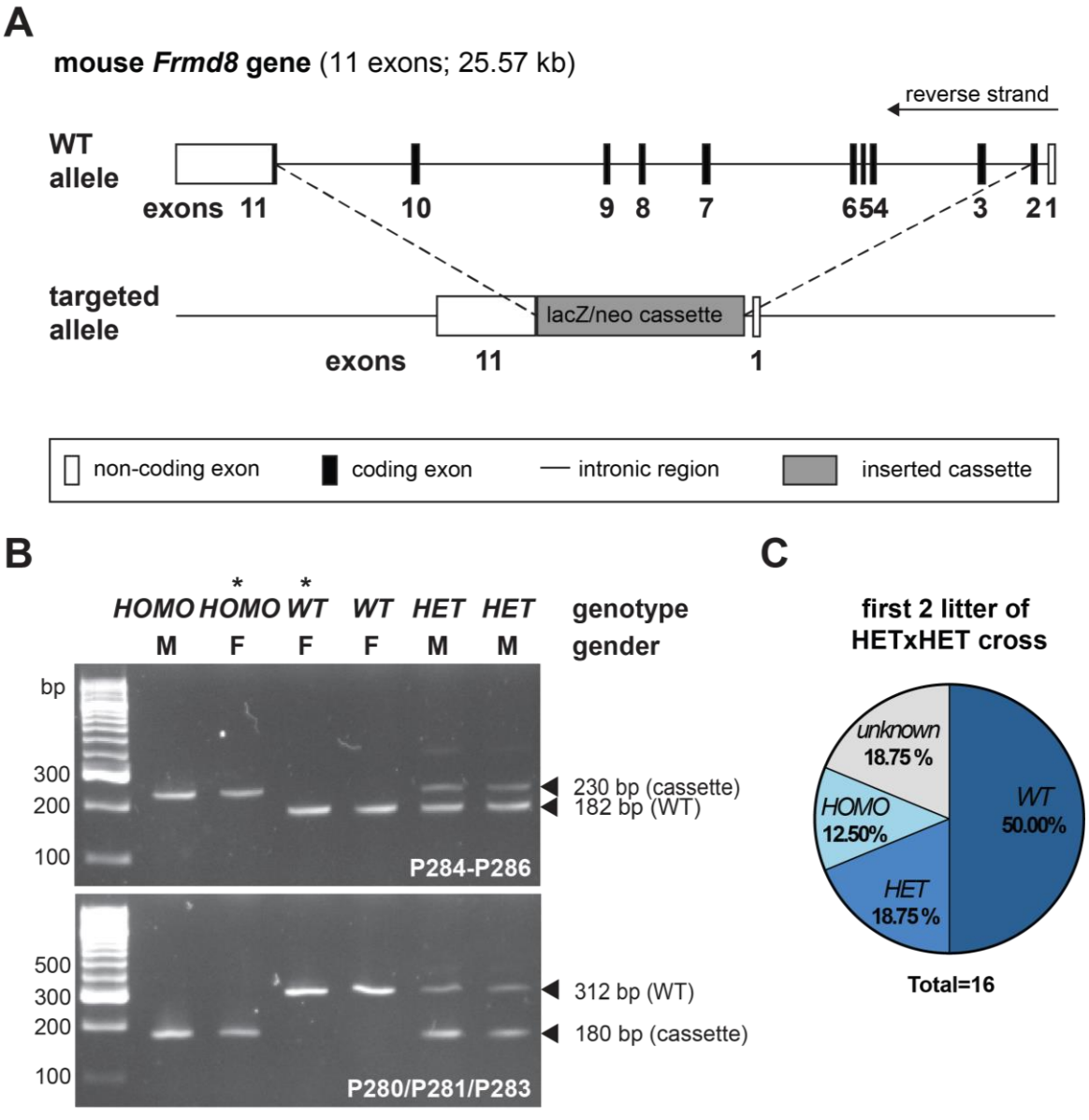


Figure 5.3 | Generation of FRMD8 KO mice. A) Schematic representation of the insertion of a lacZ/neomycin cassette into the *Frdm8* locus. The map of *Frmd8* gene is based on the Ensembl database (Yates et al., 2016). **B)** Genotyping PCR of mouse tail or ear notching samples from the first litter of a *Frdm8*$^{+/-}$ x *Frdm8*$^{+/-}$ cross analysed on an agarose gel. The genotyping strategy with primers P280-P286 is described in 2.4.2. The animals marked with an asterisk (*) were used for western blot analysis (Fig. 5.4) **C)** Genotype of first two litters of *Frdm8*$^{+/-}$ x *Frdm8*$^{+/-}$ (HET) cross as determined by genotyping PCR. Three pups are of unknown sex and genotype as they were cannibalised by the mother before the age of 3 days.

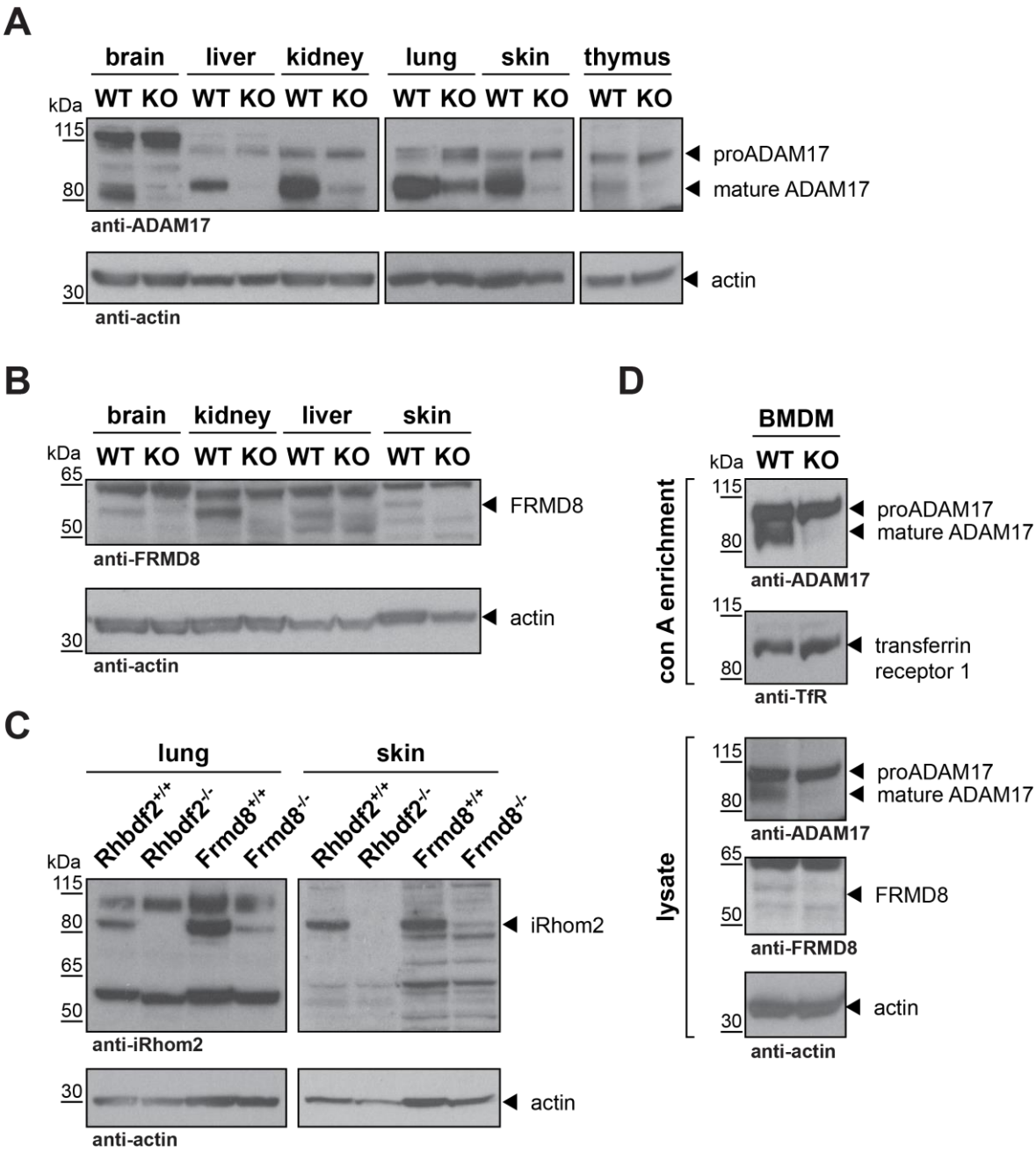


Figure 5.4 | FRMD8 stabilises iRhom2 and mature ADAM17 *in vivo*. A) - C) Western blot of mouse tissue lysates after anti-ADAM17, anti-FRMD8, anti-iRhom2 or anti-actin staining. **D)**

Western blot of lysates from bone marrow-derived macrophage lysates before and after enrichment using concanavalin A (con A) beads, stained for anti-ADAM17 or anti-transferrin receptor 1 (TfR). The shown western blot represents data from only one mouse wild-type and one knockout animal.

As my data from human cell lines suggests that FRMD8 loss destabilises iRhom2 at the protein level (Fig. 4.13C-D), I analysed iRhom2 levels in *Frmd8*$^{+/+}$ and *Frmd8*$^{-/-}$ mouse tissues, using *Rhbdf2*$^{-/-}$ tissues as a control. Using an antibody that had been generated in the lab to detect mouse iRhom2 (Adrain et al., 2012), I noted a strong decrease of iRhom2 levels in lung and skin of the *Frmd8*$^{-/-}$ pup compared to a wild-type littermate (Fig. 5.4C). This demonstrates that FRMD8 also affects iRhom2 stability *in vivo*. Future experiments will have to analyse mRNA levels in these tissues, as well as protein levels in additional tissues to confirm these data.

Macrophages are of particular interest when analysing FRMD8 function in mice as I have shown that FRMD8 plays a crucial role in controlling mature ADAM17 levels and TNFα release in human macrophages. For this reason, I cultured bone marrow-derived macrophages (BMDMs). BMDMs showed a strong decrease in mature ADAM17 levels (Fig. 5.4D) implying that these cells could also have defects in the release of TNFα, which will be analysed in future experiments.

Overall, further studies of *Frmd8*$^{-/-}$ mice will help to confirm the effects of FRMD8 loss on the iRhom/ADAM17 pathway shown in cell lines and human macrophages. More FRMD8 KO mice will have to be bred to get a full picture of the physiological role of FRMD8 in mice, and to understand the potential perinatal lethality of *Frmd8*$^{-/-}$ mice. My preliminary data from one *Frmd8*$^{-/-}$ pup, however, confirm that FRMD8 also controls mature ADAM17 and iRhom levels in mice.

5.2.3 Bili KO *Drosophila* show reduced locomotion and activity

Bili is the homologue of FRMD8 in *Drosophila melanogaster*,and shows 37% identity with human FRMD8 in the amino acid sequence. Compared to human FRMD8, Bili has an

extended N-terminus (Fig. 5.5A). As FRMD8 and iRhoms are both conserved from flies to human, I tested whether their *Drosophila* orthologues also interact. When co-expressing Bili and *Drosophila* iRhom (diRhom) in human cells, Bili-HA and diRhom-Flag interacted specifically (Fig. 5.5B), suggesting that the FRMD8-iRhom interaction might be conserved and that Bili could be involved in the regulating iRhom function in *Drosophila*.

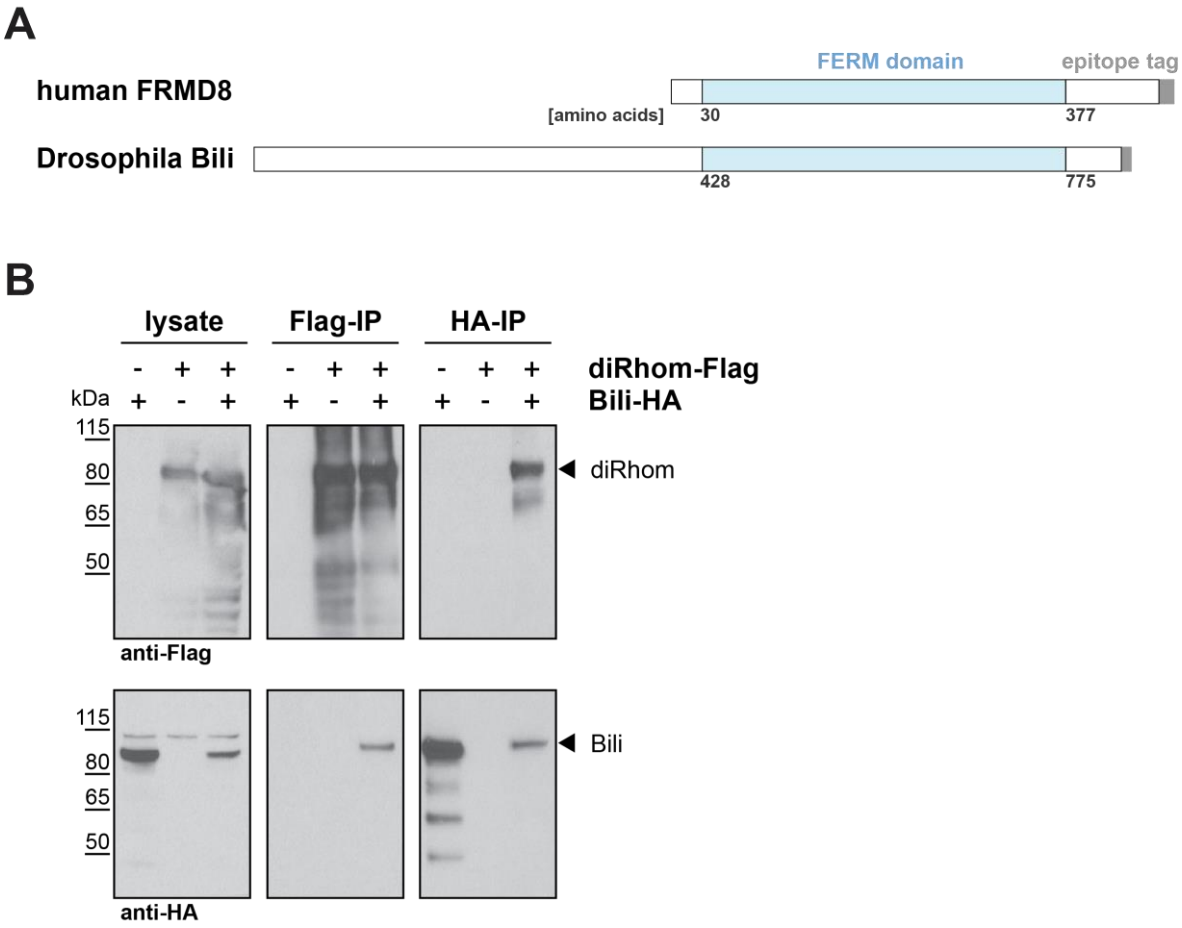


Figure 5.5 | *Drosophila* FRMD8 (Bili) binds to *Drosophila* iRhom in HEK293T cells. A) Schematic representation of the V5-tagged human FRMD8 construct used in earlier experiments and HA-tagged Bili used in B). **B)** Western blot of lysates, anti-Flag and anti-HA immunoprecipitation (Flag-IP, HA-IP) of HEK293T cells co-expressing *Drosophila* iRhom-Flag (diRhom) with *Drosophila* Bili-HA, after anti-HA or anti-Flag staining. One representative western blot out of three independent experiments is shown.

To test the biological function of Bili in *Drosophila*, I deleted the *bili* gene in flies using CRISPR/Cas9. A sgRNA targeting *bili* in exon 4 (Fig. 5.6A) was used to generated Bili KO

flies. The generated KO line had an 8-nt deletion in exon 4 of the *bili* gene (Fig. 5.6B) leading to a premature stop codon and consequently to a reduction of Bili mRNA by NMD (Fig. 5.6C). The 8-nt deletion was also found in mRNA extracted from Bili KO flies (Fig. 5.6D), proving that the mutation had not been spliced out. Although I have no data confirming the loss of Bili at the protein level, due to the lack of antibodies detecting *Drosophila* Bili, my data suggests that the premature stop codon after 131 amino acids leads to NMD of Bili mRNA and presumably to the loss of functional Bili protein.

The Bili KO flies are the first to be reported; previous work on Bili relied on RNAi knockdown (Kategaya et al., 2009). The KO flies were viable and fertile, however, I noted that they moved less frequently compared to wild-type flies. To analyse further the locomotion of Bili KO flies, I performed a negative geotaxis assay. Flies have negative geotaxis, meaning they naturally move against gravity and climb up the wall of tubes (Rhodenizer et al., 2008). However, this locomotion behaviour in *Drosophila* is impaired in neurodegenerative diseases, upon oxidative stress, bacterial infection, or age (Hosamani and Muralidhara, 2009, Llorens et al., 2007, Rhodenizer et al., 2008, Linderman et al., 2012). When I measured the climbing ability of Bili KO flies in a negative geotaxis assay (Fig. 5.7A), Bili KO flies showed a reduced climbing rate at the age of 1 day (Fig. 5.7B). This finding shows that Bili KO flies have impaired locomotion, which resembles the impaired activity and movement observed in iRhom KO flies (Zettl et al., 2011). Next, I investigated if these locomotion defects affect the life span of Bili KO flies. Bili KO flies have indeed a reduced life span and live on average 14 days shorter than wild-type flies (Fig. 5.7C), further demonstrating that Bili has an important, although not essential role in flies.

Taken together, Bili KO flies are viable, showing that Bili is not essential in *Drosophila* development, but it has importance for the activity and locomotion of the adult fly, similarly to iRhom in flies. Future investigations will have to dissect the molecular role of Bili in flies and its link to *Drosophila* iRhom.

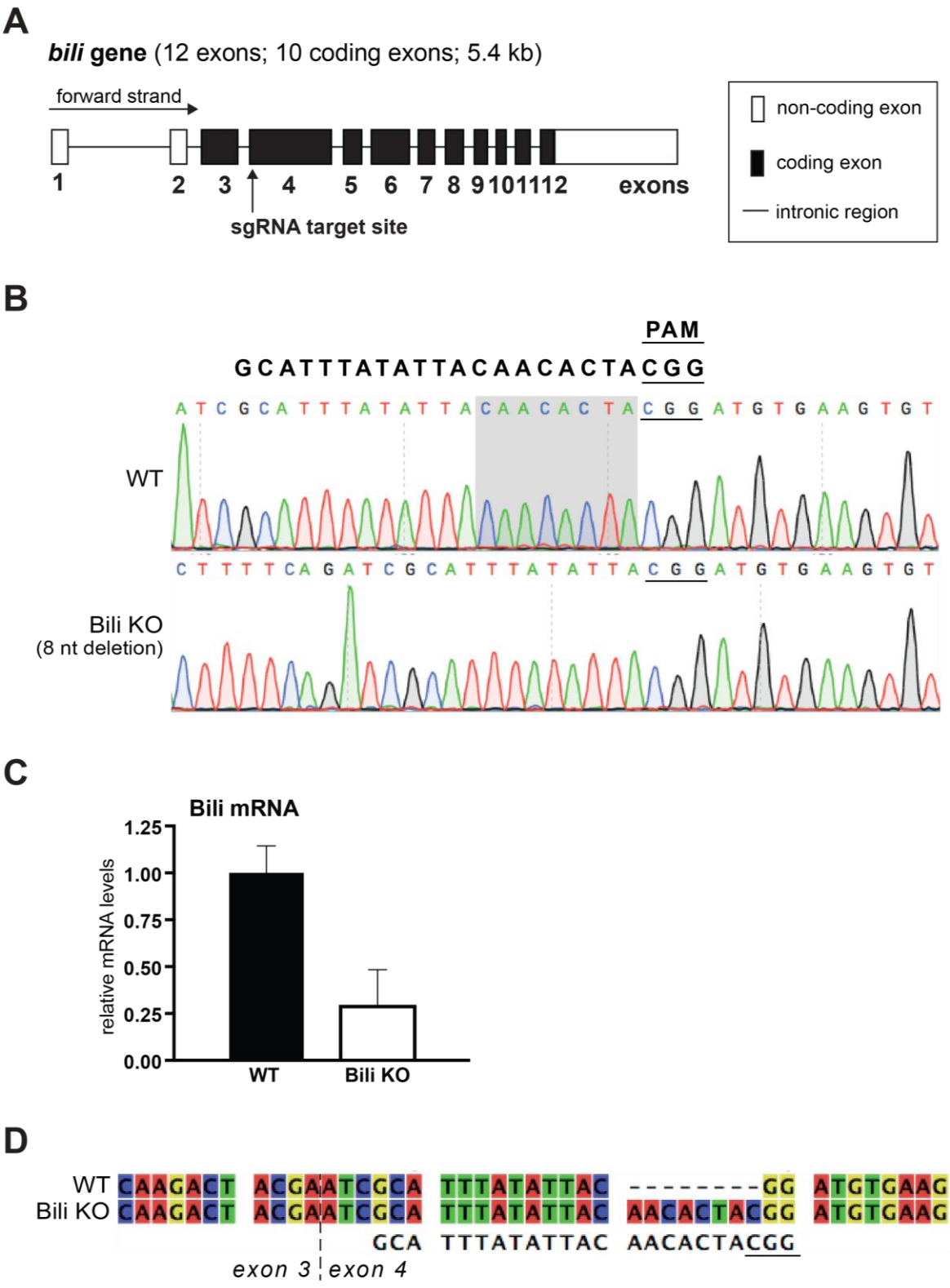


Figure 5.6 | Generation of Bili KO flies. A) Map of Bili gene based on the Ensembl database (Yates et al., 2016) with the sgRNA targeting site in exon 4. **B)** Sequence of the genomic DNA of Bili KO flies and wild-type control flies. The 23 nt sgRNA targeting sequence is shown with the PAM sequence underlined. The 8-nt deletion in the Bili KO fly line is highlighted in grey. **C)** Bili mRNA levels relative to actin mRNA levels analysed by TaqMan PCR in wild-type (WT) and Bili KO flies. **D)** Sequence alignment of fly cDNA generated from whole fly mRNA extraction and RT-PCR. The PAM sequence in sgRNA target site is underlined.

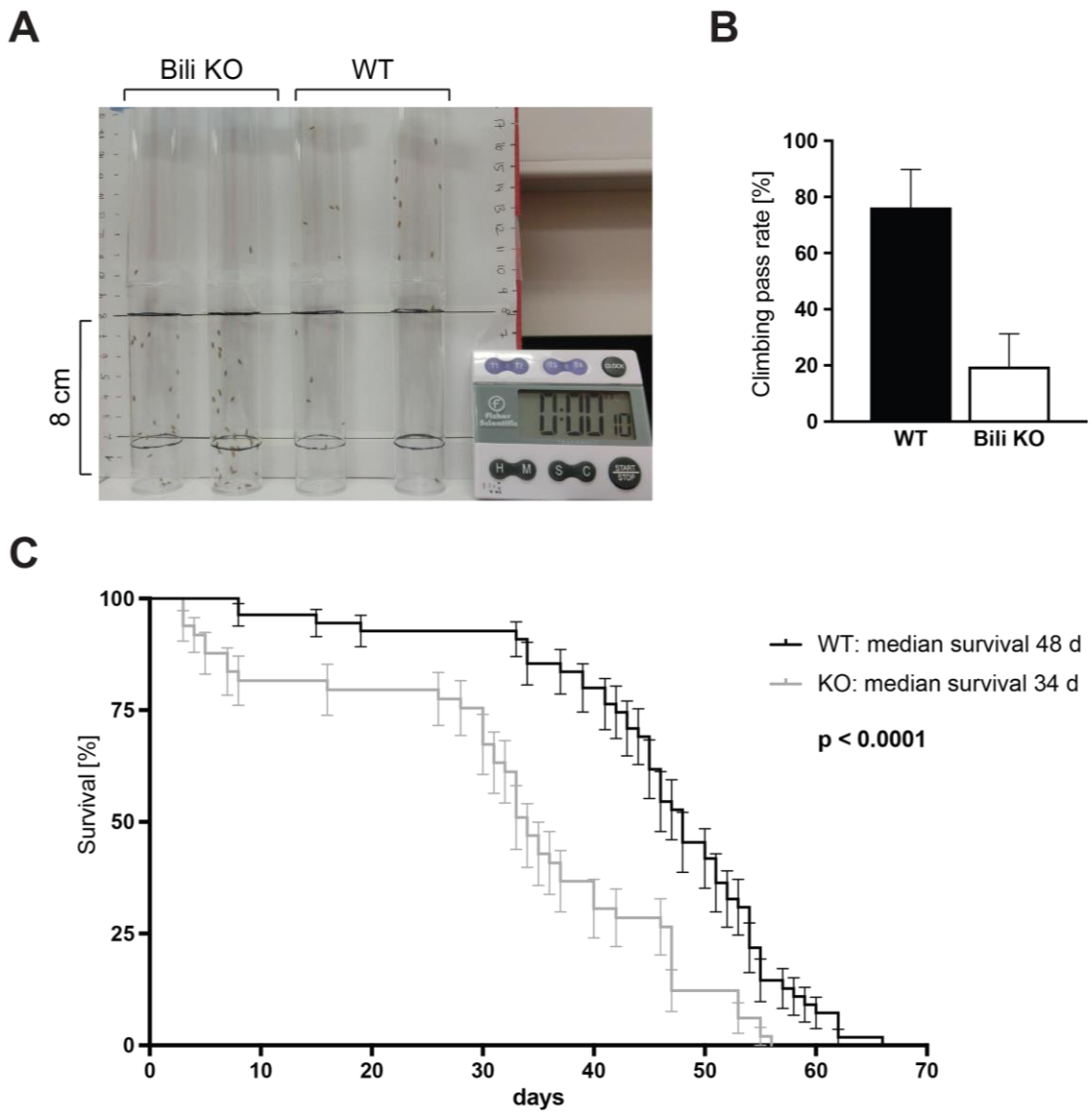


Figure 5.7 | Bili KO flies have an impaired climbing ability and a reduced life span. A) Set-up for the negative geotaxis assay measuring the percentage of flies reaching an 8-cm mark within 10 s. **B)** Results of the negative geotaxis assay described in A). Female flies at the age of 1 day were used. Results of two independent experiments are shown; n=32 (WT); n=50 (Bili KO). **C)** Survival rate of flies was measured in male flies. Flies were flipped every 2-3 days to a fresh tube to prevent sticking to the food. Data was analysed using the survival analysis in GraphPad Prism 7 (Gehan-Breslow-Wilcoxon test). n=55 (WT); n=49 (Bili KO).

5.3 Discussion

5.3.1 Analysis of the first FRMD8 KO animals

In this chapter, I reported the generation of the first FRMD8 KO flies and mice and showed that FRMD8 plays an important biological role in both model organisms. Although further investigations will have to analyse the phenotypes of these animals in more detail to understand the full implication of FRMD8 loss, my initial analysis of FRMD8 KO animals already allows me to draw conclusions about the biological relevance of FRMD8. FRMD8 is not essential for the development in *Drosophila*. Bili KO flies generated in this project were viable with no obvious developmental defects, which is consistent with the phenotype of a Bili RNAi line generated in the 'Unknome' project, which has analysed conserved, uncharacterised genes (Joao Rocha, Sean Munro, Matthew Freeman, personal communication). Given that Bili was suggested to be a negative regulator of Wnt signalling (Kategaya et al., 2009), and that the loss of axin, another negative regulator of the canonical Wnt signalling pathway, is lethal in *Drosophila* and mice (Zeng et al., 1997, Hamada et al., 1999), it is rather surprising that Bili KO flies are viable. These findings indicate that the role of Bili in Wnt/β-catenin signalling might not be essential or it is redundant to other proteins. Moreover, Bili KO flies show impaired locomotion, a phenotype that resembles iRhom KO flies. This again, is in line with the findings from the Unknome project, which found that a Bili RNAi line showed impaired locomotion at the age of 22 days (Joao Rocha, Sean Munro, Matthew Freeman, personal communication) implying that the defects caused by Bili loss increase with age. This might provide a potential explanation for the reduced life span of Bili KO flies.

In mice, it is currently unclear whether FRMD8 loss causes perinatal lethality, as the number of litters analysed from *Frmd8*$^{+/-}$ crosses is still small, and several pups were cannibalised within the first 3 days after birth without the genotype being determined. Of the two confirmed homozygous FRMD8 KO pups, one *Frmd8*$^{-/-}$ pup died 3 days after birth. It is unclear whether this was caused by biological defects due to FRMD8 loss, or if it was natural pre-weaning mortality, which is a frequent occurrence for pups (Weber et al.,

2007). A second *Frmd8*$^{-/-}$ pup, which was confirmed to be a FRMD8 KO at the protein level, survived 15 days without showing any defects, implying that FRMD8 KO mice are not embryonically lethal. Once the mouse colony is bigger, the question whether FRMD8 causes perinatal lethality can be addressed in detail.

Hypomorphic ADAM17 mice, called *Adam17*$^{ex/ex}$, show drastically reduced ADAM17 levels and are viable but show eye, heart and skin defects, and increased susceptibly to colitis upon DSS treatment (Chalaris et al., 2010). Considering the similarity of mature ADAM17 in *Frmd8*$^{-/-}$ and *Adam17*$^{ex/ex}$ mice, I would expect FRMD8 KO mice to be viable if the main function of FRMD8 was the regulation of the iRhom/ADAM17 pathway. Further studies of FRMD8 KO mice will have to investigate whether similar phenotypes to *Adam17*$^{ex/ex}$ mice can be observed, which would lead to the conclusion that the primary physiological role of FRMD8 is the regulation of the iRhom/ADAM17 pathway. Any other or more severe phenotypes could be caused by additional biological roles of FRMD8. Overall, further studies of the KO animals are required to fully understand the biological role of FRMD8 in mice and flies.

5.3.2 A role for FRMD8/Bili in regulating iRhom in flies?

My data suggest that FRMD8 has a conserved role in binding to iRhoms because I showed an interaction of Bili and *Drosophila* iRhom when expressed in human cell lines. The interaction of Bili and iRhom is, however, more difficult to prove *in vivo* and would require good antibodies for both proteins or tagged proteins expressed in flies. The fact that both Bili and iRhom are highly expressed in neuronal tissues from embryos to adults (Kategaya et al., 2009, Zettl et al., 2011, FlyAtlas (Chintapalli et al., 2007)) further supports the idea that Bili and iRhom could interact in flies. In addition, the similar phenotypes of Bili KO and iRhom KO flies suggest that these proteins could also act in the same pathway. Although the primary cellular role of iRhoms is different in flies and mammals, the iRhom-FRMD8 interaction and the basic underlying mechanism of FRMD8 regulating iRhom might be conserved. For this reason, it would be interesting to test

whether FRMD8 affects iRhom levels in flies. Future experiments will have to dissect the molecular function of Bili and its link to iRhom in *Drosophila*.

5.3.3 FRMD8 regulates TNFα signalling in human macrophages

In this chapter, I showed that loss of FRMD8 leads to a reduction of TNFα release from iPSC-derived macrophages. The iPSC-derived macrophages generated in this project developmentally resemble yolk sac-derived tissue-resident macrophages, which comprise for example microglia in the brain, Kupffer cells in the liver, and Langerhans cells in the epidermis, and are developmentally different to BMDMs (Buchrieser et al., 2017). Since all macrophages and monocytes are considered to be major producers of TNFα (Parameswaran and Patial, 2010), it will be interesting to see if a reduction of TNFα release can also be confirmed using BMDMs from FRMD8 KO mice. Given the striking reduction of mature ADAM17 levels in BMDMs from FRMD8 KO (Fig. 5.4D), and considering that ADAM17 is the primary sheddase for proTNFα in macrophages (Bell et al., 2007, Horiuchi et al., 2007a), it is likely that an effect on TNFα release will be observed.

In summary, macrophages are a suitable cell type to further investigate the mechanism of FRMD8 function, as they have high iRhom2 and FRMD8 expression levels allowing the study of endogenous protein levels, and show a significant phenotype with the impaired release of the pro-inflammatory cytokine TNFα.

CHAPTER 6

Discussion and future directions

6 Discussion and future directions

6.1 The role of FRMD8 in the iRhom/ADAM17 pathway

In this project, I identified FRMD8 as a new interaction partner of iRhom1 and iRhom2 and showed that FRMD8 has a crucial role in the iRhom/ADAM17 pathway, as evidenced by the impaired ADAM17-mediated shedding in FRMD8-deficient cells. My data suggest that FRMD8 stabilises iRhom2, and potentially iRhom1, *in vitro* and *in vivo*. FRMD8 binds to the N-terminus of iRhom2 throughout the entire secretory pathway and appears to block constitutive lysosomal degradation of iRhom2 (Fig. 6.1A). Although the mechanism by which FRMD8 leads to lysosomal degradation of iRhoms is unclear, it is tempting to speculate that FRMD8's function in the iRhom/ADAM17 pathway involves hindering a downstream protein from binding to iRhom2, similar to the described role of FRMD8 in Wnt signalling, where FRMD8 blocked the downstream interaction of the cytosolic protein axin with the Wnt signalling receptor LRP6 (Kategaya et al., 2009). This could for instance be a protein involved in cargo sorting in the endosomal/lysosomal pathway. Potential candidates are proteins of the endosomal sorting complex required for transport (ESCRT) complex, which play for example a role in cargo sorting in endosomes (Frankel and Audhya, 2017).

Furthermore, FRMD8 loss leads to a reduction of iRhom2, primarily at the cell surface. Loss of iRhom2 stability in FRMD8-deficient cells reduces mature ADAM17 levels, whereas proADAM17 levels are not affected, and ultimately results in impaired ADAM17-dependent shedding of EGFR ligands and TNFα (Fig. 6.1B). Overall, my data demonstrate that FRMD8 plays a crucial role in the iRhom/ADAM17 pathway. This raises the question whether FRMD8 is a core component or a more transient regulator of the iRhom/ADAM17 pathway. As FRMD8 was able to bind iRhom2 throughout the entire secretory pathway and potentially forms a tripartite complex with iRhom2 and ADAM17, it is likely that FRMD8 is a core protein of an iRhom-ADAM17 complex and ensures its stability. This hypothesis has, of course, to be confirmed by further studies of the potential FRMD8-iRhom-ADAM17 tripartite complex. Further supporting the hypothesis of FRMD8

as a core component of the iRhom/ADAM17 signalling pathway, as opposed to a transient regulator, are the facts that FRMD8 can bind to both iRhoms and is, according to databases, expressed in most tissues. A regulatory protein would perhaps be expected to affect a pathway only under certain circumstances or in certain tissues. So far, however, I have not identified a condition under which FRMD8 does not bind to iRhom2 or affect mature ADAM17 levels. FRMD8 loss reduces mature ADAM17 in all mouse tissues tested (Fig. 5.4A), including the brain in which iRhom1 is the primary iRhom expressed (Li et al., 2015), also supporting the idea that FRMD8 affects both iRhom1 and iRhom2. Notably, I found that the interaction of FRMD8 and iRhoms is also conserved in *Drosophila*, although *Drosophila* iRhom has no reported role in ADAM17 regulation. This might suggest that FRMD8 is also required to stabilise iRhom in *Drosophila*. The phenotype of flies mutant for Bili, the fly orthologue of FRMD8, which resembles iRhom KO flies, supports this hypothesis, and future experiments will investigate the role of FRMD8 in iRhom function in *Drosophila*.

Taken together, my data currently suggest that FRMD8 is a core factor of the iRhom/ADAM17 signalling pathway, but future experiments will have to investigate whether FRMD8's function in stabilising iRhoms and mature ADAM17 is inducible or absent under certain conditions. Despite its importance, FRMD8 is not essential for the interaction between iRhom2 and ADAM17 or ADAM17 maturation as there was still some mature ADAM17 remaining in most FRMD8-deficient tissues and cell lines (Fig. 4.4A, 5.1B and 5.4A).

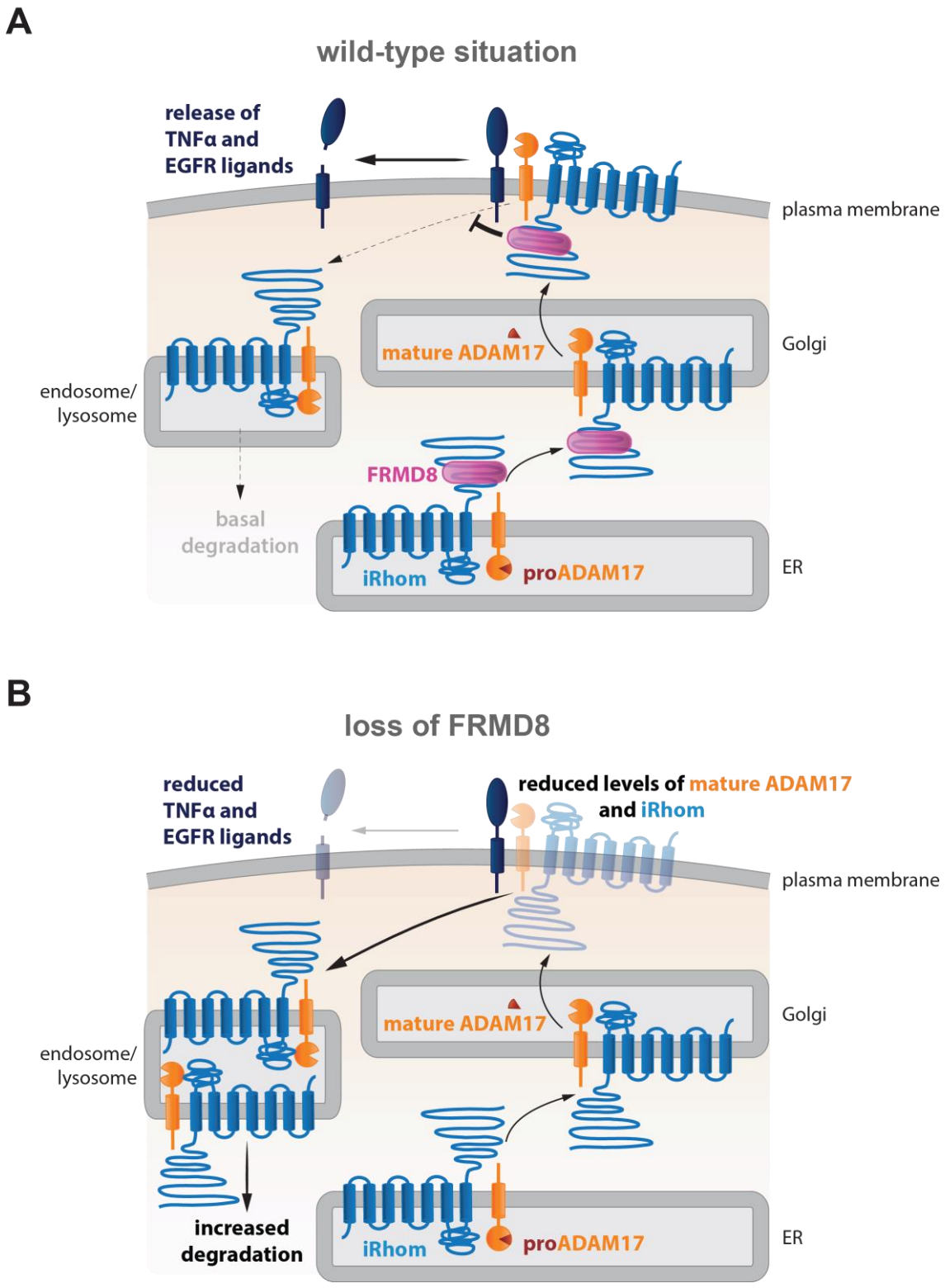


Figure 6.1 | Schematic representation of the FRMD8 function in the iRhom/ADAM17 pathway. A) The iRhom/ADAM17 pathway under wild-type conditions. **B)** Defects in the iRhom/ADAM17 pathway upon FRMD8 loss.

6.2 The function of FRMD8 in other pathways

FRMD8 was identified as a negative regulator of Wnt/β-catenin signalling in a *Drosophila* screen. The effect of FRMD8 gain- and loss-of-function on Wnt signalling was confirmed in *Drosophila*, zebrafish and human cells using a β-catenin luciferase reporter or phenotypic analysis of *Drosophila* and zebrafish embryos. FRMD8 knockdown enhanced the activation of the β-catenin reporter, suggesting that FRMD8 is a negative regulator of the Wnt signalling pathway (Kategaya et al., 2009). I have performed similar experiments using a TOPflash/FOPflash reporter assay (Korinek et al., 1997) (data not shown) confirming the data reported by Kategaya et al. (2009). The mechanistic role of FRMD8 in Wnt signalling, however, is poorly understood. It was shown that FRMD8 binds to LRP6 in human and *Drosophila* cells. The binding of axin to LRP6, which occurs upon activation of Wnt signalling, was reduced upon overexpression of FRMD8, whereas FRMD8 knockdown increased axin binding to LRP6. These experiments led to the conclusion that FRMD8 blocks the recruitment of axin to LRP6. Further experiments or follow-up studies have not been reported, so we still lack a good understanding of FRMD8 function in this pathway. It will be interesting to investigate if there are parallels between the roles of FRMD8 in regulating LRP6 and iRhoms, for instance if FRMD8 binding has consequences for LRP6 stability. It has indeed been shown that inhibition of the lysosomal pathway increased Wnt signalling (Dobrowolski et al., 2012), as LRP6 presumably has to enter the endocytic compartment in order to initialise downstream activation of β-catenin (Cruciat et al., 2010). The role of FRMD8 in controlling LRP6 and iRhom2 can be addressed in future experiments using the FRMD8-defcient cell lines and model organisms generated in this project.

FRMD8 KO mice will also help to examine whether FRMD8 has physiologically important functions in addition to its role in Wnt signalling and the iRhom/ADAM17 pathway. As I have discovered that FRMD8 stabilises iRhom2, and potentially iRhom1, FRMD8 might also have effects on other cellular functions of iRhoms, such as the regulation of STING or the degradation of EGFR ligands. FRMD8 loss mainly affected

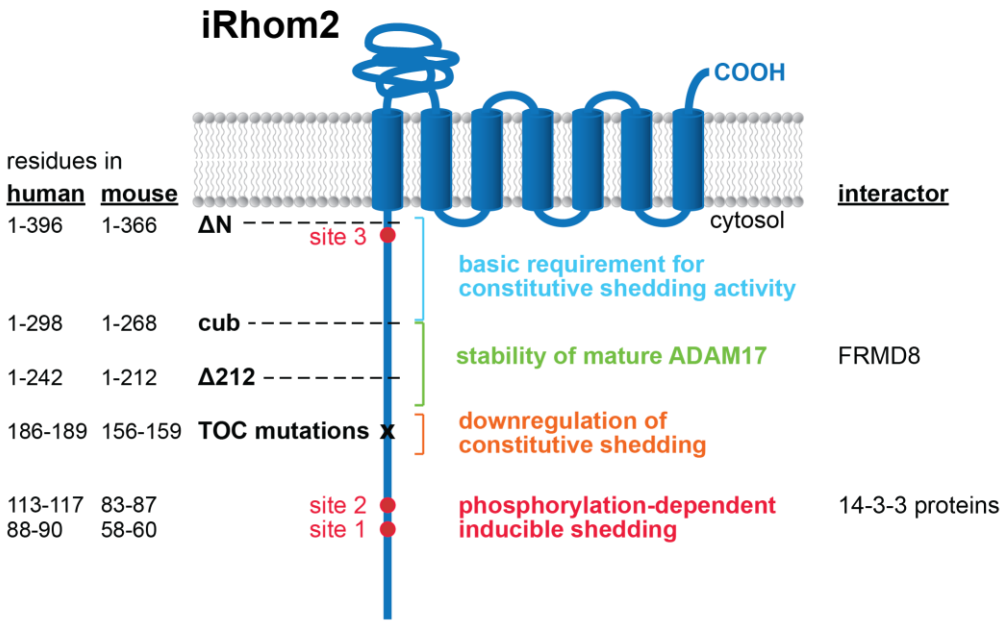
iRhom2 levels at the plasma membrane (Fig. 4.11A), which would suggest that iRhom2's function in ERAD and STING regulation, which affects mainly the ER, might not be implicated. I have not addressed the function of iRhom-mediated ERAD of EGFR ligands or the activation of type I IFN in FRMD8-deficient cells, but this is another question to be examined in the future.

Overall, the knowledge about FRMD8 is still limited, and its role in other pathways than iRhom/ADAM17 and Wnt/β-catenin signalling has not been addressed. Further studies are required to gain a more complete picture of the cellular function of FRMD8. A full analysis of the generated FRMD8 KO mice will also reveal potential other physiologically relevant roles of FRMD8.

6.3 The role of the iRhom2 N-terminus in regulating ADAM17 activity

My data that FRMD8 binds to the iRhom2 N-terminus and controls ADAM17 activity further support the increasing evidence that the iRhom N-terminus plays a key role in regulating ADAM17 function. For example, an iRhom2 mutant lacking the entire N-terminus showed no stable mature ADAM17 on the cell surface, no binding of iRhom2 to mature ADAM17, and no stimulated or constitutive ADAM17-mediated shedding (Grieve et al., 2017). When smaller parts of the iRhom2 N-terminus are deleted or mutated, distinct effects on ADAM17 activity have been observed, such as increased constitutive shedding (Brooke et al., 2014, Hosur et al., 2014, Maney et al., 2015) or loss of stimulated shedding (Siggs et al., 2014, Grieve et al., 2017), which suggests that different regions within the iRhom2 N-terminus have distinct functions. A critical review of the iRhom2 literature allows me to speculate about the location within the N-terminus of different functional and binding domains (Fig. 6.2A-B).

A



B

iRhom2 mutant	effect on ADAM17 activity	reference
ΔN (Δ366, mouse)	no stability of mature ADAM17 no binding to mature ADAM17 no constitutive shedding no stimulated shedding	(Grieve et al., 2017) (Grieve et al., 2017) (Grieve et al., 2017) (Grieve et al., 2017, Maretzky et al, 2013)
cub (Δ268, mouse)	no stability of mature ADAM17 reduced binding to mature ADAM17 elevated constitutive shedding no stimulated shedding	(Sigg et al., 2014, and unpublished) (Sigg et al., 2014) (Hosur et al., 2014) (Sigg et al., 2014)
Δ212 (mouse)	reduced stability of mature ADAM17? no binding to mature ADAM17? elevated constitutive shedding increased iRhom levels at cell surface no stimulated shedding	(Maney et al., 2015) (Maney et al., 2015) (Maney et al., 2015) (Maney et al., 2015) (Maney et al., 2015)
TOC mutations (186, 188, 189, human)	stability of mature ADAM17 elevated constitutive shedding changed iRhom localisation normal stimulated shedding	(Brooke et al., 2014) (Brooke et al., 2014, Maney et al., 2015) (Blaydon et al, 2012) (Brooke et al., 2014)
site 1-3 mutation (58-60, 83-87, 357-361, mouse)	no stimulated shedding, no 14-3-3 binding	(Grieve et al., 2017)

Figure 6.2 | Distinct functions of the iRhom2 N-terminus in regulating ADAM17 activity A) Schematic representation of the human iRhom2 and the localisation of N-terminal mutations and deletions. Deletions reported in mouse iRhom2 have been converted to the size of the corresponding human deletion (e.g. the iRhom2 cub mutation is a deletion of 1-268 in mouse and corresponds to a loss of 1-298 in human iRhom2). **B)** List of phenotypes of different iRhom2 mutants and their effect on ADAM17 activity. Red, orange, green phenotypes correspond to the different distinct regions in A). Black labelled phenotypes were not linked to a region shown in A), but might be linked to the phenotype listed one line above it.

6.3.1 Regions required for ADAM17-dependent shedding

iRhom$^{\Delta N}$, a complete deletion of the iRhom2 N-terminus, cannot perform any ADAM17-mediated shedding, whereas iRhom2^{cub} is able to support constitutive shedding (Hosur et al., 2014, Grieve et al., 2017, personal communication with Hongmei Xu). This suggests that the area between amino acids 269 to 366 of mouse iRhom2 might contain the minimum requirement for constitutive shedding (Fig. 6.2A). In addition, a second site in iRhom2 seems to be required to downregulate constitutive ADAM17-dependent shedding. Three different point mutations in the iRhom2 N-terminus (I186T, D188N, and P189L) are associated the inherited skin disease TOC (Blaydon et al., 2012, Saarinen et al., 2012) and showed higher constitutive ADAM17-mediated shedding (Brooke et al., 2014, Maney et al., 2015). The site around the TOC mutations is presumably required to downregulated constitutive shedding as cells expressing iRhom$^{\Delta 212}$, in which the TOC sites are missing, showed a similar increase in constitutive shedding to TOC mutants (Maney et al., 2015).

Recently, three sites within the iRhom2 N-terminus have been identified to be required for stimulated ADAM17-mediated shedding (Grieve et al., 2017). Upon stimulation of cells with phorbol esters or GPCR agonists these sites were phosphorylated and recruited 14-3-3 proteins, which alter the iRhom2-ADAM17 interaction and enhance ADAM17 shedding activity. Two of these sites are missing in iRhom$^{\Delta 212}$ and in iRhom2^{cub}, but not in the TOC mutants (Fig. 6.2A), probably explaining why cells from TOC patients can, in contrast to iRhom2^{cub}, still undergo stimulated shedding (Brooke et al., 2014, Hosur et al., 2014, Siggs et al., 2014).

6.3.2 The region required for mature ADAM17 stability

My work and previous reports indicate that the iRhom2 N-terminus harbours a site located approximately between amino acids 200 to 300 of human iRhom2 (Fig. 6.2A) that is required to stabilise mature ADAM17 at the cell surface. iRhom$^{\Delta N}$ and iRhom2^{cub} mutants, in which this stabilising region is missing, lack mature ADAM17 levels at the plasma membrane (Siggs et al., 2014, Grieve et al., 2017), whereas TOC mutants clearly

show mature ADAM17 levels (Brooke, 2014). The mature ADAM17 levels can be rescued in iRhom$^{\Delta N}$- and iRhom2^{cub}-expressing cells by treatment with the lysosomal inhibitor bafilomycin (personal communication with Hongmei Xu and (Grieve et al., 2017)) suggesting that mature ADAM17 is generated in these cells but quickly degraded through the lysosomal pathway. These reports about mature ADAM17 levels in iRhom$^{\Delta N}$- and iRhom2^{cub}-expressing cells are consistent with my data, which show that FRMD8 protects mature ADAM17 levels from lysosomal degradation and that FRMD8 cannot bind to iRhom2^{cub} or iRhom2 lacking its N-terminus (Fig.4.7). Loss of FRMD8 binding might therefore explain the absence of mature ADAM17 and the impaired shedding in iRhom$^{\Delta N}$ and iRhom2^{cub} cells. Maney and colleagues (Maney et al., 2015) also observed reduced mature ADAM17 levels in the mouse iRhom2$^{\Delta 212}$ mutant, which corresponds to a deletion of 242 amino acids of human iRhom2 (Fig. 6.2A). As the rescue of mature ADAM17 levels with bafilomycin treatment has not been tested in this mutant, it is currently unclear whether the reduction of mature ADAM17 is also caused by decreased stability of mature ADAM17. My data suggested that the FRMD8 binding site, and therefore the site required to stabilise mature ADAM17, is located between amino acids 242 and 298 of human iRhom2 (Fig. 4.8A). To further support this hypothesis, it would be important to generate mutants of human and mouse iRhom2 that are not able to bind to FRMD8 by making internal deletions of iRhom2, such as generating human iRhom2$^{\Delta 200\text{-}300}$. These experiments will help to confirm that the loss of mature ADAM17 at the plasma membrane, which was observed in several different iRhom2 mutants, is indeed caused by the loss of FRMD8 binding.

6.3.3 The iRhom2 cub mutation

The literature-based prediction of the distinct regulatory sites within the iRhom2 N-terminus might help to systematically investigate the role of the iRhom2 N-terminus. This will be particularly important in understanding the regulation of ADAM17 in *Rhbdf2*$^{cub/cub}$ mice, which has proven to be complex: whereas the cub mutation increased secretion of

the EGFR ligand AREG, TNFα shedding was impaired in mice (Hosur et al., 2014). There is also discrepancy of some reported iRhom2^{cub} functions with my proposed model: I have shown that loss of FRMD8 destabilises iRhom2, leading to the degradation of mature ADAM17, which is consistent with the absence of most constitutive or stimulated shedding in FRMD8-deficient cells. iRhom2^{cub} was shown to be able to support constitutive release of EGFR ligands (Hosur et al., 2014) but not stimulated shedding (Siggs et al., 2014) due to the lack of stable mature ADAM17 (Hongmei Xu, unpublished). As the elevated EGFR ligand release was not sensitive to metalloprotease inhibitors, it has been suggested by Hosur and colleagues (Hosur et al., 2014) that iRhom2 directly affects the release of AREG by proteolytically cleavage. This proposal seems very unlikely. It is not consistent with the concept of iRhoms as pseudoenzymes (Zettl et al., 2011), and it lacks biochemical and physiological evidence. It is perhaps more likely that either there was a problem with the experimental design reported by Hosur et al. (2014) or that the complexity of the cub mutant lies in the differential regulation of distinct ADAM17 substrates. It was also suggested that cub and TOC mutations increase iRhom2 stability, however, this has only been shown in transient transfections of iRhom2 constructs (Hosur et al., 2014). My own data would suggest that iRhom2^{cub} is less stable than wild-type iRhom2 due to the lack of the FRMD8 binding site. However, it is possible that regulation of the iRhom-ADAM17 relationship is even more complex than outlined here and additional sites at the beginning of the N-terminus might negatively regulate iRhom stability. Overall, as mentioned above, the iRhom2^{cub} mutation is complex, but smaller deletions of the iRhom2 N-terminus might help to reveal the underlying mechanism of ADAM17 regulation in *Rhbdf2*$^{cub/cub}$ mice.

In summary, the iRhom N-terminus has several distinct functions in regulating ADAM17 activity but the regions required for these functions have hardly been investigated using smaller truncation or point mutations of the iRhom2 N-terminus. Only recent studies on novel interaction partners, such as 14-3-3 proteins and FRMD8, have helped to shed light into the function of different regions of the iRhom2 N-terminus and contribute to a better understanding of the function of the iRhom N-terminus. At the moment it still remains

unclear which properties of iRhom2 are altered in the different mutations and how this subsequently leads to defects in constitutive shedding, stimulated shedding or stability of mature ADAM17. Future studies are required to analyse how iRhom localisation, stability or its interaction with other proteins are regulated by the iRhom N-terminus and how this affects iRhom function in regulating ADAM17 activity.

6.4 Importance of analysing endogenous iRhom levels

In this project, I demonstrated that FRMD8 stabilises iRhom2, however, the reduction of exogenously expressed iRhom2 in FRMD8-deficient cells was not obvious (Fig. 4.10A and 4.11B). This could be explained by the fact that large amounts of iRhom2 are mainly located in the ER and the Golgi (Zettl et al., 2011, Adrain et al., 2012, McIlwain et al., 2012, Luo et al., 2016), whereas FRMD8 loss mainly affected the stability of iRhom2 on the cell surface (Fig. 4.11A), and the cell surface pool of iRhom2 was reported to be relatively small in iRhom-overexpressing cells (Maney et al., 2015). However, when examining the effect of FRMD8 loss on endogenous iRhom2 levels, the reduction of iRhom2 levels was clearly detectable (Fig.4.13C). The discrepancy between exogenously expressed iRhom2 and endogenous iRhom2 might be explained by the different cellular localisation of iRhoms: a higher proportion of endogenous iRhoms might reach the cell surface compared to overexpressed iRhoms. Supporting this hypothesis, a proteomic study in HeLa cells reported that endogenous iRhom2 is localised at the plasma membrane (Itzhak et al., 2016) despite the location of overexpressed iRhom always appearing to be largely restricted to the ER. Similarly, immunofluorescence analysis of human skin showed a strong cell surface localisation of iRhom2 (Blaydon et al., 2012). These studies might imply that the amount of endogenous iRhom2 at the cell surface is higher than estimated by iRhom overexpression studies or alternatively that the cell surface levels of iRhoms are cell type-specific.

Considering that iRhoms are multi-pass membrane proteins with cysteine-rich domains, their overexpression might cause stress for the folding machinery in the ER,

leading to a higher proportion of iRhoms being retained in the ER than under endogenous conditions. However, it is important to note that overexpression of iRhom1 or iRhom2 rescues the loss of endogenous iRhoms (Grieve et al., 2017) demonstrating that overexpression does not block normal iRhom function in ADAM17 activation, and that overexpressed iRhom can reach the plasma membrane. Nevertheless, it will be necessary to further analyse the extent of endogenous iRhom1 and iRhom2 at the plasma membrane. In our endogenously tagged cell line, iRhom2 localisation could not be determined by immunofluorescence due to its low expression (data not shown). At the moment, the tools to study endogenous iRhoms are limited, but it will be important to invest in the generation of endogenously tagged cell lines and, ideally, in good antibodies. As iRhom2 is highly expressed in skin and immune cells (www.proteinatlas.org), it might be worth attempting endogenous tagging in keratinocytes, as immune cell lines are not easy to genetically modify. Alternatively, the study of the more ubiquitously expressed iRhom1 might be easier.

In conclusion, my data suggests that it is crucial to study the functions of endogenous iRhoms in order to address their role at the cell surface. The generation of good antibodies, which has proven difficult, would also improve the analysis of the function and localisation of endogenous iRhoms.

6.5 FRMD8, iRhoms and ADAM17 as potential drug targets

Here I showed that FRMD8 affects the levels of mature ADAM17 in mouse tissues, and the shedding activity of mature ADAM17 in human cell lines and macrophages. As the principle sheddase of several EGFR ligands and the inflammatory cytokine TNFα, increased ADAM17 expression has been linked to inflammatory diseases and various types of cancer (Saftig and Reiss, 2011). For this reason, it will be discussed whether FRMD8 constitutes a potential drug target for diseases linked to increased ADAM17 shedding activity.

6.5.1 ADAM17 inhibitors

ADAM17 itself has been in focus of various attempts to develop small-molecule inhibitors for the potential treatment of inflammatory diseases and cancer, but none of these compounds has successfully passed clinical testing so far (Moss et al., 2008, Mullooly et al., 2016). The main challenges for the design of ADAM17 inhibitors are on one hand the specificity for ADAM17, to prevent side effects resulting from inhibition of a broad spectrum of metalloproteases, and on the other hand, the overlapping substrate repertoire of several proteases, which might lead to ineffective drugs in patients. For this reason a detailed understanding of the pathways that are targeted is required and this might explain why early generations of small molecule inhibitors, designed to target a wide range of metalloproteases, have all failed in clinical trials due to the lack of efficiency (Vandenbroucke and Libert, 2014). Despite these discouraging results, new generations of small molecule inhibitors have been developed with selectivity for ADAM17, and several compounds showed indeed promising anti-tumour effects in preclinical studies and clinical phase I/II trials (reviewed in (Mullooly et al., 2016)). Other strategies for ADAM17 inhibition involve the use of purified ADAM17 pro-domain (Wong et al., 2016) and monoclonal anti-ADAM17 antibodies (Caiazza et al., 2015). An anti-ADAM17 and T-cell-activating bi-specific antibody showed the specific killing of ADAM17-expressing cells by T-cells (Yamamoto et al., 2012) and might prove the potential to use ADAM17 as a target for cancer immunotherapy.

When anticipating ADAM17 inhibition in disease, it has to be considered that ADAM17-deficiency leads to severe side effects as seen in ADAM17-deficient patients, which suffer from recurrent infections, hair defects, and severe skin inflammations and lesions (Blaydon et al., 2011, Bandsma et al., 2015, Tsukerman et al., 2015). For this reason, long-term treatment with ADAM17 inhibitors can potentially lead to side effects, and the tissue-specific or short-term inhibition of ADAM17 is presumably more desirable for clinical applications.

6.5.2 iRhom2 as a drug target?

iRhom2 is an immune cell-specific regulator of ADAM17 activity and TNFα release, and has for this reason been suggested as a potential drug target for the treatment of TNFα-dependent inflammatory diseases (Issuree et al., 2013). TNFα is the target of several monoclonal antibody-based drugs, which are successfully used for the treatment of rheumatoid arthritis and other chronic inflammatory diseases, although TNFα antibodies can lead to side effects including, for example, susceptibility to severe inflections (Monaco et al., 2015). Selectively targeting the iRhom2, would specifically inhibit TNFα release from immune cells as the lack of iRhom2 in other cells can be compensated by iRhom1 (Christova et al., 2013, Li et al., 2015), but macrophages rely only on iRhom2 function to secrete TNFα (Adrain et al., 2012, McIlwain et al., 2012). To inhibit iRhom2 function, the iRhom2-ADAM17 interaction would have to be targeted with small molecule or peptide-based inhibitors, which is difficult but, due to advances in computational design of TMD-binding peptides and high-throughput screening, perhaps not impossible anymore (Yin and Flynn, 2016). Given the therapeutic success of existing anti-TNFα therapies (Monaco et al., 2015), however, it is questionable whether targeting iRhom2, even if it was successful, would further improve the treatment of rheumatoid arthritis patients. At the moment, the idea of iRhom2 as a drug target seems unrealistic, especially since information, such as the structure of an iRhom2-ADAM17 complex, which would help in designing protein-protein interaction (PPI) inhibitors, are still missing.

The inhibition of the interaction of iRhom2 and 14-3-3 proteins has also been suggested as a drug target as it seems easier to target cytosolic protein-protein interactions (Grieve et al., 2017). Indeed, the inhibition of PPIs can be achieved by targeting interaction “hot spots” (Clackson and Wells, 1995) using small molecules, and several compounds are currently tested in clinical trials (Arkin et al., 2014). The inhibition of 14-3-3 PPIs has also been shown to be successfully targeted with small molecule and peptide inhibitors (Mori et al., 2013). However, it is uncertain whether blocking of the iRhom-14-3-3 interaction would be beneficial for the treatment of ADAM17-linked

diseases, as it would still enable constitutive ADAM17-dependent shedding. Elevated constitutive shedding causes hair and skin phenotypes, as well as susceptibility to cancer as seen in tylosis patients, *Rhbdf2*$^{cub/cub}$, and *Rhbdf2*$^{uncv/uncv}$ mice (Blaydon et al., 2012, Hosur et al., 2014, Leilei et al., 2014, Siggs et al., 2014). For this reason, the FRMD8-iRhom interaction might be a better drug target because FRMD8 loss decreases all ADAM17-dependent shedding without mimicking complete ADAM17 loss.

6.5.3 FRMD8 as a drug target?

Targeting FRMD8 might be beneficial for the treatment of diseases associated with excessive ADAM17-dependent shedding, such as TOC or certain types of cancer. Similar to 14-3-3 proteins, the FRMD8-iRhom interaction could be targeted with small molecules that block the interface of FRMD8 with iRhom1 and iRhom2. For the design of such compounds, structural information is very important (Mori et al., 2013), so future studies will have to analyse the structure of FRMD8, ideally co-crystallised with iRhom2 peptides. The extensive structural analysis of the FERM domain of KRIT1, a paralogue of FRMD8 (FERM domains of KRIT1 and FRMD8 share 27% identity in the amino acid sequence), might benefit purification and crystallisation attempts for FRMD8. Furthermore, detailed analysis of FRMD8 KO mice are required to investigate whether the reduced mature ADAM17 levels in *Frmd8*$^{-/-}$ mice have beneficial effects on inflammation, wound healing or tumourigenesis. At the moment, the biological role of FRMD8 is not well understood and future studies are required to determine whether FRMD8 could indeed be a drug target for disease linked to excessive ADAM17-mediated shedding. Further characterisations of FRMD8 KO mice will provide valuable information about the potential therapeutic relevance of FRMD8.

To conclude, FRMD8 is a novel component of iRhom/ADAM17 pathway both *in vitro* and *in vivo* and plays a crucial role in the ADAM17-dependent release of TNFα and EGFR ligands. My work has revealed the importance of FRMD8 but, as a poorly characterised

protein, little is yet known about the function of FRMD8. Future analysis of the FRMD8 KO mice that I have generated will help to reveal its physiological function and shed light onto its role in the iRhom/ADAM17 pathway.

Appendix

```
hiRhom1 -------MSEARRDSTSSLQRKKPPWLKLDIPSAV------------------------   28
miRhom1 -------MSEARRDSTSSLQRKKPPWLKLDIPAAV------------------------   28
hiRhom2 MASADKNGGSVSSVSSSRLQSRKPPNLSITIPPPEKETQAPGEQDSMLPEGFQNRRLKKS   60
miRhom2 MASADKNGSNLPSVSGSRLQSRKPPNLSITIPPPE--SQAPGEQDSMLPE----------   48
                ..    * * ** :*** *.: **

hiRhom1 -------PLTAEEPSFLQPLRRQAFLRSVSMPAETAHISSPHHELRRPVLQRQTSITQTI   81
miRhom1 -------PPAAEEPSFLQPLRRQAFLRSVSMPAETARVPSPHHEPRRLVLQRQTSITQTI   81
hiRhom2 QPRTWAAHTTACPPSFLPKRKNPAYLKSVSLQEPRSRW--QESSEKRPGFRRQASLSQSI  118
miRhom2 ------------------RRKNPAYLKSVSLQEPRGRW--QEGAEKRPGFRRQASLSQSI   88
                         :. *:*:***:    .:    .   :*  ::**:*::*:*

hiRhom1 RRGTADWFGVSKDSD-STQKWQRKSIRHCSQRYGKLKPQVLRELDLPSQDNVSLTSTETP  140
miRhom1 RRGTADWFGVSKDSD-STQKWQRKSIRHCSQRYGKLKPQVIRELDLPSQDNVSLTSTETP  140
hiRhom2 RKGAAQWFGVSGDWEGQRQQWQRRSLHHCSMRYGRLKASCQRDLELPSQEAPSFQGTESP  178
miRhom2 RKSTAQWFGVSGDWEGKRQNWHRRSLHHCSVHYGRLKASCQRELELPSQEVPSFQGTESP  148
        *:.:*:***** * : . *:*:*:*::*** :**:** .  *:*:****:  *: .**:*

hiRhom1 PPLYVGPCQLGMQKIIDPLARGRAFRVADDTAEGLSAPHTPVTPGAASLCSFSSSRSGFH  200
miRhom1 PPLYVGPCQLGMQKIIDPLARGRAFRMADDTADGLSAPHTPVTPGAASLCSFSSSRSGFN  200
hiRhom2 KP-------CKMPKIVDPLARGRAFRHPEEM-DRPHAPHPPLTPGVLSLTSFTSVRSGYS  230
miRhom2 KP-------CKMPKIVDPLARGRAFRHPDEV-DRPHAAHPPLTPGVLSLTSFTSVRSGYS  200
         *         * **:**********  ::  :   * * *:***. ** **:* ***:

hiRhom1 RLPRRRKRESVAKMSFRAAAALMKGRSVRDGTFR--RAQRRSFTPASFLEEDTTDFPDEL  258
miRhom1 RLPRRRKRESVAKMSFRAAAALVKGRSIRDGTLR--RGQRRSFTPASFLEEDMVDFPDEL  258
hiRhom2 HLPRR-KRMSVAHMSLQAAAALLKGRSVLDATGQRCRVVKRSFAFPSFLEEDVVDGADTF  289
miRhom2 HLPRR-KRISVAHMSFQAAAALLKGRSVLDATGQRCRHVKRSFAYPSFLEEDAVDGADTF  259
        :**** ** ***:**::*****:****: *.* :  *  :***:  ****** .*  * :

hiRhom1 DTSFFAREGILHEELSTYPDEVFESPSEAALKDWEKAPEQADLTGGALDRSELERSHLML  318
miRhom1 DTSFFAREGVLHEEMSTYPDEVFESPSEAALKDWEKAPDQADLTGGALDRSELERSHLML  318
hiRhom2 DSSFFSK-----EEMSSMPDDVFESPPLSASY-FRGIPHS---------ASPVSPDGVQI  334
miRhom2 DSSFFSK-----EEMSSMPDDVFESPPLSASY-FRGVPHS---------ASPVSPDGVHI  304
        *:***::     **:*: **:*****  :*   :.  *..          * :. . : :

hiRhom1 PLERGWRKQKEGA-AAPQPKVRLRQEVVSTAGPRRGQRIAVPVRK-LFAREKRPYGLGMV  376
miRhom1 PLERGWRKQKEGGPLAPQPKVRLRQEVVSAAGPRRGQRIAVPVRK-LFAREKRPYGLGMV  377
hiRhom2 PLK-----------------EYG--RAPVPGPRRGKRIASKVKHFAFDRKKRHYGLGVV  374
miRhom2 PLK-----------------EYSGGRALGPGTQRGKRIASKVKHFAFDRKKRHYGLGVV  346
        **:                  .     .   * :**:***  *::  * *:** ****:*

hiRhom1 GRLTNRTYRKRIDSFVKRQIEDMDDHRPFFTYWLT                           411
miRhom1 GRLTNRTYRKRIDSYVKRQIEDMDDHRPFFTYWLT                           412
hiRhom2 GNWLNRSYRRSISSTVQRQLESFDSHRPYFTYWLT                           409
miRhom2 GNWLNRSYRRSISSTVQRQLESFDSHRPYFTYWLT                           381
        *.  **:**: *.* *:**:*.:*.***:******
```

Figure A1 | Alignment of human and mouse iRhom1 and iRhom2. An asterisk (*) indicates positions which have a fully conserved residue, a colon (:) indicates strongly similar properties of the amino acids, and a period (.) indicates weakly similar properties according to the Clustal Omega tool. NLS have been predicted with the NLSmapper *(*nls-mapper.iab.keio.ac.jp/) and the NucPred tool (Brameier et al., 2007).

Table A1 | Candidate proteins identified in the iRhom1^{WT} and iRhom2^{WT} mass spectrometry screen. HEK293T cells stably expressing human iRhom1^{WT}, iRhom2^{WT} or UNC93B1 were used for mass spectrometry analysis in triplicates. The sequence coverage of each candidate protein and the p-value of differential protein abundance (performed with Perseus by Dr Monika Stegmann) are listed below. P-values that are not statistically significant (> 0.05) are indicated in grey.

Prot. ID	Protein name	Gene	p-value iRhom2^{WT} IP	Coverage [%] iRhom1^{WT} IPs	Coverage [%] iRhom2^{WT} IPs
P78536	ADAM17	ADAM17	$8.07 \cdot 10^{-3}$	67.6; 11.0; 47.2	50.5; 49.3; 49.5
Q9BZ67	FRMD8	FRMD8	$2.44 \cdot 10^{-7}$	48.5; 20.8; 48.3	46.8; 43.6; 48.3
P31947	14-3-3 protein sigma	SFN	$2.19 \cdot 10^{-2}$	21.3; 64.4; 22.2	20.4; 17.1; 17.1
P62258	14-3-3 protein epsilon	YWHAE	$6.61 \cdot 10^{-3}$	77.6; 69.8; 68.2	77.6; 77.6; 75.7
P61981	14-3-3 protein gamma	YWHAG	$3.15 \cdot 10^{-2}$	65.6; 46.2; 47.4	65.2; 66.4; 54.7
Q04917	14-3-3 protein eta	YWHAH	$2.33 \cdot 10^{-2}$	67.5; 50.8; 47.6	67.5; 64.2; 64.6
P27348	14-3-3 protein theta	YWHAQ	$1.20 \cdot 10^{-2}$	76.7; 51.4; 58.0	67.3; 69.4; 72.2
P63104	14-3-3 protein zeta/delta	YWHAZ	$9.14 \cdot 10^{-3}$	79.2; 72.7; 56.3	53.7; 69.0; 60.4
P31946	14-3-3 protein alpha/beta	YWHAB	$6.53 \cdot 10^{-2}$	69.7; 51.6; 57.4	67.6; 68.0; 63.9
P28482	MAPK1	MAPK1	$3.37 \cdot 10^{-3}$	39.4; 9.8, 14.6	41.9; 64.2; 55.0
P27361	MAPK3[#]	MAPK3	$5.34 \cdot 10^{-3}$	---	44.9; 47.0; 40.4
P51812	RSK2	RPS6KA3	$6.53 \cdot 10^{-2}$	39.3; 4.6; 38.4	33.5; 31.4; 32.0
O00629	Importin subunit alpha-3	KPNA4	$5.76 \cdot 10^{-5}$	45.3; ---	25.3; 32.8; 28.2
O00505	Importin subunit alpha-4	KPNA3	$2.33 \cdot 10^{-3}$	4.2; ---	14.0; 23.8; 25.3
Q96P70	Importin-9	IPO9	$1.25 \cdot 10^{-2}$	22.2; 20.7	21.0; 30.1; 23.9

[#] only identified with iRhom2^{WT}

Table A2 | Identified phosphorylation sites in human iRhom1 and iRhom2 by mass spectrometry. The phosphorylation sites are highlighted in red. The data on iRhom2 phosphorylation was published in (Grieve et al., 2017).

phosphorylation site	peptide sequence	ion scores
iRhom1		
8-S	RD**S**TSSLQR	49, 30
51-S	SV**S**MPAETAHISSPHHELR	42, 48, 44
56-T	SVSMPAE**T**AHIS**S**PHHELR	56, 16
61-S	SV**S**MPAETAHIS**S**PHHELR	22
76-S	QT**S**ITQTIR	40, 38, 44, 49, 31
	QT**S**ITQTIRR	21
176-S	VADDTAEGL**S**APHTPVTPGAASLCSFSSSR	62, 34, 49
180-S	VADDTAEGLSAPH**T**PVTPGAASLCSFSSSR	39, 59
183-S	VADDTAEGLSAPHTPV**T**PGAASLCSFSSSR	49, 30
390-S	RID**S**FVKR	30, 27
	ID**S**FVKR	41
iRhom2		
90-S	SV**S**LQEPR	54, 37, 57
113-S	RQA**S**LSQSIR	53, 45, 54
	QA**S**LSQSIR	50, 58, 60, 55
117-S	QASLSQ**S**IRK	49, 20
177-S	DLELPSQEAPSFQGTE**S**PKPCK	46, 30, 59, 66, 44
323-S	GIPH**S**ASPVSPDGVQIPLK	44
	GIPH**S**ASPVSPDGVQIPLKEYGR	30
325-S	GIPHSA**S**PVSPDGVQIPLK	53, 49, 55, 59, 49
328-S	GIPHSASPV**S**PDGVQIPLK	54, 31, 40, 57, 64, 42, 76
385-S	R**S**ISSTVQR	22, 25, 24
	SISSTVQR	44, 33, 38
387-S	RSI**S**STVQR	13, 25
	SI**S**STVQR	37, 62

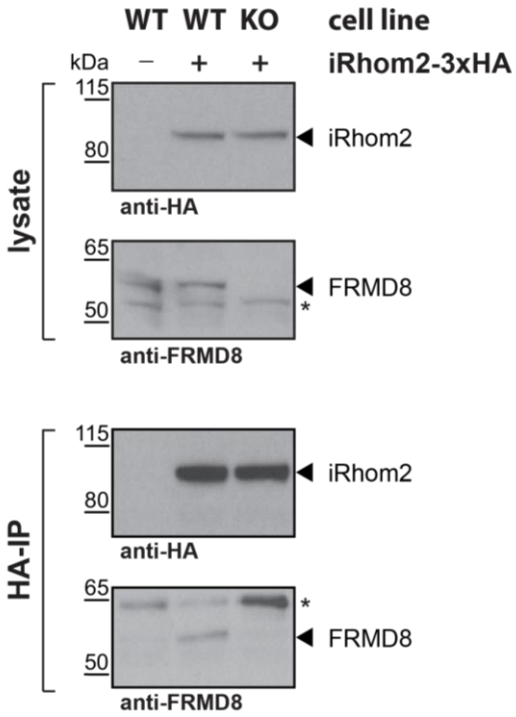


Figure A2 | Endogenous FRMD8 co-immunoprecipitates with iRhom2. Western blot of lysates and anti-HA IP from wild-type (WT) HEK293T, HEK293T cells stably expressing iRhom2-HA, and FRMD8 KO stably expressing iRhom2-HA, after anti-HA and anti-FRMD8 staining. An asterisk (*) indicates nonspecific bands detected by the FRMD8 antibody. One representative western blot out of three independent experiments is shown.

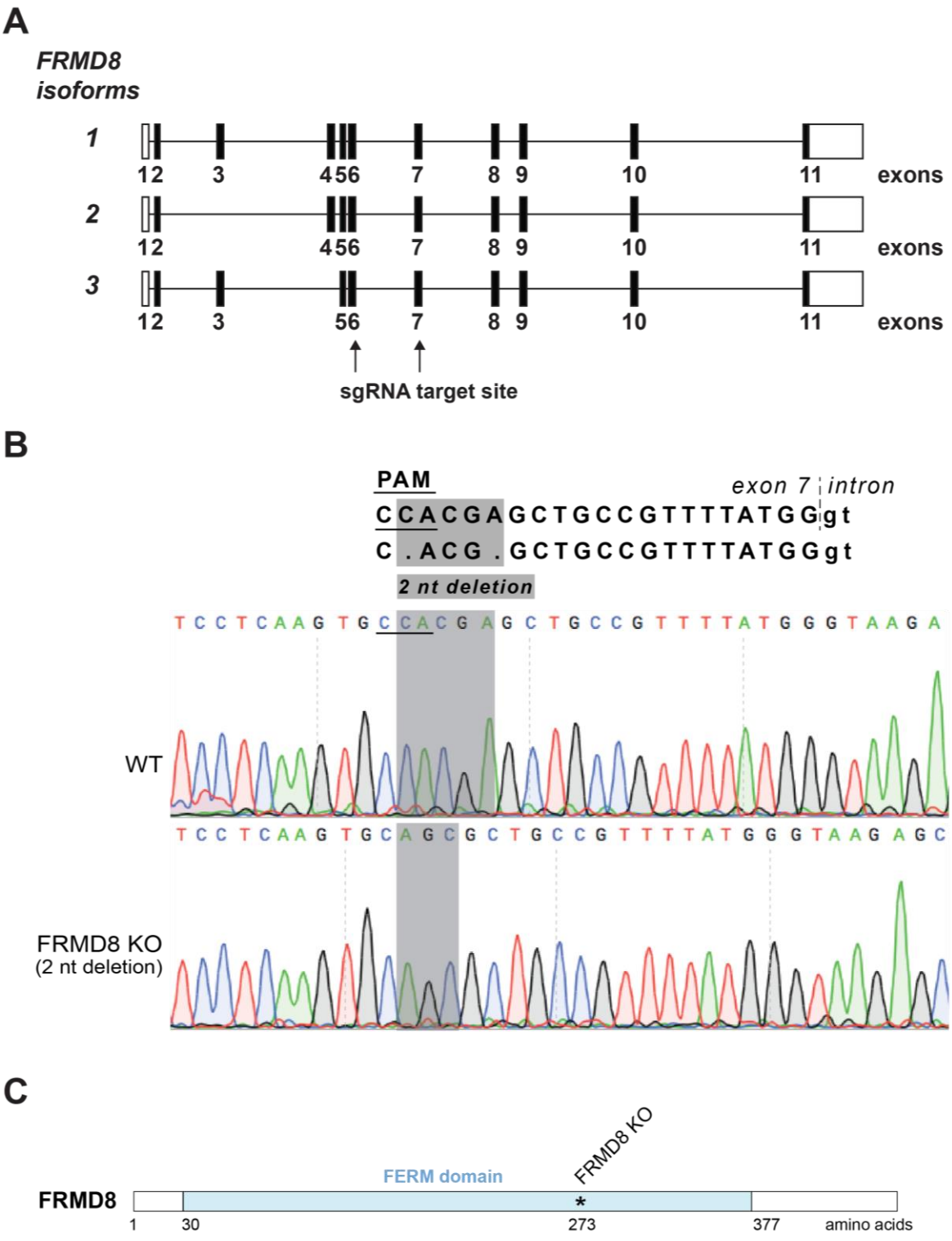


Figure A3 | Genetic analysis of FRMD8 KO HEK293T cells. A) Schematic representation of the three FRMD8 isoforms and the exons they include. **B)** Sequencing of the genomic DNA isolated from FRMD8 KO HEK293T cells. The targeting sequence of the sgRNA is shown (small letters indicate the sequence within the intronic region) with the PAM sequence underlined. **C)** Schematic representation of the FRMD8 protein and the premature stop codons (*) resulting from the frame shifts introduced by CRISPR/Cas9.

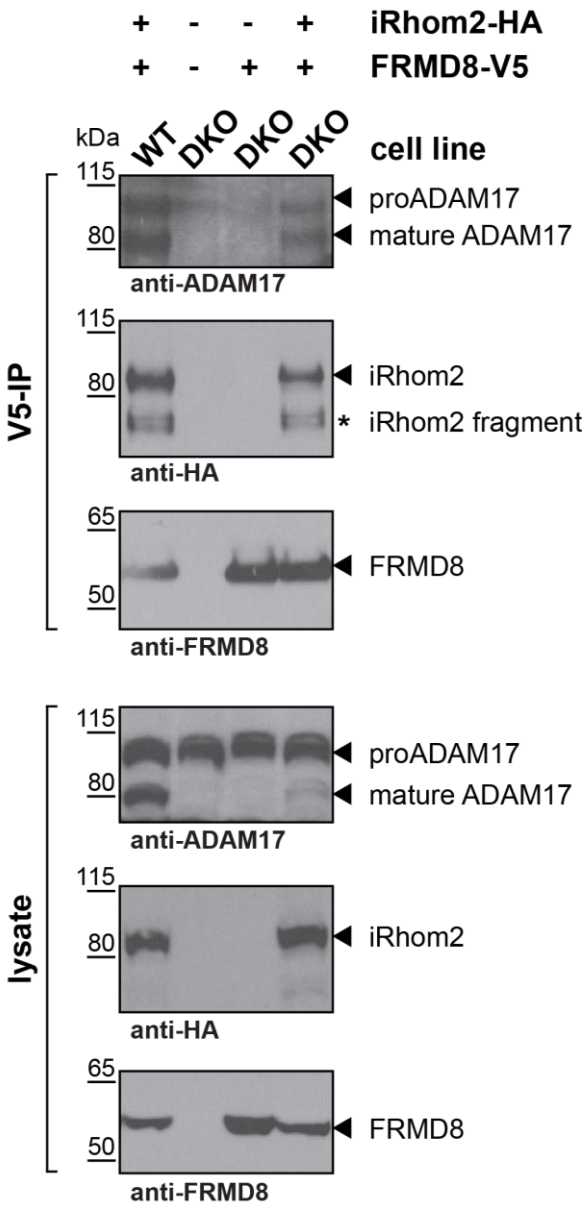


Figure A4 | ADAM17 co-immunoprecipitates with FRMD8 only in the presence of iRhom2. Western blot of lysates and anti-V5 IP from wild-type (WT) and iRhom1/2 double KO (DKO) HEK293T cells (generated by Boris Sieber, unpublished) transiently transfected with FRMD8-V5 or with iRhom2-HA and FRMD8-V5, after anti-HA, anti-ADAM17, and anti-FRMD8 staining. One representative western blot out of two independent experiments is shown.

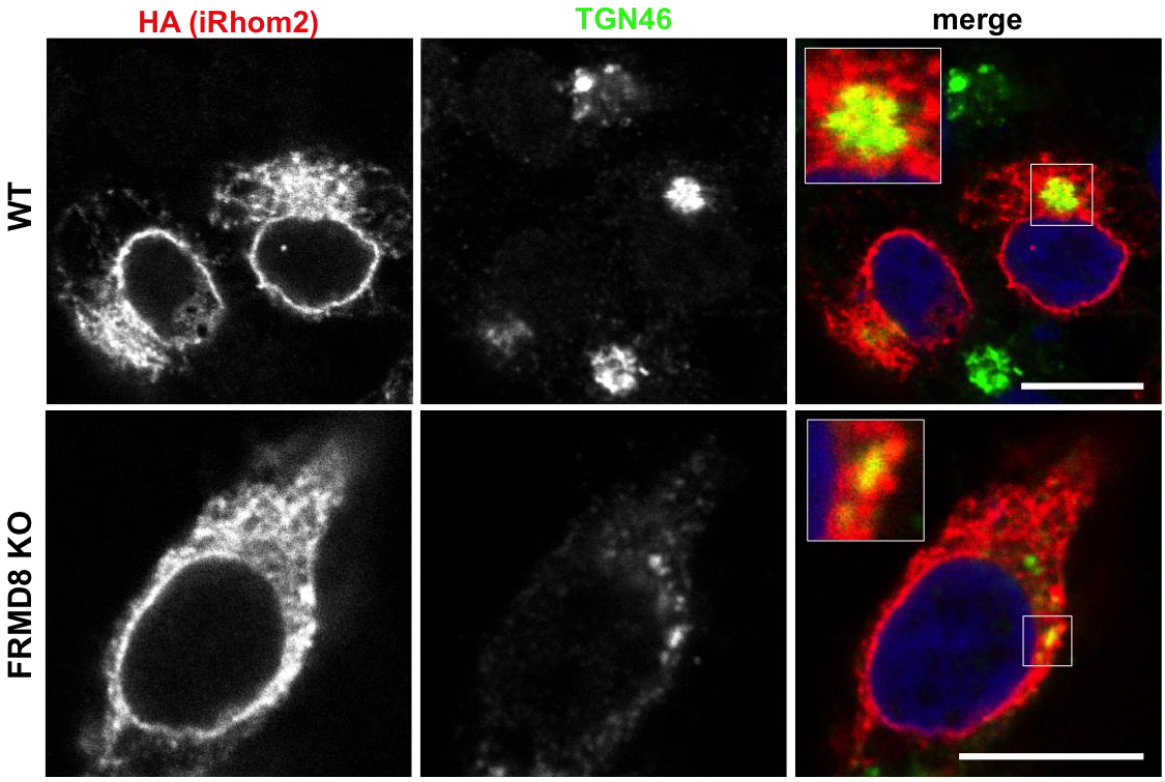


Figure A5 | iRhom2 localisation in HEK293T cells. Immunofluorescence staining of HEK293T cells transfected with iRhom2-3xHA, using 4',6-diamidino-2-phenylindole (DAPI; blue), anti-HA (red), and anti-TGN46 (green; *trans*-Golgi marker) antibody.

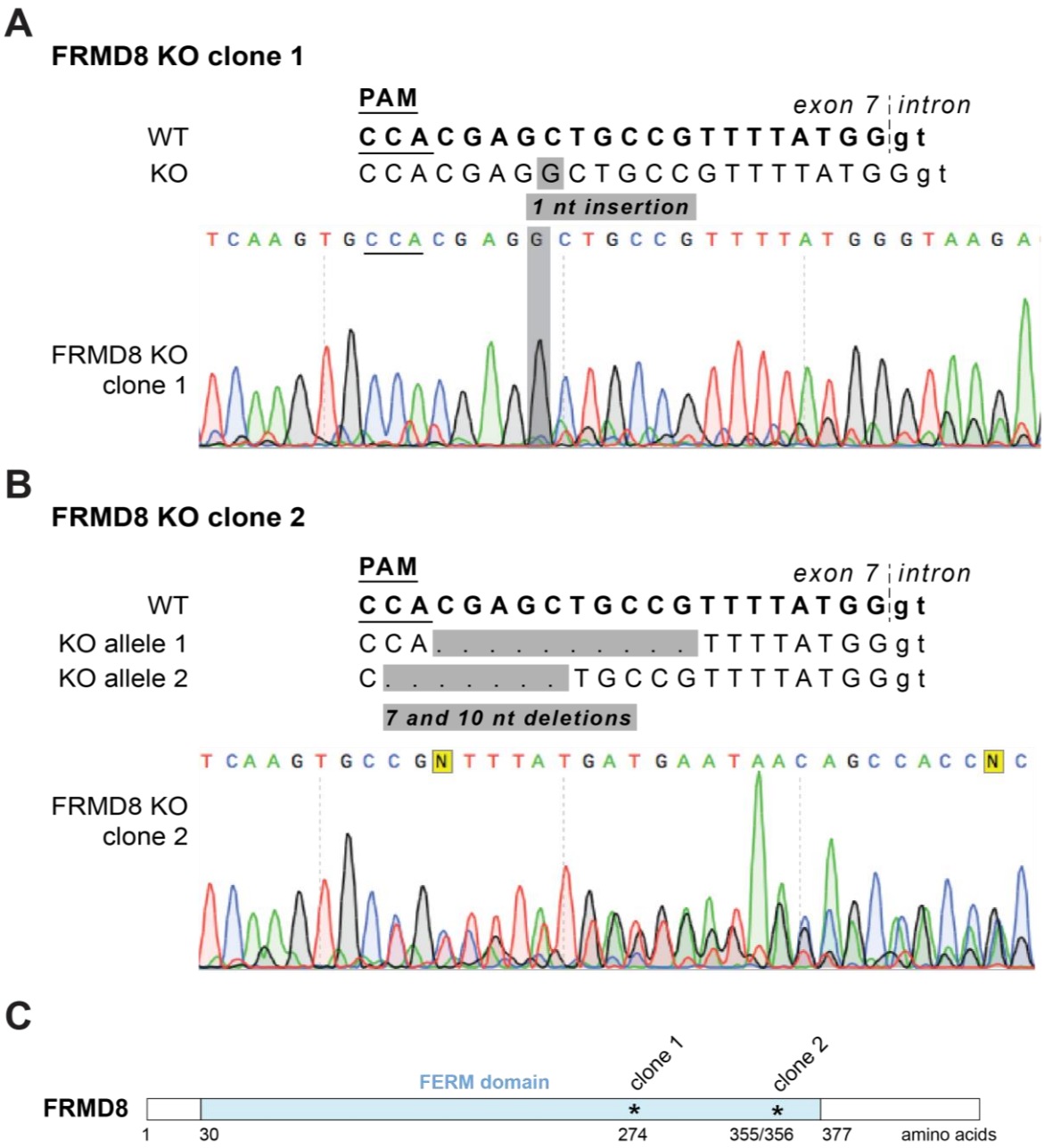


Figure A6 | Genetic analysis of FRMD8 KO iPSC lines. A) - B) Sequencing of the genomic DNA isolated from FRMD8 KO iPSC clone 1 and clone 2. Clone 1 shows a 1-nt insertion, clone 2 has a 7-nt deletion on one allele and a 10-nt deletion on the second allele. The targeting sequence of the sgRNA is shown in bold (small letters indicate the sequence within the intronic region) with the PAM sequence underlined. **C)** Schematic representation of the FRMD8 protein and the premature stop codons (*) resulting from the frame shifts introduced by CRISPR/Cas9.

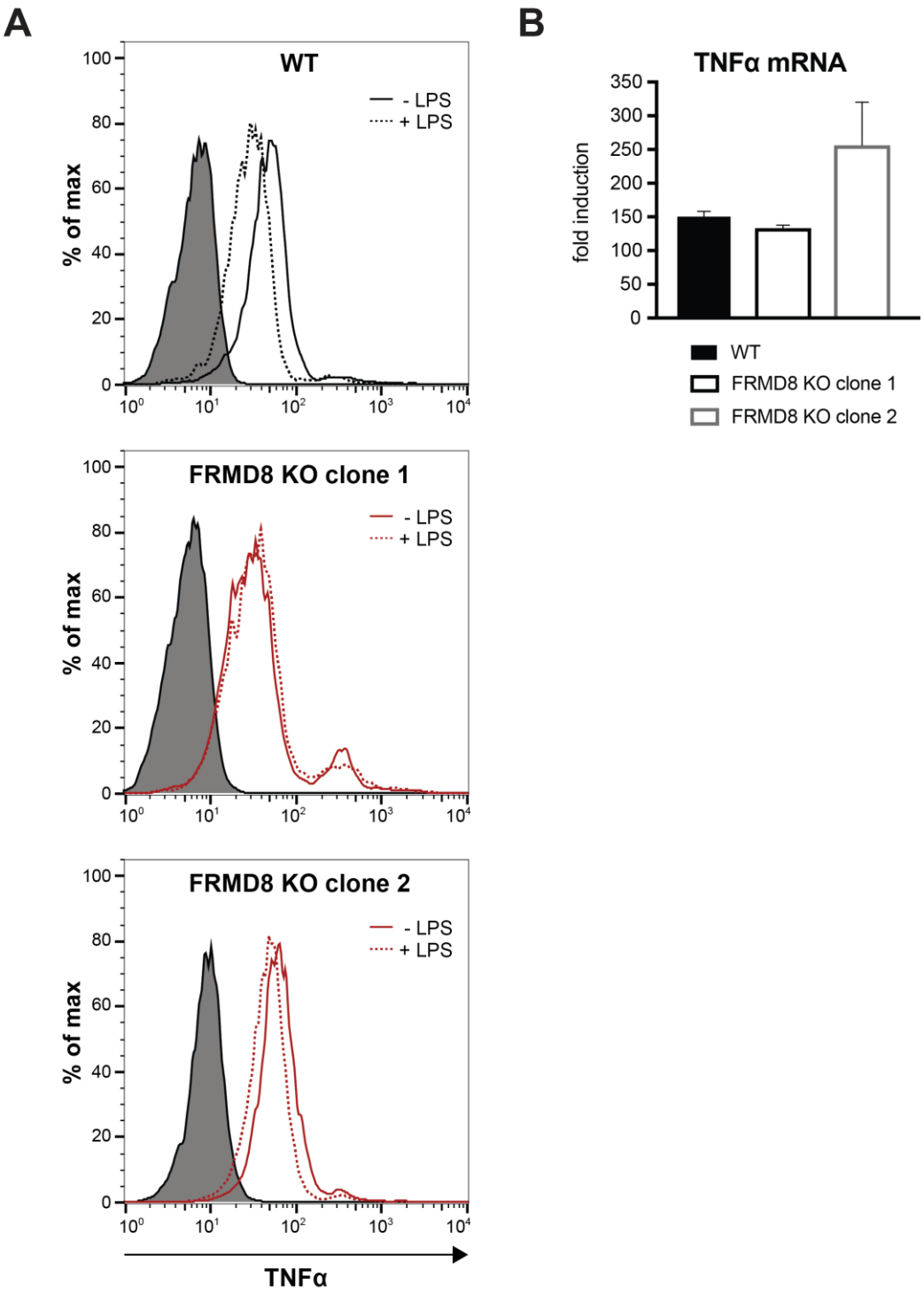


Figure A7 | Analysis of TNFα in FRMD8 KO macrophages. A) Flow cytometry analysis of cell surface levels of TNFα in unstimulated (-LPS) or LPS-stimulated (50 ng/ml for 4h) iPSC-derived macrophages (+LPS). Unpermeabilised macrophages were stained on ice for endogenous TNF, or with secondary antibody only as a control (grey). The percentage of positive cells was calculated for each experiment using FlowJo software. **B)** TNFα mRNA levels, relative to actin mRNA levels, were measured by TaqMan PCR in wild-type and FRMD8 KO iPSC-derived macrophages without stimulation or after stimulation with 100 ng/ml LPS for 4 h. The fold change of TNFα mRNA between unstimulated and stimulated cells was calculated and is presented.

References

Adrain, C. & Freeman, M. 2012. New lives for old: evolution of pseudoenzyme function illustrated by iRhoms. *Nat Rev Mol Cell Biol,* 13**,** 489-98.

Adrain, C. & Freeman, M. 2014. Regulation of receptor tyrosine kinase ligand processing. *Cold Spring Harb Perspect Biol,* 6.

Adrain, C., Strisovsky, K., Zettl, M., Hu, L., Lemberg, M. K. & Freeman, M. 2011. Mammalian EGF receptor activation by the rhomboid protease RHBDL2. *EMBO Rep,* 12**,** 421-7.

Adrain, C., Zettl, M., Christova, Y., Taylor, N. & Freeman, M. 2012. Tumor necrosis factor signaling requires iRhom2 to promote trafficking and activation of TACE. *Science,* 335**,** 225-8.

Alberts, B., Johnson, A., Lewis, J., Raff, M., Roberts, K. & Walter, P. 2002. General Principles of Cell Communication. *Molecular Biology of the Cell. 4th edition.* New York: Garland Science. Available from: http://www.ncbi.nlm.nih.gov/books/NBK26813.

Amour, A., Slocombe, P. M., Webster, A., Butler, M., Knight, C. G., Smith, B. J., Stephens, P. E., Shelley, C., Hutton, M., Knauper, V., Docherty, A. J. P. & Murphy, G. 1998. TNF-alpha converting enzyme (TACE) is inhibited by TIMP-3. *FEBS Lett,* 435**,** 39-44.

Arachea, B. T., Sun, Z., Potente, N., Malik, R., Isailovic, D. & Viola, R. E. 2012. Detergent selection for enhanced extraction of membrane proteins. *Protein Expr Purif,* 86**,** 12-20.

Arkin, M. R., Tang, Y. & Wells, J. A. 2014. Small-molecule inhibitors of protein-protein interactions: progressing toward the reality. *Chem Biol,* 21**,** 1102-14.

Bandsma, R. H., Van Goor, H., Yourshaw, M., Horlings, R. K., Jonkman, M. F., Scholvinck, E. H., Karrenbeld, A., Scheenstra, R., Komhoff, M., Rump, P., Koopman-Keemink, Y., Nelson, S. F., Escher, J. C., Cutz, E. & Martin, M. G. 2015. Loss of ADAM17 is associated with severe multiorgan dysfunction. *Hum Pathol,* 46**,** 923-8.

Bassett, A. & Liu, J. L. 2014. CRISPR/Cas9 mediated genome engineering in Drosophila. *Methods,* 69**,** 128-36.

Bax, D. V., Messent, A. J., Tart, J., Van Hoang, M., Kott, J., Maciewicz, R. A. & Humphries, M. J. 2004. Integrin alpha5beta1 and ADAM-17 interact in vitro and co-localize in migrating HeLa cells. *J Biol Chem,* 279**,** 22377-86.

Bell, J. H., Herrera, A. H., Li, Y. & Walcheck, B. 2007. Role of ADAM17 in the ectodomain shedding of TNF-alpha and its receptors by neutrophils and macrophages. *J Leukoc Biol,* 82**,** 173-6.

Bergbold, N. & Lemberg, M. K. 2013. Emerging role of rhomboid family proteins in mammalian biology and disease. *Biochim Biophys Acta,* 1828**,** 2840-8.

Black, R. A., Rauch, C. T., Kozlosky, C. J., Peschon, J. J., Slack, J. L., Wolfson, M. F., Castner, B. J., Stocking, K. L., Reddy, P., Srinivasan, S., Nelson, N., Boiani, N., Schooley, K. A., Gerhart, M., Davis, R., Fitzner, J. N., Johnson, R. S., Paxton, R. J., March, C. J. & Cerretti, D. P. 1997. A metalloproteinase disintegrin that releases tumour-necrosis factor-alpha from cells. *Nature,* 385**,** 729-33.

Blaydon, D. C., Biancheri, P., Di, W. L., Plagnol, V., Cabral, R. M., Brooke, M. A., Van Heel, D. A., Ruschendorf, F., Toynbee, M., Walne, A., O'toole, E. A., Martin, J. E., Lindley, K., Vulliamy, T., Abrams, D. J., Macdonald, T. T., Harper, J. I. & Kelsell, D. P. 2011. Inflammatory skin and bowel disease linked to ADAM17 deletion. *N Engl J Med,* 365**,** 1502-8.

Blaydon, D. C., Etheridge, S. L., Risk, J. M., Hennies, H. C., Gay, L. J., Carroll, R., Plagnol, V., Mcronald, F. E., Stevens, H. P., Spurr, N. K., Bishop, D. T., Ellis, A., Jankowski, J., Field, J. K., Leigh, I. M., South, A. P. & Kelsell, D. P. 2012. RHBDF2 mutations are associated with tylosis, a familial esophageal cancer syndrome. *Am J Hum Genet,* 90**,** 340-6.

Blobel, C. P. 2005. ADAMs: key components in EGFR signalling and development. *Nat Rev Mol Cell Biol,* 6**,** 32-43.

Blobel, C. P., Carpenter, G. & Freeman, M. 2009. The role of protease activity in ErbB biology. *Exp Cell Res,* 315**,** 671-82.

Bosanquet, D. C., Ye, L., Harding, K. G. & Jiang, W. G. 2014. FERM family proteins and their importance in cellular movements and wound healing (Review). *Int J Mol Med,* 34**,** 3-12.

Brameier, M., Krings, A. & Maccallum, R. M. 2007. NucPred--predicting nuclear localization of proteins. *Bioinformatics,* 23**,** 1159-60.

Brooke, M. A., Etheridge, S. L., Kaplan, N., Simpson, C., O'toole, E. A., Ishida-Yamamoto, A., Marches, O., Getsios, S. & Kelsell, D. P. 2014. iRHOM2-dependent regulation of ADAM17 in cutaneous disease and epidermal barrier function. *Hum Mol Genet,* 23**,** 4064-76.

Buchrieser, J., James, W. & Moore, M. D. 2017. Human Induced Pluripotent Stem Cell-Derived Macrophages Share Ontogeny with MYB-Independent Tissue-Resident Macrophages. *Stem Cell Reports,* 8**,** 334-345.

Caiazza, F., Mcgowan, P. M., Mullooly, M., Murray, A., Synnott, N., O'donovan, N., Flanagan, L., Tape, C. J., Murphy, G., Crown, J. & Duffy, M. J. 2015. Targeting ADAM-17 with an inhibitory monoclonal antibody has antitumour effects in triple-negative breast cancer cells. *Br J Cancer,* 112**,** 1895-1903.

Chalaris, A., Adam, N., Sina, C., Rosenstiel, P., Lehmann-Koch, J., Schirmacher, P., Hartmann, D., Cichy, J., Gavrilova, O., Schreiber, S., Jostock, T., Matthews, V., Hasler, R., Becker, C., Neurath, M. F., Reiss, K., Saftig, P., Scheller, J. & Rose-John, S. 2010. Critical role of the disintegrin metalloprotease ADAM17 for intestinal inflammation and regeneration in mice. *J Exp Med,* 207**,** 1617-24.

Chintapalli, V. R., Wang, J. & Dow, J. a. T. 2007. Using FlyAtlas to identify better Drosophila melanogaster models of human disease. *Nat Genet,* 39**,** 715-720.

Christova, Y., Adrain, C., Bambrough, P., Ibrahim, A. & Freeman, M. 2013. Mammalian iRhoms have distinct physiological functions including an essential role in TACE regulation. *EMBO Rep,* 14**,** 884-90.

Citri, A. & Yarden, Y. 2006. EGF-ERBB signalling: towards the systems level. *Nat Rev Mol Cell Biol,* 7**,** 505-16.

Clackson, T. & Wells, J. A. 1995. A hot spot of binding energy in a hormone-receptor interface. *Science,* 267**,** 383-6.

Cook, P. W., Brown, J. R., Cornell, K. A. & Pittelkow, M. R. 2004. Suprabasal expression of human amphiregulin in the epidermis of transgenic mice induces a severe, early-onset, psoriasis-like skin pathology: expression of amphiregulin in the basal epidermis is also associated with synovitis. *Exp Dermatol,* 13**,** 347-56.

Cook, P. W., Piepkorn, M., Clegg, C. H., Plowman, G. D., Demay, J. M., Brown, J. R. & Pittelkow, M. R. 1997. Transgenic expression of the human amphiregulin gene induces a psoriasis-like phenotype. *J Clin Invest,* 100**,** 2286-94.

Cox, J. & Mann, M. 2008. MaxQuant enables high peptide identification rates, individualized p.p.b.-range mass accuracies and proteome-wide protein quantification. *Nat Biotechnol,* 26**,** 1367-1372.

Cox, J., Neuhauser, N., Michalski, A., Scheltema, R. A., Olsen, J. V. & Mann, M. 2011. Andromeda: A Peptide Search Engine Integrated into the MaxQuant Environment. *J Proteome Res,* 10**,** 1794-1805.

Cruciat, C. M., Ohkawara, B., Acebron, S. P., Karaulanov, E., Reinhard, C., Ingelfinger, D., Boutros, M. & Niehrs, C. 2010. Requirement of prorenin receptor and vacuolar H+-ATPase-mediated acidification for Wnt signaling. *Science,* 327**,** 459-63.

Dahlhoff, M., Muller, A. K., Wolf, E., Werner, S. & Schneider, M. R. 2010. Epigen transgenic mice develop enlarged sebaceous glands. *J Invest Dermatol,* 130**,** 623-6.

De Jager, P. L., Srivastava, G., Lunnon, K., Burgess, J., Schalkwyk, L. C., Yu, L., Eaton, M. L., Keenan, B. T., Ernst, J., Mccabe, C., Tang, A., Raj, T., Replogle, J., Brodeur, W., Gabriel, S., Chai, H. S., Younkin, C., Younkin, S. G., Zou, F., Szyf, M., Epstein, C. B., Schneider, J. A., Bernstein, B. E., Meissner, A., Ertekin-Taner, N., Chibnik, L. B., Kellis, M., Mill, J. & Bennett, D. A. 2014. Alzheimer's disease: early alterations in brain DNA methylation at ANK1, BIN1, RHBDF2 and other loci. *Nat Neurosci,* 17**,** 1156-63.

Dobrowolski, R., Vick, P., Ploper, D., Gumper, I., Snitkin, H., Sabatini, D. D. & De Robertis, E. M. 2012. Presenilin deficiency or lysosomal inhibition enhances Wnt signaling through relocalization of GSK3 to the late-endosomal compartment. *Cell Rep,* 2**,** 1316-28.

Dombernowsky, S. L., Samsoe-Petersen, J., Petersen, C. H., Instrell, R., Hedegaard, A. M., Thomas, L., Atkins, K. M., Auclair, S., Albrechtsen, R., Mygind, K. J., Frohlich, C., Howell, M., Parker, P., Thomas, G. & Kveiborg, M. 2015. The sorting protein PACS-2 promotes ErbB signalling by regulating recycling of the metalloproteinase ADAM17. *Nat Commun,* 6**,** 7518.

Doudna, J. A. & Charpentier, E. 2014. Genome editing. The new frontier of genome engineering with CRISPR-Cas9. *Science,* 346**,** 1258096.

Dusterhoft, S., Kunzel, U. & Freeman, M. 2017. Rhomboid proteases in human disease: Mechanisms and future prospects. *Biochim Biophys Acta*.

Endres, K., Anders, A., Kojro, E., Gilbert, S., Fahrenholz, F. & Postina, R. 2003. Tumor necrosis factor-alpha converting enzyme is processed by proprotein-convertases to its mature form which is degraded upon phorbol ester stimulation. *Eur J Biochem,* 270**,** 2386-2393.

Fernandes, H. J., Hartfield, E. M., Christian, H. C., Emmanoulidou, E., Zheng, Y., Booth, H., Bogetofte, H., Lang, C., Ryan, B. J., Sardi, S. P., Badger, J., Vowles, J., Evetts, S., Tofaris, G. K., Vekrellis, K., Talbot, K., Hu, M. T., James, W., Cowley, S. A. & Wade-Martins, R. 2016. ER Stress and Autophagic Perturbations Lead to Elevated Extracellular alpha-Synuclein in GBA-N370S Parkinson's iPSC-Derived Dopamine Neurons. *Stem Cell Reports,* 6**,** 342-56.

Fischer, O. M., Hart, S., Gschwind, A. & Ullrich, A. 2003. EGFR signal transactivation in cancer cells. *Biochem Soc Trans,* 31**,** 1203-8.

Fleck, D., Van Bebber, F., Colombo, A., Galante, C., Schwenk, B. M., Rabe, L., Hampel, H., Novak, B., Kremmer, E., Tahirovic, S., Edbauer, D., Lichtenthaler, S. F., Schmid, B., Willem, M. & Haass, C. 2013. Dual cleavage of neuregulin 1 type III by BACE1 and ADAM17 liberates its EGF-like domain and allows paracrine signaling. *J Neurosci,* 33**,** 7856-69.

Frame, M. C., Patel, H., Serrels, B., Lietha, D. & Eck, M. J. 2010. The FERM domain: organizing the structure and function of FAK. *Nat Rev Mol Cell Biol,* 11**,** 802-14.

Franzke, C. W., Cobzaru, C., Triantafyllopoulou, A., Loffek, S., Horiuchi, K., Threadgill, D. W., Kurz, T., Van Rooijen, N., Bruckner-Tuderman, L. & Blobel, C. P. 2012. Epidermal ADAM17 maintains the skin barrier by regulating EGFR ligand-dependent terminal keratinocyte differentiation. *J Exp Med,* 209**,** 1105-19.

Freeman, M. 2009. Rhomboids: 7 years of a new protease family. *Semin Cell Dev Biol,* 20**,** 231-9.

Freeman, M. 2014. The rhomboid-like superfamily: molecular mechanisms and biological roles. *Annu Rev Cell Dev Biol,* 30**,** 235-54.

Galvan, A., Frullanti, E., Anderlini, M., Manenti, G., Noci, S., Dugo, M., Ambrogi, F., De Cecco, L., Spinelli, R., Piazza, R., Pirola, A., Gambacorti-Passerini, C., Incarbone, M., Alloisio, M., Tosi, D., Nosotti, M., Santambrogio, L., Pastorino, U. & Dragani, T. A. 2013. Gene expression signature of non-involved lung tissue associated with survival in lung adenocarcinoma patients. *Carcinogenesis,* 34**,** 2767-73.

Gibson, D. G., Young, L., Chuang, R. Y., Venter, J. C., Hutchison, C. A. & Smith, H. O. 2009. Enzymatic assembly of DNA molecules up to several hundred kilobases. *Nature Methods,* 6**,** 343-U41.

Gingras, A. C., Gstaiger, M., Raught, B. & Aebersold, R. 2007. Analysis of protein complexes using mass spectrometry. *Nat Rev Mol Cell Biol,* 8**,** 645-54.

Gooz, P., Dang, Y. J., Higashiyama, S., Twal, W. O., Haycraft, C. J. & Gooz, M. 2012. A Disintegrin and Metalloenzyme (ADAM) 17 Activation Is Regulated by alpha 5 beta 1 Integrin in Kidney Mesangial Cells. *PLoS One,* 7.

Grieve, A. G., Xu, H., Kunzel, U., Bambrough, P., Sieber, B. & Freeman, M. 2017. Phosphorylation of iRhom2 at the plasma membrane controls mammalian TACE-dependent inflammatory and growth factor signalling. *Elife,* 6.

Grotzinger, J., Lorenzen, I. & Dusterhoft, S. 2017. Molecular insights into the multilayered regulation of ADAM17: The role of the extracellular region. *Biochim Biophys Acta*.

Hamada, F., Tomoyasu, Y., Takatsu, Y., Nakamura, M., Nagai, S., Suzuki, A., Fujita, F., Shibuya, H., Toyoshima, K., Ueno, N. & Akiyama, T. 1999. Negative regulation of Wingless signaling by D-axin, a Drosophila homolog of axin. *Science,* 283**,** 1739-42.

Harris, R. C., Chung, E. & Coffey, R. J. 2003. EGF receptor ligands. *Exp Cell Res,* 284**,** 2-13.

Hayashida, K., Bartlett, A. H., Chen, Y. & Park, P. W. 2010. Molecular and cellular mechanisms of ectodomain shedding. *Anat Rec (Hoboken),* 293**,** 925-37.

Hirano, Y., Hendil, K. B., Yashiroda, H., Iemura, S., Nagane, R., Hioki, Y., Natsume, T., Tanaka, K. & Murata, S. 2005. A heterodimeric complex that promotes the assembly of mammalian 20S proteasomes. *Nature,* 437**,** 1381-5.

Hochberg, Y. & Benjamini, Y. 1990. More Powerful Procedures for Multiple Significance Testing. *Stat Med,* 9**,** 811-818.

Holbro, T. & Hynes, N. E. 2004. ErbB receptors: directing key signaling networks throughout life. *Annu Rev Pharmacol Toxicol,* 44**,** 195-217.

Horiuchi, K., Kimura, T., Miyamoto, T., Takaishi, H., Okada, Y., Toyama, Y. & Blobel, C. P. 2007a. Cutting edge: TNF-alpha-converting enzyme (TACE/ADAM17) inactivation in mouse myeloid cells prevents lethality from endotoxin shock. *J Immunol,* 179**,** 2686-9.

Horiuchi, K., Le Gall, S., Schulte, M., Yamaguchi, T., Reiss, K., Murphy, G., Toyama, Y., Hartmann, D., Saftig, P. & Blobel, C. P. 2007b. Substrate selectivity of epidermal growth factor-receptor ligand sheddases and their regulation by phorbol esters and calcium influx. *Mol Biol Cell,* 18**,** 176-88.

Hosamani, R. & Muralidhara 2009. Neuroprotective efficacy of Bacopa monnieri against rotenone induced oxidative stress and neurotoxicity in Drosophila melanogaster. *Neurotoxicology,* 30**,** 977-85.

Hosur, V., Johnson, K. R., Burzenski, L. M., Stearns, T. M., Maser, R. S. & Shultz, L. D. 2014. Rhbdf2 mutations increase its protein stability and drive EGFR hyperactivation through enhanced secretion of amphiregulin. *Proc Natl Acad Sci U S A,* 111**,** E2200-9.

Hosur, V., Low, B. E., Shultz, L. D. & Wiles, M. V. 2017. Genetic deletion of amphiregulin restores the normal skin phenotype in a mouse model of the human skin disease tylosis. *Biol Open,* 6**,** 1174-1179.

Huet, O. & Chin-Dusting, J. P. 2014. Septic shock: desperately seeking treatment. *Clin Sci (Lond),* 126**,** 31-9.

Hundhausen, C., Misztela, D., Berkhout, T. A., Broadway, N., Saftig, P., Reiss, K., Hartmann, D., Fahrenholz, F., Postina, R., Matthews, V., Kallen, K. J., Rose-John, S. & Ludwig, A. 2003. The disintegrin-like metalloproteinase ADAM10 is involved in constitutive cleavage of CX3CL1 (fractalkine) and regulates CX3CL1-mediated cell-cell adhesion. *Blood,* 102**,** 1186-95.

Ishikawa, H., Ma, Z. & Barber, G. N. 2009. STING regulates intracellular DNA-mediated, type I interferon-dependent innate immunity. *Nature,* 461**,** 788-92.

Issuree, P. D., Maretzky, T., Mcilwain, D. R., Monette, S., Qing, X., Lang, P. A., Swendeman, S. L., Park-Min, K. H., Binder, N., Kalliolias, G. D., Yarilina, A., Horiuchi, K., Ivashkiv, L. B., Mak, T. W., Salmon, J. E. & Blobel, C. P. 2013. iRHOM2 is a critical pathogenic mediator of inflammatory arthritis. *J Clin Invest,* 123**,** 928-32.

Itzhak, D. N., Tyanova, S., Cox, J. & Borner, G. H. 2016. Global, quantitative and dynamic mapping of protein subcellular localization. *Elife,* 5.

Iwamoto, R., Yamazaki, S., Asakura, M., Takashima, S., Hasuwa, H., Miyado, K., Adachi, S., Kitakaze, M., Hashimoto, K., Raab, G., Nanba, D., Higashiyama, S., Hori, M., Klagsbrun, M. & Mekada, E. 2003. Heparin-binding EGF-like growth factor and ErbB signaling is essential for heart function. *Proc Natl Acad Sci U S A,* 100**,** 3221-3226.

Jackson, L. F., Qiu, T. H., Sunnarborg, S. W., Chang, A., Zhang, C., Patterson, C. & Lee, D. C. 2003. Defective valvulogenesis in HB-EGF and TACE-null mice is associated with aberrant BMP signaling. *EMBO J,* 22**,** 2704-16.

Jinek, M., Chylinski, K., Fonfara, I., Hauer, M., Doudna, J. A. & Charpentier, E. 2012. A programmable dual-RNA-guided DNA endonuclease in adaptive bacterial immunity. *Science,* 337**,** 816-21.

Jurgens, G., Wieschaus, E., Nusslein-Volhard, C. & Kluding, H. 1984. Mutations affecting the pattern of the larval cuticle inDrosophila melanogaster : II. Zygotic loci on the third chromosome. *Wilehm Roux Arch Dev Biol,* 193**,** 283-295.

Kalliolias, G. D. & Ivashkiv, L. B. 2016. TNF biology, pathogenic mechanisms and emerging therapeutic strategies. *Nat Rev Rheumatol,* 12**,** 49-62.

Kategaya, L. S., Changkakoty, B., Biechele, T., Conrad, W. H., Kaykas, A., Dasgupta, R. & Moon, R. T. 2009. Bili inhibits Wnt/beta-catenin signaling by regulating the recruitment of axin to LRP6. *PLoS One,* 4**,** e6129.

Koehn, J., Huesken, D., Jaritz, M., Rot, A., Zurini, M., Dwertmann, A., Beutler, B. & Korthauer, U. 2007. Assessing the function of human UNC-93B in Toll-like receptor signaling and major histocompatibility complex II response. *Hum Immunol,* 68**,** 871-8.

Koonin, E. V., Makarova, K. S., Rogozin, I. B., Davidovic, L., Letellier, M. C. & Pellegrini, L. 2003. The rhomboids: a nearly ubiquitous family of intramembrane serine proteases that probably evolved by multiple ancient horizontal gene transfers. *Genome Biol,* 4**,** R19.

Korinek, V., Barker, N., Morin, P. J., Van Wichen, D., De Weger, R., Kinzler, K. W., Vogelstein, B. & Clevers, H. 1997. Constitutive transcriptional activation by a beta-catenin-Tcf complex in APC-/- colon carcinoma. *Science,* 275**,** 1784-7.

Kose, M. 2017. GPCRs and EGFR - Cross-talk of membrane receptors in cancer. *Bioorg Med Chem Lett,* 27**,** 3611-3620.

Le Gall, S. M., Maretzky, T., Issuree, P. D. A., Niu, X. D., Reiss, K., Saftig, P., Khokha, R., Lundell, D. & Blobel, C. P. 2010. ADAM17 is regulated by a rapid and reversible mechanism that controls access to its catalytic site. *J Cell Sci,* 123**,** 3913-3922.

Lee, J. R., Urban, S., Garvey, C. F. & Freeman, M. 2001. Regulated intracellular ligand transport and proteolysis control EGF signal activation in Drosophila. *Cell,* 107**,** 161-71.

Lee, W., Kim, Y., Park, J., Shim, S., Lee, J., Hong, S. H., Ahn, H. H., Lee, H. & Jung, Y. K. 2015. iRhom1 regulates proteasome activity via PAC1/2 under ER stress. *Sci Rep,* 5**,** 11559.

Leilei, Y., Bing, L., Yang, L., Shaoxia, W., Yuan, X., Dongping, W., Huahu, Y., Shichen, S., Guangzhou, Z., Ruiyun, P., Lin, Z. & Wenlong, L. 2014. iRhom2 mutation leads to aberrant hair follicle differentiation in mice. *PLoS One,* 9**,** e115114.

Lemberg, M. K. & Freeman, M. 2007. Functional and evolutionary implications of enhanced genomic analysis of rhomboid intramembrane proteases. *Genome Res,* 17**,** 1634-46.

Lemberg, M. K., Menendez, J., Misik, A., Garcia, M., Koth, C. M. & Freeman, M. 2005. Mechanism of intramembrane proteolysis investigated with purified rhomboid proteases. *EMBO J,* 24**,** 464-72.

Lewis, M., Tartaglia, L. A., Lee, A., Bennett, G. L., Rice, G. C., Wong, G. H., Chen, E. Y. & Goeddel, D. V. 1991. Cloning and expression of cDNAs for two distinct murine tumor necrosis factor receptors demonstrate one receptor is species specific. *Proc Natl Acad Sci U S A,* 88**,** 2830-4.

Li, X., Maretzky, T., Weskamp, G., Monette, S., Qing, X., Issuree, P. D., Crawford, H. C., Mcilwain, D. R., Mak, T. W., Salmon, J. E. & Blobel, C. P. 2015. iRhoms 1 and 2 are essential upstream regulators of ADAM17-dependent EGFR signaling. *Proc Natl Acad Sci U S A,* 112**,** 6080-5.

Lichtenthaler, S. F. 2013. iRHOM2 takes control of rheumatoid arthritis. *J Clin Invest,* 123**,** 560-2.

Lichtenthaler, S. F., O'hara, B. F. & Blobel, C. P. 2015. iRhoms in the brain - a new frontier? *Cell Cycle,* 14**,** 3003-4.

Linderman, J. A., Chambers, M. C., Gupta, A. S. & Schneider, D. S. 2012. Infection-related declines in chill coma recovery and negative geotaxis in Drosophila melanogaster. *PLoS One,* 7**,** e41907.

Llorens, J. V., Navarro, J. A., Martinez-Sebastian, M. J., Baylies, M. K., Schneuwly, S., Botella, J. A. & Molto, M. D. 2007. Causative role of

oxidative stress in a Drosophila model of Friedreich ataxia. *FASEB J,* 21**,** 333-44.

Lorenzen, I., Lokau, J., Korpys, Y., Oldefest, M., Flynn, C. M., Kunzel, U., Garbers, C., Freeman, M., Grotzinger, J. & Dusterhoft, S. 2016. Control of ADAM17 activity by regulation of its cellular localisation. *Sci Rep,* 6**,** 35067.

Luetteke, N. C., Qiu, T. H., Fenton, S. E., Troyer, K. L., Riedel, R. F., Chang, A. & Lee, D. C. 1999. Targeted inactivation of the EGF and amphiregulin genes reveals distinct roles for EGF receptor ligands in mouse mammary gland development. *Development,* 126**,** 2739-50.

Luetteke, N. C., Qiu, T. H., Peiffer, R. L., Oliver, P., Smithies, O. & Lee, D. C. 1993. TGF alpha deficiency results in hair follicle and eye abnormalities in targeted and waved-1 mice. *Cell,* 73**,** 263-78.

Luo, W. W., Li, S., Li, C., Lian, H., Yang, Q., Zhong, B. & Shu, H. B. 2016. iRhom2 is essential for innate immunity to DNA viruses by mediating trafficking and stability of the adaptor STING. *Nat Immunol,* 17**,** 1057-66.

Maney, S. K., Mcilwain, D. R., Polz, R., Pandyra, A. A., Sundaram, B., Wolff, D., Ohishi, K., Maretzky, T., Brooke, M. A., Evers, A., Vasudevan, A. A., Aghaeepour, N., Scheller, J., Munk, C., Haussinger, D., Mak, T. W., Nolan, G. P., Kelsell, D. P., Blobel, C. P., Lang, K. S. & Lang, P. A. 2015. Deletions in the cytoplasmic domain of iRhom1 and iRhom2 promote shedding of the TNF receptor by the protease ADAM17. *Sci Signal,* 8**,** ra109.

Mann, G. B., Fowler, K. J., Gabriel, A., Nice, E. C., Williams, R. L. & Dunn, A. R. 1993. Mice with a null mutation of the TGF alpha gene have abnormal skin architecture, wavy hair, and curly whiskers and often develop corneal inflammation. *Cell,* 73**,** 249-61.

Maretzky, T., Evers, A., Zhou, W., Swendeman, S. L., Wong, P. M., Rafii, S., Reiss, K. & Blobel, C. P. 2011. Migration of growth factor-stimulated epithelial and endothelial cells depends on EGFR transactivation by ADAM17. *Nat Commun,* 2**,** 229.

Maretzky, T., Mcilwain, D. R., Issuree, P. D., Li, X., Malapeira, J., Amin, S., Lang, P. A., Mak, T. W. & Blobel, C. P. 2013. iRhom2 controls the substrate selectivity of stimulated ADAM17-dependent ectodomain shedding. *Proc Natl Acad Sci U S A,* 110**,** 11433-8.

Marino, M. W., Dunn, A., Grail, D., Inglese, M., Noguchi, Y., Richards, E., Jungbluth, A., Wada, H., Moore, M., Williamson, B., Basu, S. & Old, L. J. 1997. Characterization of tumor necrosis factor-deficient mice. *Proc Natl Acad Sci U S A,* 94**,** 8093-8.

Maruthappu, T., Chikh, A., Fell, B., Delaney, P. J., Brooke, M. A., Levet, C., Moncada-Pazos, A., Ishida-Yamamoto, A., Blaydon, D., Waseem, A., Leigh, I. M., Freeman, M. & Kelsell, D. P. 2017. Rhomboid family member 2 regulates cytoskeletal stress-associated Keratin 16. *Nat Commun,* 8**,** 14174.

Mcilwain, D. R., Lang, P. A., Maretzky, T., Hamada, K., Ohishi, K., Maney, S. K., Berger, T., Murthy, A., Duncan, G., Xu, H. C., Lang, K. S., Haussinger, D., Wakeham, A., Itie-Youten, A., Khokha, R., Ohashi, P. S., Blobel, C. P. & Mak, T. W. 2012. iRhom2 regulation of TACE controls TNF-mediated protection against Listeria and responses to LPS. *Science,* 335**,** 229-32.

Milla, M. E., Leesnitzer, M. A., Moss, M. L., Clay, W. C., Carter, H. L., Miller, A. B., Su, J. L., Lambert, M. H., Willard, D. H., Sheeley, D. M., Kost, T. A., Burkhart, W., Moyer, M., Blackburn, R. K., Pahel, G. L., Mitchell, J. L., Hoffman, C. R. & Becherer, J. D. 1999. Specific sequence elements are

required for the expression of functional tumor necrosis factor-alpha-converting enzyme (TACE). *J Biol Chem,* 274**,** 30563-70.
Moleirinho, S., Tilston-Lunel, A., Angus, L., Gunn-Moore, F. & Reynolds, P. A. 2013. The expanding family of FERM proteins. *Biochem J,* 452**,** 183-93.
Monaco, C., Nanchahal, J., Taylor, P. & Feldmann, M. 2015. Anti-TNF therapy: past, present and future. *Int Immunol,* 27**,** 55-62.
Mori, M., Vignaroli, G. & Botta, M. 2013. Small molecules modulation of 14-3-3 protein-protein interactions. *Drug Discov Today Technol,* 10**,** e541-7.
Moss, M. L., Jin, S. L., Milla, M. E., Bickett, D. M., Burkhart, W., Carter, H. L., Chen, W. J., Clay, W. C., Didsbury, J. R., Hassler, D., Hoffman, C. R., Kost, T. A., Lambert, M. H., Leesnitzer, M. A., Mccauley, P., Mcgeehan, G., Mitchell, J., Moyer, M., Pahel, G., Rocque, W., Overton, L. K., Schoenen, F., Seaton, T., Su, J. L., Becherer, J. D. & Et Al. 1997. Cloning of a disintegrin metalloproteinase that processes precursor tumour-necrosis factor-alpha. *Nature,* 385**,** 733-6.
Moss, M. L., Sklair-Tavron, L. & Nudelman, R. 2008. Drug insight: tumor necrosis factor-converting enzyme as a pharmaceutical target for rheumatoid arthritis. *Nature Clinical Practice Rheumatology,* 4**,** 300-309.
Mullooly, M., Mcgowan, P. M., Crown, J. & Duffy, M. J. 2016. The ADAMs family of proteases as targets for the treatment of cancer. *Cancer Biol Ther,* 17**,** 870-880.
Nakagawa, T., Guichard, A., Castro, C. P., Xiao, Y., Rizen, M., Zhang, H. Z., Hu, D., Bang, A., Helms, J., Bier, E. & Derynck, R. 2005. Characterization of a human rhomboid homolog, p100hRho/RHBDF1, which interacts with TGF-alpha family ligands. *Dev Dyn,* 233**,** 1315-31.
Nelson, M. D. & Fitch, D. H. 2011. Overlap extension PCR: an efficient method for transgene construction. *Methods Mol Biol,* 772**,** 459-70.
Nusse, R. & Clevers, H. 2017. Wnt/beta-Catenin Signaling, Disease, and Emerging Therapeutic Modalities. *Cell,* 169**,** 985-999.
Obenauer, J. C., Cantley, L. C. & Yaffe, M. B. 2003. Scansite 2.0: proteome-wide prediction of cell signaling interactions using short sequence motifs. *Nucleic Acids Res,* 31**,** 3635-3641.
Ohtsu, H., Dempsey, P. J. & Eguchi, S. 2006. ADAMs as mediators of EGF receptor transactivation by G protein-coupled receptors. *American Journal of Physiology-Cell Physiology,* 291**,** C1-C10.
Parameswaran, N. & Patial, S. 2010. Tumor necrosis factor-alpha signaling in macrophages. *Crit Rev Eukaryot Gene Expr,* 20**,** 87-103.
Pearson, M. A., Reczek, D., Bretscher, A. & Karplus, P. A. 2000. Structure of the ERM protein moesin reveals the FERM domain fold masked by an extended actin binding tail domain. *Cell,* 101**,** 259-70.
Peschon, J. J., Slack, J. L., Reddy, P., Stocking, K. L., Sunnarborg, S. W., Lee, D. C., Russell, W. E., Castner, B. J., Johnson, R. S., Fitzner, J. N., Boyce, R. W., Nelson, N., Kozlosky, C. J., Wolfson, M. F., Rauch, C. T., Cerretti, D. P., Paxton, R. J., March, C. J. & Black, R. A. 1998. An essential role for ectodomain shedding in mammalian development. *Science,* 282**,** 1281-4.
Popp, M. W. & Maquat, L. E. 2016. Leveraging Rules of Nonsense-Mediated mRNA Decay for Genome Engineering and Personalized Medicine. *Cell,* 165**,** 1319-1322.
Prenzel, N., Zwick, E., Daub, H., Leserer, M., Abraham, R., Wallasch, C. & Ullrich, A. 1999. EGF receptor transactivation by G-protein-coupled receptors requires metalloproteinase cleavage of proHB-EGF. *Nature,* 402**,** 884-8.

Reddy, P., Slack, J. L., Davis, R., Cerretti, D. P., Kozlosky, C. J., Blanton, R. A., Shows, D., Peschon, J. J. & Black, R. A. 2000. Functional analysis of the domain structure of tumor necrosis factor-alpha converting enzyme. *J Biol Chem,* 275**,** 14608-14.

Rhodenizer, D., Martin, I., Bhandari, P., Pletcher, S. D. & Grotewiel, M. 2008. Genetic and environmental factors impact age-related impairment of negative geotaxis in Drosophila by altering age-dependent climbing speed. *Exp Gerontol,* 43**,** 739-48.

Rose-John, S. 2013. ADAM17, shedding, TACE as therapeutic targets. *Pharmacol Res,* 71**,** 19-22.

Saarinen, S., Vahteristo, P., Lehtonen, R., Aittomaki, K., Launonen, V., Kiviluoto, T. & Aaltonen, L. A. 2012. Analysis of a Finnish family confirms RHBDF2 mutations as the underlying factor in tylosis with esophageal cancer. *Fam Cancer,* 11**,** 525-8.

Saftig, P. & Reiss, K. 2011. The "A Disintegrin And Metalloproteases" ADAM10 and ADAM17: novel drug targets with therapeutic potential? *Eur J Cell Biol,* 90**,** 527-35.

Sahin, U. & Blobel, C. P. 2007. Ectodomain shedding of the EGF-receptor ligand epigen is mediated by ADAM17. *FEBS Lett,* 581**,** 41-4.

Sahin, U., Weskamp, G., Kelly, K., Zhou, H. M., Higashiyama, S., Peschon, J., Hartmann, D., Saftig, P. & Blobel, C. P. 2004. Distinct roles for ADAM10 and ADAM17 in ectodomain shedding of six EGFR ligands. *J Cell Biol,* 164**,** 769-79.

Scheller, J., Chalaris, A., Garbers, C. & Rose-John, S. 2011. ADAM17: a molecular switch to control inflammation and tissue regeneration. *Trends Immunol,* 32**,** 380-7.

Shi, Y., Inoue, H., Wu, J. C. & Yamanaka, S. 2017. Induced pluripotent stem cell technology: a decade of progress. *Nat Rev Drug Discov,* 16**,** 115-130.

Shirakata, Y., Kimura, R., Nanba, D., Iwamoto, R., Tokumaru, S., Morimoto, C., Yokota, K., Nakamura, M., Sayama, K., Mekada, E., Higashiyama, S. & Hashimoto, K. 2005. Heparin-binding EGF-like growth factor accelerates keratinocyte migration and skin wound healing. *J Cell Sci,* 118**,** 2363-2370.

Shirasawa, S., Sugiyama, S., Baba, I., Inokuchi, J., Sekine, S., Ogino, K., Kawamura, Y., Dohi, T., Fujimoto, M. & Sasazuki, T. 2004. Dermatitis due to epiregulin deficiency and a critical role of epiregulin in immune-related responses of keratinocyte and macrophage. *Proc Natl Acad Sci U S A,* 101**,** 13921-13926.

Siggs, O. M., Grieve, A., Xu, H., Bambrough, P., Christova, Y. & Freeman, M. 2014. Genetic interaction implicates iRhom2 in the regulation of EGF receptor signalling in mice. *Biol Open,* 3**,** 1151-7.

Siggs, O. M., Xiao, N., Wang, Y., Shi, H., Tomisato, W., Li, X., Xia, Y. & Beutler, B. 2012. iRhom2 is required for the secretion of mouse TNFalpha. *Blood,* 119**,** 5769-71.

Sommer, A., Kordowski, F., Buch, J., Maretzky, T., Evers, A., Andra, J., Dusterhoft, S., Michalek, M., Lorenzen, I., Somasundaram, P., Tholey, A., Sonnichsen, F. D., Kunzelmann, K., Heinbockel, L., Nehls, C., Gutsmann, T., Grotzinger, J., Bhakdi, S. & Reiss, K. 2016. Phosphatidylserine exposure is required for ADAM17 sheddase function. *Nature Communications,* 7.

Soond, S. M., Everson, B., Riches, D. W. & Murphy, G. 2005. ERK-mediated phosphorylation of Thr735 in TNFalpha-converting enzyme and its potential role in TACE protein trafficking. *J Cell Sci,* 118**,** 2371-80.

Stanley, P., Schachter, H. & Taniguchi, N. 2009. N-Glycans. *In:* Varki, A., Cummings, R. D., Esko, J. D., Freeze, H. H., Stanley, P., Bertozzi, C. R., Hart, G. W. & Etzler, M. E. (eds.) *Essentials of Glycobiology.* 2nd ed. Cold Spring Harbor (NY).

Stoll, S. W., Johnson, J. L., Bhasin, A., Johnston, A., Gudjonsson, J. E., Rittie, L. & Elder, J. T. 2010. Metalloproteinase-mediated, context-dependent function of amphiregulin and HB-EGF in human keratinocytes and skin. *J Invest Dermatol,* 130**,** 295-304.

Sun, L., Wu, J., Du, F., Chen, X. & Chen, Z. J. 2013. Cyclic GMP-AMP synthase is a cytosolic DNA sensor that activates the type I interferon pathway. *Science,* 339**,** 786-91.

Takahashi, K. & Yamanaka, S. 2006. Induction of pluripotent stem cells from mouse embryonic and adult fibroblast cultures by defined factors. *Cell,* 126**,** 663-76.

Tokumaru, S., Higashiyama, S., Endo, T., Nakagawa, T., Miyagawa, J., Yamamori, K., Hanakawa, Y., Ohmoto, H., Yoshino, K., Shirakata, Y., Matsuzawa, Y., Hashimoto, K. & Taniguchi, N. 2000. Ectodomain shedding of epidermal growth factor receptor ligands is required for keratinocyte migration in cutaneous wound healing. *J Cell Biol,* 151**,** 209-219.

Trad, A., Riese, M., Shomali, M., Hedeman, N., Effenberger, T., Grotzinger, J. & Lorenzen, I. 2013. The disintegrin domain of ADAM17 antagonises fibroblastcarcinoma cell interactions. *Int J Oncol,* 42**,** 1793-800.

Trudgian, D. C., Ridlova, G., Fischer, R., Mackeen, M. M., Ternette, N., Acuto, O., Kessler, B. M. & Thomas, B. 2011. Comparative evaluation of label-free SINQ normalized spectral index quantitation in the central proteomics facilities pipeline. *Proteomics,* 11**,** 2790-7.

Truett, G. E., Heeger, P., Mynatt, R. L., Truett, A. A., Walker, J. A. & Warman, M. L. 2000. Preparation of PCR-quality mouse genomic DNA with hot sodium hydroxide and tris (HotSHOT). *Biotechniques,* 29**,** 52, 54.

Tsukerman, P., Eisenstein, E. M., Chavkin, M., Schmiedel, D., Wong, E., Werner, M., Yaacov, B., Averbuch, D., Molho-Pessach, V., Stepensky, P., Kaynan, N., Bar-On, Y., Seidel, E., Yamin, R., Sagi, I., Elpeleg, O. & Mandelboim, O. 2015. Cytokine secretion and NK cell activity in human ADAM17 deficiency. *Oncotarget,* 6**,** 44151-60.

Uhlen, M., Fagerberg, L., Hallstrom, B. M., Lindskog, C., Oksvold, P., Mardinoglu, A., Sivertsson, A., Kampf, C., Sjostedt, E., Asplund, A., Olsson, I., Edlund, K., Lundberg, E., Navani, S., Szigyarto, C. A., Odeberg, J., Djureinovic, D., Takanen, J. O., Hober, S., Alm, T., Edqvist, P. H., Berling, H., Tegel, H., Mulder, J., Rockberg, J., Nilsson, P., Schwenk, J. M., Hamsten, M., Von Feilitzen, K., Forsberg, M., Persson, L., Johansson, F., Zwahlen, M., Von Heijne, G., Nielsen, J. & Ponten, F. 2015. Proteomics. Tissue-based map of the human proteome. *Science,* 347**,** 1260419.

Urban, S., Lee, J. R. & Freeman, M. 2001. Drosophila rhomboid-1 defines a family of putative intramembrane serine proteases. *Cell,* 107**,** 173-82.

Van Wilgenburg, B., Browne, C., Vowles, J. & Cowley, S. A. 2013. Efficient, long term production of monocyte-derived macrophages from human pluripotent stem cells under partly-defined and fully-defined conditions. *PLoS One,* 8**,** e71098.

Vandenbroucke, R. E. & Libert, C. 2014. Is there new hope for therapeutic matrix metalloproteinase inhibition? *Nature Reviews Drug Discovery,* 13**,** 904-927.

Vassar, R. & Fuchs, E. 1991. Transgenic Mice Provide New Insights into the Role of Tgf-Alpha during Epidermal Development and Differentiation. *Gene Dev,* 5**,** 714-727.

Vuckovic, D., Dagley, L. F., Purcell, A. W. & Emili, A. 2013. Membrane proteomics by high performance liquid chromatography-tandem mass spectrometry: Analytical approaches and challenges. *Proteomics,* 13**,** 404-23.

Weber, E. M., Olsson, A. S. & Algers, B. 2007. High mortality rates among newborn laboratory mice - is it natural and which are the causes? *Acta Vet Scand,* 49.

Wisniewski, J. R., Zougman, A., Nagaraj, N. & Mann, M. 2009. Universal sample preparation method for proteome analysis. *Nat Methods,* 6**,** 359-62.

Wong, E., Cohen, T., Romi, E., Levin, M., Peleg, Y., Arad, U., Yaron, A., Milla, M. E. & Sagi, I. 2016. Harnessing the natural inhibitory domain to control TNFalpha Converting Enzyme (TACE) activity in vivo. *Sci Rep,* 6**,** 35598.

Wu, C., Jin, X., Tsueng, G., Afrasiabi, C. & Su, A. I. 2016. BioGPS: building your own mash-up of gene annotations and expression profiles. *Nucleic Acids Res,* 44**,** D313-6.

Xu, P. & Derynck, R. 2010. Direct activation of TACE-mediated ectodomain shedding by p38 MAP kinase regulates EGF receptor-dependent cell proliferation. *Mol Cell,* 37**,** 551-66.

Xu, P., Liu, J., Sakaki-Yumoto, M. & Derynck, R. 2012. TACE activation by MAPK-mediated regulation of cell surface dimerization and TIMP3 association. *Sci Signal,* 5**,** ra34.

Yamamoto, K., Trad, A., Baumgart, A., Huske, L., Lorenzen, I., Chalaris, A., Grotzinger, J., Dechow, T., Scheller, J. & Rose-John, S. 2012. A novel bispecific single-chain antibody for ADAM17 and CD3 induces T-cell-mediated lysis of prostate cancer cells. *Biochem J,* 445**,** 135-44.

Yan, Z., Zou, H., Tian, F., Grandis, J. R., Mixson, A. J., Lu, P. Y. & Li, L. Y. 2008. Human rhomboid family-1 gene silencing causes apoptosis or autophagy to epithelial cancer cells and inhibits xenograft tumor growth. *Mol Cancer Ther,* 7**,** 1355-64.

Yang, L., Li, W., Liu, B., Wang, S., Zeng, L., Zhang, C. & Li, Y. 2016. iRhom2 (Uncv) mutation blocks bulge stem cells assuming the fate of hair follicle. *Arch Dermatol Res,* 308**,** 503-10.

Yarden, Y. & Pines, G. 2012. The ERBB network: at last, cancer therapy meets systems biology. *Nat Rev Cancer,* 12**,** 553-63.

Yarden, Y. & Sliwkowski, M. X. 2001. Untangling the ErbB signalling network. *Nat Rev Mol Cell Biol,* 2**,** 127-37.

Yates, A., Akanni, W., Amode, M. R., Barrell, D., Billis, K., Carvalho-Silva, D., Cummins, C., Clapham, P., Fitzgerald, S., Gil, L., Giron, C. G., Gordon, L., Hourlier, T., Hunt, S. E., Janacek, S. H., Johnson, N., Juettemann, T., Keenan, S., Lavidas, I., Martin, F. J., Maurel, T., Mclaren, W., Murphy, D. N., Nag, R., Nuhn, M., Parker, A., Patricio, M., Pignatelli, M., Rahtz, M., Riat, H. S., Sheppard, D., Taylor, K., Thormann, A., Vullo, A., Wilder, S. P., Zadissa, A., Birney, E., Harrow, J., Muffato, M., Perry, E., Ruffier, M., Spudich, G., Trevanion, S. J., Cunningham, F., Aken, B. L., Zerbino, D. R. & Flicek, P. 2016. Ensembl 2016. *Nucleic Acids Res,* 44**,** D710-6.

Yin, H. & Flynn, A. D. 2016. Drugging Membrane Protein Interactions. *Annu Rev Biomed Eng,* 18**,** 51-76.

Zeng, L., Fagotto, F., Zhang, T., Hsu, W., Vasicek, T. J., Perry, W. L., 3rd, Lee, J. J., Tilghman, S. M., Gumbiner, B. M. & Costantini, F. 1997. The mouse

Fused locus encodes Axin, an inhibitor of the Wnt signaling pathway that regulates embryonic axis formation. *Cell,* 90**,** 181-92.
Zettl, M., Adrain, C., Strisovsky, K., Lastun, V. & Freeman, M. 2011. Rhomboid family pseudoproteases use the ER quality control machinery to regulate intercellular signaling. *Cell,* 145**,** 79-91.
Zhou, Z., Liu, F., Zhang, Z. S., Shu, F., Zheng, Y., Fu, L. & Li, L. Y. 2014. Human rhomboid family-1 suppresses oxygen-independent degradation of hypoxia-inducible factor-1alpha in breast cancer. *Cancer Res,* 74**,** 2719-30.
Zou, H., Thomas, S. M., Yan, Z. W., Grandis, J. R., Vogt, A. & Li, L. Y. 2009. Human rhomboid family-1 gene RHBDF1 participates in GPCR-mediated transactivation of EGFR growth signals in head and neck squamous cancer cells. *FASEB J,* 23**,** 425-32.
Zunke, F. & Rose-John, S. 2017. The shedding protease ADAM17: Physiology and pathophysiology. *Biochim Biophys Acta*.